DOE F 241.3
(2-01) p.1 of 2

UNITED STATES DEPARTMENT OF ENERGY (DOE)
Announcement of Scientific and Technical Information (STI)
(For Use By Financial Assistance Recipients and Non-M&O/M&I Contractors)

OMB CONTROL NO. 1910-1400

PART I: STI PRODUCT DESCRIPTION
(To be completed by Recipient/Contractor)

A. STI Product Identifiers

1. REPORT/PRODUCT NUMBER(s)
None

2. DOE AWARD/CONTRACT NUMBER(s)
DE-FC36-97ID13554

3. OTHER IDENTIFYING NUMBER(s)
None

B. Recipient/Contractor

CANMET-Materials Technology Laboratory, 568 Booth St., Ottawa, ON K1A0G1 Canada

C. STI Product Title

Properties of Galvanized and Galvannealed Advanced High Strength Hot Rolled Steels

D. Author(s)

V.Y. Guertsman, E. Essadiqi, S. Dionne, O. Dremailova
R. Bouchard, B. Voyzelle, J. McDermid, R. Fourmentin

E-mail Address(es):
vgertsma@nrcan.gc.ca

E. STI Product Issue Date/Date of Publication

04 (MM) 01 (DD) 2008 (YYYY)

F. STI Product Type (*Select only one*)

☒ 1. TECHNICAL REPORT
☒ *Final* ☐ *Other (specify)* _____

☐ 2. CONFERENCE PAPER/PROCEEDINGS

Conference Information (title, location, dates)

☐ 3. JOURNAL ARTICLE
a. TYPE: ☐ *Announcement Citation Only* ☐ *Preprint* ☐ *Postprint*
b. JOURNAL NAME
c. VOLUME _____ *d. ISSUE* _____
e. SERIAL IDENTIFIER (e.g. ISSN or CODEN)

☐ 4. OTHER, SPECIFY

G. STI Product Reporting Period

06 (MM) 28 (DD) 2005 (YYYY) Thru 04 (MM) 01 (DD) 2008 (YYYY)

H. Sponsoring DOE Program Office

Office of Industrial Technologies (OIT)(EE20)

I. Subject Categories (*list primary one first*)

32 Energy Conservation, Consumption and Utilization

Keywords: Advanced high strength steel, HSLA, DP, TRIP, Galvanizing, Galvannealling

J. Description/Abstract

The objectives of the project were (i) to develop the coating process information to achieve good quality coatings on 3 advanced high strength hot rolled steels while retaining target mechanical properties, (ii) to obtain precise knowledge of the behavior of these steels in the various forming operations and (iii) to establish accurate user property data in the coated conditions. Three steel substrates (HSLA, DP, TRIP) with compositions providing yield strengths in the range of 400-620 MPa were selected. Only HSLA steel was found to be suitable for galvanizing and galvannealing in the hot-rolled condition.

K. Intellectual Property/Distribution Limitations

(*must select at least one; if uncertain contact your Contracting Officer (CO)*)

☒ 1. UNLIMITED ANNOUNCEMENT (*available to U.S. and non-U.S. public; the Government assumes no liability for disclosure of such data*)

☐ 2. COPYRIGHTED MATERIAL: *Are there any restrictions based on copyright?* ☐ *Yes* ☐ *No.*
If yes, list the restrictions as contained in your award document

☐ 3. PATENTABLE MATERIAL: THERE IS PATENTABLE MATERIAL IN THE DOCUMENT.
INENTION DISCLOSURE SUBMITTED TO DOE:
DOE Docket Number: S-
(Sections are marked as restricted distribution pursuant to 35 USC 205)

☐ 4. PROTECTED DATA: ☐ CRADA ☐ *Other, specify*
Release date (required) no more than 5 years from date listed in Part I.E. above ___ (MM) ___ (DD) ____ (YYYY)

☐ 5. SMALL BUSINESS INNOVATION RESEARCH (SBIR) DATA
Release date (required) no more than 4 years from date listed in Part I.E. above ___ (MM) ___ (DD) ____ (YYYY)

☐ 6. SMALL BUSINESS TECHNOLOGY TRANSFER RESEARCH (STTR) DATA
Release date (required) no more than 4 years from date listed in Part I.E. above ___ (MM) ___ (DD) ____ (YYYY)

☐ 7. OFFICE OF NUCLEAR ENERGY APPLICED TECHNOLOGY

L. Recipient/Contract Point of Contact *Contact for additional information (contact or organization name To be included in published citations and who would Receive any external questions about the content of the STI Product or the research contained herein)*

Dr. Val Guertsman
Name and/or Position
vgertsma@nrcan.gc.ca *(613) 995-2132*
E-mail *Phone*
CANMET-Materials Technology Laboratory, 568 Booth St.
Ottawa, ON K1A0G1 Canada

UNITED STATES DEPARTMENT OF ENERGY (DOE)
Announcement of Scientific and Technical Information (STI)
(For Use By Financial Assistance Recipients and Non-M&O/M&I Contractors)

OMB CONTROL NO.
1910-1400

PART II: STI PRODUCT MEDIA/FORMAT and LOCATION/TRANSMISSION
(To be completed by Recipient/Contractor)

A. Media/Format Information:

1. MEDIUM OF STI PRODUCT IS:
   [X] Electronic Document [ ] Computer Medium
   [ ] Audiovisual Material [ ] Paper [ ] No Full-text
2. SIZE OF STI PRODUCT 204 Pages, 49,937 KB
3. SPECIFY FILE FORMAT OF ELECTRONIC DOCUMENT BEING TRANSMITTED, INDICATE:
   [ ] SGML [ ] HTML [ ] XML [X] PDF Normal
   [ ] PDF Image [ ] TIFFG4
   [ ] WP-indicate Version *(5.0 or greater)* _____
   Platform/operation system _____
   [ ] MS-indicate Version *(5.0 or greater)* _____
   Platform/operation system _____
   [ ] Postscript _____
4. IF COMPUTER MEDIUM OR AUDIOVISUAL MATERIAL:
   a. Quantity/type *(specify)* _____
   b. Machine compatibility *(specify)* _____
   c. Other information about product format a user needs to know:
   _____

B. Transmission Information:

1. STI PRODUCT IS BEING TRANSMITTED:
   [X] a. Electronically via E-Link
   b. Via mail or shipment to address indicated in award document *(Paper product, CD-ROM, diskettes, video cassettes, etc.)*
   _____
2. INFORMATION PRODUCT FILE NAME
   [X] *(of transmitted electronic format)*
   TRP9946NonPropFinalReport

PART III: STI PRODUCT REVIEW/RELEASE INFORMATION
(To be completed by DOE)

A. STI Product Reporting Requirements Review.

[ ] 1. THIS DELIVERABLE COMPLETES ALL REQUIRED DELIVERABLES FOR THIS AWARD
[ ] 2. THIS DELIVERABLE FULFILLS A TECHNICAL INFORMATION REPORTING REQUIREMENT, BUT SHOULD NOT BE DISSEMINATED BEYOND DOE.

B. Award Office Is the Source of STI Product Availability

[ ] THE STI PRODUCT IS NOT AVAILABLE IN AN ELECTRONIC MEDIUM. THE AWARDING OFFICE WILL SERVE AS THE INTERIM SOURCE OF AVAILABILITY.

C. DOE Releasing Official

[ ] 1. I VERIFY THAT ALL NECESSARY REVIEWS HAVE BEEN COMPLETED AS DESCRIBED IN DOE G 241.1-1A, PART II, SECTION 3.0 AND THAT THE STI PRODUCT SHOULD BE RELEASED IN ACCORDANCE WITH THE INTELLECTUAL PROPERTY/DISTRIBUTION LIMITATION ABOVE.

Release by *(name)* _____

Date ___ ___ _____
MM DD YYYY

E-Mail _____

Phone _____

REPORT DOCUMENTATION PAGE

Title and Subtitle:

AISI/DOE Technology Roadmap Program for the Steel Industry
TRP 9946: Properties of Galvanized and Galvannealed Advanced High Strength Hot Rolled Steels

Authors:

V.Y. Guertsman
E. Essadiqi
S. Dionne
J. McDermid
O. Dremailova
R. Bouchard
B. Voyzelle
R. Fourmentin

Performing Organization

CANMET - Materials Technology Laboratory
568 Booth Street
Ottawa, ON K1A0G1 Canada

Abstract

The objectives of the project were: (i) to develop the coating process information to achieve good quality coatings on three advanced high strength hot-rolled steels while retaining target mechanical properties, (ii) to obtain precise knowledge of the behavior of these steels in the various forming operations required by automobile parts manufacturers, and (iii) to establish accurate user property data in the coated conditions. Three steel substrates with compositions providing yield strength in the range of 400-620 MPa were selected for this project. These were: high-strength low alloyed (HSLA) steel with Ti, Nb and V precipitation-strengthening additions, an Mn-Mo dual-phase (DP) steel, and an Al-base transformation-induced plasticity (TRIP) steel. The coating regimes were established using heat treatment experiments and a galvanizing simulator. The microstructures of the steels were characterized in the as-received (hot-rolled), heat-treated, and coated conditions. The static and dynamic tensile properties, as well as stretch-flange formability, were determined for different conditions. Only HSLA steel was found to be suitable for galvanizing and galvanneling in the as-received hot-rolled condition; the DP and TRIP grades did not have the required microstructure and properties in the as-received hot-rolled condition. Therefore, additional heat treatment would be necessary to bring those grades to the required condition before coating.

Keywords: Advanced high-strength steels, high strength low alloy (HSLA) steel, dual-phase (DP) steel, transformation induced plasticity (TRIP) steel, Galvanizing, Galvannealing

DOCUMENT AVAILABILITY

Reports are available free via the U.S. Department of Energy (DOE) Information Bridge:

Website: http://www.osti.gov/bridge

Reports are available to DOE employees, DOE contractors, Energy Technology Data Exchange (ETDE) representatives, and Informational Nuclear Information System (INIS) representatives from the following source:

Office of Scientific and Technical Information
P.O. Box 62
Oak Ridge, TN 37831
Tel: (865) 576-8401
Fax: (865) 576-5728
E-mail: reports@osti.gov
Website: http://www.osti.gov/contract.html

Acknowledgement: "This report is based upon work supported by the U.S. Department of Energy under Cooperative Agreement No. DE-FC36-97ID13554."

AISI/DOE Technology Roadmap Program

Final Report

TRP 9946 - Properties of Galvanized and Galvannealed Advanced High Strength Hot Rolled Steels

By

V.Y. Guertsman, E. Essadiqi, S. Dionne, O. Dremailova, R. Bouchard, B. Voyzelle, J. McDermid, R. Fourmentin

April 2008

Work Performed under Cooperative Agreement No. DE-FC36-97ID13554

Prepared for
U.S. Department of Energy

Prepared by
American Iron and Steel Institute
Technology Roadmap Program Office
Pittsburgh, PA 15222

TRP 9946: "Properties of Galvanized and Galvannealed Advanced High Strength Hot Rolled Steels"

Report No. 2008-11(CF)

CANMET-Materials Technology Laboratory
568 Booth Street, Ottawa, ON, K1A0G1, Canada

V.Y. Guertsman, E. Essadiqi, S. Dionne, O. Dremailova, R. Bouchard, B. Voyzelle,
J. McDermid, R. Fourmentin

April 2008

Work on this project was funded by AISI.

DISCLAIMER

Natural Resources Canada makes no representations or warranties respecting the contents of this report, either expressed or implied, arising by law or otherwise, including but not limited to implied warranties or conditions of merchantability or fitness for a particular purpose.

EXECUTIVE SUMMARY

This report was prepared at the request of the American Iron and Steel Institute (AISI) as one of the deliverables of the TRP 9946 program entitled "Properties of Galvanized and Galvannealed Advanced High Strength Hot-rolled Steels". The objectives of the project were: (i) to develop the coating process information to achieve good quality coatings on three advanced high strength hot-rolled steels while retaining target mechanical properties, (ii) to obtain precise knowledge of the behavior of these steels in the various forming operations required by automobile parts manufacturers, and (iii) to establish accurate user property data in the coated conditions.

The project participants were:
Research organizations: CANMET-Materials Technology Laboratory, Ottawa, Canada; McGill University, Montreal, Canada; McMaster University, Hamilton, Canada;
Industry participants: International Lead Zinc Research Organization (ILZRO); Nucor Steel, SC, SeverStal N.A., Dearborn, MI; US Steel, Pittsburgh, PA.

Recent advances in hot rolling technology have made possible the production of hot-rolled products with more consistent gauge, shape, profile and surface quality. These improved hot-rolled products may be suitable for galvanizing after pickling and, therefore, finished galvanized strip could be produced without a cold reduction step, resulting in significant energy and cost savings. Advanced high strength steels are of great interest to the automotive industry for fabrication of components such as engine cradles, sub frames and structural closures. Three steel substrates with compositions providing yield strength in the range of 400-620 MPa were selected for this project. These were advanced high strength hot-rolled steels: high-strength low alloyed (HSLA) steel, dual-phase (DP) steel and transformation-induced plasticity (TRIP) steel.

The microstructure, inclusions and surface of the as-rolled steels in the as-received condition were characterized. The tensile properties of the as-rolled steels in the as-received condition were determined and are compared with the target properties identified in the ILZRO reports ZCO-21-1 and ZCO-21-2 [1,2].

The HSLA steel in this project was a grade with Ti, Nb and V precipitation-strengthening additions. The hot-rolled HSLA steel did meet the target mechanical properties in the as-received condition. Those properties were retained after galvanizing and galvannealing. Stretch-flange formability of this steel in the galvanized condition measured through the hole expansion tests is what is expected from this steel grade. In the galvannealed condition, however, the hole expansion ratio was lower; the fractography showed that fracture was more brittle than with the galvanized coating. The results of dynamic tensile tests, performed to assess crashworthiness, indicate that there is an increase in stress at higher strain rates coupled with a small decrease in total elongation to failure. The energy absorbed at high strain rates is above that at a quasi-static rate, and is similar in the galvanized and galvannealed conditions.

The material received as a DP grade was an Mn-Mo steel. The tensile properties of this steel in the as-received hot-rolled condition did not meet the target yield strength and ultimate tensile strength. Microstructural studies showed that there was almost no martensite in the as-received condition which explained its low strength properties. Using trial heat treatments, consisting of intercritical

annealing followed by rapid cooling, it was possible to determine a schedule producing enough martensite in the microstructure to increase hardness. However, that schedule would be difficult to implement in actual galvanizing lines. Moreover, additional hold at galvanizing temperature of 460°C destroyed the DP microstructure. Because of that as well as the very limited amount of material of this grade received, it was decided to terminate the work on this particular grade.

The TRIP steel received for this project was an Al-base grade. The tensile properties of this steel in the as-received hot-rolled condition did not meet the target yield strength and ultimate tensile strength and were barely on the margins of what is expected from TRIP grades. Microstructural studies showed that there was very little retained austenite in the as-received condition, which is necessary to provide for TRIP effect. Heat treatment regimes were developed to produce enough austenite in the microstructure. The optimal schedule includes intercritical annealing followed by overaging at 460°C (galvanizing temperature). The tensile properties of the heat-treated samples improved compared with the as-received condition. That heat treatment regime could be included in the galvanizing schedule. The tensile properties were retained after galvanizing of the TRIP steel. The hole expansion (stretch) ratio for TRIP steel was significantly lower than that measured for the HSLA steel and was near the lower limit of what is expected for high-strength steels. Dynamic tensile test results indicate an increase in stress at higher strain rates coupled with a small decrease in total elongation to failure. The increase in UTS at high strain rates is greater for the TRIP steel than for the HSLA steel. The energy absorbed at high strain rates is above that at a quasi-static rate and is similar to the results obtained on the HSLA samples.

It must be noted that there were significant delays in obtaining the project materials. Moreover, the DP and TRIP materials did not have the required microstructure and properties in the as-received hot-rolled conditions. Significant efforts were therefore undertaken to bring those materials up to the target properties. As a result of the late delivery of materials and additional work on the pre-coated conditions, it was not possible to complete all the stages of the project envisaged in the project plan, even though the total amount of experimental work was the same as planned.

Summarizing, in this study, only HSLA steel was found to be suitable for galvanizing and galvanneling in the as-received hot-rolled condition. DP and TRIP grades did not have the required microstructure and properties in the as-received hot-rolled condition, therefore, additional heat treatment would be necessary to bring those grades to the required condition before coating. Even though some of the heat treatment schedules could be incorporated into the galvanizing procedure, this may mean an increase in energy consumption.

CONTENTS

CANMET MATERIALS TECHNOLOGY LABORATORY

REPORT MTL 2008-11(CF)

TRP 9946: "PROPERTIES OF GALVANIZED AND GALVANNEALED ADVANCED HIGH STRENGTH HOT ROLLED STEELS"

by

V.Y. Guertsman, E. Essadiqi, S. Dionne, O. Dremailova, R. Bouchard, B. Voyzelle,

J. McDermid, R. Fourmentin

ABSTRACT

The objectives of the project were: (i) to develop the coating process information to achieve good quality coatings on three advanced high strength hot-rolled steels while retaining target mechanical properties, (ii) to obtain precise knowledge of the behavior of these steels in the various forming operations required by automobile parts manufacturers, and (iii) to establish accurate user property data in the coated conditions. Three steel substrates with compositions providing yield strength in the range of 400-620 MPa were selected for this project. These were: high-strength low alloyed (HSLA) steel with Ti, Nb and V precipitation-strengthening additions, an Mn-Mo dual-phase (DP) steel, and an Al-base transformation-induced plasticity (TRIP) steel. The coating regimes were established using heat treatment experiments and a galvanizing simulator. The microstructures of the steels were characterized in the as-received (hot-rolled), heat-treated, and coated conditions. The static and dynamic tensile properties, as well as stretch-flange formability, were determined for different conditions. Only HSLA steel was found to be suitable for galvanizing and galvanneling in the as-received hot-rolled condition; the DP and TRIP grades did not have the required microstructure and properties in the as-received hot-rolled condition. Therefore, additional heat treatment would be necessary to bring those grades to the required condition before coating.

Keywords: Advanced high-strength steels, high strength low alloy (HSLA) steel, dual-phase (DP) steel, transformation induced plasticity (TRIP) steel, Galvanizing, Galvannealing

INTRODUCTION

PROJECT OBJECTIVES

1. To develop the coating process information to achieve good quality coatings on three advanced high strength hot-rolled steels (HSLA, DP and TRIP) while retaining target mechanical properties.

2. To obtain precise knowledge of the behavior of these steels in the various forming operations required by automobile parts manufacturers.

3. To establish accurate user property data in the galvanized and galvannealed conditions.

BACKGROUND

Recent advances in hot rolling technology have made possible the production of hot-rolled products with more consistent gauge, shape, profile and surface quality. These improved hot-rolled products are suitable for galvanizing after pickling and, therefore, finished galvanized strip can be produced without a cold reduction step, resulting in significant energy and cost savings. Advanced high strength hot-rolled steels have been developed based on precipitation (HSLA), Dual-phase (DP) and Transformation-induced Plasticity (TRIP) strengthening mechanisms. Thermo-mechanical processing routes exist to produce these grades as 1 to 3 mm hot-rolled strip that can achieve target yield strength (YS) of 350-600 MPa (50-85 ksi) [1,2]. These grades are of great interest to the automotive industry for fabrication of components such as engine cradles, sub frames and structural closures.

From 2000-2005, CANMET-MTL, Noranda Inc. and ILZRO completed a comprehensive research project to develop hot-dip galvanizing processing windows for several high strength hot-rolled steel grades and to determine the effect of galvanizing on their tensile properties. The results were summarized in several reports [3-7]. Good quality coatings were obtained on both hot-rolled HSLA-type and TRIP steels with Mn content ranging from 0.5 to 1.5% and Si content from 0.1 to 1.5%. However, additional effort is required to extend these galvanizing windows to the DP grades and to develop suitable galvannealing process conditions. There is a lack of precise knowledge of the behavior of galvanized and galvannealed high strength hot-rolled steels in the various forming operations required by parts manufacturers and automobile producers. Among these, stretch-flange-formability is a property critical to avoiding fracture during forming of actual parts. Since some forming operations are applied by hydroforming, there is also a need to develop property data in the welded tube state. Accurate user property data for the high strength hot-rolled steels in the galvanized and galvannealed conditions is also required. Fatigue resistance and crashworthiness are the two properties most relevant to automotive applications.

In the current research, CANMET-MTL, in partnership with ILZRO, McMaster University and McGill University, aimed at developing the required coating process information, formability and user property data for advanced high strength hot-rolled grades for automotive applications. Selected hot-rolled steels, that is, HSLA, DP and TRIP grades, were going to be hot dip galvanized and

galvannealed using McMaster University's galvanizing simulator. A range of mechanical and formability properties were to be determined in the as-received and coated conditions.

PROPOSED TEST MATRIX

Three steel substrates with compositions providing yield strength in the range of 350-570 MPa were proposed for this project. Table 2 lists the target composition and properties of each grade, including some alternative compositions that were considered acceptable for the project objectives. The steels included a precipitation-strengthened high strength low alloy (HSLA) grade, a transformation induced plasticity (TRIP) grade and a dual-phase (DP) grade. The chemistries were based on the results of the ILZRO ZCO-21 project [1-5] and on the recommendations made by the project sponsors during the kick-off meeting in July 2006. The desired steel thickness was 2.0 to 2.5 mm; the maximum thickness that could be used in the galvanizing simulator was 3.0 mm, however, thinner material was preferable as it is more representative of the automotive applications targeted for this project. The preferred source of hot-rolled steel would be commercial mills as this ensures that the hot-rolled surface quality is representative of industrial practice. With the assistance of AISI and ILZRO, the project team attempted to obtain all of the steels from the program sponsors.

Three organizations supplied material for the program. Organization A provided an HSLA grade with Ti, Nb and V precipitation-strengthening additions; organization B provided an Mn-Mo DP grade, but the amount of steel was not sufficient for all the stages planned for this project; and organization C provided an Al-base TRIP grade. All three materials were somewhat similar to the alternative grades of the corresponding steels listed in Table 2.

Detailed data on the composition, thickness and initial surface condition of each material, as well as the processing information provided by each supplier, are given in the corresponding sections below.

PROJECT DELIVERABLES

1. Coating process information to achieve galvanized and galvannealed advanced high strength hot-rolled steels with good coating quality that meet the target mechanical properties for automotive applications.

2. Knowledge of the behavior of these steels during stretch-flange-formability and hydroforming operations.

3. Static and dynamic property data for these steels in the galvanized and galvannealed conditions.

The research program was designed to accomplish these deliverables by performing the 12 tasks and sub-tasks listed in Table 1. However, significant delays were encountered in obtaining the steels due to the limited availability of some of the desired compositions in the hot-rolled condition. Because of the delays and the unsuitability of some of the received materials, not all the tasks were performed on all steel grades.

HSLA STEEL

OBTAINING THE STEEL SUBSTRATE

Organization A provided an HSLA grade steel with Ti, Nb and V precipitation-strengthening additions. Its chemistry is similar to the alternative composition requested at the start of the project (see Table 2). The composition, thickness and initial surface condition of each material, as well as the processing information provided by the supplier, are summarized in Tables 3-5.

Characterization of the As-Received Hot-rolled HSLA Steel

Microstructure of the As-Received HSLA Steel

The as-rolled microstructure of the steels was characterized using light optical and scanning electron microscopy techniques. Longitudinal and transverse metallographic cross-sections were etched in 3% Nital. To reveal the martensite-austenite constituent, dual-phase samples were etched using the etchant developed by LePera [8]. This etchant colors ferrite light tan, bainite brown, pearlite black, and martensite-austenite islands white. As-polished longitudinal cross-sections were examined using SEM equipped with Energy Dispersive Spectroscopy (EDS) to characterize the inclusions in the as-rolled steels.

The microstructure of the as-received HSLA steel was composed of fine-grained ferrite interspersed with a few pearlite grains (Figs. 1 and 2). The fine pearlite lamellae and small grain boundary carbides are visible at higher magnification in the SEM (Fig. 2d).

The HSLA steel was supplied in the pickled condition. No residual scale or internal oxidation was detected on SEM cross-sections.

Typical inclusions observed in the as-received HSLA steel were complex oxide and sulfide phases up to 10 μm in diameter. The large inclusion shown in Fig. 3a is composed of a core of Mg-Al-Ca oxide (Fig. 3b) and Al-Ca oxide (Fig. 3c) with an Al-Ca sulfide shell (Fig. 3d). Figure 3e shows a smaller inclusion composed of Mg-Al oxide (Fig. 3f) and Ca sulfide (Fig. 3g). Two other complex inclusions are shown in Fig. 3h. One inclusion is composed of Ca sulfide and Mg-Al oxide (Figs. 3i and 3j), whereas the other is composed of a Mg-Al oxide core surrounded by a Ca sulfide shell (Figs. 3k and 3l). Two smaller inclusions (Fig. 3m) are composed of Ca sulfide (Figs. 3n and 3o). Many of these inclusions also contained small amounts of Ti and Mn. These observations suggest that the steel was calcium-treated to obtain round sulfide inclusions instead of the usual elongated manganese sulfide inclusions.

Tensile Properties of the As-Received HSLA Steel

The tensile properties of the as-rolled steel were determined using flat tensile specimens with 80 mm gauge length and 20 mm gauge width. Specimens were cut using electric discharge machining with their long axes aligned parallel (longitudinal orientation) or perpendicular (transverse orientation) to the rolling direction. For each condition, three to six specimens were tested on an Instron 100 kN frame using a crosshead speed of 2.5 mm/min and extensometers to measure displacements. The yield strength (stress at 0.2% offset), ultimate tensile strength and total elongation were determined

per ASTM E 8. The strain hardening exponent and plastic strain ratio were measured per ASTM E 517 and E 698.

The average and standard deviation of the tensile test results are presented in Table 6. In the as-received condition, the HSLA steel exceeded the target yield strength and ultimate tensile strength of the proposed HSLA grade by 10 to 40 MPa depending on whether the longitudinal or transverse properties are considered. The target elongation was met in the longitudinal direction but was slightly below the target value in the transverse direction due to the anisotropy of the tensile properties. The strain hardening exponent (n) and plastic strain ratio (r) are commensurate with the values expected for hot-rolled products.

HOT DIP GALVANIZING

Coupon Preparation and Pickling Procedures

Coupons with the dimensions 12 cm x 20 cm were machined with the long dimension parallel to the rolling direction (Fig. 4). A type K thermocouple was attached at the location indicated in Fig. 1 to record the sample temperature during each trial. The coupons were solvent degreased and pickled using the following procedure:

- Before using the pickling solution, the panels were degreased:
  - brush in NaOH (2%) at 80°C for 2 min,
  - rinse in distilled water for 1 min, and
  - dry coupons
- Immersion in the flash pickling solution at 21°C for 1 min:
  477 ml concentrated HCl (36.5-38 %, SP 1.19 g/cm^3),
  645 ml deionized Type IV water, and
  2 g hexamethylene tetramine (Aldrich, FW 140.19);
- Rinse in Type IV water at 21°C for 20 s; and
- Dry coupons.

Reheating and Galvanizing Procedures

To minimize energy consumption, galvanizing of hot-rolled steel should be performed using the lowest reheating temperature that provides acceptable coating quality. Typically, the strip is heated to a temperature above that of the galvanizing bath for a short time immediately prior to entering the zinc bath. If the reheating temperature is too high, the mechanical properties of some steel grades may be altered. On the other hand, insufficient reduction of surface oxides/hydroxides can result in poor coating quality if the reheating temperature is too low [9]. Furthermore, the coating quality can be affected by problems such as incomplete pickling of the hot-rolled scale, rust staining of the prepared surface during storage after pickling and segregation of carbon on the strip surface before hot dipping [10]. The coating quality can often be improved by increasing the reheating temperature

and/or the hydrogen content of the reheating atmosphere, which decreases surface contamination. Alternatively, higher bath and/or strip entry temperatures can be used to enhance coating wettability by increasing the chemical reactivity of the galvanizing bath.

In the present work, laboratory reheating and galvanizing trials were conducted on the McMaster Galvanizing Simulator to determine the effects of the reheating temperature, hydrogen content and dew point of the reheating atmosphere on the coating quality of the hot-rolled steels. The technical specifications and a schematic of the McMaster Galvanizing Simulator are presented in Appendix 1.

The following thermal cycles and conditions were used for the HSLA steel:

- Heating in an infrared furnace at 5°C/s to 600°C.
- Holding at 600°C for 60 s or 120 s. The reheating atmosphere: 20% H_2 in N_2 with a dew point of -30°C.
- Cooling at 5°C/s down to the strip entry temperature of 465°C.
- Dipping at 460°C for 4 s. Zinc bath with 0.20% effective Al and Fe saturated.
- Cooling after galvanizing at 3-5°C/s.

Figure 5 shows typical temperature vs. time plots for representative coupons reheated for 60 and 120 s. The observed thermal profiles show a good fit with the desired heat-to-coat schedule.

Three coupons were first tested and thoroughly examined for each of the two thermal cycles, i.e. 60 s and 120 s holding times at 600°C. As shown below, these two regimes resulted in similar characteristics in terms of the obtained microstructure, and the quality of the coating and the inhibition layer. Therefore, according to recommendations of the sponsors, the holding time of 60 s was chosen. Overall, 39 HSLA coupons were galvanized according to that schedule.

Characterization of Galvanized Coupons

The coating quality was assessed by visual inspection and quantitative measurements of the population of coating defects. Selected galvanized samples were also subjected to an in-depth evaluation using optical microscopy and SEM. A chemical dissolution technique was used to determine the coating mass and composition (Fe and Al contents).

Visual Inspection

Visual inspection indicated good coating quality on the galvanized samples. The typical appearance of the galvanized coupons can be seen in Fig. 6. More detailed photographs of both sides of the galvanized coupons are presented in Appendix 2. A few coupons show linear defects that could be associated with scratches made during handling. It should be noted that, due to the design of the McMaster simulator, the bottom part of the coupons is known to be cooler than the rest of the coupon (up to 10ºC cooler, depending on the reheating temperature). Consequently, the difference between the strip and bath temperatures is smaller in this part of the coupon, leading to reduced wettability. Therefore, the sampling pattern used for the coating quality evaluation was adjusted to reflect this characteristic of the McMaster simulator.

Coating Thickness and Mass

The coating thickness was evaluated on the cross-section samples using optical microscopy (Fig. 7). The thickness observed in a microscope roughly corresponds to the thickness evaluated using the glow discharge optical emission spectrometer (GDOES, as described below). The mass of the coating on the galvanized coupons was determined using a modified ASTM A90 [11] chemical dissolution procedure ("weigh-strip-weigh") developed by Noranda Inc. The following sample dimensions were used: 2×0.000167 m^2 (the sample after 60 s hold at 600°C) and 2×0.000165 m^2 (the sample after 120 s hold at 600°C). The samples were weighed before and after stripping in a fuming nitric acid. The measured coating mass was 210 g/m^2 and 138 g/m^2 for the 60 s and 120 s samples, respectively - significantly higher than the expected value of 60 g/m^2. This might be due to the rough surface of the hot-rolled steel.

Quantitative Evaluation of Coating Defects

The quantitative evaluation of coating defects was performed using optical microscopy and an image analysis system. For the bare spot area evaluation, the counting was carried out for the two samples (60 s and 120 s), with 18 fields (9 for each side, front and back) and with a total area of 391 mm^2. The results are summarized in Fig. 8. The following fractions for the bare area were obtained – 2.9% for the 60 s sample and 1.4% for the 120 s sample.

GDOES of Coupons

Elemental depth profiles of coupons that had been reheated in the -5ºC dew point atmospheres were obtained using a glow discharge optical emission spectrometer (GDOES). The measurements were performed with a JY Horiba HR GDOES instrument using an argon pressure of 885 Pa and a power of 35 W. The results of GDOES profiling for selected coupons after different stages of processing are shown in Fig. 9. One can see that the GDOES profiles exhibited the expected succession of layers on the galvanized coupons: zinc, the inhibition layer and the steel substrate.

Microstructure of the Steel Substrate of Galvanized Coupons

Figure 10 shows typical microstructures of the HSLA steel substrate after the galvanizing cycle. Comparison with the as-received microstructure (cf. Fig. 2) indicates that galvanizing did not change the steel microstructure, i.e. it consists mostly of fine-grained ferrite with a few pearlite colonies.

Inhibition Layer on Galvanized Coupons

The inhibition layer was examined on selected galvanized coupons after chemically removing the zinc layer; typical appearance is shown in Fig. 11a. Defects, such as that shown in Fig. 11b, were rarely observed. The presence of the Fe_2Al_5 phase was confirmed by X-ray diffractometry (Fig. 12). Because of the small thickness of the inhibition layer, the peaks of Fe_2Al_5 were weak, but still distinguishable.

Coating Quality (Bending test 180°)

Coating adhesion was determined using 180° bend testing per ASTM A653/A635M-03 on galvanized samples (Fig. 13). The results did not show any evidence of splitting of the coating nor of edge cracking. These results confirm that the galvanizing of these steel resulted in good reactive wetting and a complete Fe_2Al_5 layer.

GALVANNEALING

Galvannealing trials were conducted on the same McMaster Galvanizing Simulator as galvanizing (see above). The following parameters were tested:

- Heating at 5°C/s up to 600°C.
- Holding at 600°C for 60s
- Cooling at -5°C/s to the strip entry temperature of 465°C.
- Dipping at 460°C for 4 s.
- Cooling after galvanizing at 3-5°C/s.
- The reheating atmosphere 20% H_2 in N_2 with a dew point of -30°C.
- Zinc bath with 0.136% and 0.123% effective Al and Fe saturated.

The optimal galvannealing parameters were determined as follows:

- Effective Al concentration = 0.123 wt.%.
- Galvannealing temperature = 510°C.
- Galvannealing time = 30 s.

Figure 14 shows typical temperature vs. time plot for a representative coupon galvannealed under the optimal parameters. Visual inspection indicated good coating quality on the samples galvannealed under such conditions, except for the bottom portions of the coupons where Zn coating was thicker. The typical appearance of the galvannealed coupons can be seen in Fig. 15. More detailed photographs of both sides of the galvannealed coupons are presented in Appendix 3.

The thermal cycles at 500, 510 and 520°C for 30 s produced well-developed galvannealed coatings with ~10 wt.% of iron according to GDOES results (Fig. 16). After stripping the galvannealed coating using a 10% sulfuric acid solution, inductively coupled plasma (ICP) analysis confirmed the GDOES results concerning the iron content: 8.2 wt.% for 500°C, 11.3 wt.% for 510°C and 13.0 wt.%

for 520°C. The density of Fe-Zn intermetallics was as follows: for the GA 510°C 30 s – 65 g/m^2, for GA 520°C 30 s – 81 g/m^2.

Examples of SEM observations of galvannealed coating are shown in Fig. 17. Three layers of Fe-Zn intermetallics (i.e. Γ, δ and ζ) were observed, and X-ray diffraction confirmed the presence of these phases (Fig. 18).

USER PROPERTIES

Standard Tensile Tests

Standard subsized flat specimens (25 mm gauge length), with their axes in transverse and longitudinal to the rolling direction, were machined from galvanized and galvannealed coupons to evaluate their mechanical properties. Samples were cut away from the edges of the coupons to keep uniform microstructure. Tests were carried out at room temperature with a servo-hydraulic universal testing machine. The tests were done according to the ASTM E 8 standard at a constant crosshead rate of 1 mm/min. Instron Series IX software was used to control the machine, and to record and process data. Strain measurements were done up to the fracture by an extensometer attached to the sample.

The summary results on the HSLA steel samples are presented in Table 7. The results obtained on the samples in the uncoated, as-received condition are also included for comparison. Typical stress-strain curves are shown in Fig. 19. One can see that the target properties were retained after galvanizing and galvannealing. While the strength remained the same after both types of coating as in the as-received condition, the elongation seems to have increased. There could be two reasons for such an increase. First, the specimens with longer gauge length (80 mm) were tested in the as-received condition. Second, and probably the most likely reason: the as-received surface was very rough, while the surface defects, which might contribute to premature failure, were smoothed during pickling and coating procedures.

Dynamic Tensile Tests

Dynamic tensile tests were performed to assess crashworthiness. The tension experiments were conducted using the MTS hydraulic testing equipment for the quasi-static tests, whereas the Direct Split Hopkinson Pressure Bars set-up (McGill University, Montreal) was used for the high strain rate tests. The detailed results are reported in Appendices 4-6, while only a brief summary is given in this Section.

The schematics of the sample for dynamic tests, as well as a photograph of the actual samples before and after the tests, are shown in Fig. 20. Three strain rates were employed: 10^{-3} s^{-1} (quasi-static tests), 900 s^{-1}, and 1600 s^{-1}. The typical strain-stress curves are presented in Fig. 21, and the

summarized results of the dynamic tensile tests are presented in Tables 8 and 9. They indicate that there is an increase in stress at higher strain rates coupled with a small decrease in total elongation to failure. The energy absorbed at high strain rates is above that at a quasi-static rate, and is similar in the galvanized and galvannealed conditions. One can notice that, after the quasi-static tests, the UTS is comparable with the standard tensile tests, but the elongation is higher (see Table 8). An explanation for this could be the differences in geometry (length-to-width ratio) of the samples for the two types of tests.

Figures 22-24 present examples of fracture surfaces after the quasi-static and dynamic tests. Even though the fractured samples have somewhat different appearances on the macro-scale, the fracture surfaces are very similar on the micro-scale – it is a dimpled (ductile) fracture. The aforementioned Appendices 4-6 contain more examples.

Stretch-Flange Formability

Stretch-flange formability is an important property for press-forming of high strength steels. The objective of this task was to obtain a better understanding of the mechanisms that govern the fracture of the steels investigated. Press-formability of steel sheets is classified into four basic modes: stretch-flange formability, deep draw-ability, bulge-ability and bend-ability. Among them, stretch-flange formability is sometimes a critical property for avoiding fractures in actual parts. Stretch-flange formability tests were conducted on galvanized and galvannealed coupons at room temperature using conventional hole-punching (ISO/TS 16630:2003 standard). The schematic diagram of the test is shown in Fig. 25. First, a hole was punched in the center of the coupons. The punch and die diameters used for punching were 10.0 mm and 10.3 mm, respectively. The hole was then expanded using a conical punch until fracture occurred at the hole edge. The limiting hole expansion ratio was calculated as follows:

$$\lambda = \frac{D_h - D_o}{D_o} \times 100\%,$$

where D_o is the original hole diameter and D_h is the hole diameter after rupture (see Fig. 25).

Photographs of the test coupons are presented in Appendix 7. Table 10 gives the full numerical results of the tests of the HSLA coupons. After the tests, the hole diameters were measured at four points in each coupon, and the results were averaged. The hole expansion (stretch) ratio for galvanized HSLA steel was $\lambda = 67.4 \pm 5.2\%$, which is close to the $\lambda = 65$ reported in [12] for uncoated HSLA340 steel. At the same time, the hole expansion ratio for galvannealed HSLA samples was significantly lower at $\lambda = 34.7 \pm 2.5\%$. This is somewhat surprising since the standard tensile mechanical properties of the two coating conditions of this steel were very similar (see above).

Fractographic investigation of the tested coupons was undertaken in an attempt to uncover the reason for the difference between the behavior of the galvanized and galvannealed coupons during the stretch flanging tests. The formed specimens were characterized using scanning electron microscopy to reveal the influence of the microstructure on the initiation and propagation of cracks during stretch flanging.

For the galvanized coating condition, sample HSLA 32 (Fig. 26) was examined in great detail, and the results are presented in Figs. 27-32. The investigation revealed ductile fracture; in some places the crack followed carbide chains. The galvanized (zinc) coating mostly withstood the hole expansion test without cracking and/or delaminating, even in the most bent parts. Microcracks appeared in the coating only in the immediate vicinity of the main crack (see Figs. 28c and 29).

Galvannealed coupon HSLA GA-30 (Fig. 33) was examined in great detail, and the results are presented in Figs. 34-37. One can see that the fracture in this case appears much more brittle than in the case of the galvanized coupon. The galvannealed coating is cracked all over the bend parts, and the steel substrate is exposed in many places (see Fig. 35). The brittleness of the galvannealed coating may not be surprising since it consists mostly of Fe-Zn intermetallic phases, which are brittle by nature. However, it appears that the brittle coating also promotes brittle fracture in the steel substrate itself; this effect needs to be studied in more detail in future research.

DUAL-PHASE STEEL

OBTAINING THE STEEL SUBSTRATE

Organization B provided an Mn-Mo dual-phase (DP) steel grade. The composition, thickness and initial surface condition of this material, as well as the processing information provided by the supplier, are summarized in Tables 11 and 12.

Characterization of the As-Received Hot-rolled Dual-Phase Steel

Microstructure of the As-Received DP Steel

The as-rolled microstructure of the steel was characterized using the same techniques as described above for the HSLA steel. The microstructure of the as-received dual-phase steel was composed of equiaxed ferrite grains interspersed with pearlite and bainite islands (Figs. 38, 39). A few martensite grains were also observed (Fig. 39b). The center of the strip contained bands of martensite and pearlite grains (Figs. 38a, b and e). Figure 39c shows a detail of the pearlite structure in the banded region.

The DP steel was supplied in the unpickled condition. Examination of SEM cross-sections showed that the hot-rolled scale was thicker on one side (Fig. 40a) than on the other (Fig. 40b). The average scale thickness was 11.0 ± 1.4 μm on one side and 8.2 ± 1.4 μm on the opposite side. No internal oxidation was detected using SEM.

Typical inclusions observed on the as-received DP steel were elongated MnS up to 10 μm in length (Figs. 41a, b, f and g). Some MnS were associated with Al oxide inclusions (Figs. 41c-e and h-j).

Tensile Properties of the As-Received HSLA Steel

The tensile properties of the as-rolled steels were determined using flat tensile specimens with 80 mm gauge length and 20 mm gauge width using the same technique as described above for the HSLA steel.

The tensile test results are presented in Table 13. The tensile properties of the dual-phase steel in the as-received condition did not meet the target yield strength and ultimate tensile strength. The yield strength was about 30 MPa higher and the tensile strength 125 MPa lower than the target values proposed in Table 2. On the other hand, the elongation was quite high (30% instead of 20%). These discrepancies are due to the ferrite + pearlite microstructure of the as-received steel. There were no significant differences between the properties in the transverse and longitudinal direction for this grade. Stress-strain curves for the as-received hot-rolled dual-phase steel shows yield point elongation behavior (Fig. 42), which is not characteristic of dual-phase steels.

Dilatometer Trials of Dual-Phase Steel

Since the material received as dual-phase steel did not conformed to the dual-phase grade specifications, it was decided to perform simulated heat treatment trials in order to bring it to the required mechanical properties. This was to be achieved by a heat treatment that would transform the as-received ferrite + pearlite microstructure into the desired ferrite + martensite microstructure. A galvanizing schedule for the DP steel could then be designed to incorporate that heat treatment.

The fraction of austenite that formed during heating of the dual-phase steel was measured with a dilatometer BAËHR DIL 805 A/D. From 600 to 1050ºC, a heating rate of 2 K/s was selected to ensure that conditions close to equilibrium were obtained. Figure 43 is a plot of the measured fraction of austenite formed during heating versus temperature. A significant amount of austenite began to form at about 750ºC. Intercritical annealing at 820ºC produced about 50% austenite and complete austenitization was obtained at 920ºC. Figure 44 shows the fractions of austenite transformed during cooling of samples from different temperatures. Full results of the dilatometer trials are displayed in Table 14. The fraction of the martensite-austenite (MA) phase was determined using an automated image analysis of metallographic samples after the LePera etch (Fig. 45). One can see that the MA fraction was very low in the as-received condition (see the first line in Table 14). It was possible to find several schedules that increased the MA fraction and thereby improved the steel hardness (see Table 14). However, even though those heat treatments could be incorporated into the galvanizing schedule on the galvanizing simulator; they do not seem compatible with existing industrial galvanizing lines. Moreover, an additional hold at the galvanizing temperature of 460ºC seems to destroy the DP microstructure (see the last line in Table 14 and Fig. 45t). Therefore, after consultations with sponsors at the AISI Project Review Meeting held in Ottawa on February 8, 2007, it was decided to drop this steel grade from the test matrix.

TRIP STEEL

OBTAINING THE STEEL SUBSTRATE

Organization C provided an Al-based TRIP steel, which contains about 1.5% Mn, 1% Al, 0.2% C and very little Si. The exact composition and processing information are not reported here at the request of the supplier. The material was delivered in the form of pickled plates 2.6 mm thick. A piece of unpickled plated was also delivered at our request for the analysis of the oxide scale.

Characterization of the As-Received Hot-Rolled TRIP Steel

Microstructure of the As-Received TRIP Steel

The as-rolled microstructure of the steel was characterized using light optical and scanning electron microscopy techniques as described above for the HSLA and DP steels. The microstructure was examined on the cross-sections, and typical images are presented in Figs. 46-55.

Examination of the polished cross-sections (see Figs. 46, 47, 53) showed that the hot-rolled surface was rather rough and oxide scale on both sides was of uneven thickness – generally only a few microns. No internal oxidation was detected using SEM; EDS in SEM found only Fe and O in the surface oxide scale.

Examination of the microstructure of the Nital-etched cross-sections (see Figs. 48, 49) revealed mostly equiaxed ferrite grains interspersed with bainite islands. Microstructural banding is also apparent.

In the samples cut out of the unpickled piece (i.e. near the edge of the rolling strip), LePera etch revealed bands of MA (martensite-austenite) grains, mostly in the mid-section of the rolled plate (see Figs. 50, 51, 54). It is noteworthy that the LePera etch cannot distinguish between martensite and austenite, therefore the white (unetched) grains are commonly called MA phase. X-ray diffraction measurements have shown that there is only about 1.7 vol.% of retained austenite in these samples (the XRD technique is presented in Appendix 8). As such, the observed MA phase in the as-received sample is mostly martensite.

Almost no MA was observed in the middle of the rolling plate, where the microstructure is mostly ferrite-bainite (see Fig. 52). Apparently, the presence of martensite in the unpickled piece, which was cut near the end of the rolling strip, is due to a higher cooling rate after hot rolling in that region.

Typical inclusions observed on the as-received TRIP steel were extremely elongated manganese sulphites (see Figs. 53a, c, g). Some MnS inclusions were associated with aluminum oxide inclusions (see Fig. 54g) and, very occasionally, with complex inclusions containing Ti, C and P (see Figs. 53c and f). Also found were separate Al oxide and Al nitride inclusions (see Figs. 53a and g).

Tensile Properties of the As-Received TRIP Steel

The tensile properties of the TRIP steel were determined using the same techniques for sample preparation and testing as described above for the HSLA and DP steels. The tensile test results are presented in Table 15. A typical stress-strain curve is shown in Fig. 56. The properties of the heat-treated conditions also included in the table will be discussed in the next section. The tensile properties of the TRIP steel in the as-received condition did not meet the target yield strength and ultimate tensile strength (cf. with Table 2 above). Moreover, the mechanical properties of the as-received material are barely on the margins of what is expected from TRIP grades. One can notice that supplier's data on the strength of the steel (see row 1 of Table 15) are higher than those obtained at CANMET-MTL (rows 2 and 3). However, the supplier tested a single sample cut out near the edge of the strip (the same piece of material we examined in the unpickled condition), where there was significant amount of martensite (see above). Therefore, it shows a higher yield stress and lower strain hardening exponent. The samples tested at CANMET-MTL for the as-received condition were cut out of the middle of the plate where the microstructure was mostly ferrite-bainite.

HOT DIP GALVANIZING

Since the material received as TRIP steel did not conform to the TRIP grade specifications, it was decided to perform simulated heat treatment trials in order to increase its mechanical properties. A galvanizing schedule for the TRIP steel could then be designed to incorporate the optimal heat treatment regime found.

Dilatometer Trials of TRIP Steel

The fraction of austenite that forms during heating of TRIP steel was measured with a dilatometer BAËHR DIL 805 A/D. The dimensions of the sample used were 2.6 mm square by 10 mm in length. Between 600 and 1050ºC, a heating rate of 2 K/s was selected to ensure that conditions close to equilibrium were obtained. Figure 57 is a plot of the measured fraction of austenite formed during heating versus temperature for 2 tests. This shows an excellent reproducibility. Significant amounts of austenite start to form above 750ºC. Intercritical annealing at 850ºC produces about 50% austenite, and complete austenitization is obtained at 965ºC. Based on these results, the intercritical annealing temperature of 850ºC was chosen for the trial heat treatments.

The samples were then heat treated in the dilatometer according to the following regimes (Fig. 58):
HT1: heating at 10°C/s + 850°C x 120 s + cooling at 10°C/s + 460°C x 60 s + cooling at 10°C/s;
HT3: heating at 10°C/s + 850°C x 120 s + cooling at 10°C/s + 400°C x 60 s + heating at 10°C/s + 460°C x 60 s + cooling at 10°/s.

The microstructures of the samples were then examined using optical microscopy and XRD. The optical micrographs are presented in Figs. 59-62. One can see that numerous white grains (MA phase) appeared as a result of heat treatments, their volume fraction being significantly higher after the HT1 regime (see Figs. 59 and 60) than after the HT3 regime (see Figs. 61 and 62). The original microstructure of those samples corresponded to Fig. 52 with almost no MA phase. Since the amount of retained austenite was lower after HT3, it was decided not to work with that schedule any longer.

X-ray diffraction determined that the volume fraction of retained austenite was 19% after HT1 and 13% after HT3, indicating that the MA phase observed by optical metallography was actually austenite, not martensite.

Gleeble and Furnace Heat Treatments of TRIP Steel

Using the results of the dilatometer trials, larger samples were heat treated in the Gleeble 2000 simulator of thermo-mechanical processes. Figure 63 shows the sample dimensions and thermo-couple locations. The following heat treatment regimes were employed (Fig. 64):
HT1: heating at 9°C/s + 850°C x 120 s + cooling at 9°C/s + 460°C x 60 s + cooling at 9°C/s;
HT2: heating at 5°C/s + 850°C x 60 s + cooling at 9°C/s + 460°C x 60 s + cooling at 9°C/s,.

The heating and cooling rates were slightly lower in the Gleeble experiments than in the dilatometer trials (see above) since those rates could not be achieved for large samples in the Gleeble simulator.

The volume fraction of retained austenite determined by X-ray diffractometry was almost identical after both heat treatments – 12% after HT1 and 11% after HT3. Two reasons for the lower amounts of austenite measured in the Gleeble samples than in the dilatometer samples could be: 1) the statistical scatter, the heat treated microstructure is not uniform (see Figs. 59-62); and 2) the dilatometer heat treatment schedules were more precise and utilized faster cooling rates (compare Figs. 58 and 64).

The HT2 heat treatment regime, with the holding time of 1 min at 850°C, was eventually chosen to be incorporated in the galvanizing schedule since it reflects industrial practice better than 2-min holds in regime HT1. This schedule was also tried on samples of TRIP steel simulating large parts using furnace heating and sand-bath cooling. Figures 65 and 66 present optical microstructures of a 5 in-diameter tubes heat treated according to the HT2 regime. One can see that they are very similar to the microstructures produced during dilatometer trials (see Figs. 59 and 60). XRD has shown the amounts of retained austenite of 10% and 12% in the two tube samples examined – very close to the figures obtained on the Gleeble samples. Thus, this heat treatment can be reproduced on large parts.

Tensile Properties of Heat Treated TRIP Steel

Mechanical properties obtained during standard ASTM tensile tests are listed in Table 15 along with the properties for the as-received condition. The heat-treated samples were flat specimens (25-mm gage) cut from the center of the large strips used for Gleeble heat treatment simulations (see Fig. 63). A typical stress-strain curve for a heat treated TRIP sample is shown in Fig. 67. The tensile properties of the steel were similar after both heat treatment regimes, HT1 and HT2. The strength properties of the TRIP steel were still below the target values envisaged at the start of the project (see Table 2), apparently due to very low alloying of this particular grade – particularly very low Si content. However, in the heat treated conditions they were within characteristic TRIP range. Since no other hot-rolled material of the TRIP grade was available, it was decided to continue the work with this steel.

Galvanizing of TRIP Steel Coupons in the Galvanizing Simulator

Coupons 12 cm x 20 cm were machined with the long dimension parallel to the rolling direction (the same geometry as described above for the HSLA coupons). The coupons were degreased in a 2% NaOH solution, rinsed with water, and flash pickled at 21°C for 1 min using 210 g/L HCl and 1.78 g/L hexamethylene tetramine in deionized water.

The regimes used for galvanizing are listed in Table 16. They differ only in the galvanizing atmosphere while the thermal profile was the same; an example of the actual curve recorded by the thermocouple attached to the coupon is shown in Fig. 68. The thermal profile corresponded to previously established heat treatment schedule HT2 (see Fig. 64). Macro photographs of the galvanized TRIP coupons are presented in Figs. 69-72. One can notice a relatively large amount of bare spots on the galvanized coating, the reason for which has not yet been established.

USER PROPERTIES

Standard Tensile Tests

Standard subsized flat specimens (25 mm gauge length) with their axes in the transverse and longitudinal to the rolling direction were machined from galvanized and galvannealed coupons to evaluate the mechanical properties. Samples were removed away from the edges of the coupons to keep uniform microstructure. The tests were carried out at room temperature with a servo-hydraulic universal testing machine according to the ASTM E 8 standard, at a constant crosshead rate of 1 mm/min. Instron Series IX software was used to control the machine, and record and process the data. Strain measurements were done up to the fracture by an extensometer attached to the sample.

The summary results on the TRIP steel samples are presented in Table 15. One can see that the tensile properties after galvanizing were similar to those in the heat-treated conditions, confirming that galvanizing could follow heat treatment without deterioration of mechanical properties. Somewhat better plasticity obtained in the coated condition is probably due to the same reason mentioned above for the HSLA steel: i.e., the as-received surface of the steel was very rough, while the surface defects, which might contribute to premature failure, were smoothed during the pickling and coating procedures.

Dynamic Tensile Testing

Dynamic tensile tests were performed at McGill University in Montreal in the same way as described above for HSLA steel. The tension experiments were conducted using the MTS hydraulic testing equipment for the quasi-static tests, whereas the Direct Split Hopkinson Pressure Bars were used for the high strain rate tests. The detailed results are reported in Appendix 7, while only a brief summary is given in this Section.

The samples of the same shape and dimensions as the HSLA sample shown above in Fig. 20 were machined from TRIP steel. Due to time constrains to allow meeting the project deadline, coupons with simulated heat treatment HT2 rather than actual galvanized coupons were used. Three strain rates were employed: 10^{-3} s^{-1} (quasi-static tests), 900 s^{-1} and 1600 s^{-1}. The typical strain-stress curves are presented in Fig. 73, and the summarized results of the dynamic tensile tests are presented in Tables 17 and 18. They indicate an increase in stress at higher strain rates coupled with a small decrease in total elongation to failure. The increase in UTS at high strain rates is greater for the TRIP steel than for the HSLA steel (compare Tables 17, 18 with Tables 8, 9). The energy absorbed at high strain rates is above that at a quasi-static rate and is similar to the results obtained on the HSLA samples. One can notice that after the quasi-static tests, the UTS was comparable with the standard tensile tests, but elongation was higher (see Table 15). An explanation for this could be the same as for the similar effect observed on the HSLA samples, i.e. different geometry (length-to-width ratio) of the samples for the two types of tests.

Figures 74 and 75 present examples of fracture surfaces after the quasi-static and dynamic tests. The fractures were very similar after the quasi-static and dynamic tensile tests on both the microscale and microscale. The appearance of the fracture surface is different from that of the HSLA samples (see above) – on the microscale, there are apparent striations of the fracture surfaces (see Figs.74a, b and 75a, b). On the microscale, the fracture is non-uniform – dimples (ductile) areas are intermixed with more brittle regions (see Figs.74c, d and 75d, e).

Stretch-Flange Formability

Stretch-flange-formability was evaluated through hole-expansion tests using the same equipment and technique as described above for the HSLA steel, i.e. according to the ISO/TS 16630:2003 standard as shown in Fig. 25. The tests were conducted on coupons after simulated heat treatment in the McMaster Galvanizing Simulator according to the thermal profile shown above in Fig. 68. Table 19 gives the full numerical results of the tests of the TRIP coupons. The hole expansion (stretch) ratio for the TRIP steel was $\lambda = 24.7 \pm 3.4\%$, which is significantly lower than the ratio measured for the HSLA steel and is near the lower limit of what is expected for high-strength steels. It is generally known (see e.g. [14]) that TRIP steels show poor hole expandability even though they may exhibit high total elongation during tensile tests. Such a behavior is usually explained by the fact that homogeneous microstructure cannot be obtained in the process that produces the microstructure providing for the TRIP phenomenon.

CONCLUSIONS

1 The HSLA steel in this project was a grade with Ti, Nb and V precipitation-strengthening additions. In the as-received, hot-rolled condition its microstructure was composed of fine-grained ferrite interspersed with a few pearlite grains. The yield stress was 580-610 MPa, the UTS was 630-655 MPa, and the total elongation was about 20%.

2 After galvanizing and galvannealing, the mechanical properties of the HSLA steel remained the same as in the as-received condition. The galvanized samples exhibited yield stress of 590-610 MPa, UTS of 630-650 MPa and total elongation of 28-29%. The galvanized samples had a YS of 600-620 MPa, UTS of 635-650 MPa and total elongation of about 25%. The better plasticity of the coated samples was apparently due to the smoother surface.

3 Dynamic tensile tests performed to assess the crashworthiness of the HSLA steel indicated that there was an increase in stress at higher strain rates (UTS up to 740 MPa) coupled with a small decrease (of about one third) in the total elongation to failure. The energy absorbed at high strain rates was above that at a quasi-static rate, and was similar in the galvanized and galvannealed conditions.

4 Stretch-flange formability of the HSLA steel in the galvanized condition measured through the hole expansion tests was as expected from this steel grade; the hole expansion ratio was about 67%. In the galvannealed condition, however, the hole expansion ratio was lower – about 35%; the fractography showed that fracture was more brittle than with the galvanized coating.

5 The material received as a DP grade was an Mn-Mo steel. Microstructural studies showed that the as-received steel was composed of equiaxed ferrite grains interspersed with pearlite and bainite islands. There was almost no martensite in the as-received condition. The tensile properties of this steel in the as-received hot-rolled condition did not meet the target yield strength and ultimate tensile strength. The yield stress was measured to be about 390 MPa and UTS about 475 MPa.

6 Using trial heat treatments consisting of intercritical annealing followed by rapid cooling, it was possible to determine a schedule producing enough martensite in the microstructure of the DP steel (up to 7.5 vol.%) to increase hardness. However, that schedule would be difficult to implement in industrial galvanizing lines. Moreover, additional hold at a galvanizing temperature of 460°C destroyed the DP microstructure.

7 The TRIP steel examined in this project was an Al-base grade. Microstructural studies showed that there was very little retained austenite in the as-received condition, and the microstructure consisted mostly of ferrite and bainite. The tensile properties of this steel in the as-received hot-rolled condition did not meet the target yield strength and ultimate tensile strength: YS 400-445 MPa, UTS 570-595 MPa.

8 Heat treatment regimes were developed in order to produce enough austenite in the microstructure of the TRIP steel. The optimal schedule included intercritical annealing at 850°C followed by overaging at 460°C (galvanizing temperature). The tensile properties of the heat-treated samples relative to the as-received condition: YS 410-455 MPa, UTS 635-645 MPa, δ ~30%.

9 The developed heat treatment regime could be included in the galvanizing schedule of the TRIP steel. However, the quality of coating after galvanizing simulator trials was poor (unlike the HSLA steel). The tensile properties retained after galvanizing: YS 440-450 MPa, UTS ~635 MPa, δ ~ 30%.

10 Dynamic tensile tests of the TRIP samples indicated that there was an increase in stress at higher strain rates (UTS up to 750 MPa) coupled with a small decrease in total elongation to failure. The energy absorbed at high strain rates is above that at a quasi-static rate and is similar to the results obtained on the HSLA samples.

11 The hole expansion ratio for TRIP steel was about 25%, which is near the lower limit of what is expected for high-strength steels.

ACKNOWLEDGMENTS

The authors are grateful to David Ashe, Rino Canaj, Robert Eagleson, Mark LaRonde, Pei Liu and Russ Orr who helped with laboratory work at CANMET-MTL.

REFERENCES

[1] A. Gibson and R.L. Seufert, "Improving Properties of Cold Formable Galvanized Hot-rolled Strip – ZCO-21-1: Market and Application Review", (ILZRO Report, 1999).

[2] A. Marder, "Improving Properties of Cold Formable Galvanized Hot-rolled Strip – ZCO-21-2: Literature and Practice Review", (ILZRO Report, 1999).

[3] S. Dionne, B. Voyzelle, E. Essadiqi, J. McDermid and E. Baril, First Progress Report ZCO-21-3: "Galvanizing Simulator Trials" and ZCO-21-4: "User Properties Evaluation, MTL 2002-45(CF), August 2002.

[4] S. Dionne, B. Voyzelle, E. Essadiqi, J. McDermid and E. Baril, Second Progress Report ZCO-21-3: "Galvanizing Simulator Trials" and ZCO-21-4: "User Properties Evaluation, MTL 2003-12(CF), February 2003.

[5] S. Dionne, J.R. Brown, B. Voyzelle, E. Essadiqi, J. McDermid and E. Baril, Third Progress Report ZCO-21-3: "Galvanizing Simulator Trials" and ZCO-21-4: "User Properties Evaluation", MTL 2004-39(CF), September 2004.

[6] S. Dionne, B. Voyzelle, E. Essadiqi, J. McDermid and E. Baril, Fourth Progress Report ZCO-21-3: "Galvanizing Simulator Trials" and ZCO-21-4: "User Properties Evaluation", MTL 2004-50(CF), January 2005.

[7] S. Dionne, J.R. Brown, C. Bibby, E. Essadiqi, V.Y. Guertsman, J. Li, J. Neima, B. Voyzelle, J. McDermid and É. Baril, Final Report ZCO-21-3: "Galvanizing Simulator Trials" and ZCO-21-4: "User Properties Evaluation", MTL 2005-7(CF), April 2005.

[8] F.S. LePera, "Improved Etching Technique to Emphasize Martensite and Bainite in High-strength Dual-phase Steel", Journal of Metallography, (32), (1980), pp.380-39.

[9] S. Claessens et al., "Influence of Surface Composition and Morphology on the Galvanizing Behaviour of Hot-rolled Steel", Proc. 5th Int. Conf. on Zinc and Zinc Alloy Coated Steel Sheet (Galvatech 2001), Brussels, Belgium, Verlag-Stahleisen, Düsseldorf, Germany, 2001, p.631.

[10] L. Bordignon, "Galvanising of Hot-rolled Strip", Proc. 5th Int. Conf. on Zinc and Zinc Alloy Coated Steel Sheet (Galvatech 2001), Brussels, Belgium, Verlag-Stahleisen, Düsseldorf, Germany, 2001, p.19.

[11] ASTM A 90 / A 90M, "Standard Test Method for Weight [Mass] of Coating on Iron and Steel Articles with Zinc or Zinc-Alloy Coatings", ASTM International.

[12] X.M. Chen, P.M. McKune and D.G. Prince, Automotive applications of stretch flange high strength steel. – In: Innovations in Steel Sheet and Bar Products. SP-1764, SAE International, Warendale, PA, 2003, pp.77-505.

[13] K. Hasegawa, K. Kawamura, T. Urabe and Y. Hosoya, Effects of Microstructure on Stretch-Flange-Formability of Cold-Rolled Ultra High Strength Steels. – In: Proc. 45th MWSP Conference. MS&T 2003, Nov. 9-12, 2003, Chicago, IL. ISS and TMS Publ. Vol. XLI, p.495-505.

[14] IISI-AutoCo AHSS Guidelines - March 2004, p. 3.5 (www.ulsab.org/AHSSGuidelinesDocs/3_5_AHSS_Flanging.pdf)

Table 1 – Project Tasks

Task/Sub-Task	Description
A	Galvanizing Simulator Trials
A.1.	Obtaining the Steels
A.2.	Hot Dip Galvanizing
A.3.	Galvannealing
B.	Formability Evaluation
B.1.	Stretch-Flange-Formability
B.2.	Tube Welding
B.3.	Hydroforming Characteristics
C.	User Properties
C.1.	Fatigue
C.2.	Dynamic Tensile Testing
D.	Reporting

Table 2 – Target Composition and Properties of High Strength Hot-rolled Steels for TRP 9946.

Type	Target Composition (wt.%)						Target Properties		
	C	Si	Mn	Nb	Ti	Other	Yield Strength (MPa)	Tensile Strength (MPa)	Total Elongation (%)
HSLA	0.08	0.01	0.54	0.04	0.05	-	570	620	23
Alternative HSLA grades	0.06-0.08	0.01-0.14	0.5-1.4	Precipitation strengthening based on Ti, Nb and/or V					
TRIP	0.18	1.5	1.4	0.025	0.005	-	500	900	20
Alternative TRIP grades	0.1-0.2	0.5-1.5	<1.5	0.05 to 1.0 Al (depending on Si content) Nb and/or P to obtain desired strength level					
DP	0.08	<0.3	1.5	0.03	0.002	0.25 Mo, 0.5 Cr	350	600	20
Alternative DP grades	<0.1		1.6-2.0	Nb, Cr and/or Mo additions					

Table 3 - Coil Data Provided by the Supplier of the Hot-rolled HSLA Steel.

Coil Id.	Heat Number	Surface Condition	Nominal Coil Width (m)	Nominal Thickness (mm)	Mechanical Properties *		
					Yield Strength (MPa)	Tensile Strength (MPa)	Elongation (%)
HSM 00521698	77132D	Pickled and oiled	1.17	2.6	618	631	26

* Tail end sample testing performed by supplier.

Table 4 – Hot Mill Process Control Data for Heat 77132D.

	Roughmill Exit Temp. (°C)	Finishing Mill Exit Temp. (°C)	Intermediate Temp. (°C)	Coiling Temp. (°C)
Aim	1079	889	655	635
Head	1073	902	672	672
Body	1056	897	-	-
Tail	-	-	633	619
Average	-	886	645	612

Table 5 – Composition of the Hot-rolled HSLA Steel.
(Optical Emission Spectroscopy and Leco C, S, O and N Analysis).

Element	Concentration (wt.%)
Boron	<0.0005
Carbon	0.065
Nitrogen	0.0057
Oxygen	0.0016
Aluminum	0.035
Silicon	0.076
Phosphorus	0.009
Sulfur	0.005
Calcium	0.0033
Titanium	0.014

Element	Concentration (wt.%)
Vanadium	0.064
Chromium	0.034
Manganese	1.35
Iron	balance
Nickel	0.015
Copper	0.022
Niobium	0.052
Molybdenum	0.004
Tin	0.005
Vanadium	0.064

Table 6 - Tensile Properties of the As-received Hot-rolled HSLA Steel
(flat specimens with 80 mm gauge length).

Steel Grade	Orientation	Stress at 0.2% Offset (MPa)	Ultimate Tensile Stress (MPa)	Total Elongation (%)	*n*	r at ε = 0.10
HSLA	Transverse	613±12	654±13	19±1	0.07	0.68
	Longitudinal	580±5	633±2	22±1	0.09	0.59

Table 7 – Tensile Properties of the HSLA Steel in Different Conditions.

Condition	Orientation	Stress at 0.2% Offset (MPa)	Ultimate Tensile Stress (MPa)	Total Elongation (%)	Reduction in Area (%)	Strain hardening *n*
As-received (hot-rolled)	Transverse	613±12	654±13	19±1		0.07
	Longitudinal	580±5	633±2	22±1		0.09
Galvanized	Transverse	608±8	647±2	28±1	54±2	0.07
	Longitudinal	590±5	632±1	29±1	61±1	0.08
Galvannealed	Transverse	616±4	646±1	25±1	55±5	0.07
	Longitudinal	598±9	635±3	26±1	54±1	0.07

Table 8 – Summary Results of Dynamic Tensile Tests of the HSLA Steel in Different conditions.

Strain Rate	UTS (MPa)	Total Elongation (%)
HSLA Galvanized		
10^{-3} s^{-1}	638	36
900 s^{-1}	698	27
1600 s^{-1}	740	26
HSLA Galvannealed		
10^{-3} s^{-1}	658	37
900 s^{-1}	735	27
1600 s^{-1}	735	28

Table 9 – Energy Absorbed During Dynamic Tensile Tests of the HSLA Samples.

	Galvanized (N/m^2)			Galvannealed (N/m^2)		
Strain Rate	at 10% strain	at 15% strain	at 20% strain	at 10% strain	at 15% strain	at 20% strain
10^{-3} s^{-1}	59.3	90.6	123	61.2	94.5	127
900 s^{-1}	70.2	105	138	71.5	108	143
1600 s^{-1}	72.3	108	140	70.9	107	142

Table 10 – Results of the Hole Expansion Tests of HSLA Coupons
(all dimensions – in mm).

Galvanized Coupons

Sample Number	Dia.-Org., D_o	Diameter – Final, D_h				Average D_h	Stretch, λ %
HSLA 25	10.0965	17.6276	17.7292	17.7038	17.6911	17.6879	75.2
HSLA 36	10.0965	16.4719	16.4338	16.4592	16.4465	16.4529	63.0
HSLA 41	10.0965	17.3609	17.3482	17.3736	17.3609	17.3609	71.9
HSLA 60	10.0965	16.7005	16.6624	16.6751	16.6878	16.6815	65.2
HSLA 46	10.0838	16.3449	16.2941	16.3195	16.3068	16.3163	61.8
HSLA 32	10.0838	16.8656	16.9037	16.8783	16.8910	16.8847	67.4
					Avg.	**16.8974**	**67.4**
					St.Dev.	**0.5333**	**5.2**

Galvannealed Coupons

Sample Number	Dia.-Org., D_o	Diameter - Final, D_h				Average D_h	Stretch, λ %
HSLA GA 30	10.0711	13.8176	13.7795	13.8049	13.8303	13.8081	37.1
HSLA GA 33	10.0711	13.3604	13.3858	13.3477	13.3858	13.3699	32.8
HSLA GA 35	10.0838	13.5001	13.4366	13.5001	13.4874	13.4811	33.7
HSLA GA 36	10.0838	13.8684	13.8557	13.8938	13.8811	13.8748	37.6
HSLA GA 37	10.0711	13.3477	13.2969	13.3731	13.3096	13.3318	32.4
					Avg.	**13.5731**	**34.7**
					St.Dev.	**0.2521**	**2.5**

Table 11 - Hot Strip Mill Processing Data Provided by the Supplier
of the Hot-rolled Dual-phase Steel
(preliminary unpickled material supplied to CANMET-MTL in January 2006).

Hot Mill Id.	Coiling Temp. (°C)	Finishing Temp. (°C)	Furnace Residence Time (h)	Surface Condition	Nominal Coil Width (m)	Nominal Thickness (mm)
4042-100605	640	895	21.0-21.3 *	Unpickled	1.6	2.9

* The supplier indicated that the furnace residence times for these coils were extremely long, possibly due to a line downturn. Normally, the residence times are on the order of 1-10 h.

Table 12 – Composition of the Hot-rolled Dual-phase Steel
(Optical Emission Spectroscopy and Leco C, S, O and N Analysis).

Element	Concentration (wt.%)
Boron	<0.0003
Carbon	0.062
Nitrogen	0.0071
Oxygen	0.0037
Aluminum	0.046, 0.054
Silicon	0.036, 0.039
Phosphorus	0.0097
Sulfur	0.0039
Calcium	<0.001
Titanium	0.0032
Vanadium	0.003
Chromium	0.037, 0.037
Manganese	1.62, 1.66
Iron	balance
Nickel	0.018, 0.025
Copper	0.028, 0.031
Niobium	<0.003
Molybdenum	0.16, 0.17
Tin	0.0015

Table 13 – Tensile Properties of Hot-rolled Dual-Phase Steel in the As-received Condition (flat specimens with 80 mm gauge length).

Steel Grade	Orientation	Stress at 0.2% Offset (MPa)	Ultimate Tensile Stress (MPa)	Total Elongation (%)	n	r at ε = 0.10
DP	Transverse	393±4	476±1	31±2	0.15	0.77
	Longitudinal	386±9	476±4	30±2	0.14	0.66

Table 14 – Results of Heat Treatment Schedules for Dual-phase Steel Simulated Using A Dilatometer

Sample Id.	Schedule	T_{START} (°C)	T_{FINISH} (°C)	Volume % MA	Vickers Hardness
Hot-rolled	-	-	-	<2	148±13
DP214	776°C/1 min + 10°C/s	717	615	5.9±0.2	160±2
DP450	776°C/2 min + 25°C/s	689	458	5.1±0.4	174±3
DP440	776°C/5 min + 25°C/s	674	433	7.4±0.6	179±2
DP215	795°C/1 min + 10°C/s	718	460	5.4±0.3	158±12
DP216	820°C/1 min + 10°C/s	755	450	3.7±0.2	153±3
DP246	820°C/2 min + 10°C/s	755	490	4.4±0.4	153±1
DP249	820°C/1 min + 25°C/s	744	481	4.7±0.4	169±4
DP248	820°C/2 min + 25°C/s	749	473	5.8±0.4	168±3
DP252	950°C/5 min + 10°C/s	736	453	6.4±0.5	158±2
DP253	950°C/5 min + 25°C/s	716	490	4.8±0.3	177±2
DP255	950°C/5 min + 50°C/s	761	481	4.6±0.3	201±2
DP438	950°C/5 min + 50°C/s	688	438	4.4±0.3	188±1
DP254	820°C/2 min + 10°C/s + 460°C/1 min	760	506	0.8±0.1	153±1

Table 15 – Tensile Properties of Hot-rolled TRIP Steel in the As-received and Heat-Treated Conditions.

Condition	Orientation	Stress at 0.2% Offset (MPa)	Ultimate Tensile Stress (MPa)	Total Elongation (%)	Reduction of Area (%)	Strain hardening *n*
Supplier's data	unknown	478	631	27		0.15
As-received (hot-rolled)	Transverse	446±2	595±1	30±1	50±1	0.16±0.01
	Longitudinal	398±18	569±20	36±3	65±4	0.18±0.01
HT1: 850°C×2min + 460°C×1min	Transverse	436±5	646±4	32±1	50±3	0.20±0.01
	Longitudinal	407±4	643±3	31±1	47±2	0.21±0.01
HT2 850°C×1min + 460°C×1min	Transverse	453±8	642±3	30±1	49±1	0.19±0.01
	Longitudinal	417±5	634±1	29±1	45±2	0.20±0.01
Galvanized	Transverse	450±4	634±6	32±1	44±0	0.19±0.01
	Longitudinal	442±5	634±1	34±1	56±4	0.19±0.01

Table 16 – Galvanizing Parameters Tested for TRIP steel

Schedule	Atmosphere		Heating Rate	Intercritical Anneal		Cooling Rate	Overaging		Zn Bath Temp.	Dipping Time	Effective Al
	Dew Point	% H2		Temp.	Time		Temp.	Time			
TRIP-GI01	-30°C	5%	5°C/s	850°C	60s	9°C/s	460°C	60 s	460°C	4 s	0.20%
TRIP-GI02	-30°C	20%	5°C/s	850°C	60s	9°C/s	460°C	60 s	460°C	4 s	0.20%
TRIP-GI03	-40°C	20%	5°C/s	850°C	60s	9°C/s	460°C	60 s	460°C	4 s	0.20%
TRIP-GI04	5°C	20%	5°C/s	850°C	60s	9°C/s	460°C	60 s	460°C	4 s	0.20%

Table 17 – Summary Results of Dynamic Tensile Tests of TRIP Steel

Strain Rate	UTS (MPa)	Total Elongation (%)
10^{-3} s^{-1}	635	43
900 s^{-1}	720	26
1600 s^{-1}	750	36

Table 18 – Energy Absorbed During Dynamic Tensile Tests of the TRIP Samples

Strain Rate	at 10 % strain	at 15 % strain	at 20 % strain
10^{-3} s^{-1}	49	78	109
900 s^{-1}	66	102	139
1600 s^{-1}	71	108	145

Table 19 – Results of the Hole Expansion Tests of TRIP Coupons.

Sample Number	Dia.-Org., D_o	Diameter - Final, D_h				Average D_h	Stretch, λ %
TRIP-A1	10.08	12.51	12.47	12.55	12.56	12.51	24.1
TRIP-A2	10.08	12.94	12.91	12.98	12.97	12.94	28.4
TRIP-A3	10.08	12.43	12.41	12.44	12.47	12.43	23.3
TRIP-A4	10.08	12.64	12.63	12.62	12.64	12.63	25.3
TRIP-A5	10.08	11.98	12.02	12.01	11.96	12.00	19.1
TRIP-A6	10.08	12.89	12.93	12.90	12.95	12.91	28.0
					Avg.	**12.57**	**24.7**
					St.Dev.	**0.35**	**3.4**

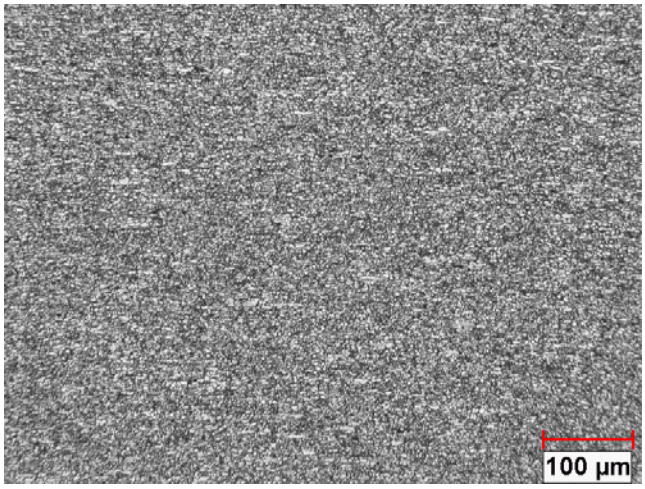

(a) Transverse section.

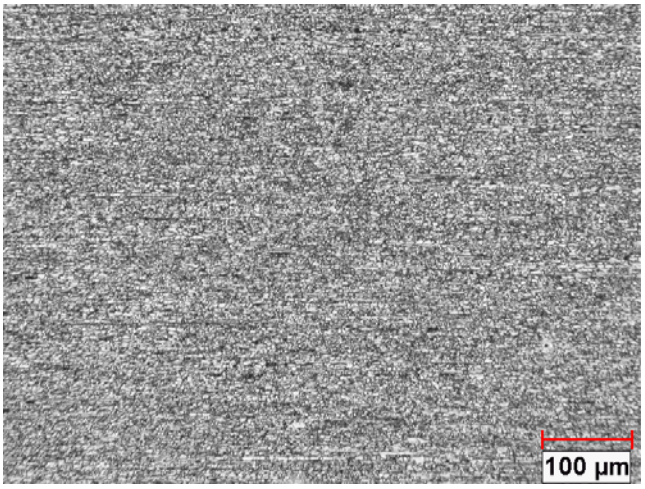

(b) Longitudinal section.

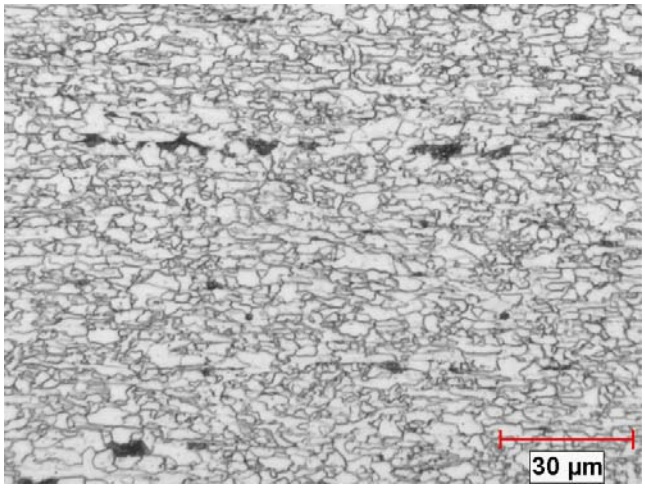

(c) Detail of transverse section.

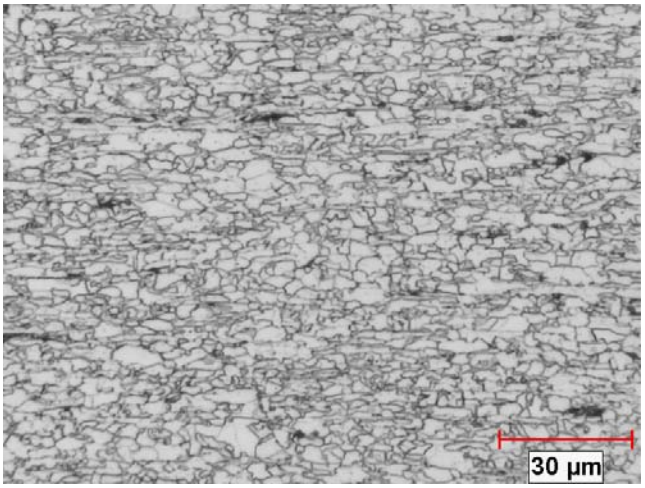

(d) Detail of longitudinal section.

Fig. 1 – Optical micrographs of Nital-etched metallographic cross-sections of the as-received hot-rolled HSLA steel.

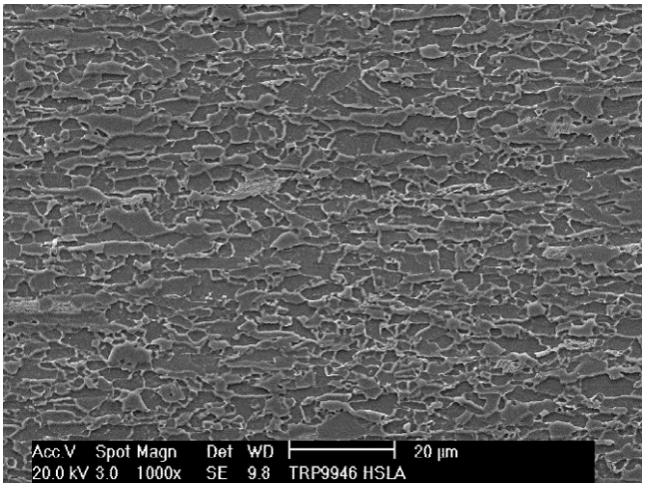

(a) The microstructure is composed mainly of ferrite grains.

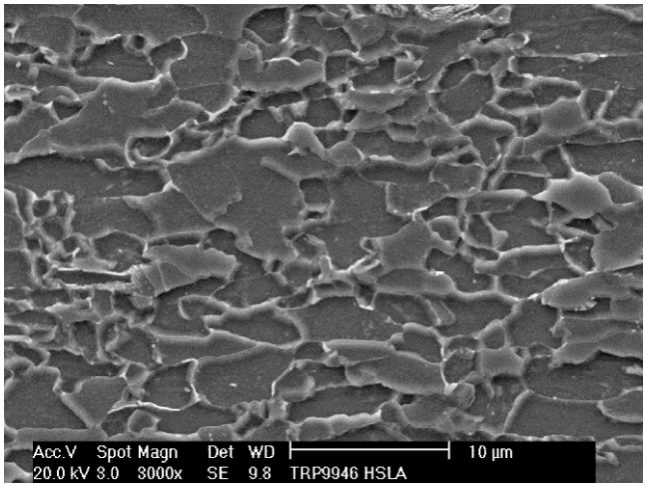

(b) Detail showing fine ferrite grain structure.

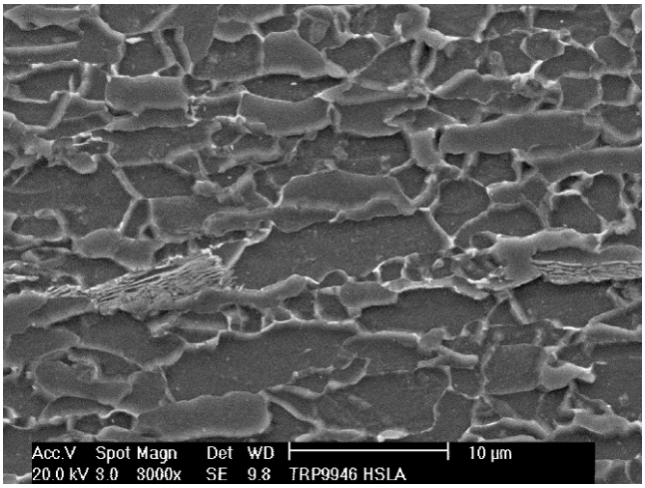

(c) Detail showing sporadic pearlite islands.

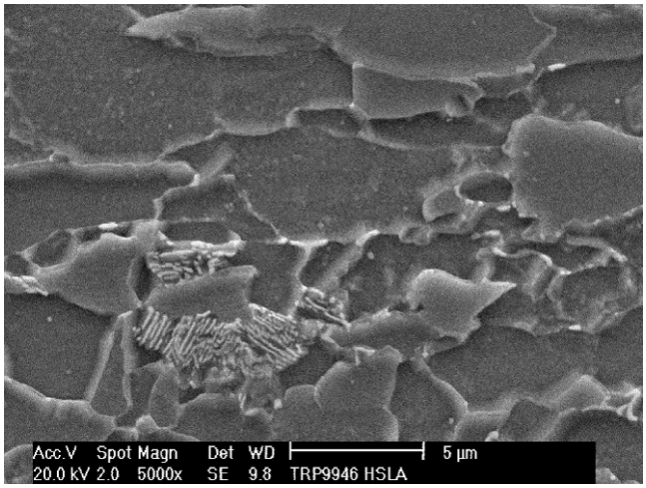

(d) Fine pearlite lamellae and small grain boundary carbides are visible at higher magnification.

Fig. 2 – Scanning electron micrographs of a Nital-etched transverse cross-section of the as-received hot-rolled HSLA steel.

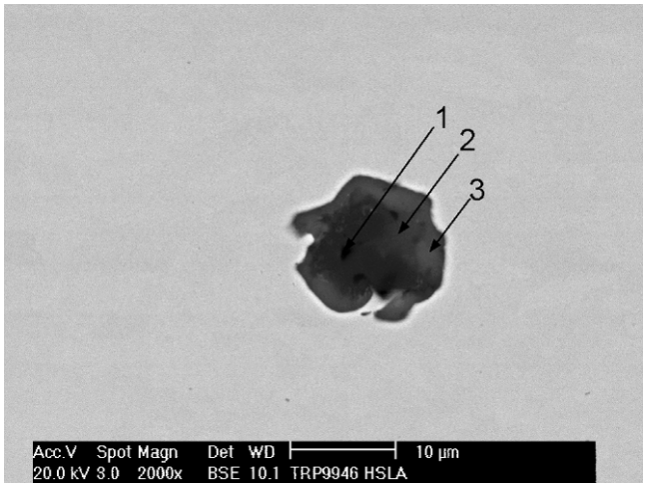

(a) Back scattered electron (BSE) micrograph of a large complex oxide (spots 1 and 2) and sulfide (spot 3) inclusion.

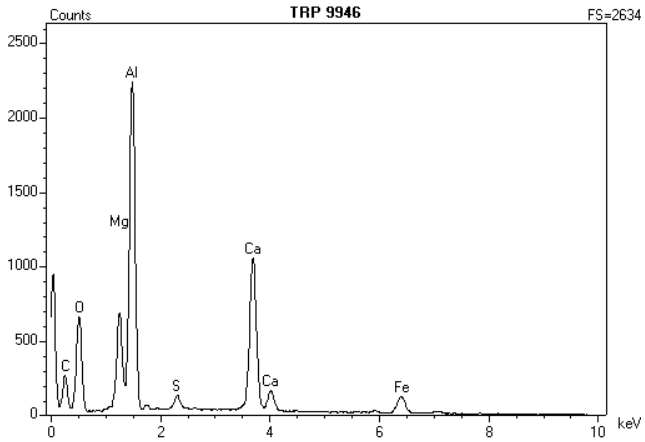

(b) EDS spectrum obtained from spot 1 on (a).

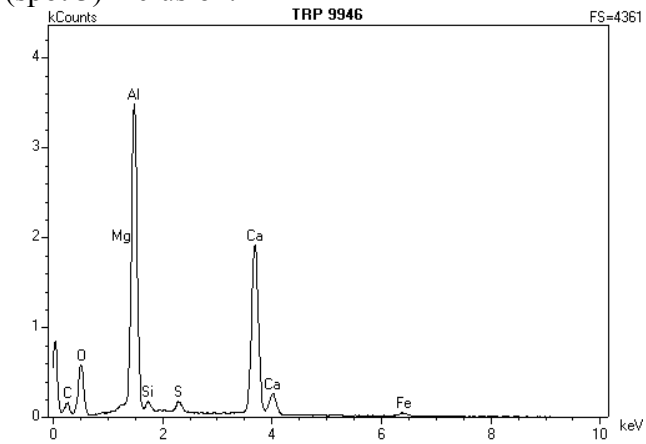

(c) EDS spectrum obtained from spot 2 on (a).

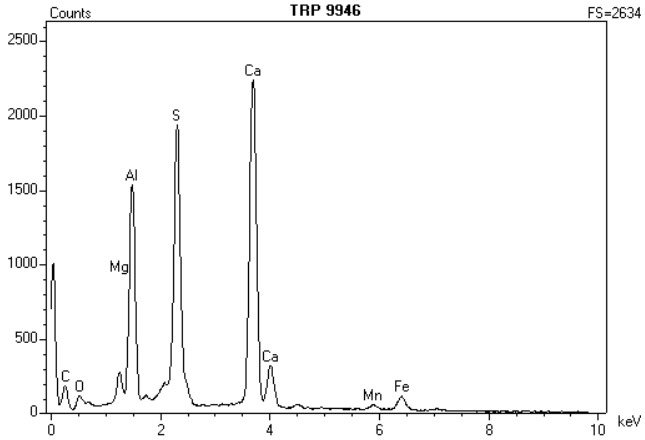

(d) EDS spectrum obtained from spot 3 on (a).

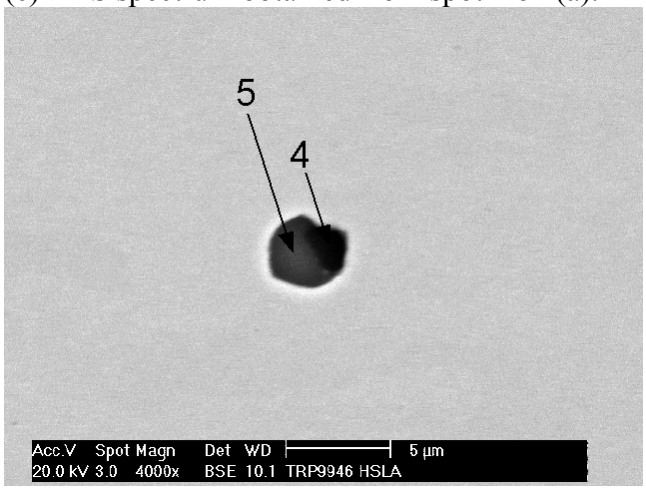

(e) BSE image of a complex mixed oxide (spot 4) and sulfide (spot 5) inclusion.

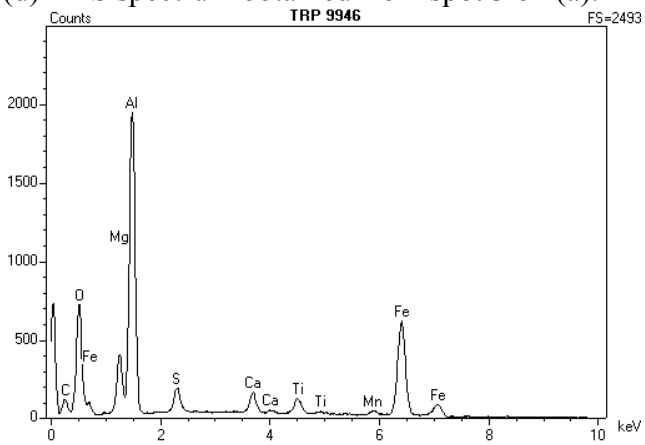

(f) EDS spectrum obtained from spot 4 on (e).

Fig. 3 – Scanning electron micrographs and EDS spectra of typical inclusions on an as-polished longitudinal cross-section of the as-received hot-rolled HSLA steel.

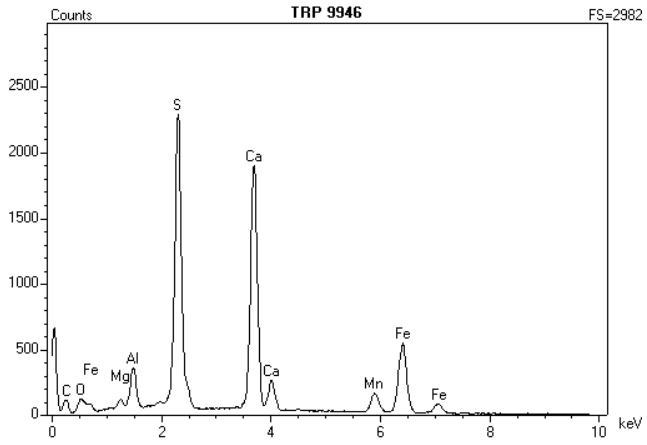

(g) EDS spectrum obtained from spot 5 on (e).

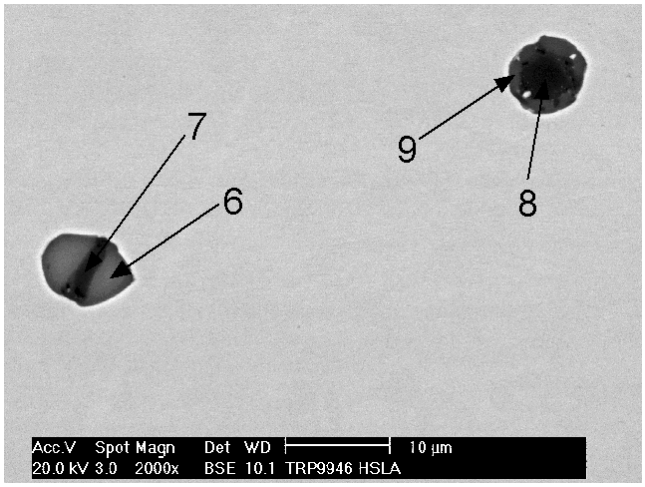

(h) BSE image showing two complex inclusions.

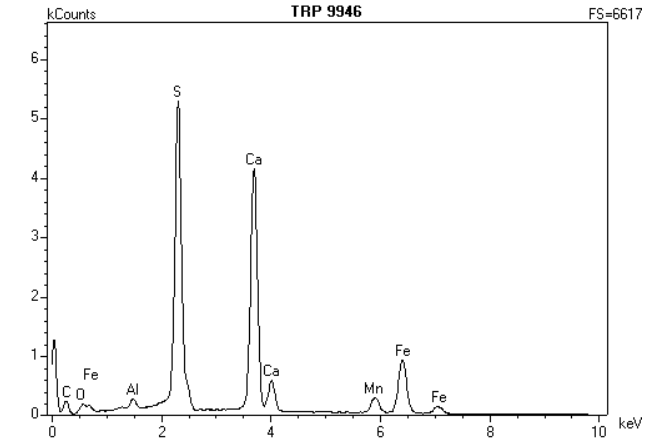

(i) EDS spectrum obtained from spot 6 on (h).

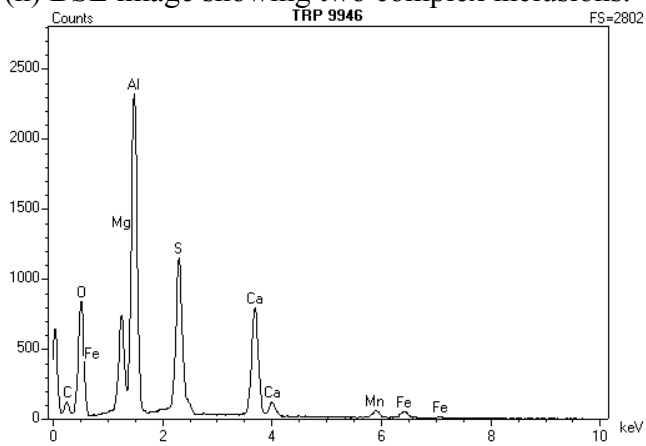

(j) EDS spectrum obtained from spot 7 on (h).

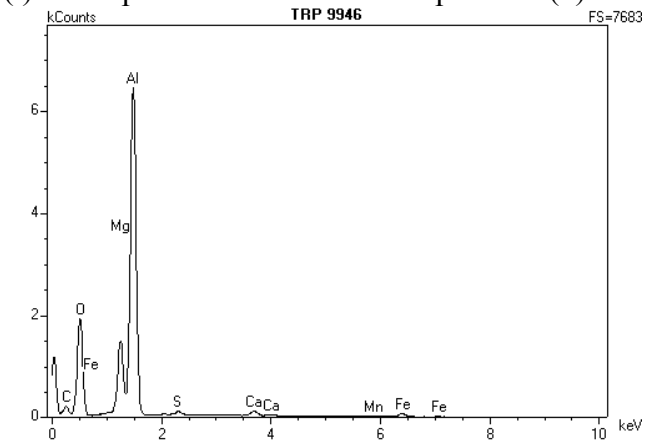

(k) EDS spectrum obtained from spot 8 on (h).

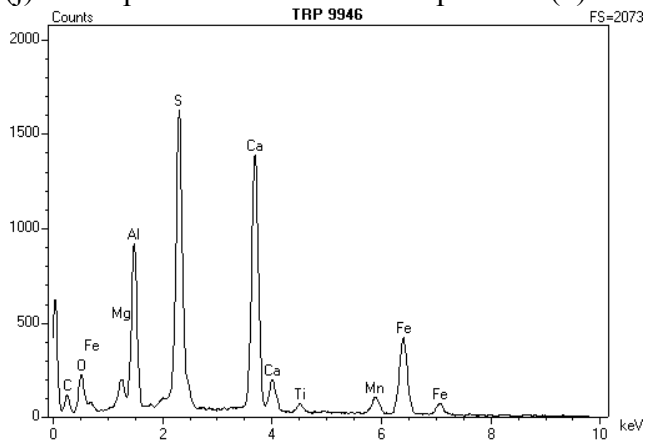

(l) EDS spectrum obtained from spot 9 on (h).

Fig. 3 – Scanning electron micrographs and EDS spectra of typical inclusions on an as-polished longitudinal cross-section of the as-received hot-rolled HSLA steel (continued).

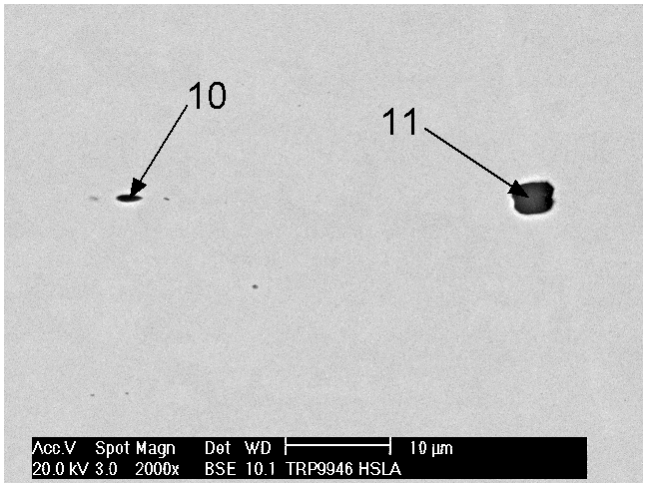

(m) BSE image showing two smaller inclusions.

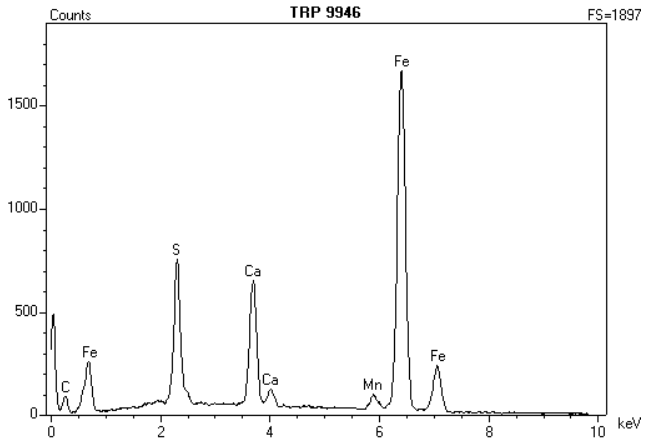

(n) EDS spectrum obtained from spot 10 on (m).

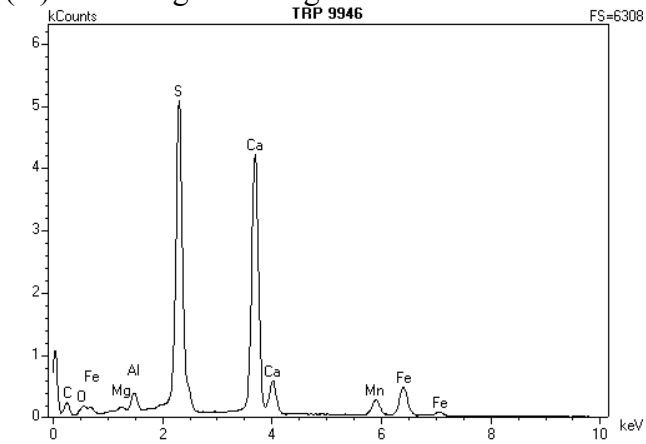

(o) EDS spectrum obtained from spot 11 on (m).

Fig. 3 – Scanning electron micrographs and EDS spectra of typical inclusions on an as-polished longitudinal cross-section of the as-received hot-rolled HSLA steel (continued).

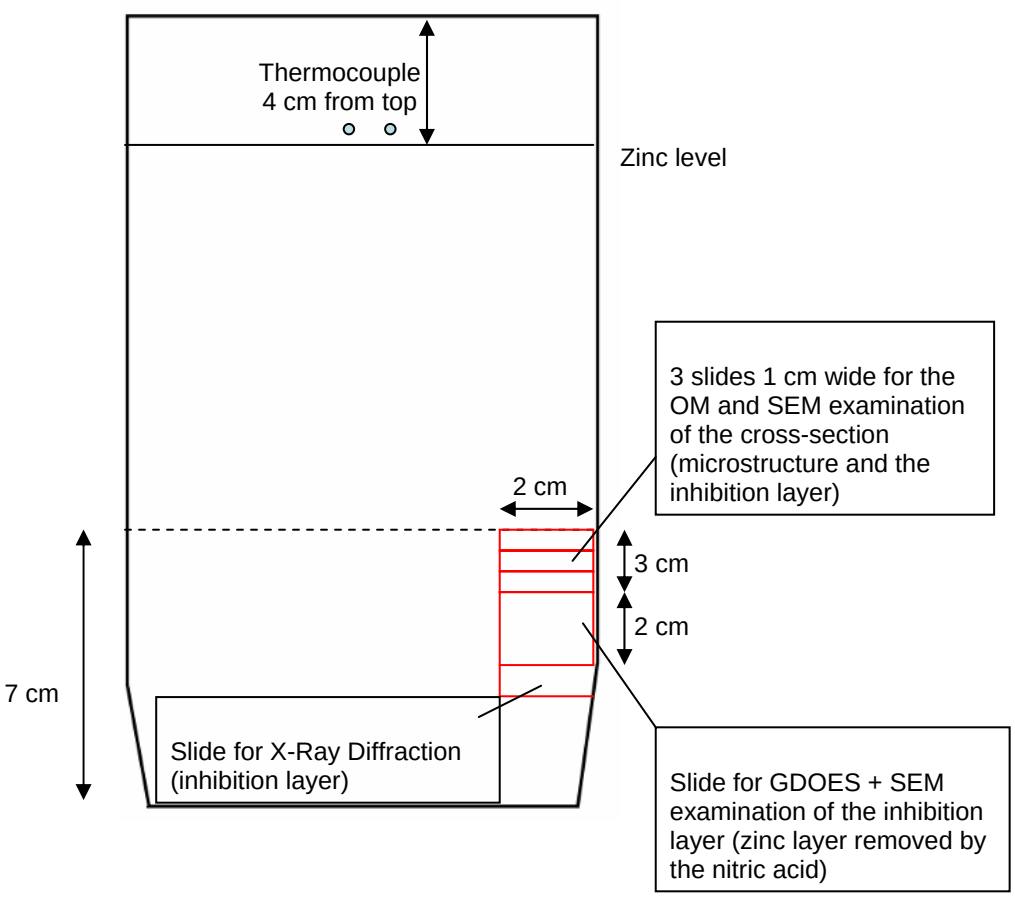

Fig. 4 – Coupon pattern for galvanized coupons. Side 1 was defined as the side to which the thermo-couple was attached, the opposite was Side 2.

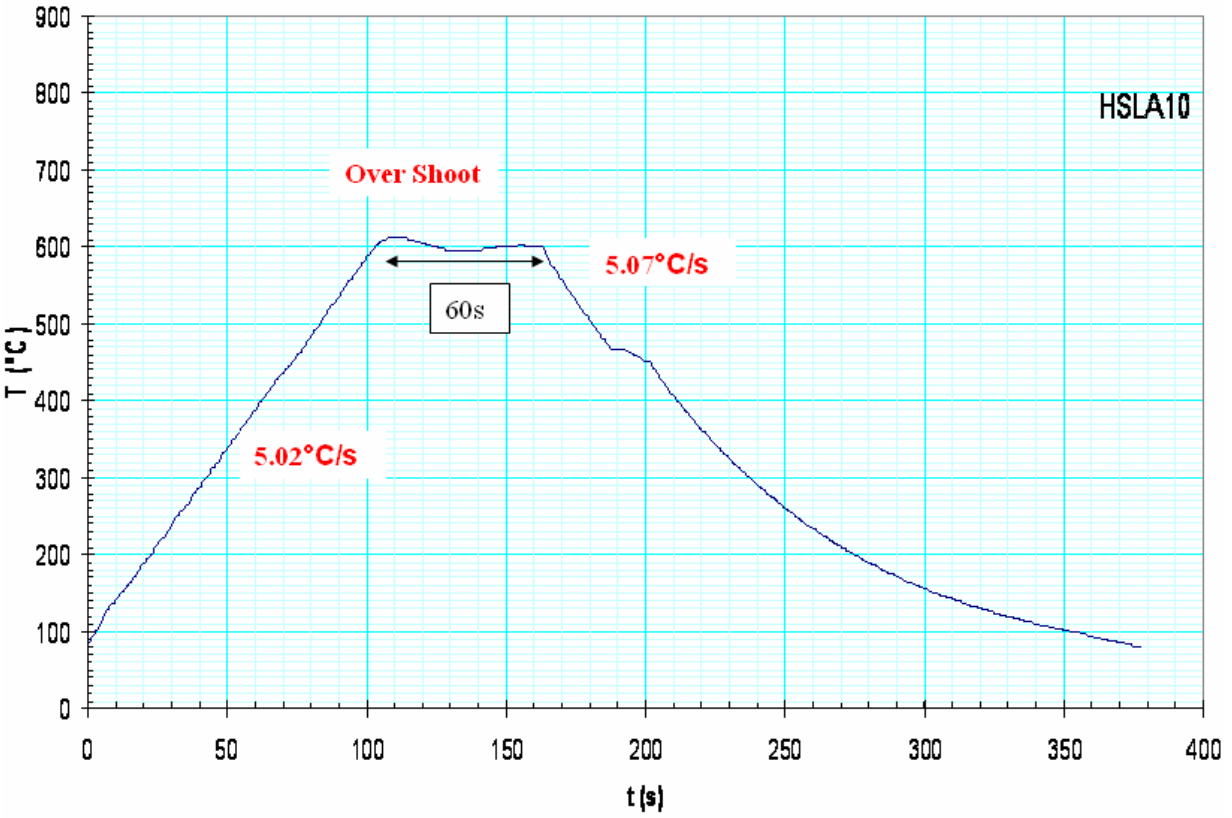

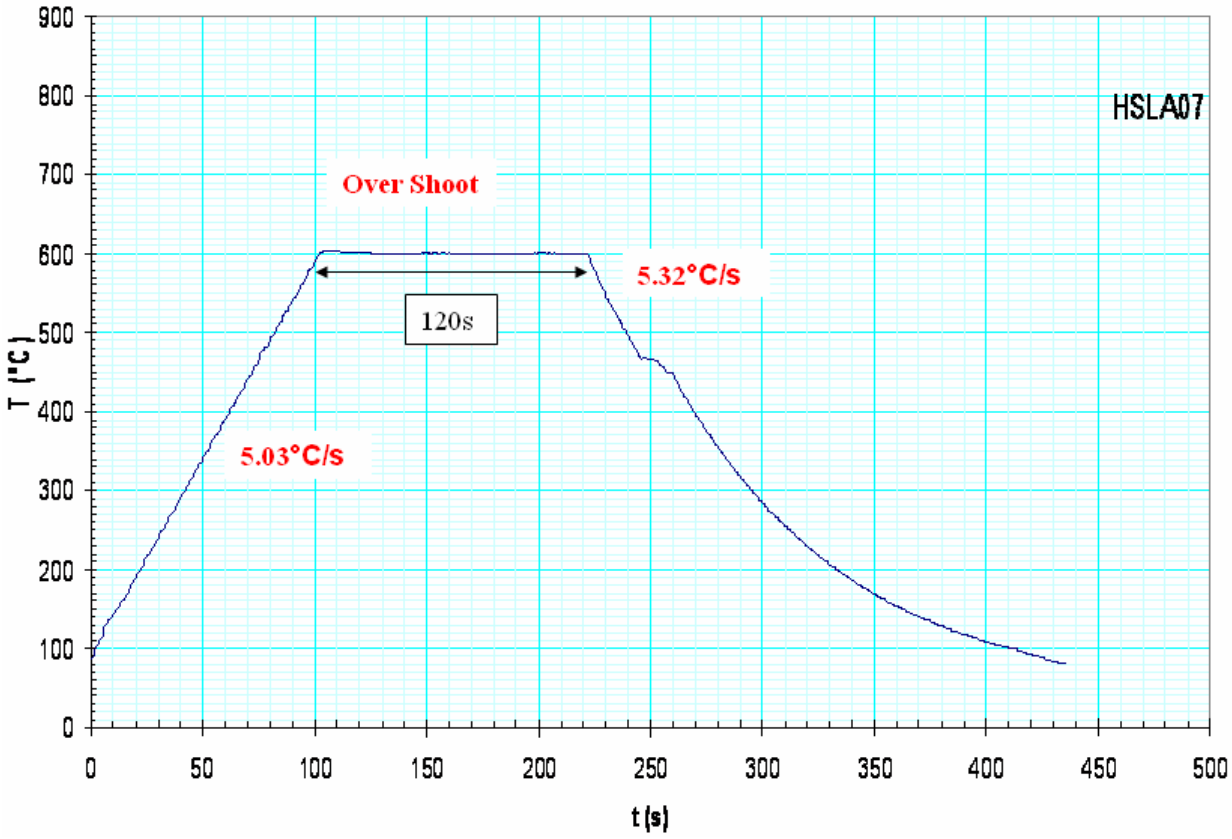

Fig. 5 – Thermal cycles for HSLA coupons (temperature vs. time plots).

Fig. 6 – Examples of galvanized coupons.

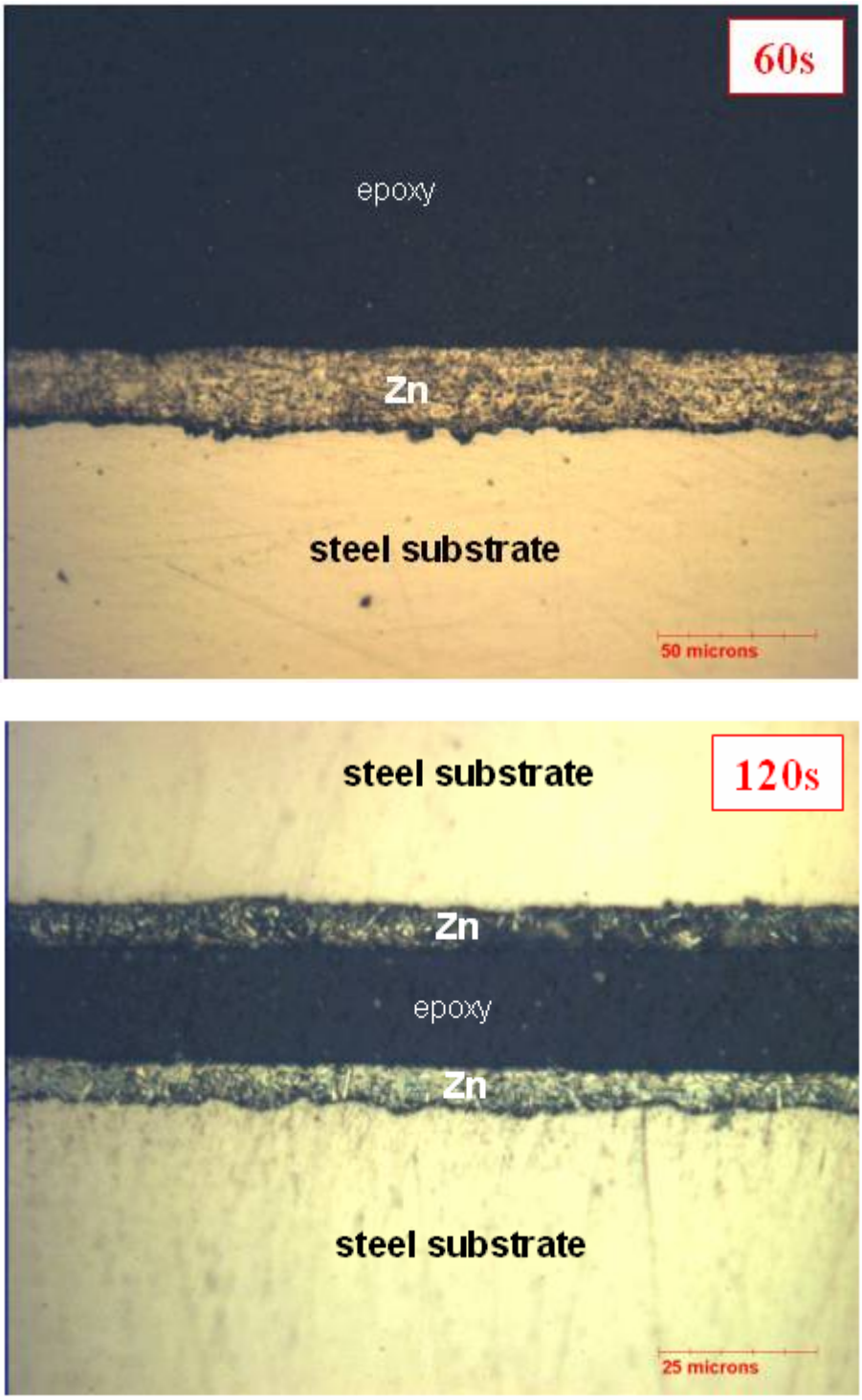

Fig. 7 – Examples of cross-sections of galvanized coupons (optical microscopy).

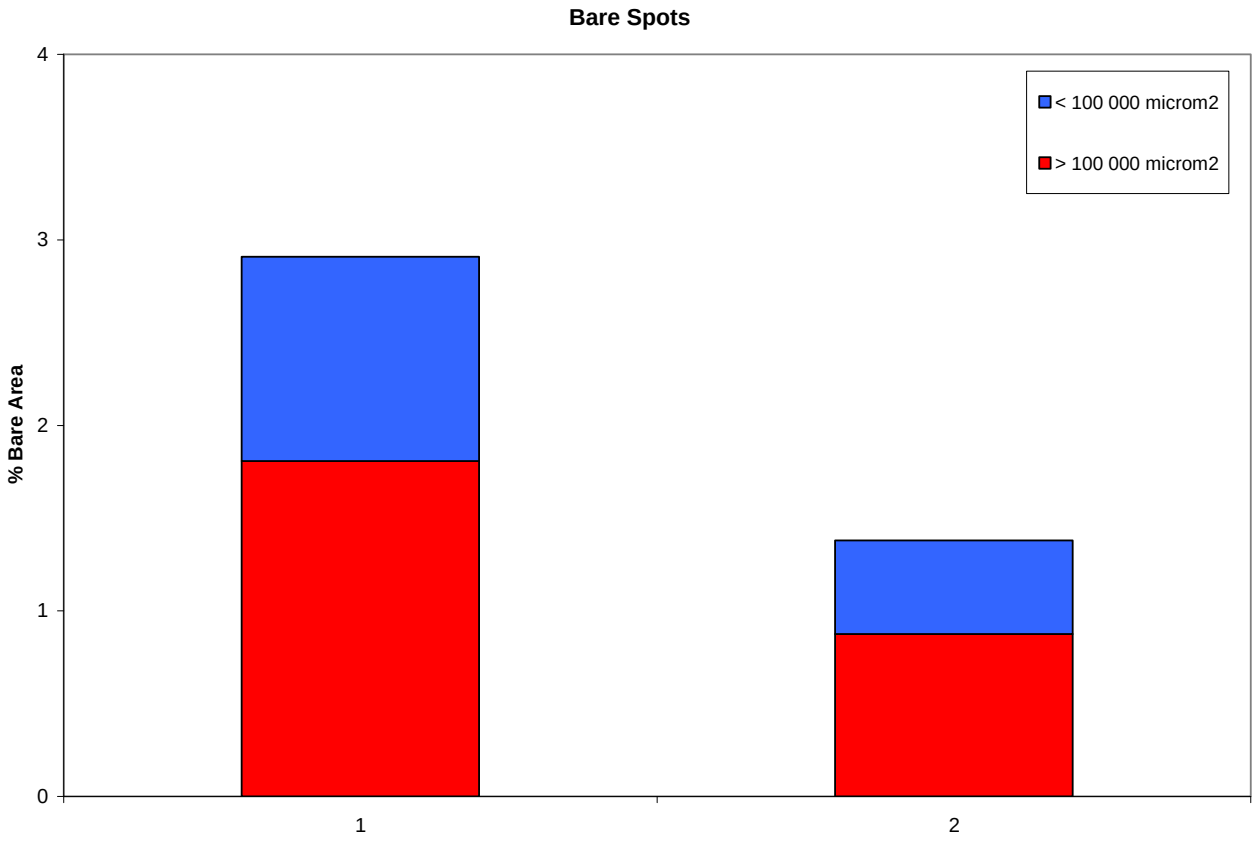

Fig. 8 – Proportions of the bare spot areas in the HSLA samples after 60 s (1) and 120 s (2) hold times.

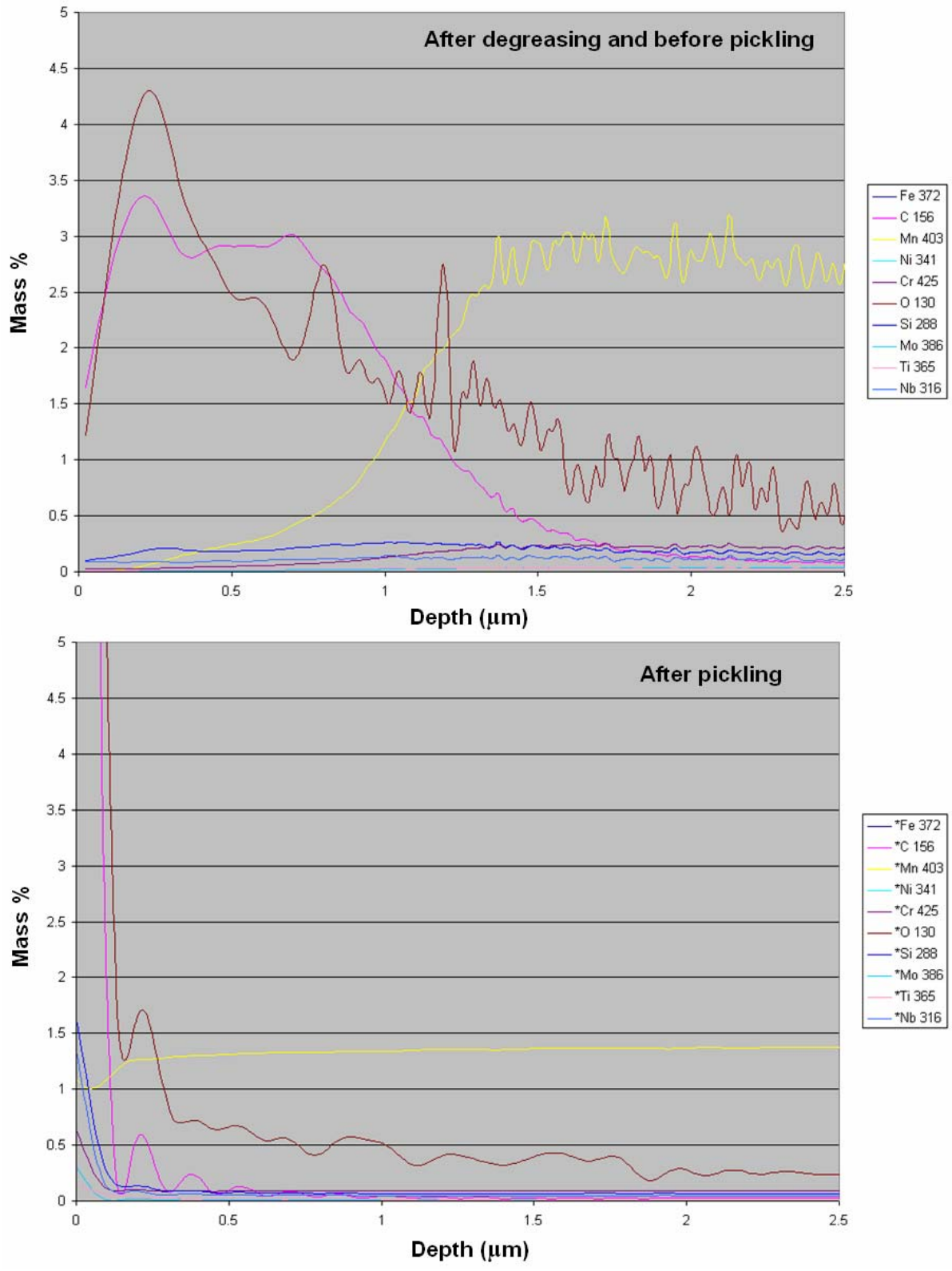

Fig. 9 – GDOES depth profiles obtained from selected galvanized hot-rolled HSLA steel coupons.

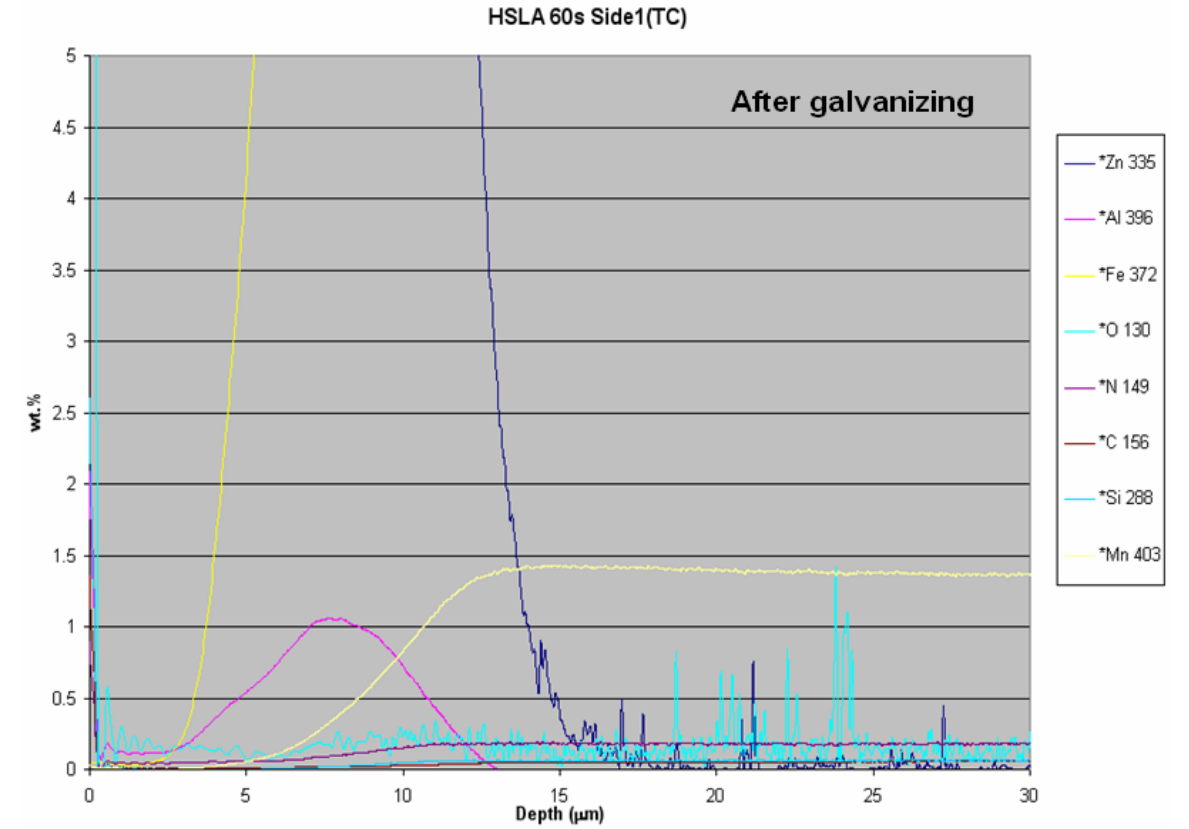

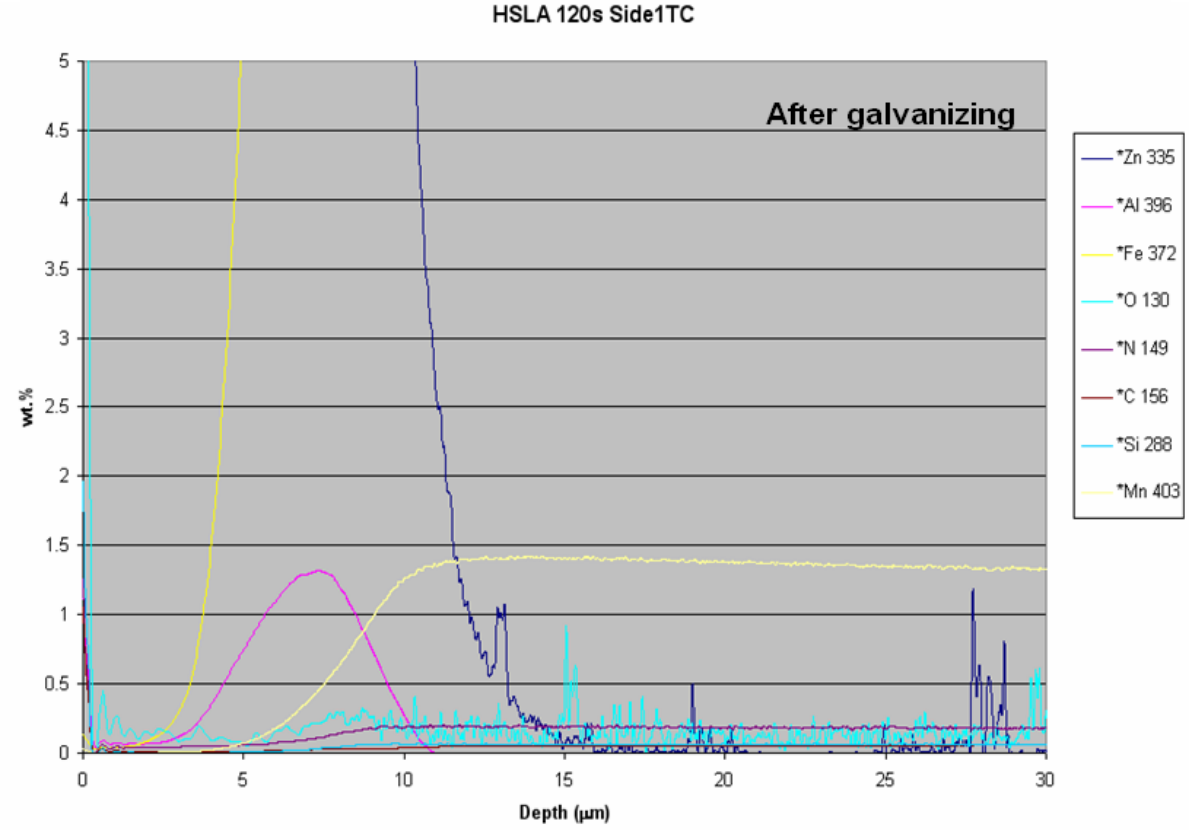

Fig. 9 – GDOES depth profiles obtained from selected galvanized HSLA steel coupons. (continued).

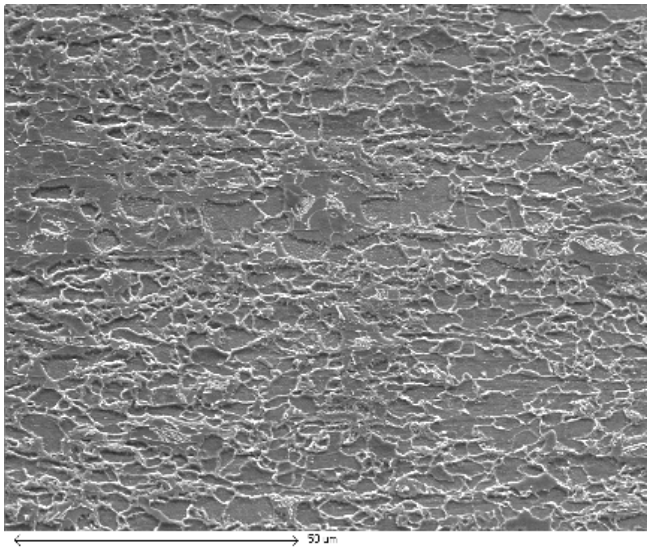

60 s hold at 600°C

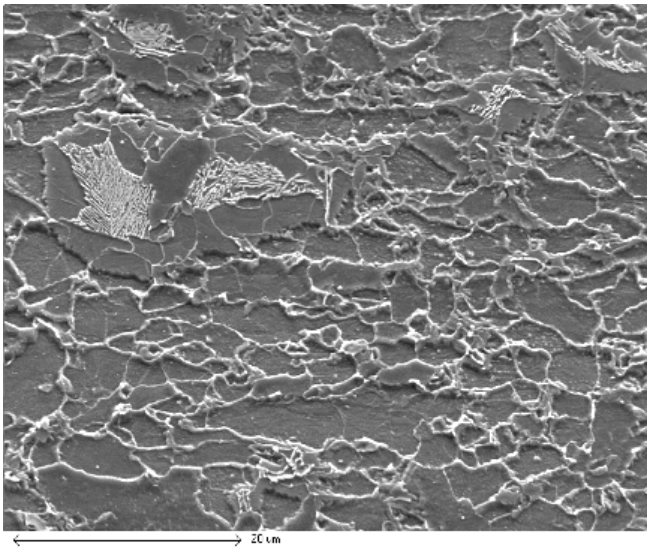

60 s hold at 600°C

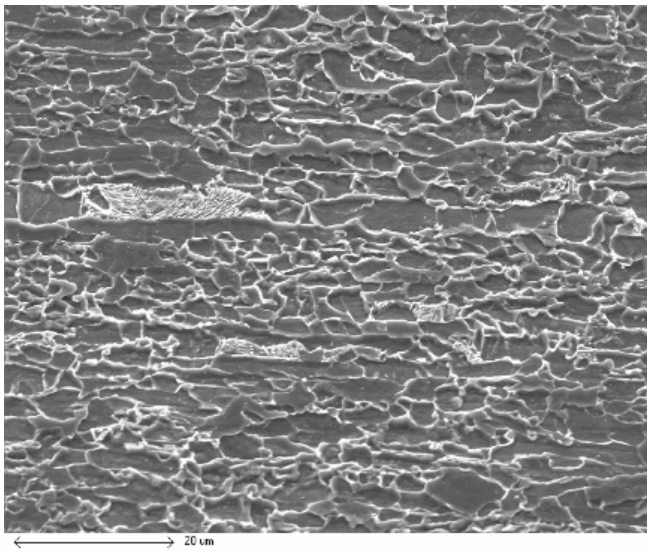

120 s hold at 600°C

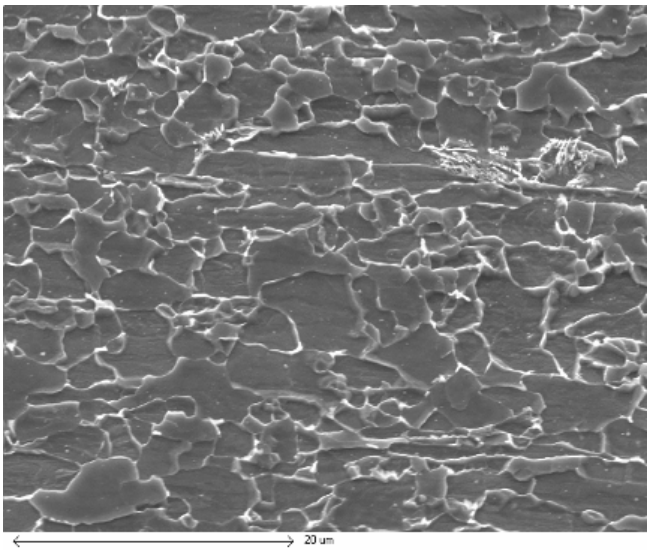

120 s hold at 600°C

Fig. 10 – SEM micrographs of the microstructure of the HSLA steel substrate in the galvanized coupons. Rolling direction is parallel to the longer side in each micrograph.

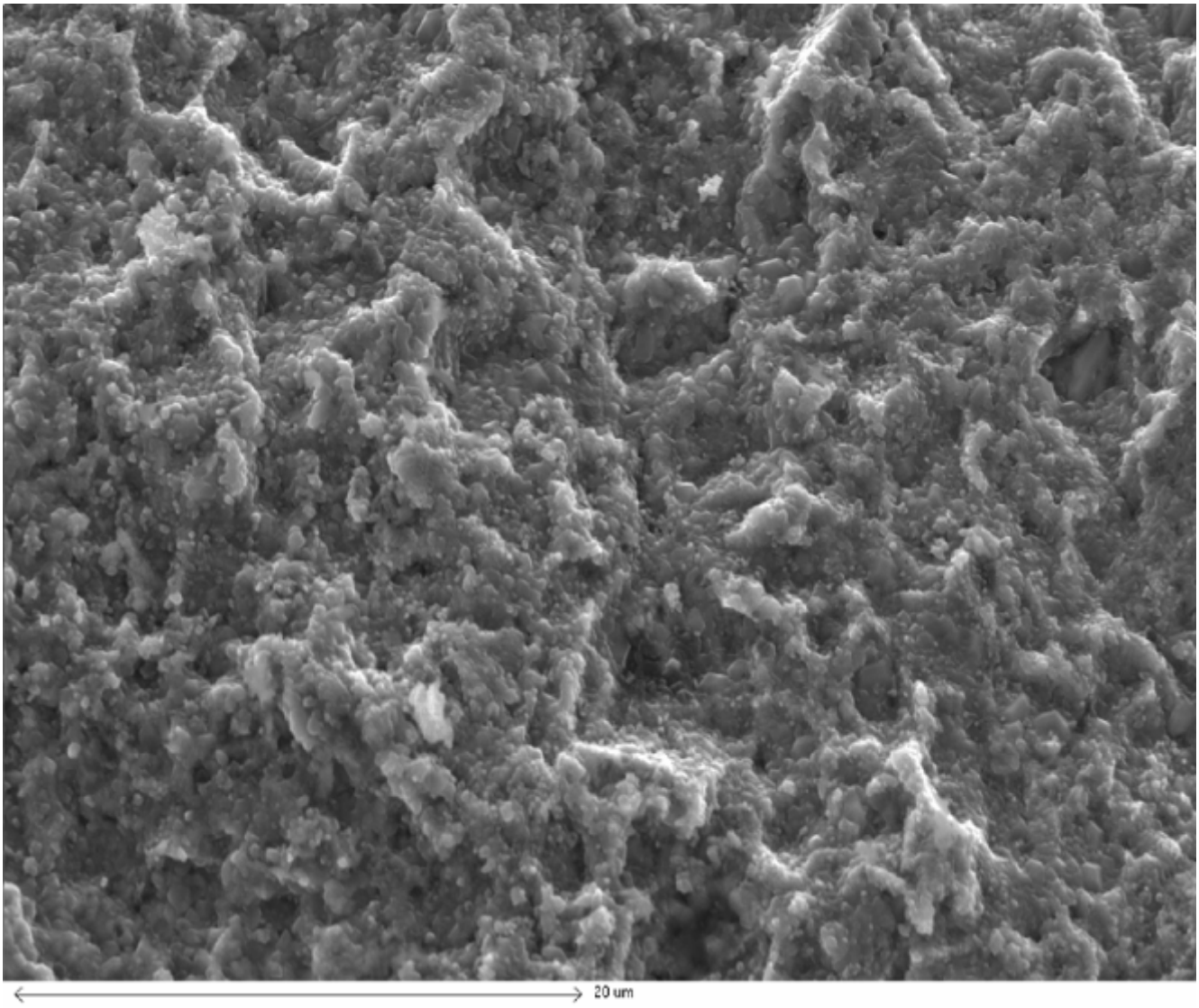

(a) sample after 60 s hold at 600°C

Fig. 11 – SEM micrographs of inhibition layer on galvanized coupons.

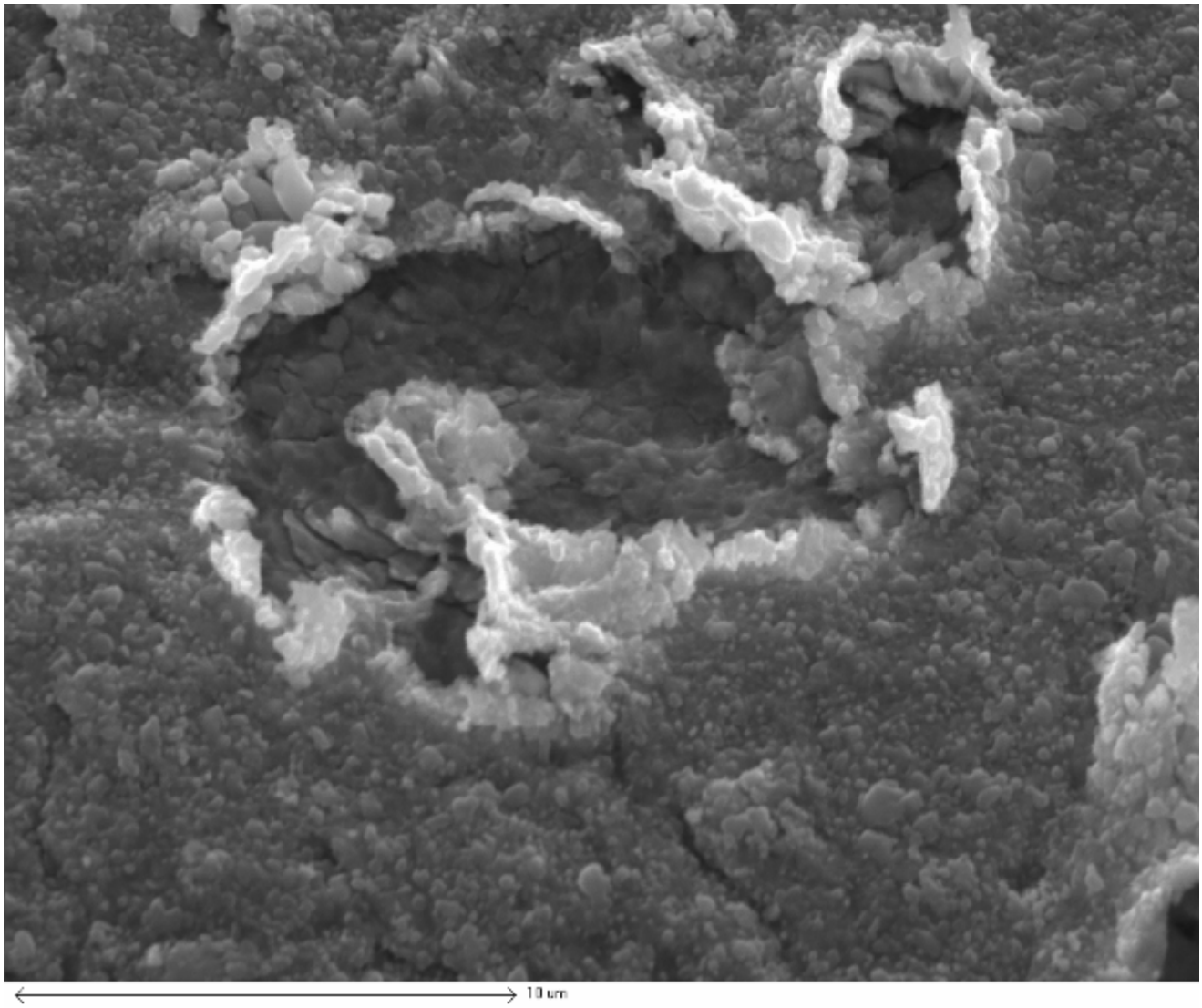

(b) sample after 120 s hold at 600°C

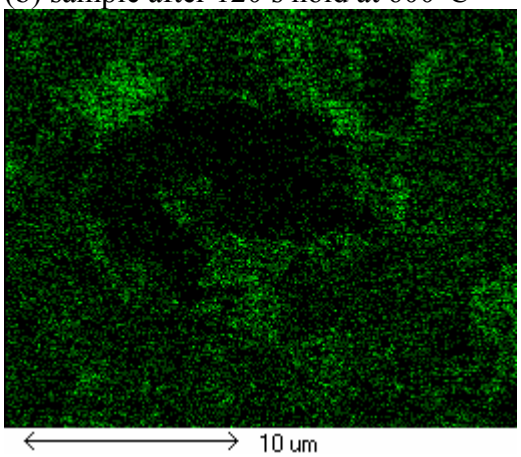

(c) EDS map of Al

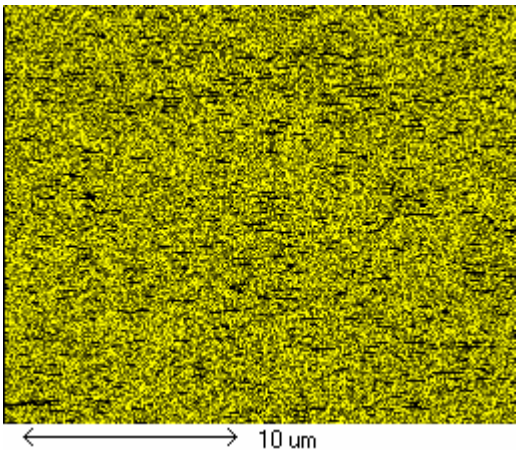

(d) EDS map of Fe

Fig. 11 – SEM micrographs of inhibition layer on galvanized coupons. (continued).

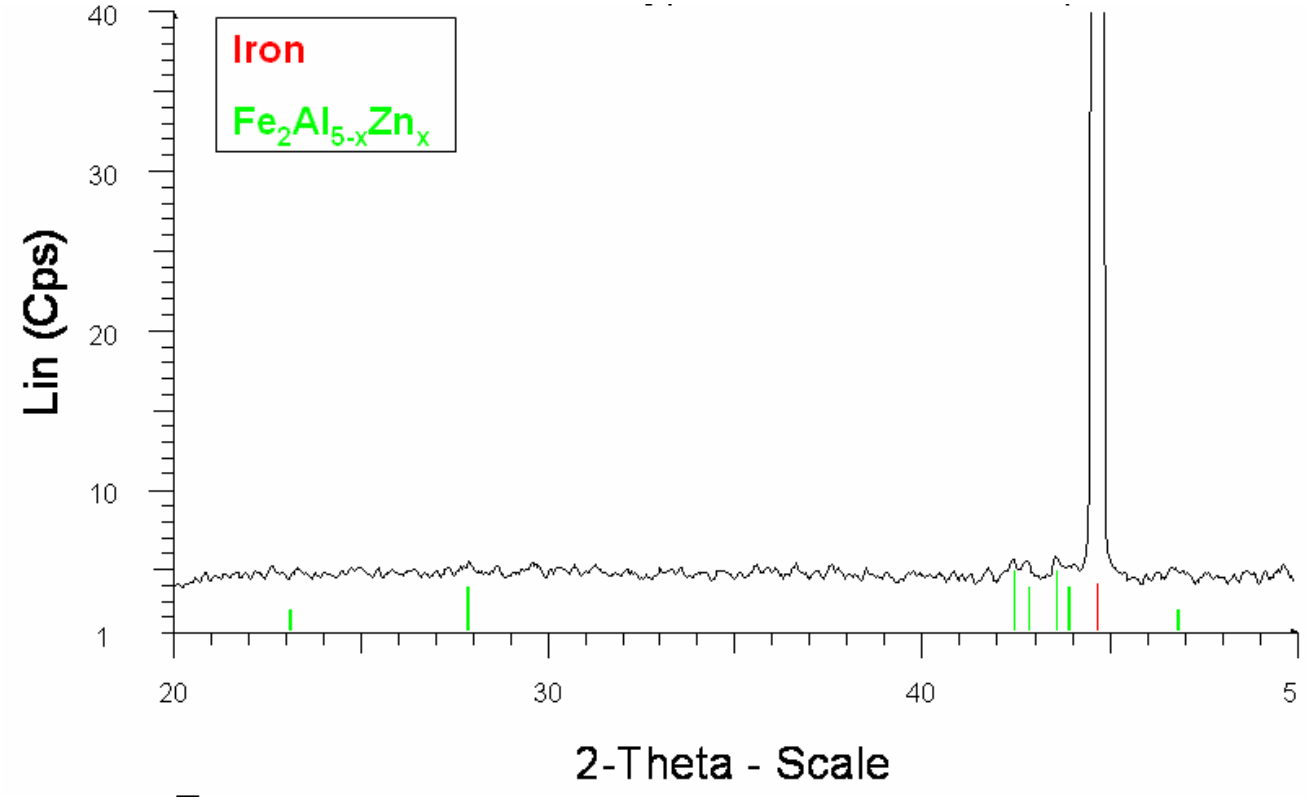

(a) sample after 60 s hold at 600°C

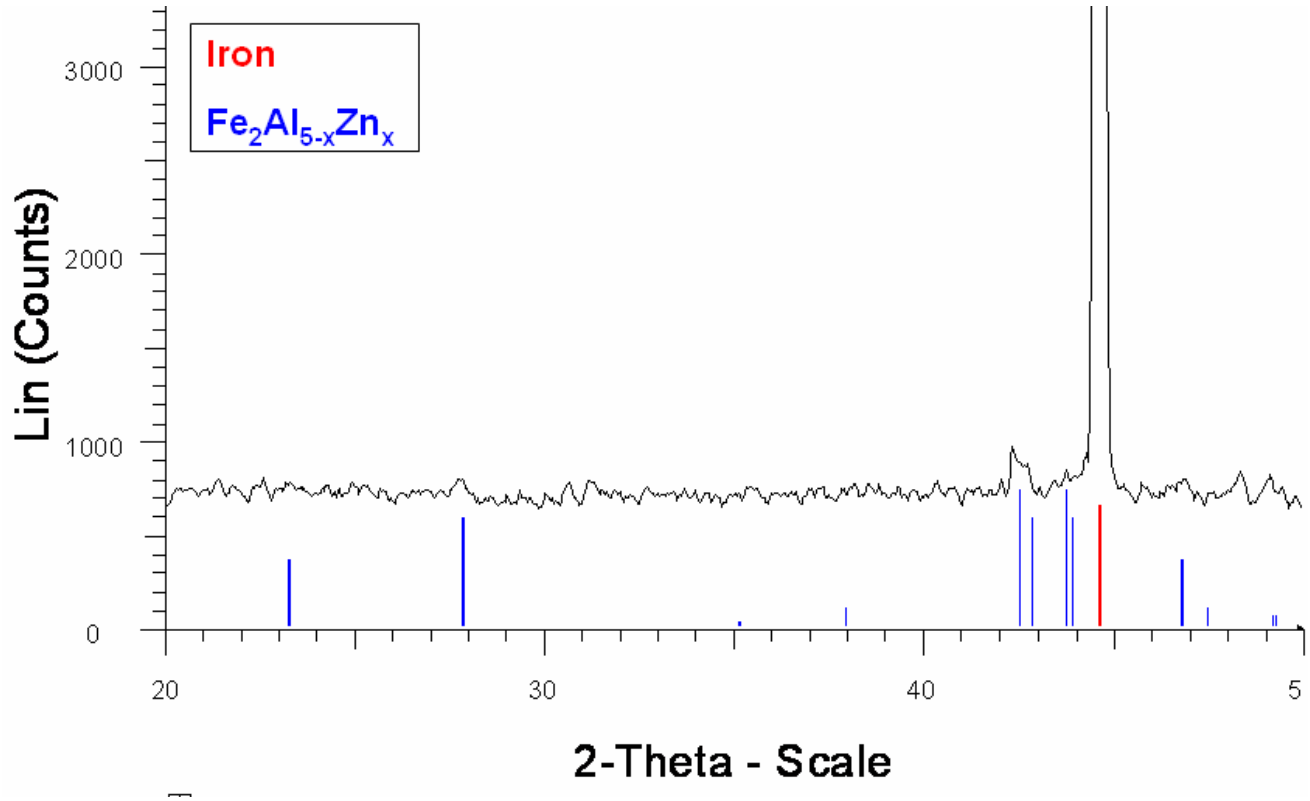

(b) sample after 120 s hold at 600°C

Fig. 12 – X-ray spectra of the inhibition layer on the steel substrate.

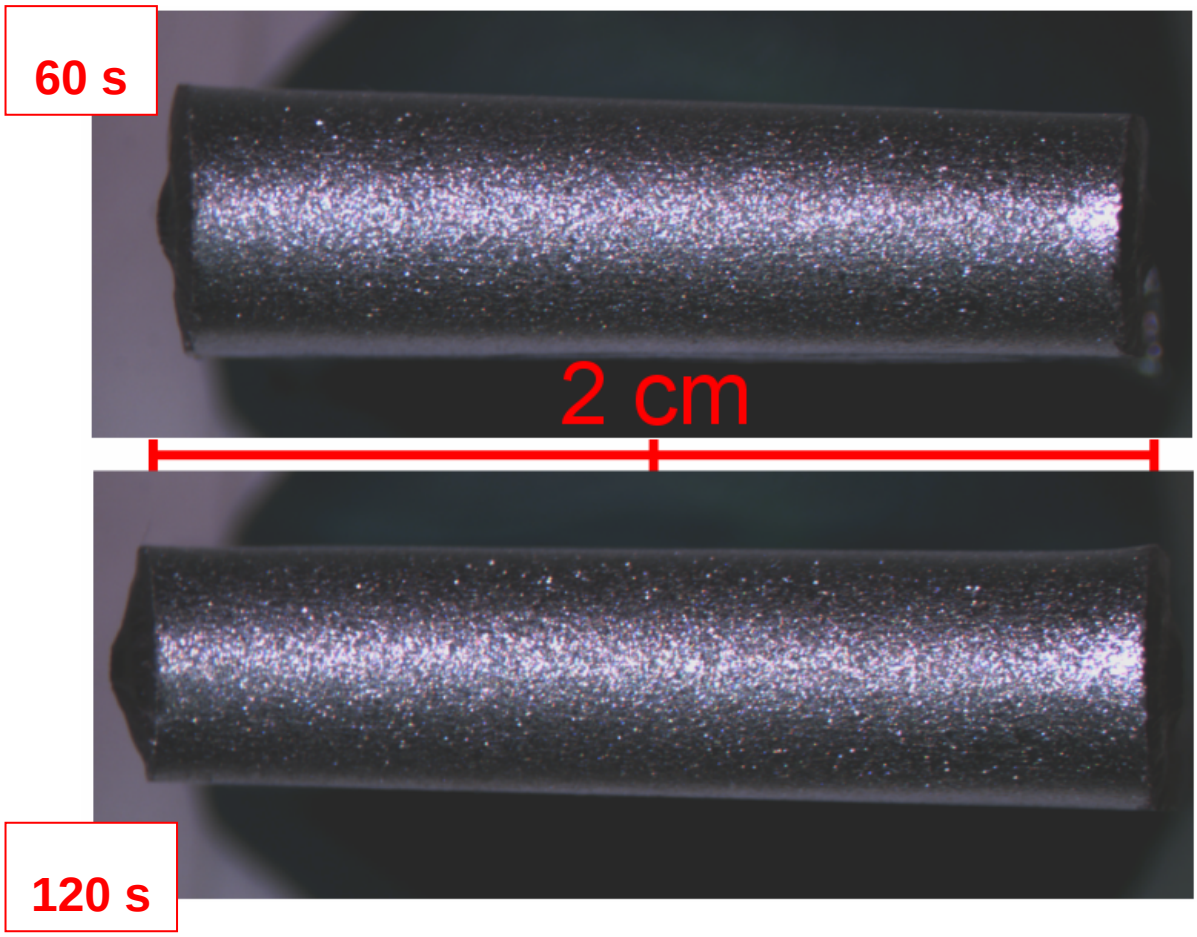

Fig. 13 – Galvanized samples after 180° bending test to assess the coating quality.

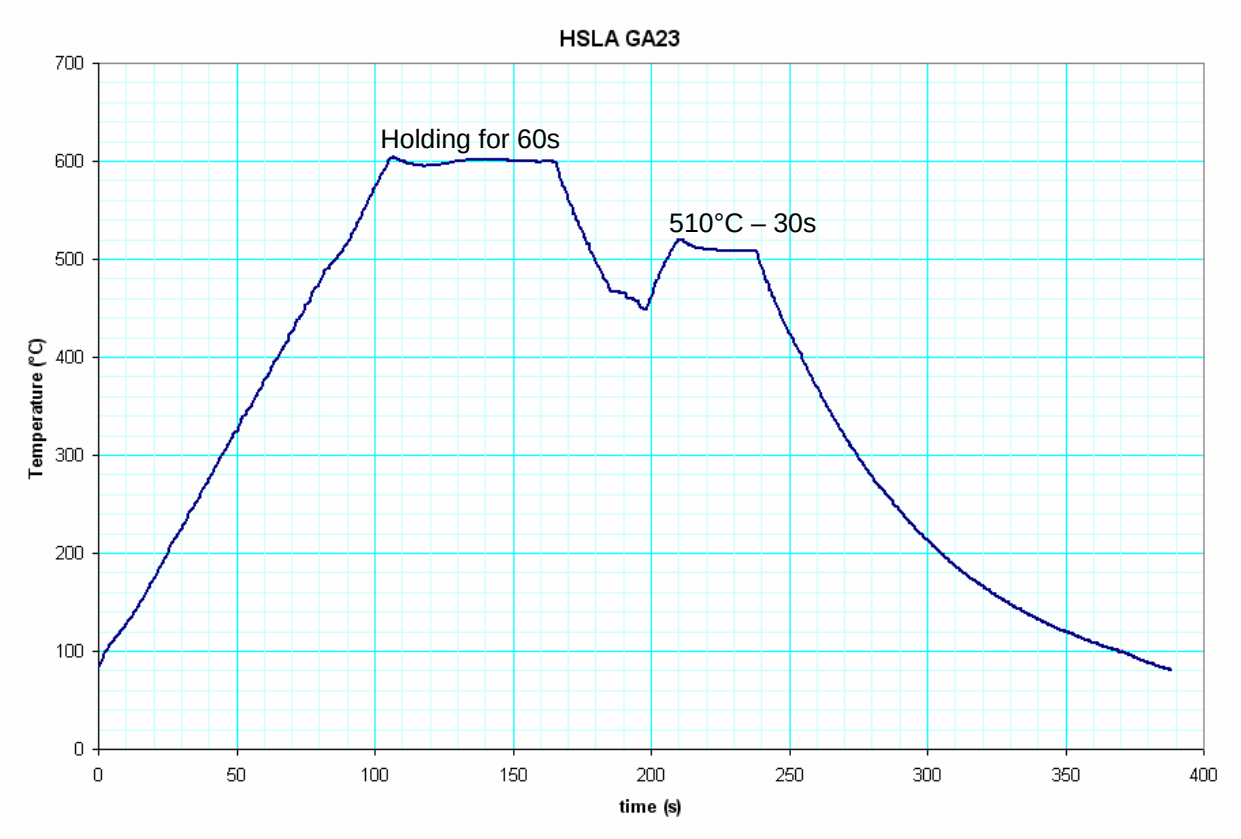

Fig. 14 – Example of galvannealing thermal cycle.

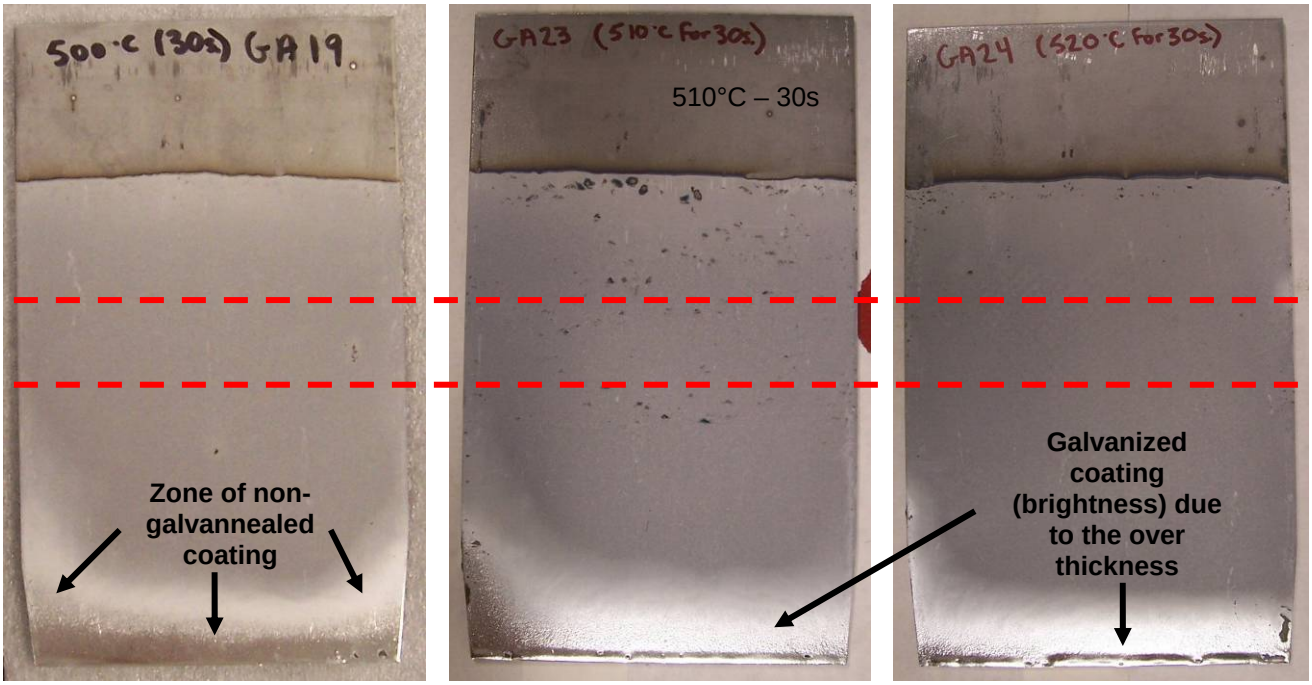

Fig. 15 – Examples of galvannealed coupons. The red lines delineate the portions cut for detailed microscopic examination and other analyses.

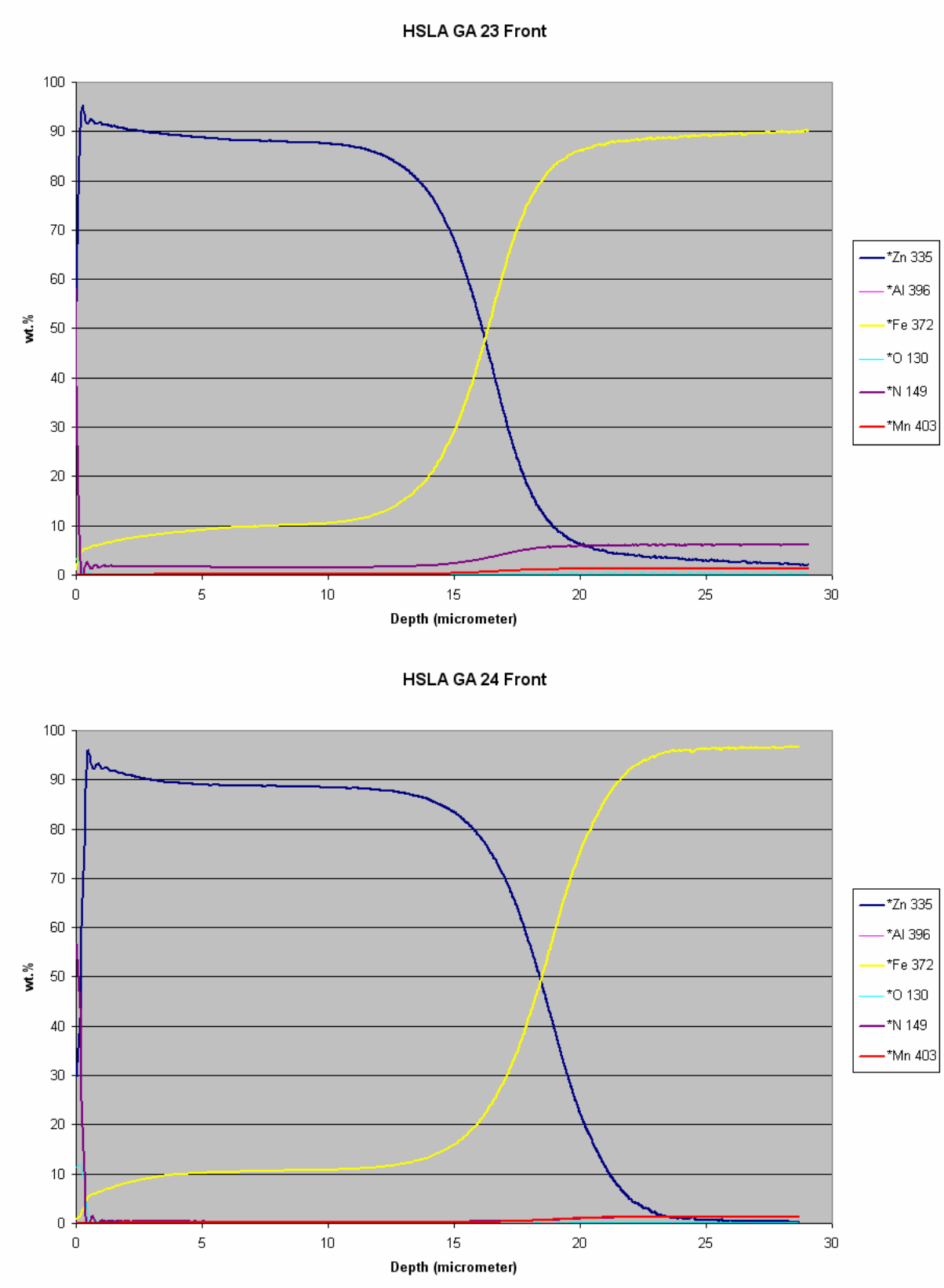

Fig. 16 –Examples of GDOES depth profiles obtained from selected galvannealed hot-rolled HSLA steel coupons.

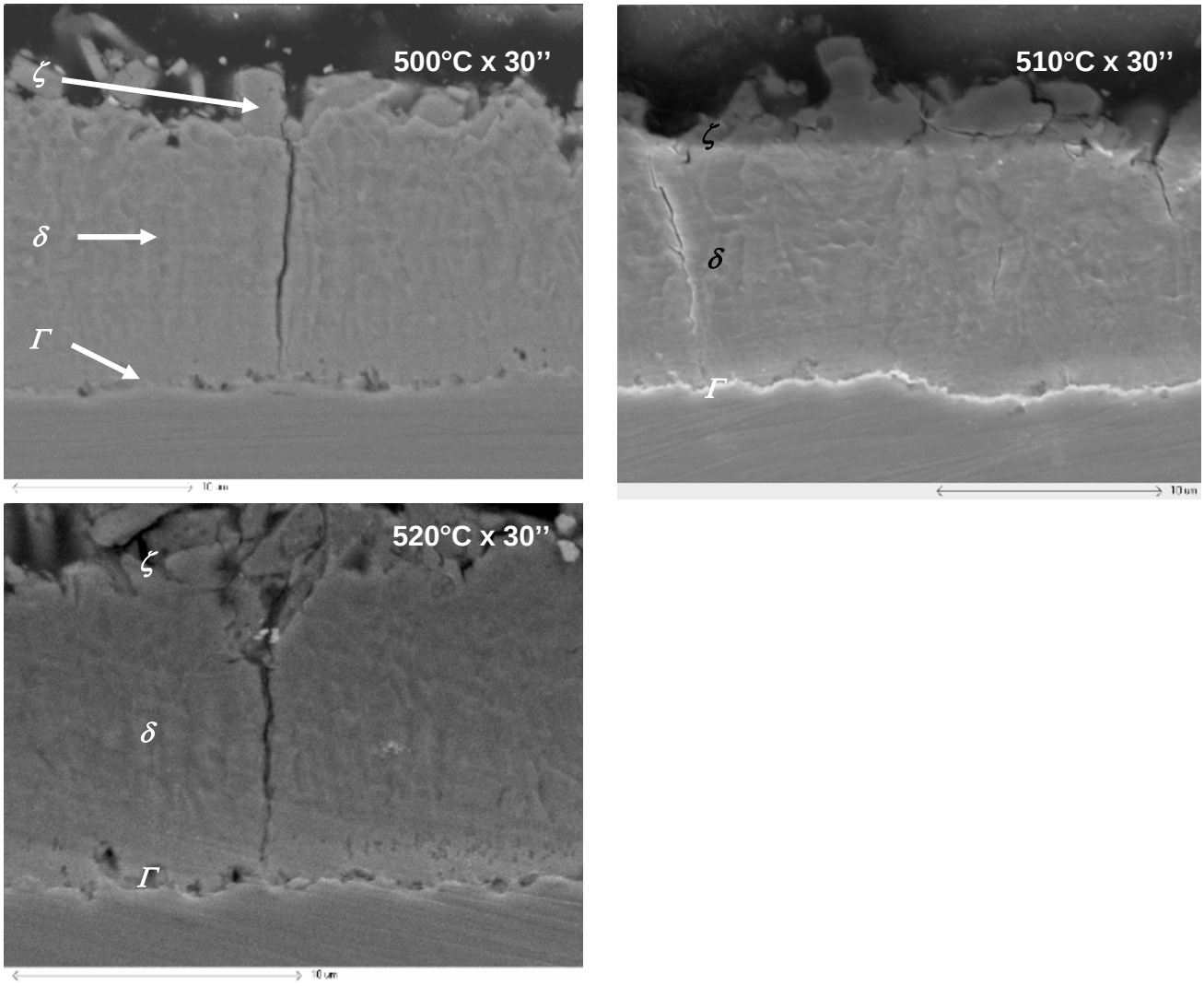

Fig. 17 – Cross-section SEM of the galvannealed samples etched in 0.5% Nital for 2 s.

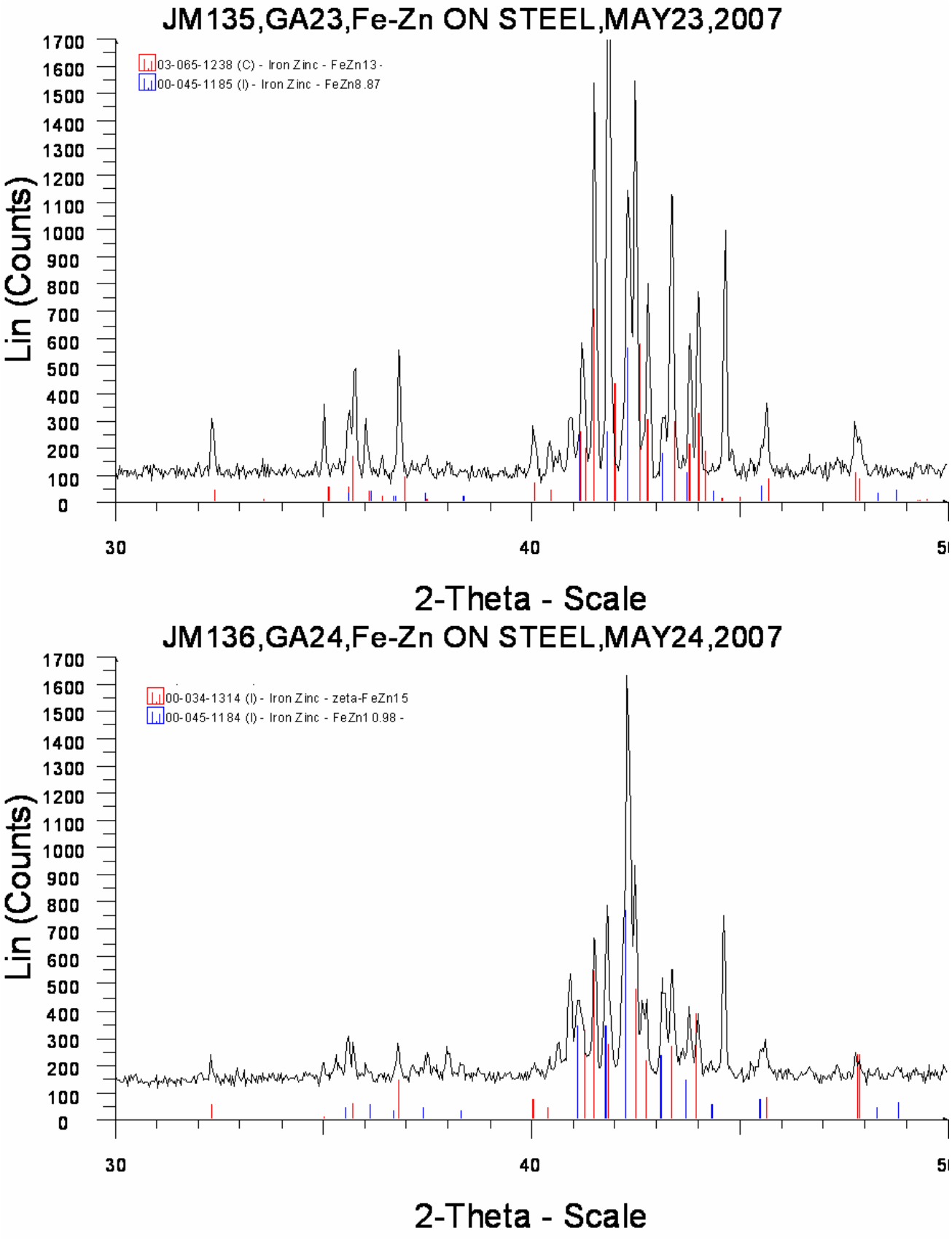

Fig. 18 – Examples of X-ray spectra of galvannealed coating on the hot-rolled HSLA steel substrate.

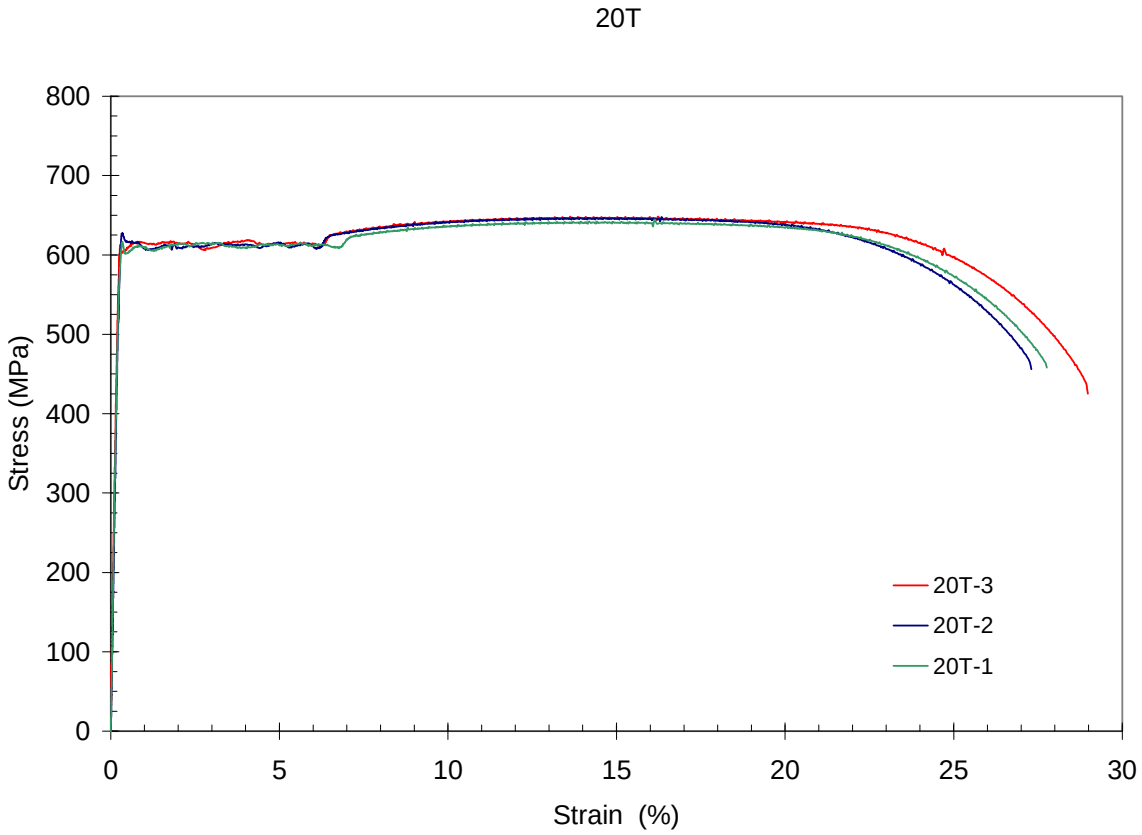

Fig. 19 – Typical stress-strain curves for the HSLA steel samples.

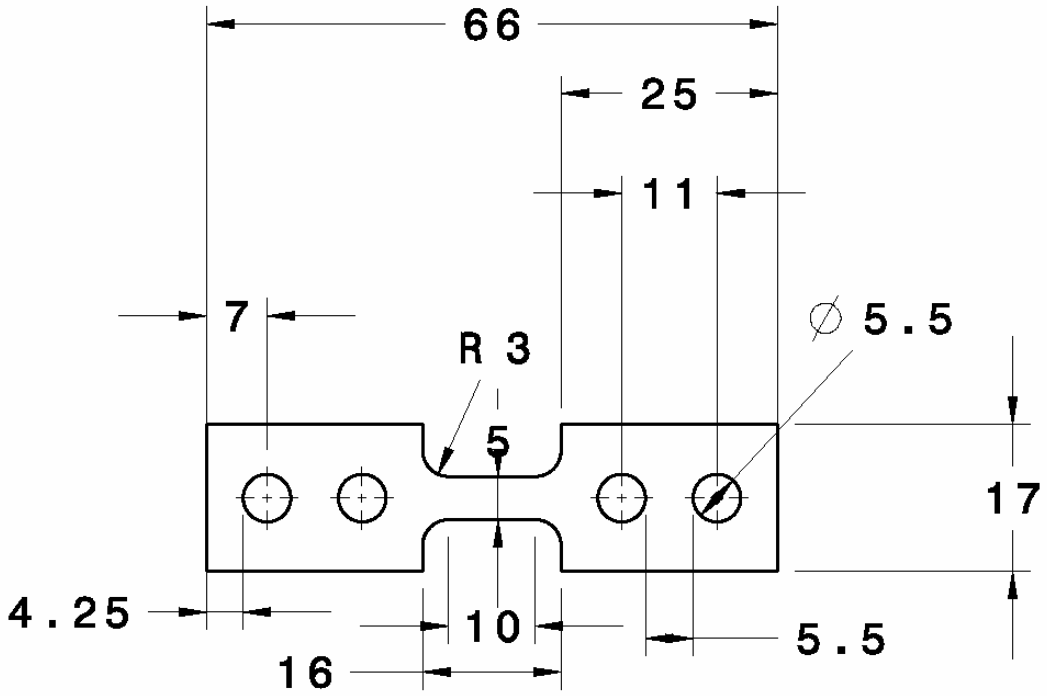

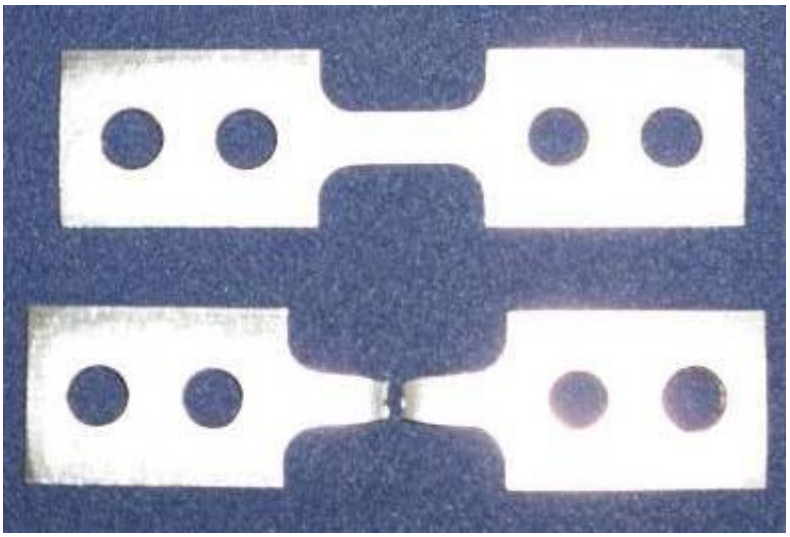

Fig. 20 – The geometry (dimensions in mm) and photos of the specimens for dynamic tensile tests.

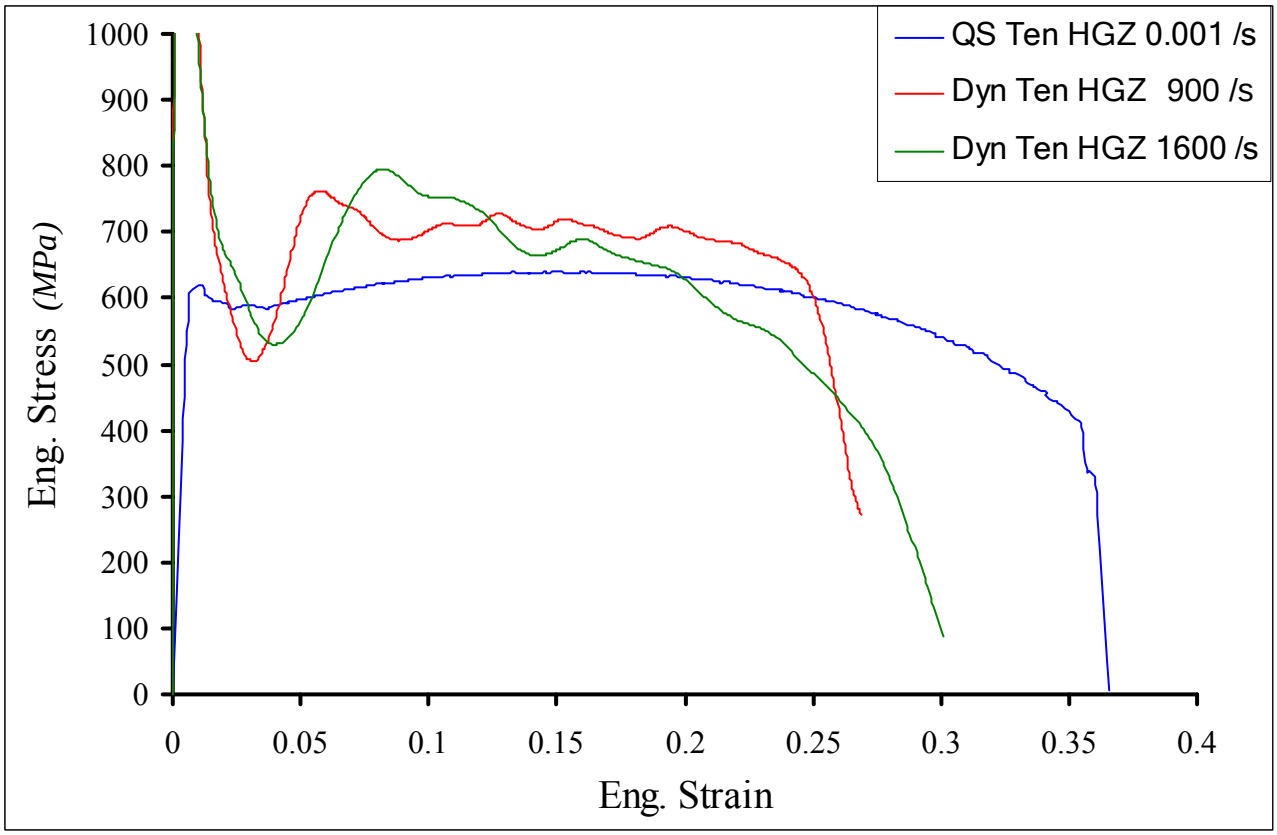

Fig. 21 – Examples of stress-strain curves (galvanized HSLA steel).

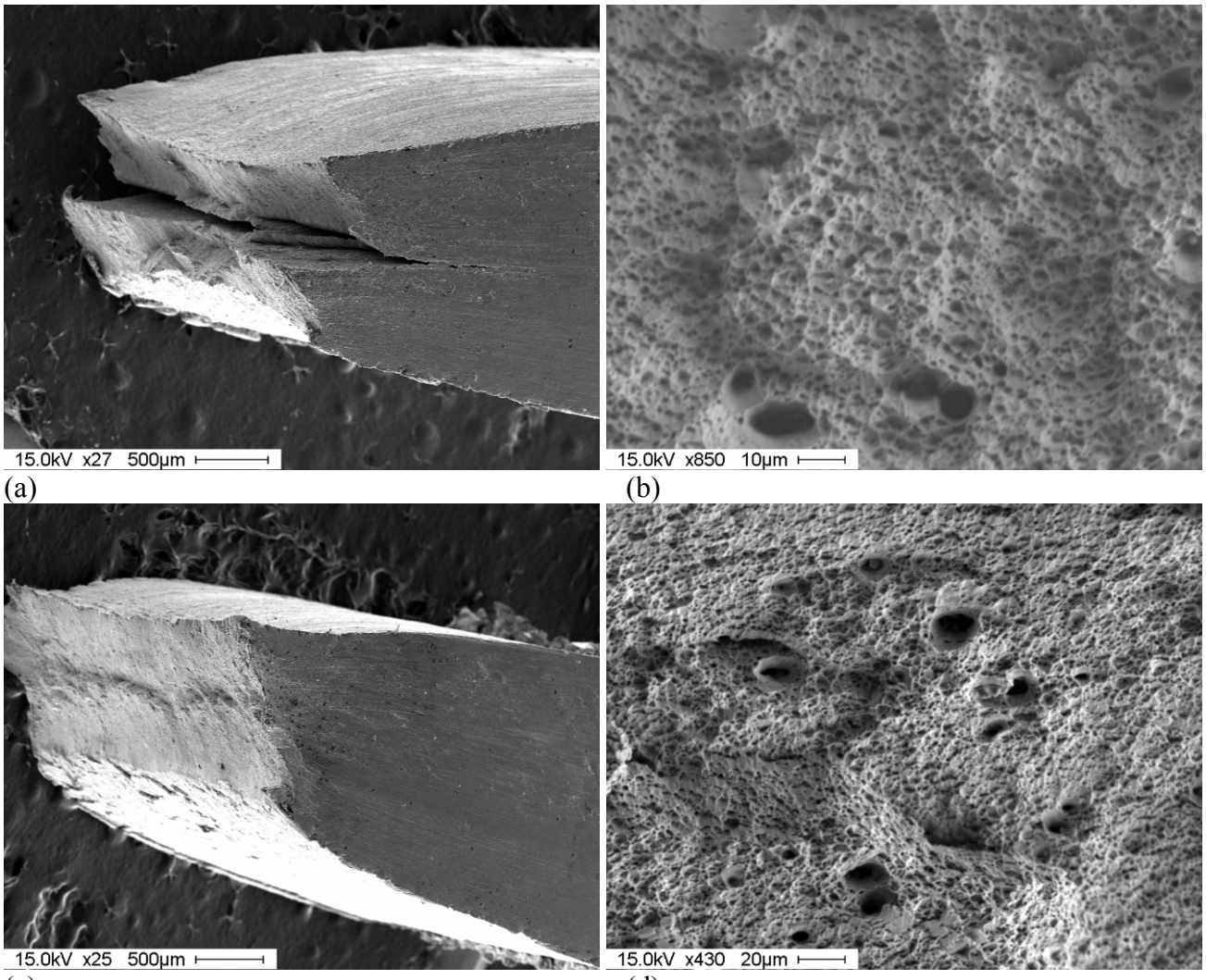

(a) (b)

(c) (d)

Fig. 22 – Examples of fractographic examination of the galvanized HSLA steel samples after quasi-static (a, b) and dynamic (c, d) tensile tests.

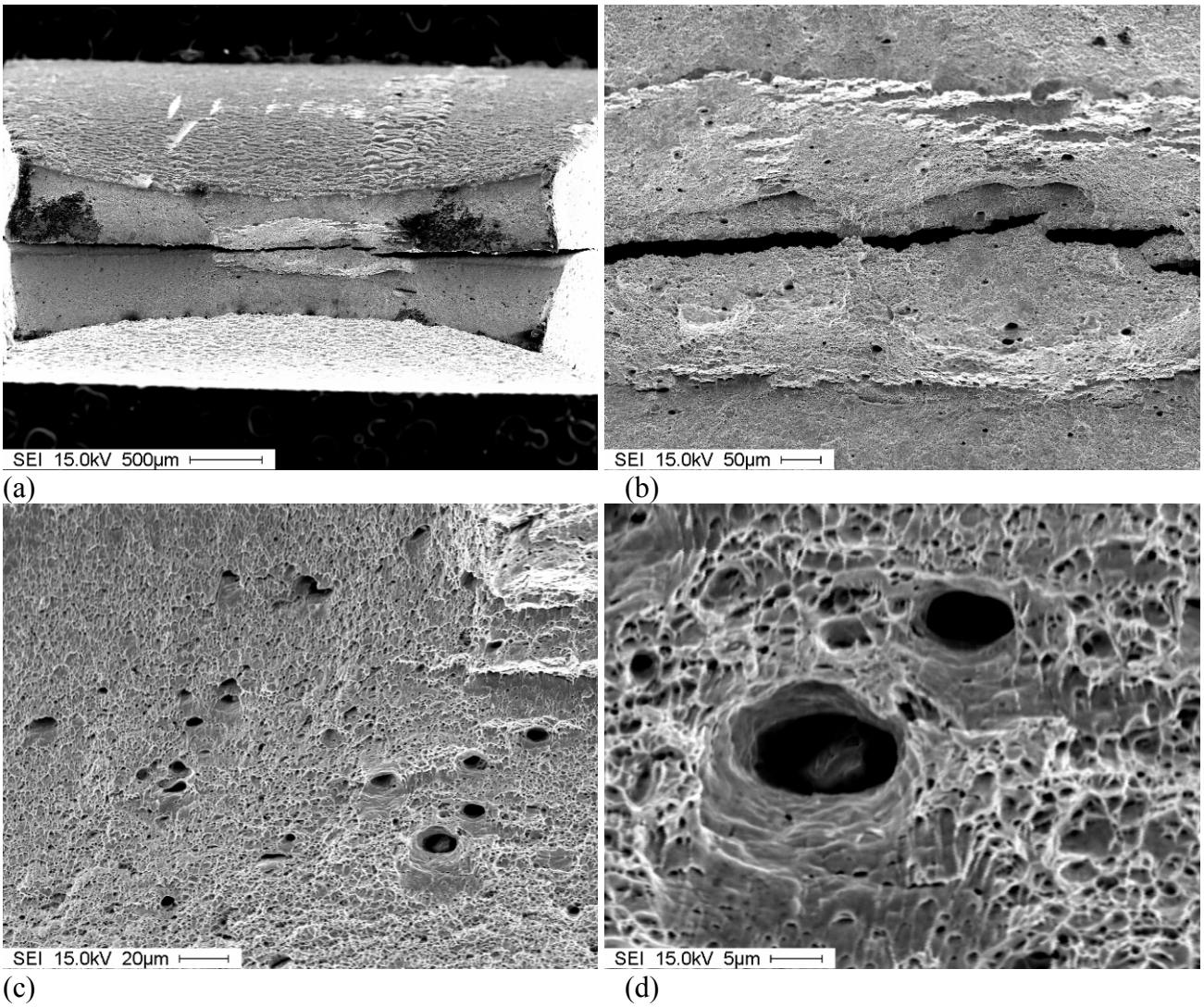

Fig. 23 – Examples of fractographic examination of the galvannealed HSLA steel samples after quasi-static tensile tests.

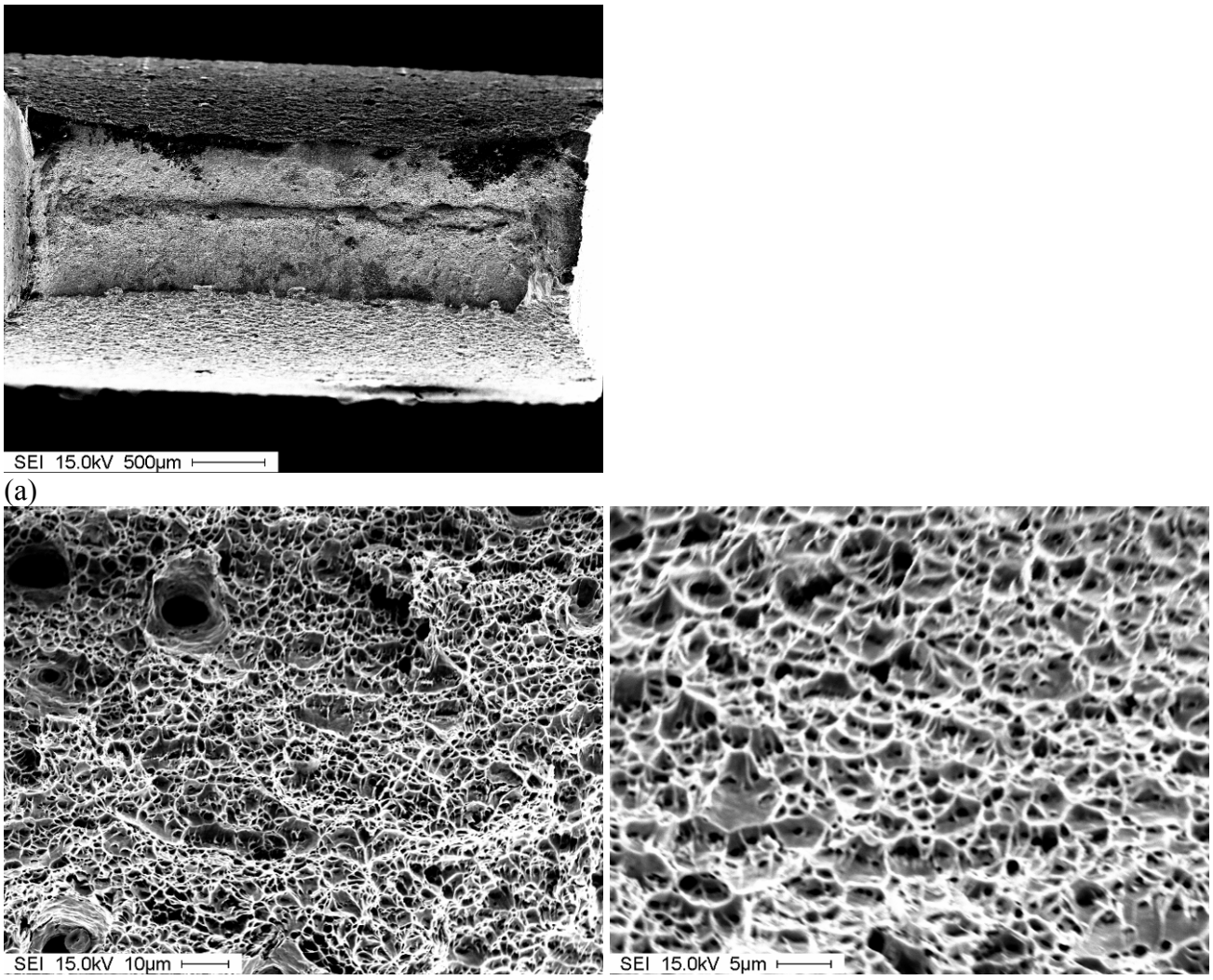

Fig. 24 – Examples of fractographic examination of the galvannealed HSLA steel samples after high strain rate tensile tests.

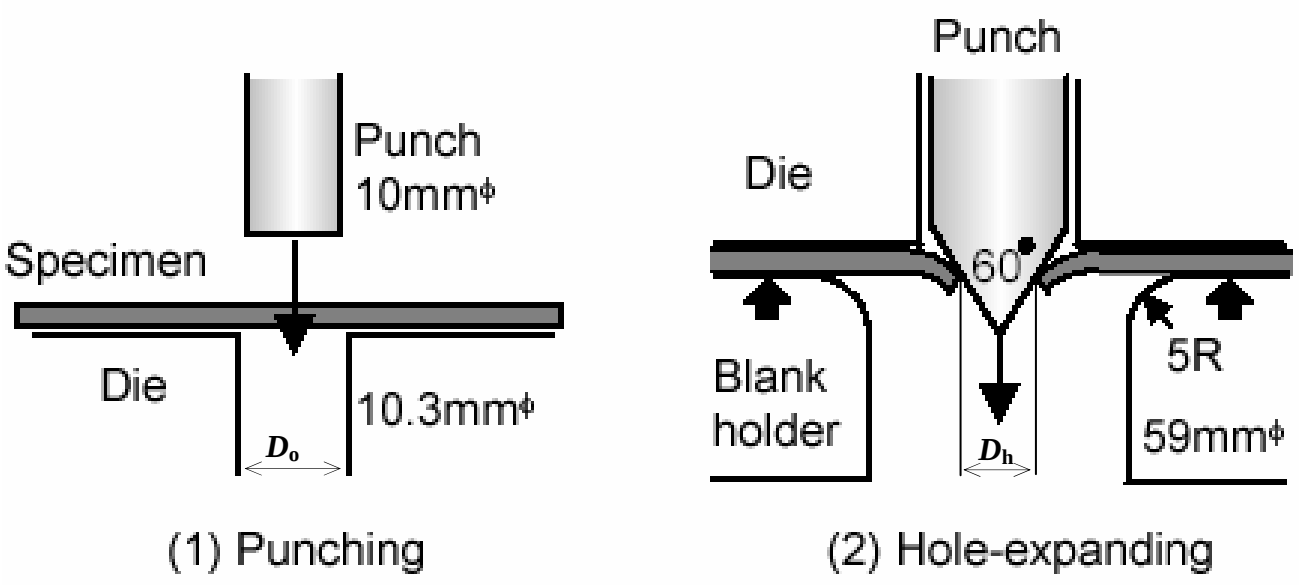

Fig. 25 – Schematics of the hole-expansion test.

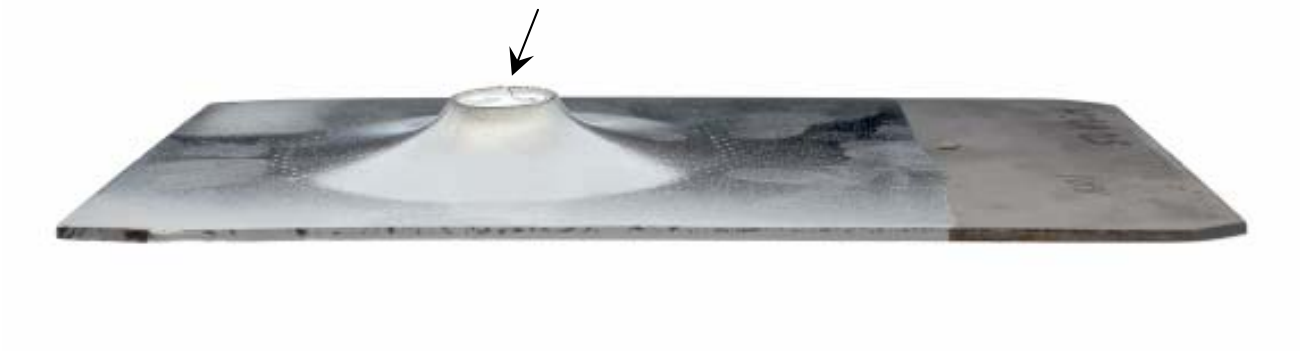

Fig. 26 – General appearance of the HSLA-32 coupon after the hole-expansion test. The arrow points to the crack.

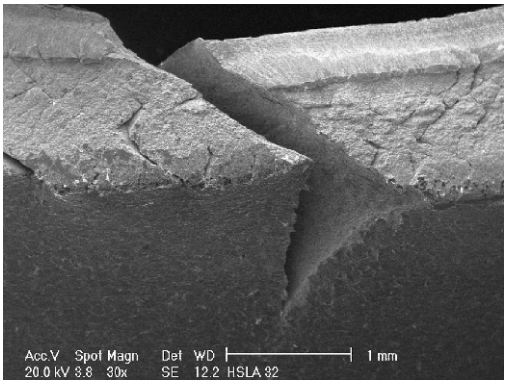

(a) SE image

(b) BSE image shows burnished surface indicated by the arrow.

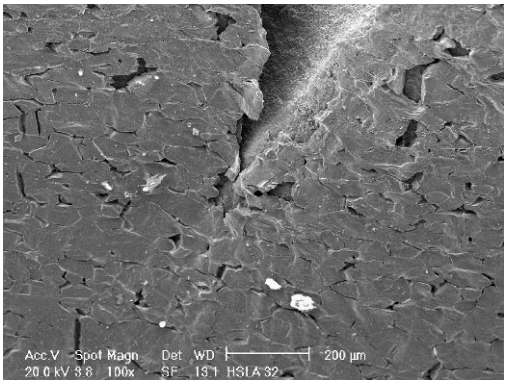

(c) SE image shows the end of the crack

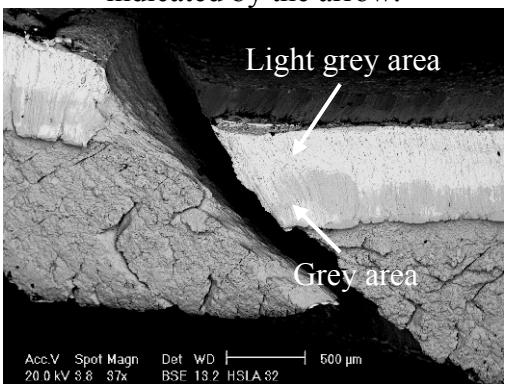

(d) BSE image of tilted sample revealing Zn coating (light gray)

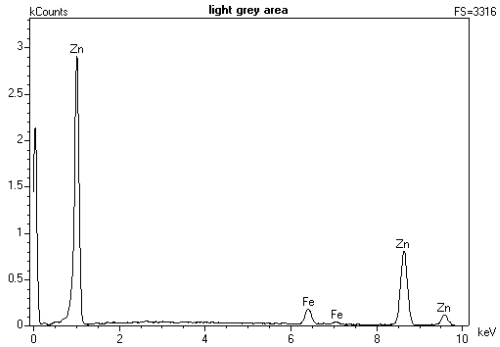

(e) EDS spectrum of light gray area

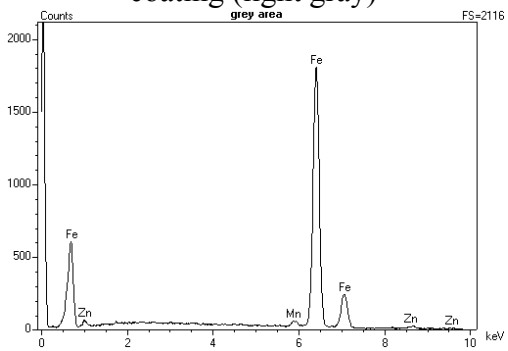

(f) EDS spectrum of gray area

Fig. 27 – Secondary-electron (SE) and back-scattered electron (BSE) SEM images and EDS spectra of the HSLA 32 sample after the hole expansion test.

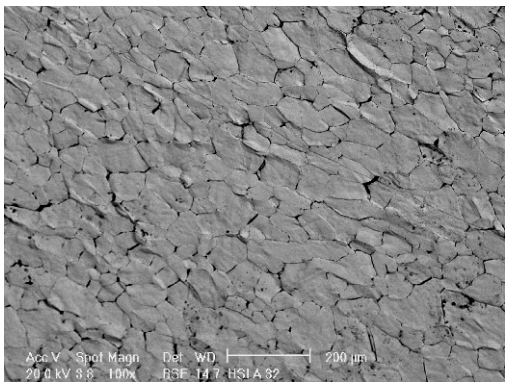

(a) BSE image of the coating near the crack

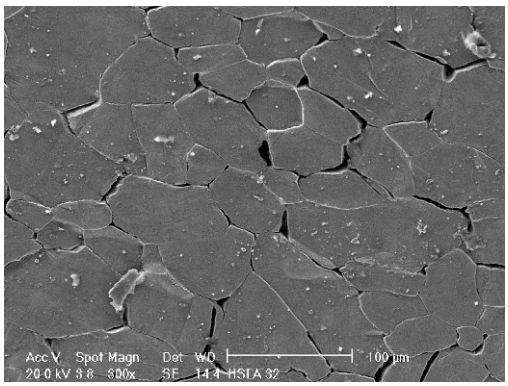

(b) Higher magnification SE image

Fig. 28 – SEM images of the galvanized coupon after hole expansion test.

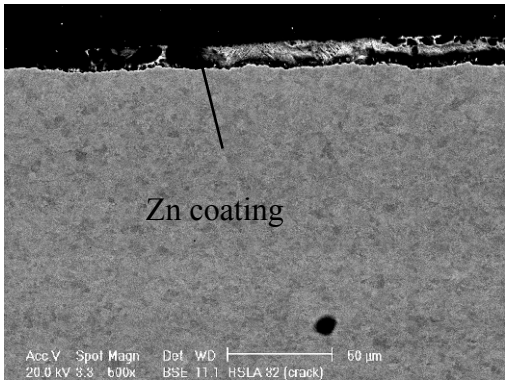

(a) BSE image revealing discontinuous coating

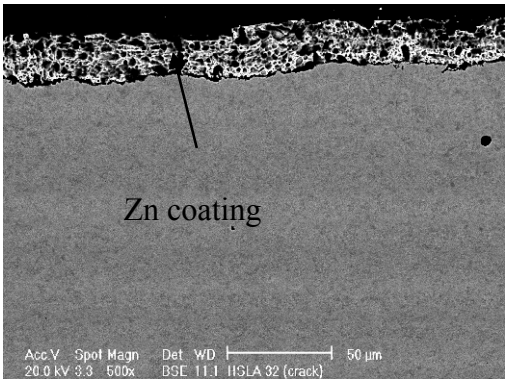

(b) BSE image of the side opposite (a) revealing a thicker continuous coating

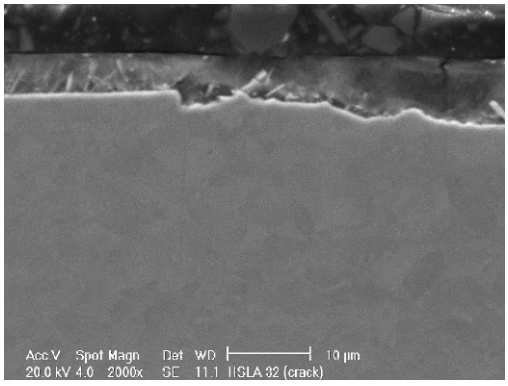

(c) Higher magnification SE image of the coating

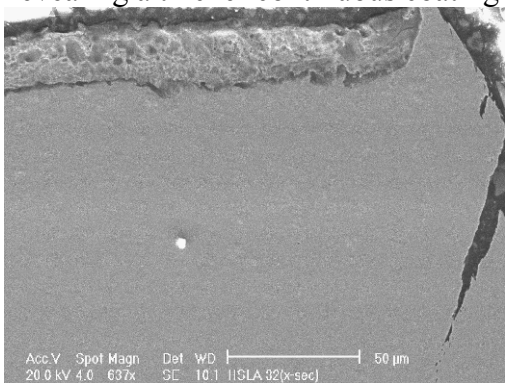

(d) Higher magnification SE image of the coating near the crack

Fig. 29 – SEM images of the polished cross-section of the HSLA 32 sample taken 10 mm away from the crack revealing the coating on both sides (after the hole expansion test).

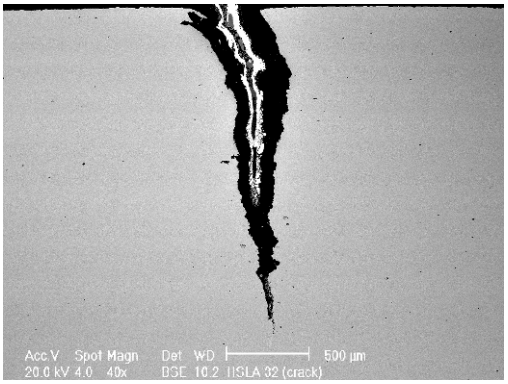

(a) BSE image

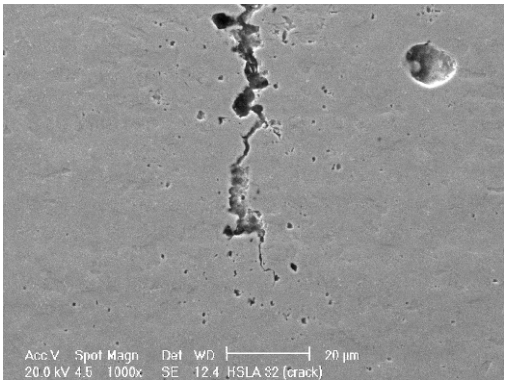

(b) Higher magnification of SE image of the end of the crack

Fig. 30 – SEM images of the crack (polished cross-section).

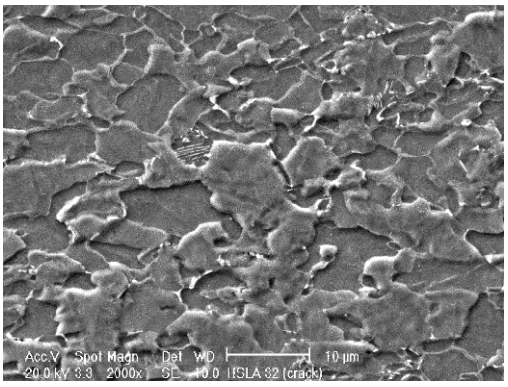

(a) SE image of the steel microstructure

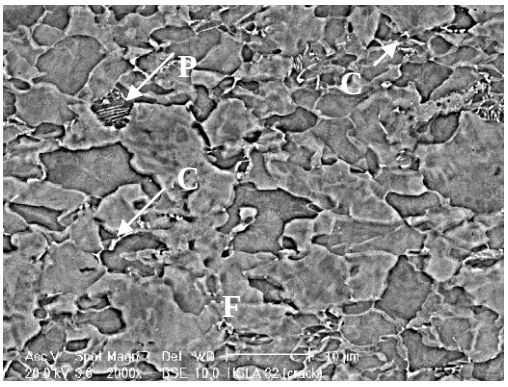

(b) BSE image revealing three microstructural constituents indicated by the arrows (ferrite, perlite and carbides)

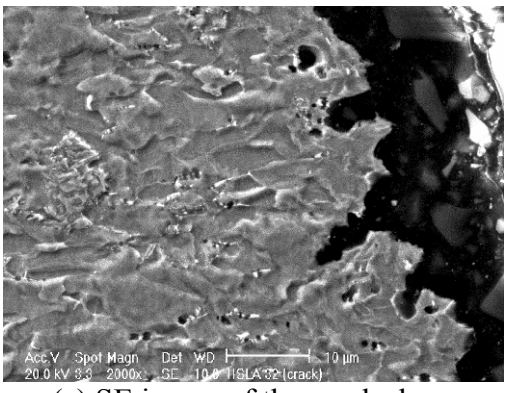

(c) SE image of the crack shore

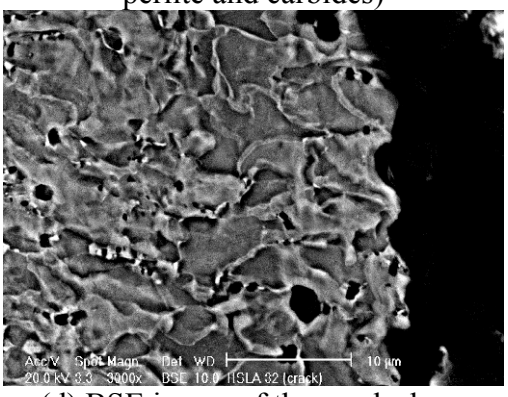

(d) BSE image of the crack shore

Fig. 31 – SEM images of the cross-section etched with 2% Nital.

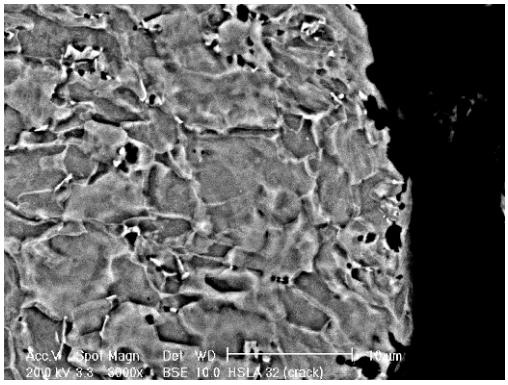

(e) BSE image of the crack shore

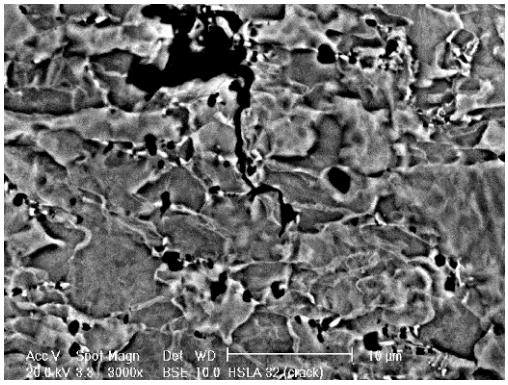

(d) BSE image shows the propagation of the end of the crack through the grains

Fig. 32 – SEM images of the cross-section etched with 2% Nital (continued).

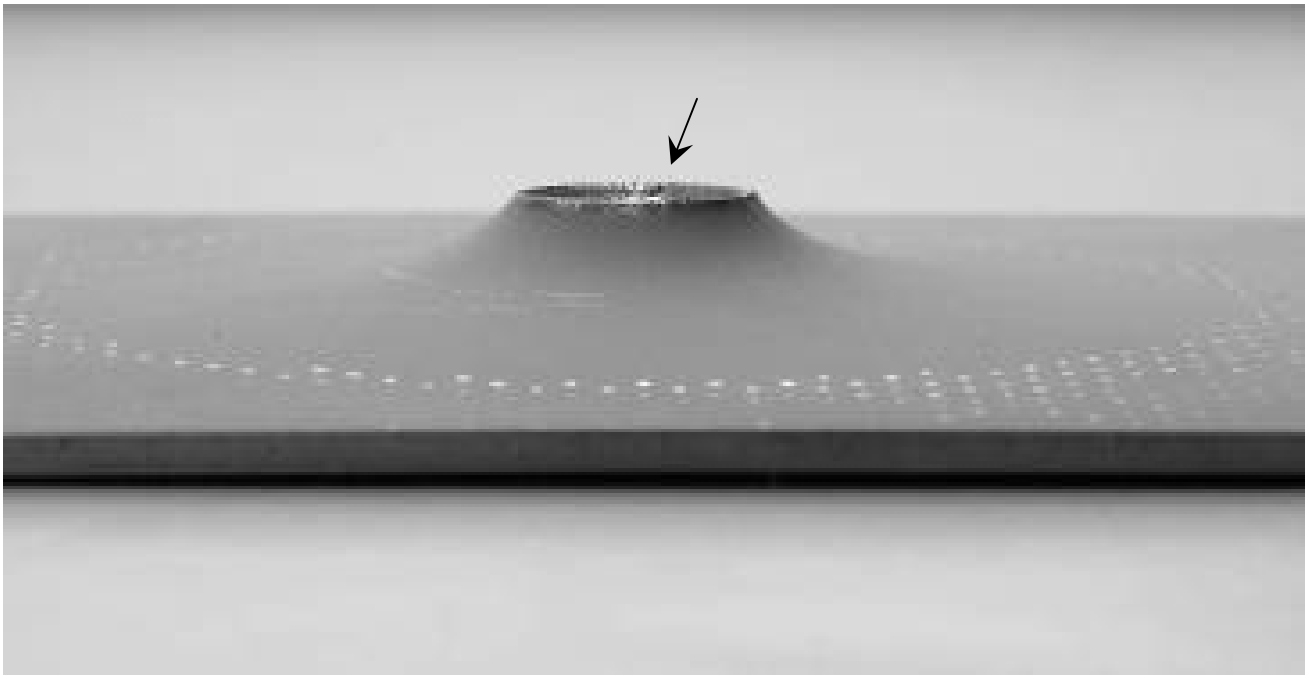

Fig. 33 – General appearance of the HSLA-GA30 coupon after the hole-expansion test. The arrow points to the crack.

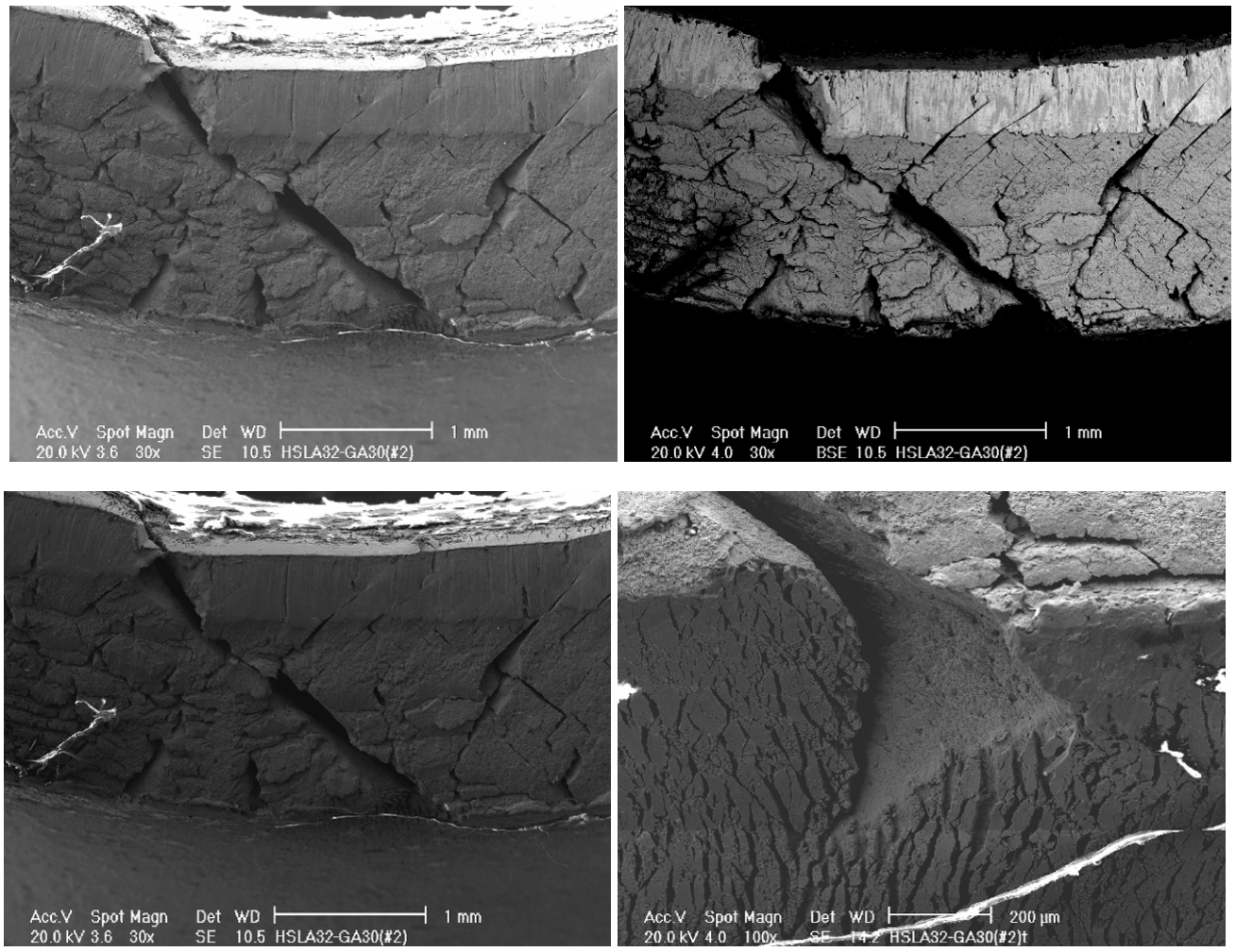

Fig. 34 – SEM images of the as-tested HSLA GA-30 sample (hole expansion test).

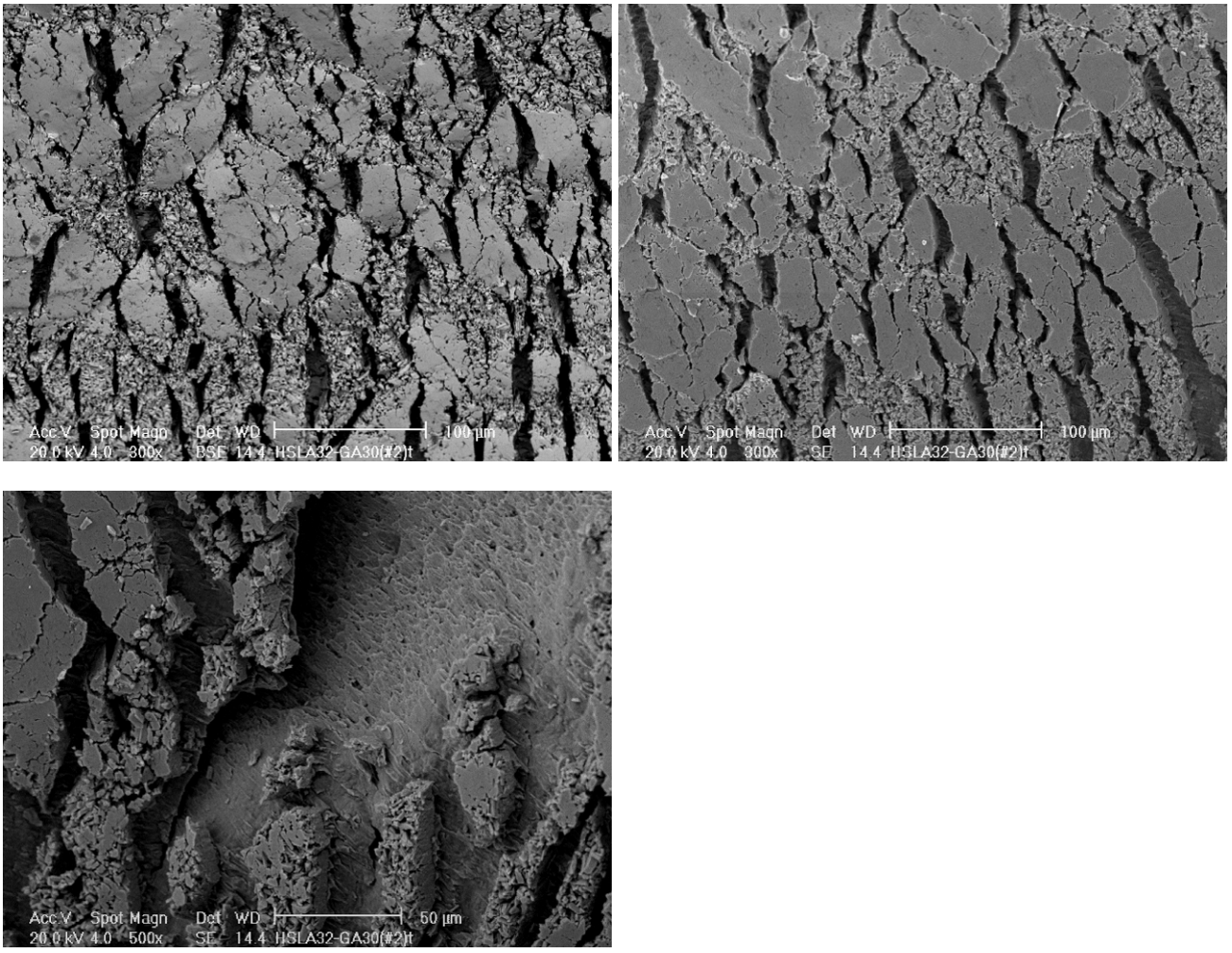

Fig. 35 – SEM images of galvannealed coating after the hole expansion test.

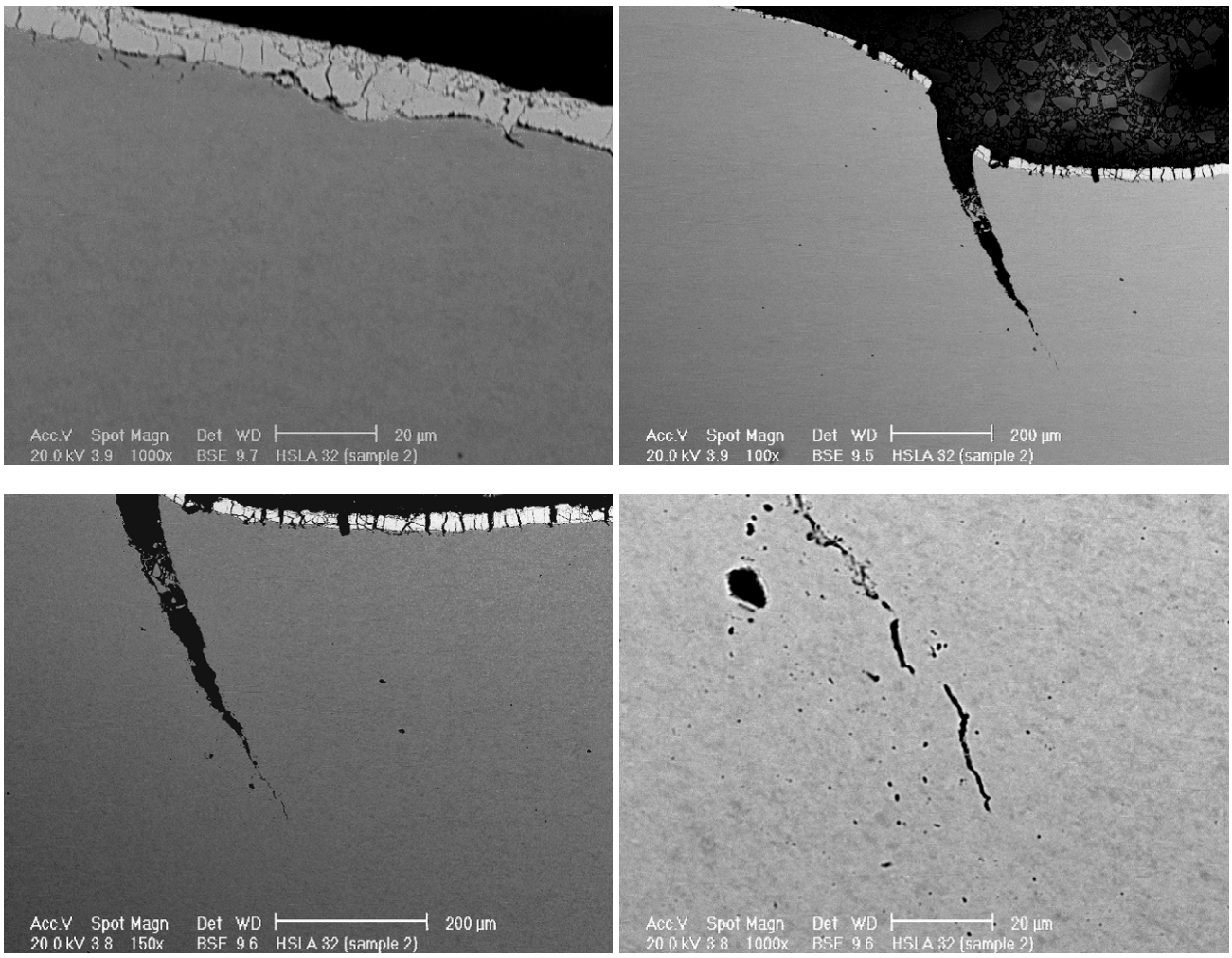

Fig. 36 – SEM images of the polished cross-section of the HSLA GA-30 sample after the hole expansion test.

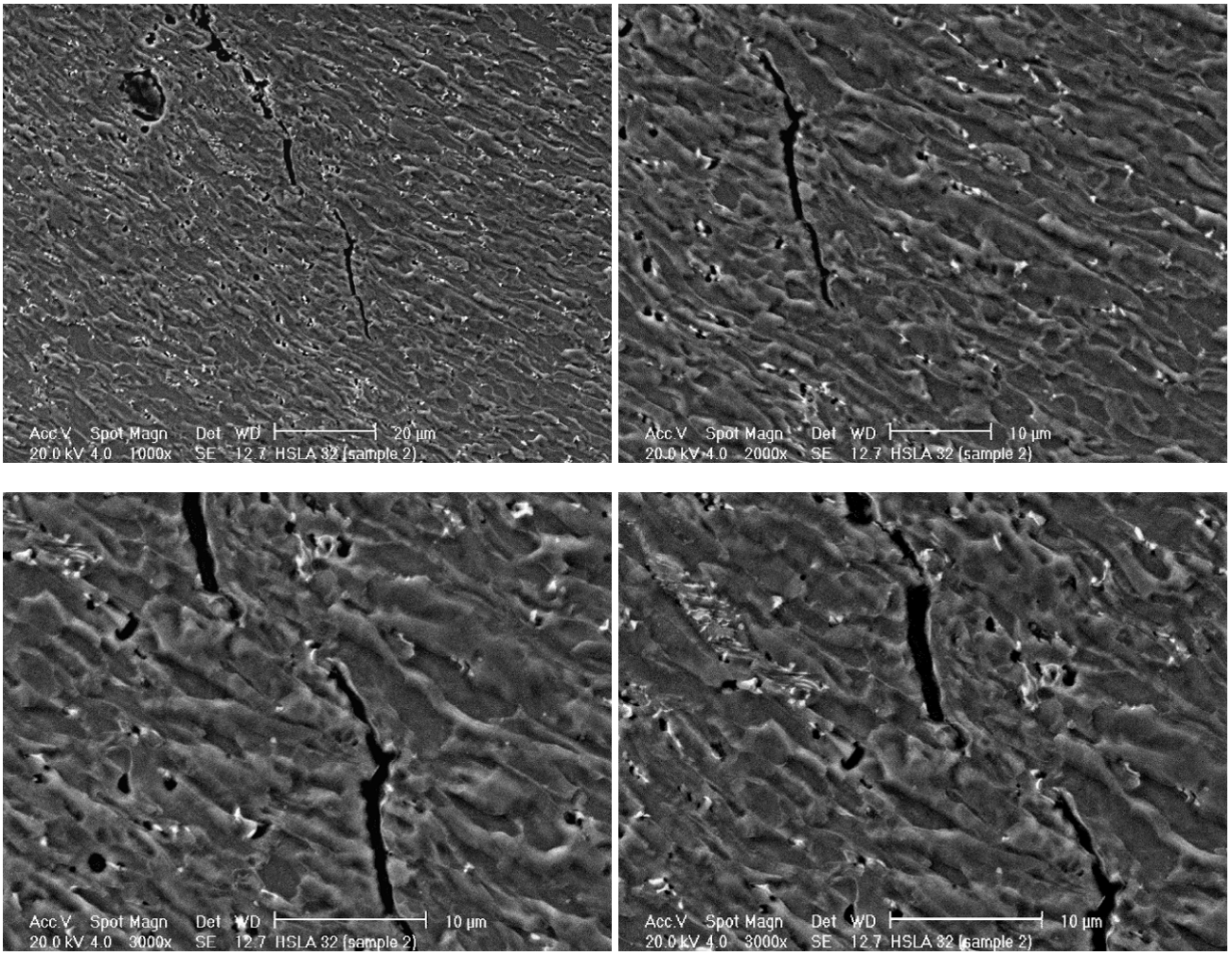

Fig. 37 – SEM images of the cross-section (sample HSLA GA-30) etched with 2% Nital.

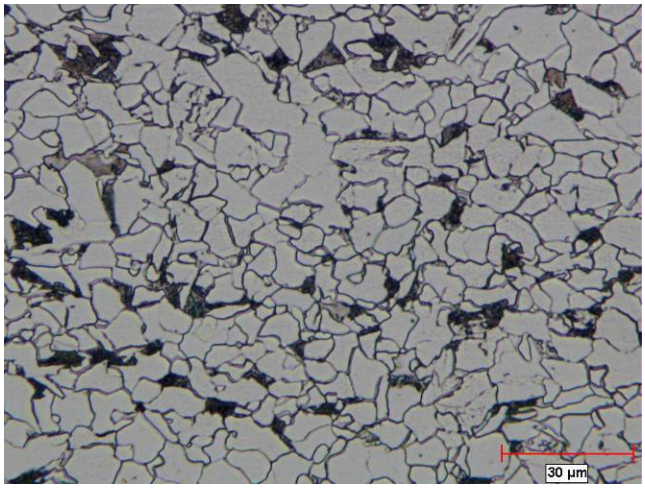

(c) Detail of transverse section.

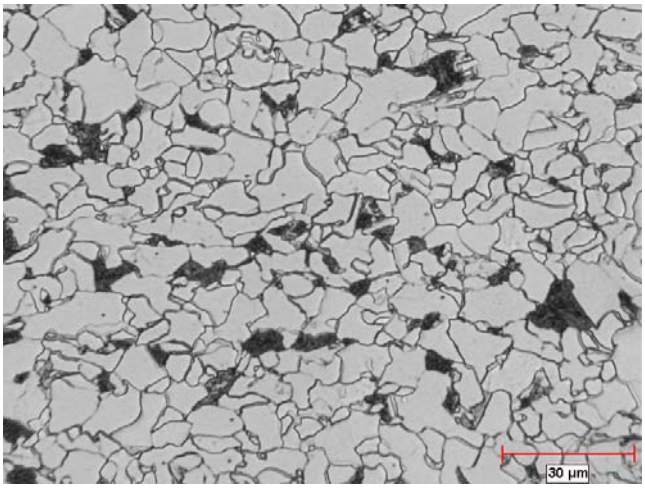

(d) Detail of longitudinal section.

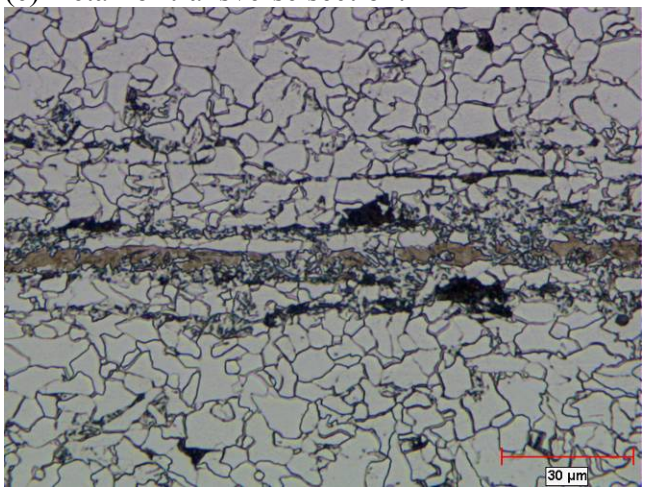

(e) Detail of transverse section showing microstructural banding.

Fig. 38 – Optical micrographs of Nital-etched metallographic cross-sections of the as-received hot-rolled dual-phase steel.

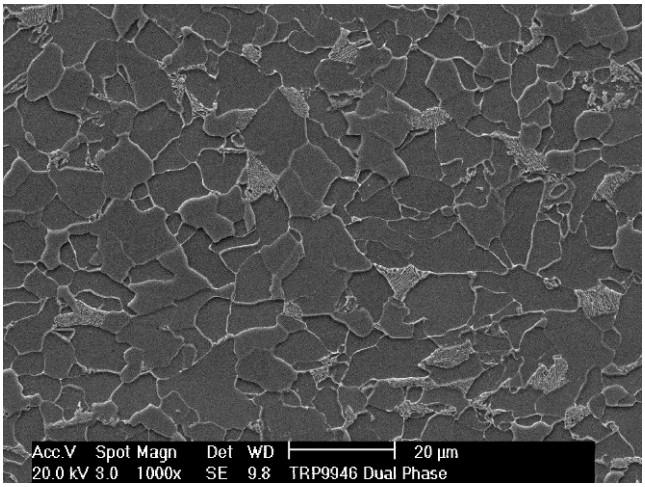

(a) The microstructure is composed of a mixture of ferrite and pearlite grains.

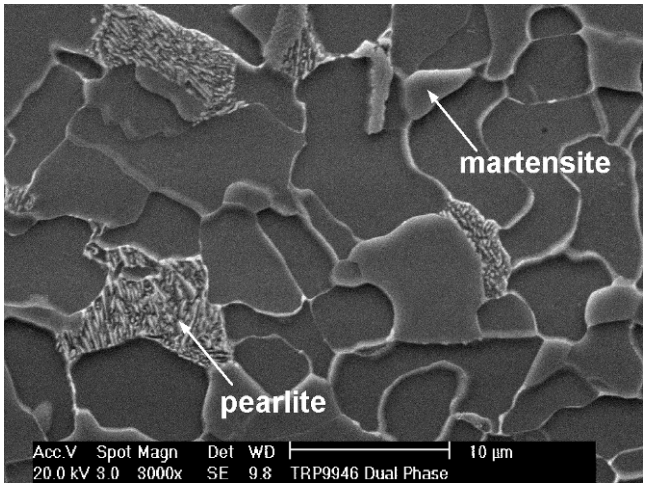

(b) Small martensite grains are also visible at higher magnification.

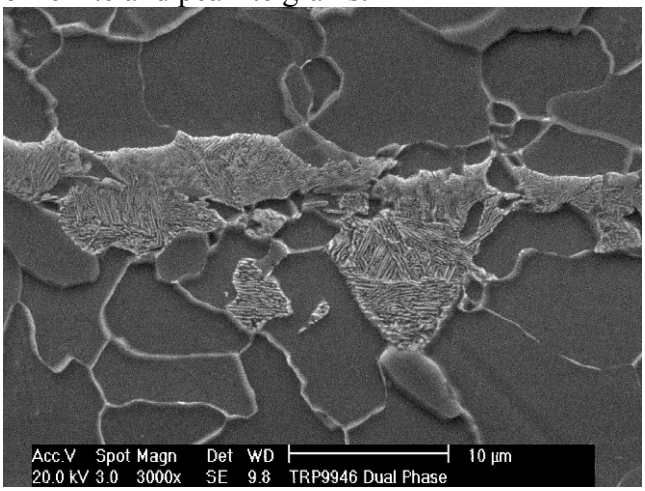

(c) Detail of pearlite islands in banded region.

Fig. 39 – SEM micrographs of a Nital-etched transverse cross-section of the as-received hot-rolled dual-phase steel.

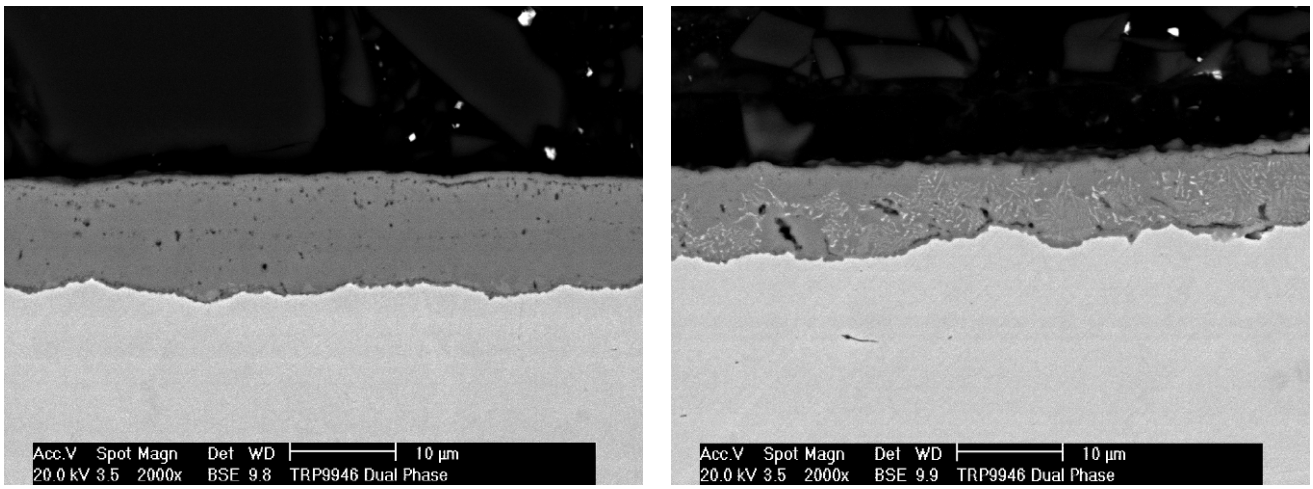

(a) Hot-rolled scale on one side of the panel. (b) Hot-rolled scale on opposite side of panel.

Fig. 40 – SEM micrographs of as-polished longitudinal cross-section showing the surface condition of the as-received hot-rolled dual-phase steel panels.

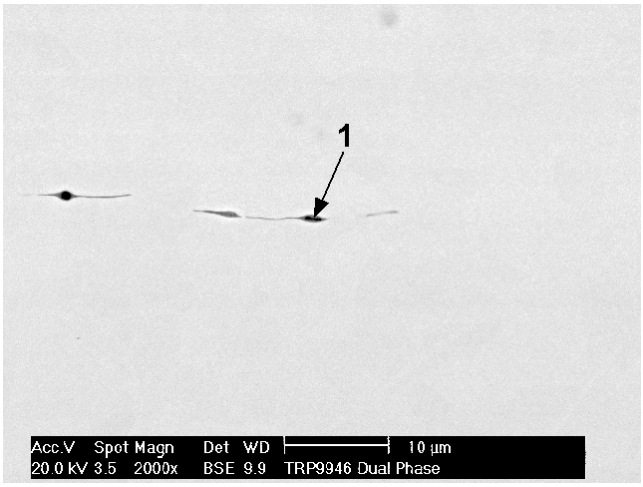

(a) BSE micrograph of an elongated MnS inclusion (spot 1).

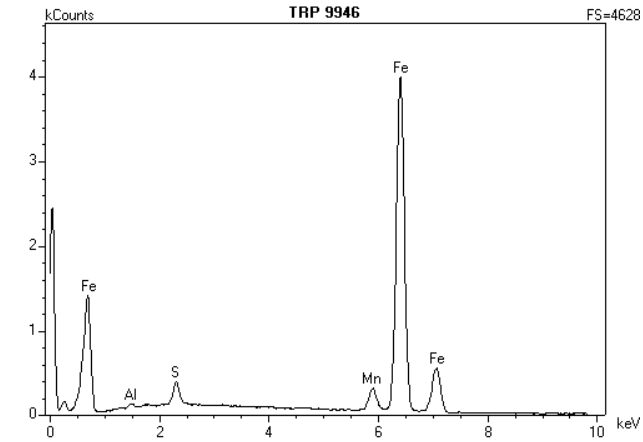

(b) EDS spectrum obtained from spot 1 on (a).

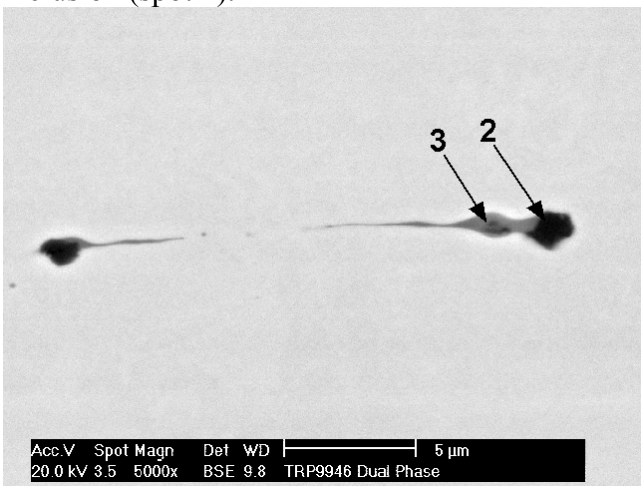

(c) BSE image of an Al_2O_3 inclusion (spot 2) attached to an elongated MnS (spot 3).

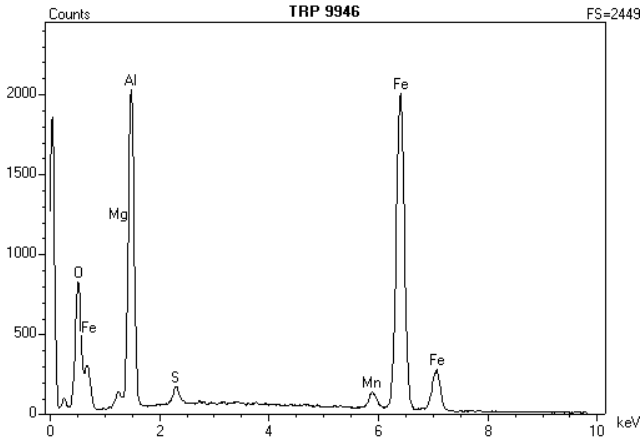

(d) EDS spectrum obtained from spot 2 on (c).

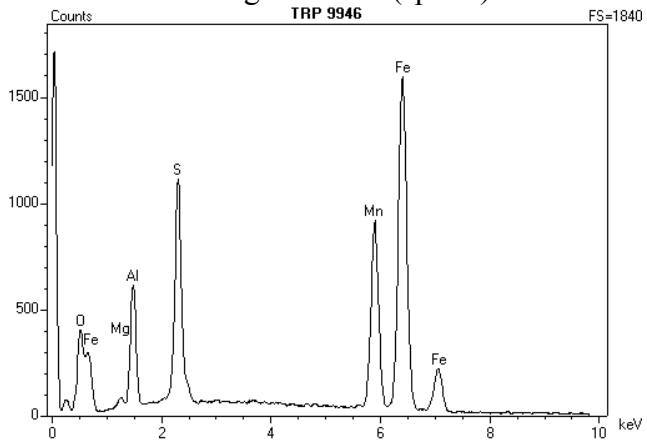

(e) EDS spectrum obtained from spot 3 on (c).

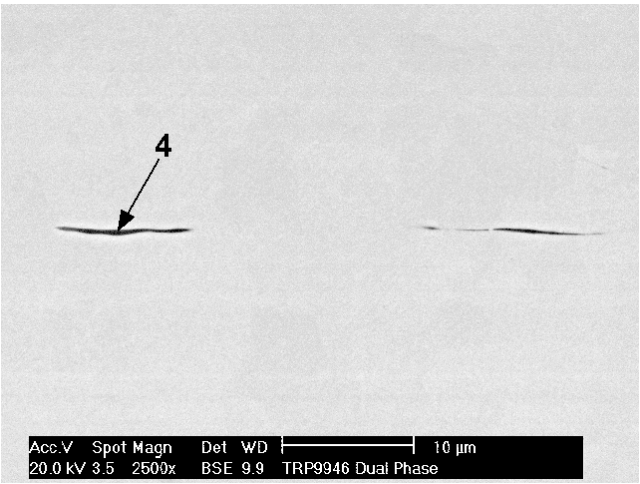

(f) BSE image of an elongated MnS (spot 4).

Fig. 41 – SEM micrographs and EDS spectra of typical inclusions on an as-polished longitudinal cross-section of the as-received hot-rolled dual-phase steel.

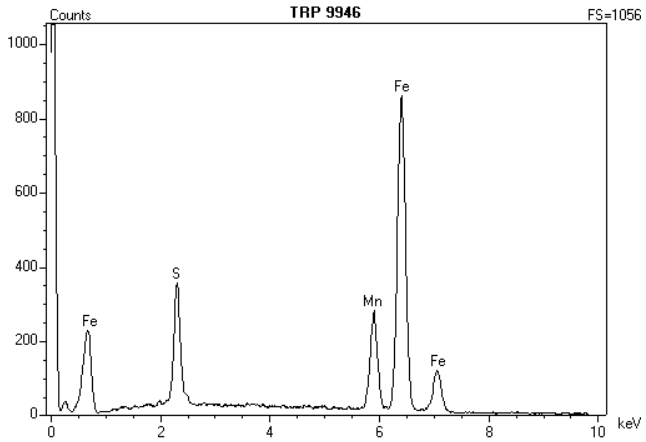

(g) EDS spectrum obtained from spot 4 on (f).

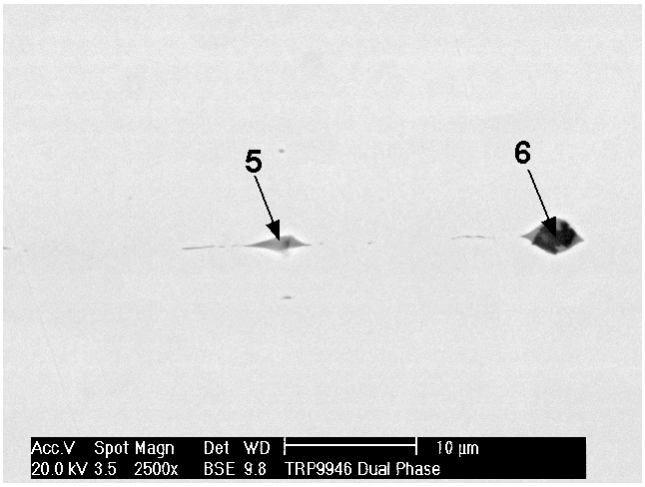

(h) BSE image of MnS (spot 5) and oxide (spot 6) inclusions.

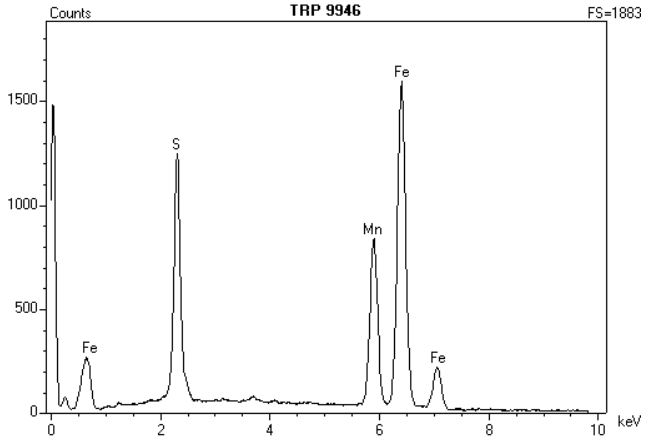

(i) EDS spectrum obtained from spot 5 on (h).

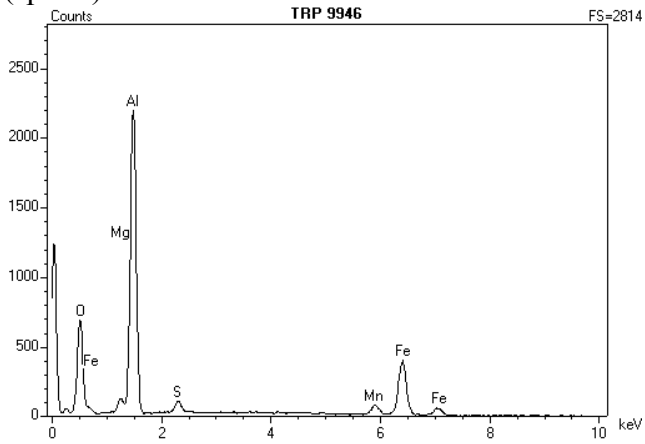

(j) EDS spectrum obtained from spot 6 on (h).

Fig. 41 – SEM micrographs and EDS spectra of typical inclusions on an as-polished longitudinal cross-section of the as-received hot-rolled dual-phase steel (continued).

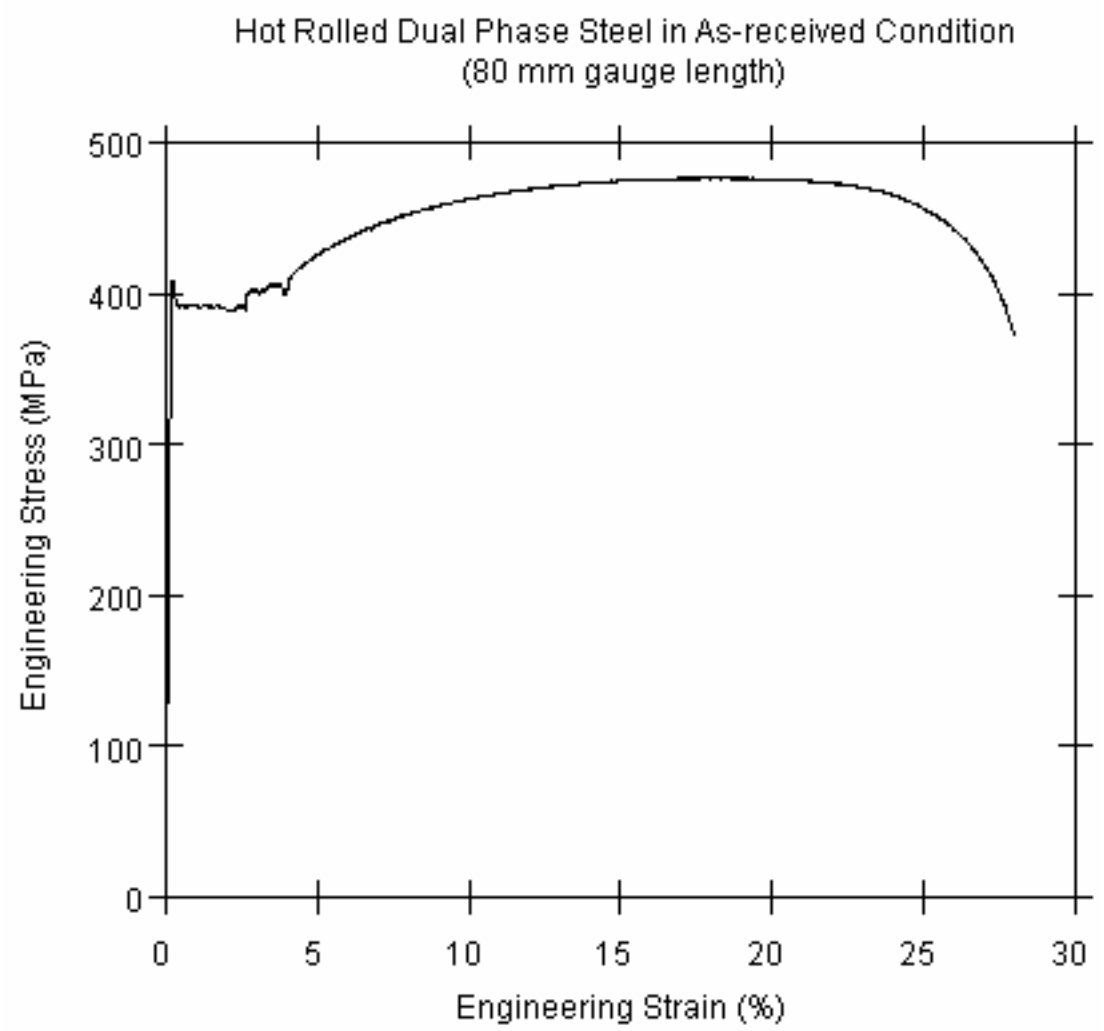

Fig. 42 – Representative engineering stress versus engineering strain plot for the as-received hot-rolled dual-phase steel showing yield point elongation behavior.

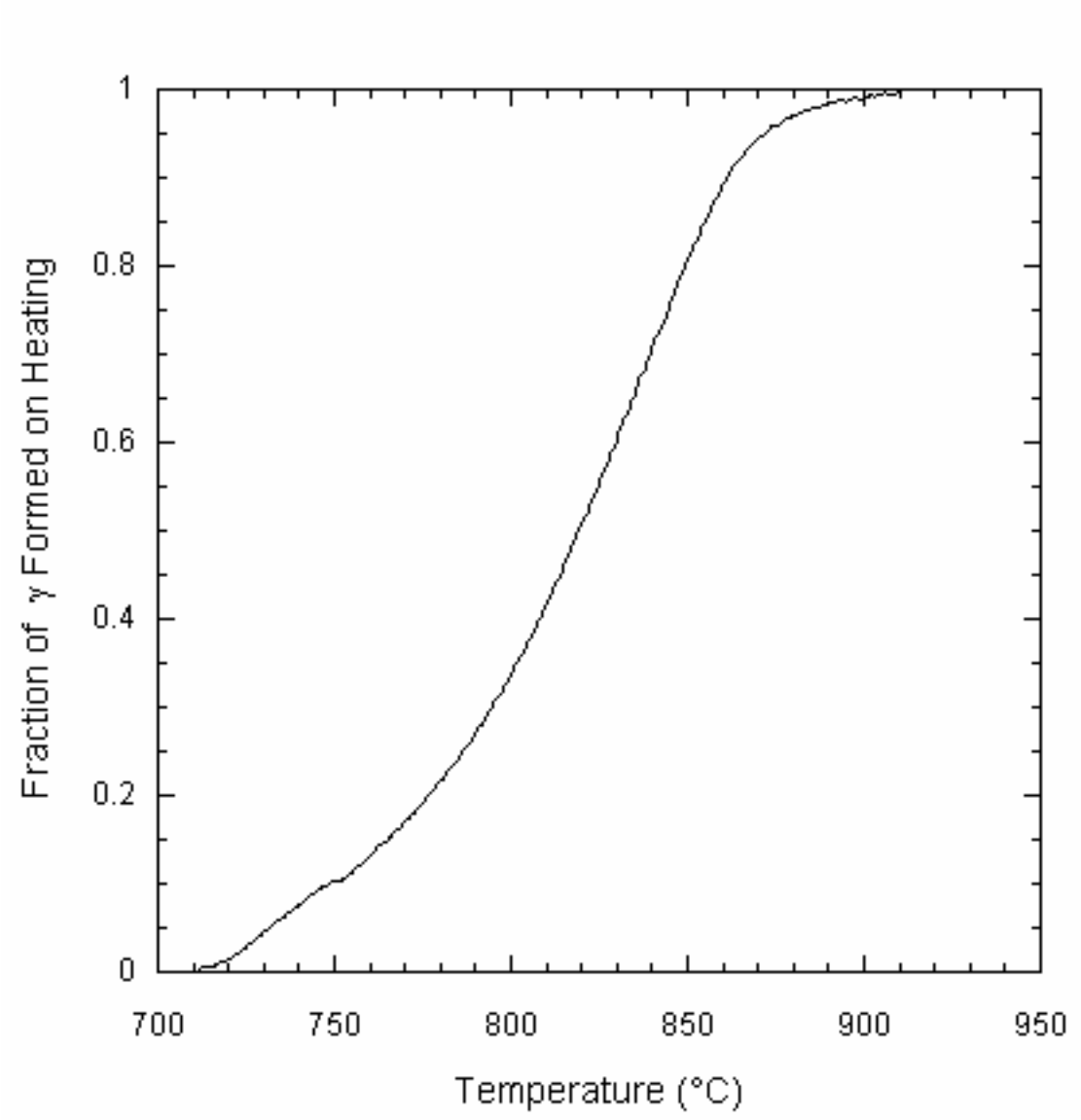

Fig. 43 – Formation of austenite on heating of dual-phase steel.

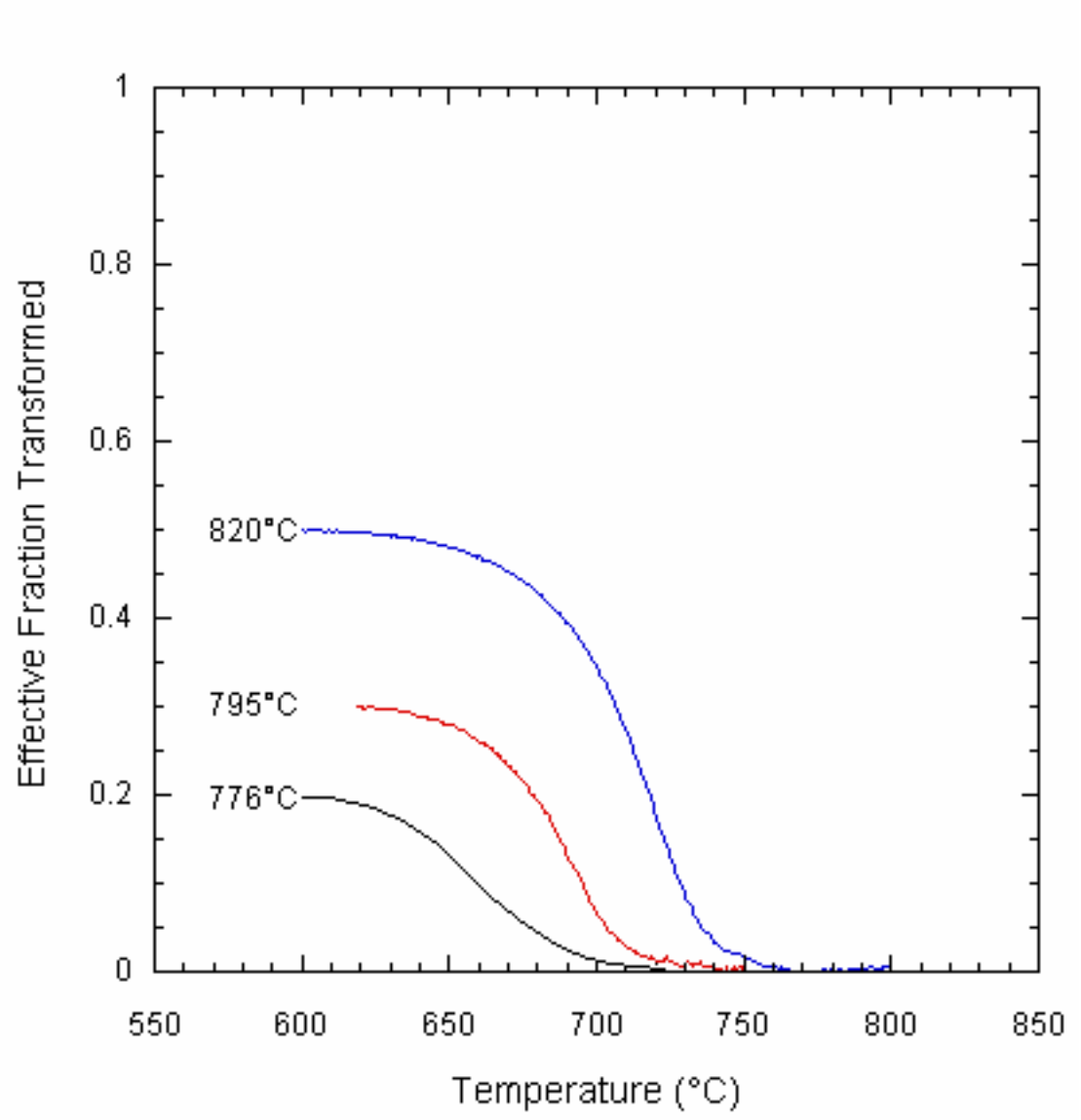

Fig. 44 – Transformation of austenite on cooling of dual-phase steel.

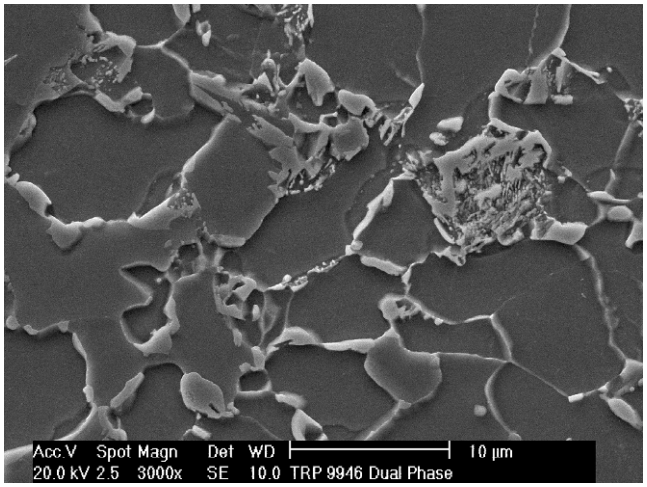

(a) DP214: 776°C/1 min + 10°C/s (Nital etch).

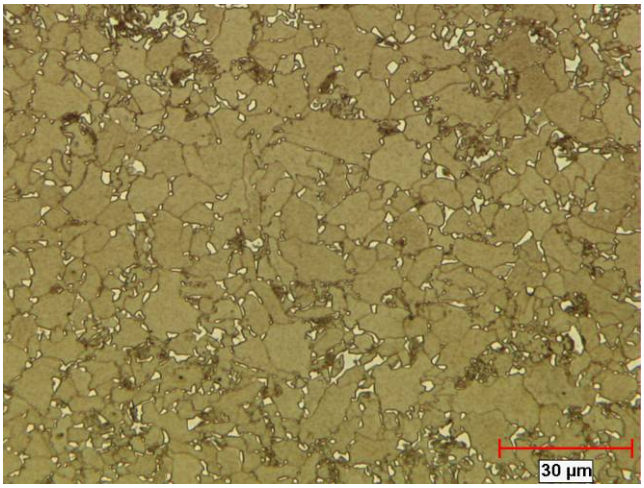

(b) DP214: 776°C/1 min + 10°C/s (LePera etch).

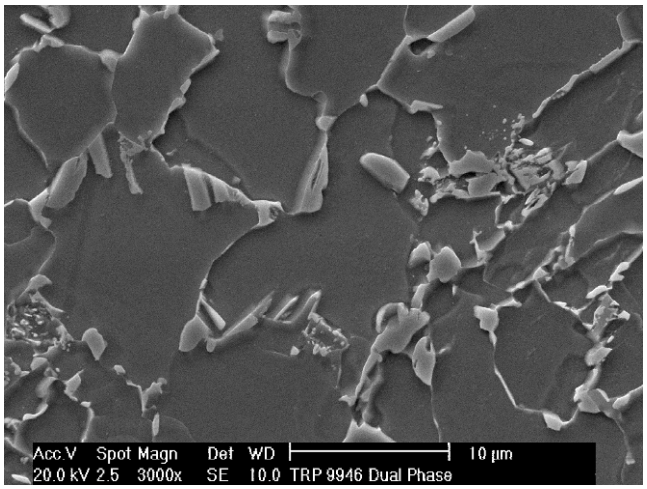

(c) DP215: 795°C/1 min + 10°C/s (Nital etch).

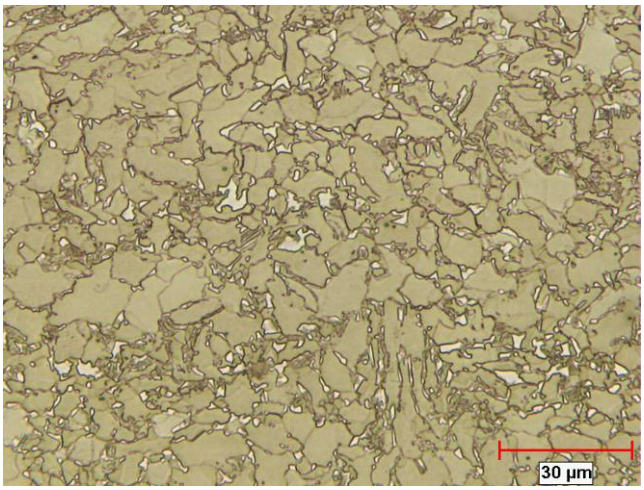

(d) DP215: 795°C/1 min + 10°C/s (LePera etch).

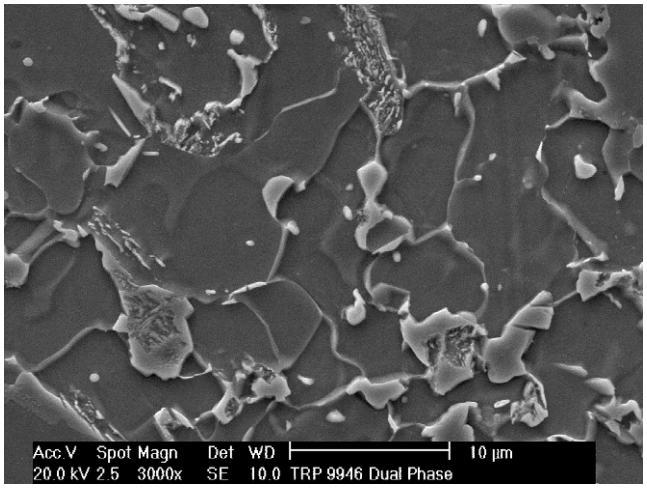

(e) DP216: 820°C/1 min + 10°C/s (Nital etch).

(f) DP216: 820°C/1 min + 10°C/s (LePera etch).

Fig. 45 – Optical micrographs of the microstructures of the samples after dilatometer trials.

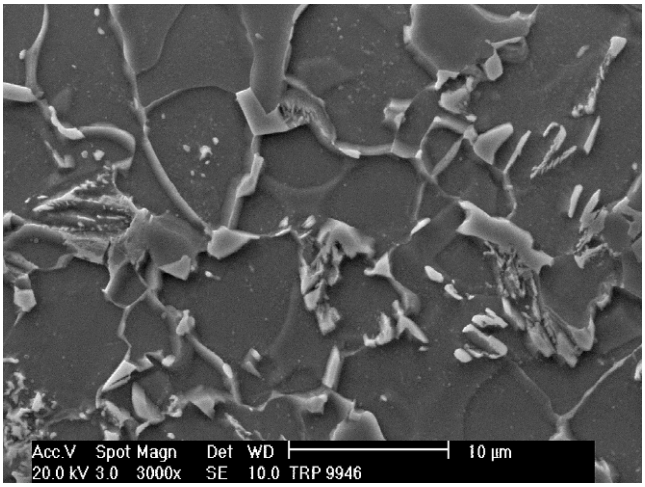

(g) DP246: 820°C/2 min + 10°C/s (Nital etch).

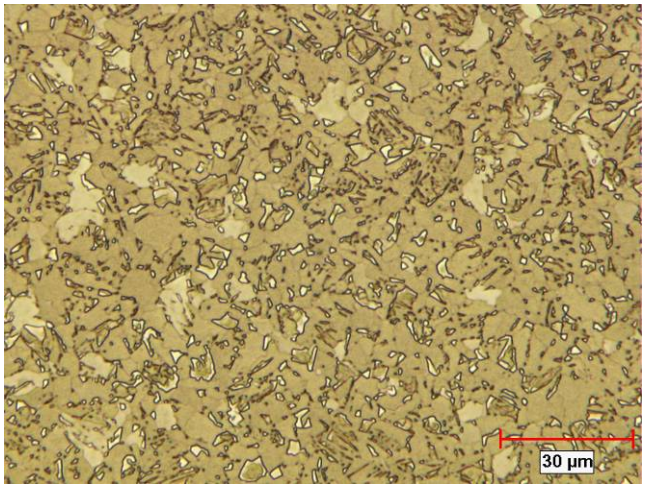

(h) DP246: 820°C/2 min + 10°C/s (LePera etch).

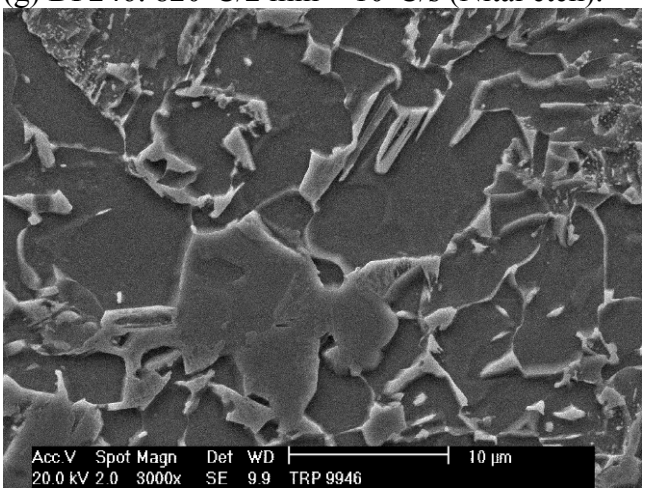

(i) DP249: 820°C/1 min + 25°C/s (Nital etch).

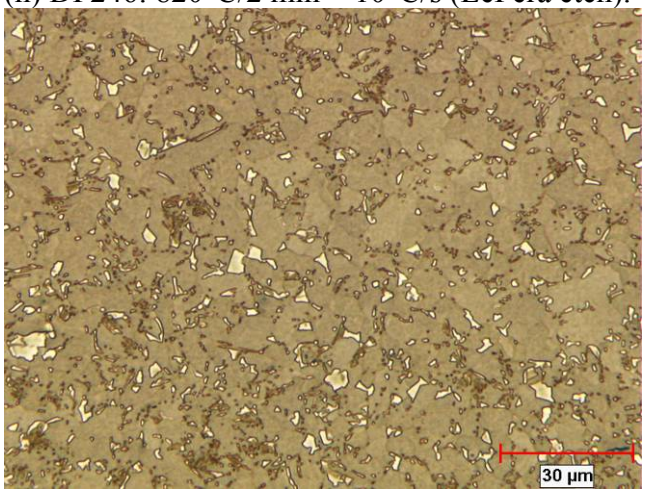

(j) DP249: 820°C/1 min + 25°C/s (LePera etch).

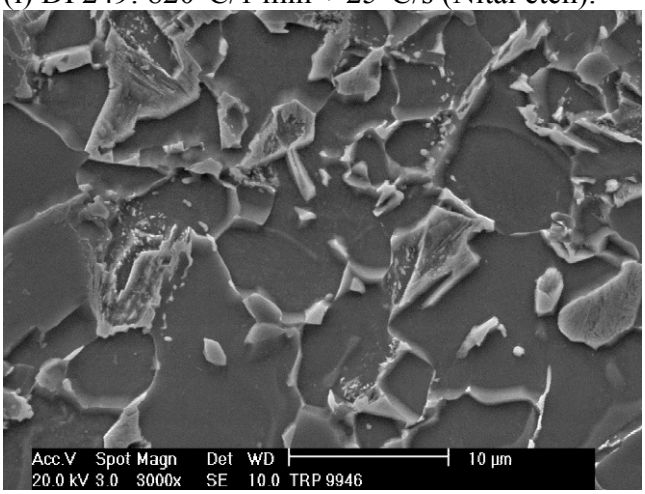

(k) DP248: 820°C/2 min + 25°C/s (Nital etch).

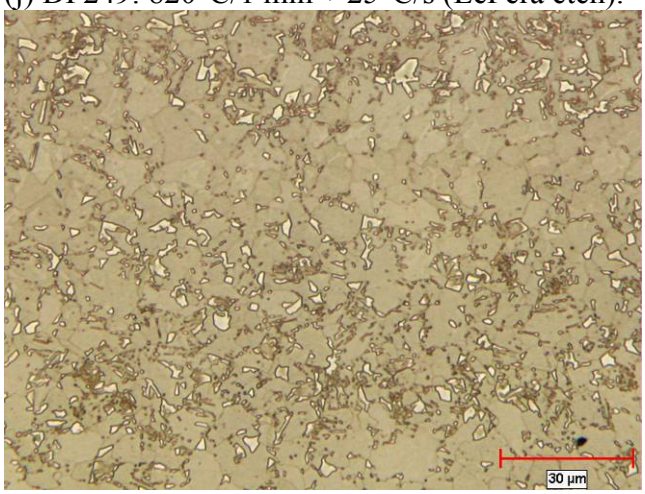

(l) DP248: 820°C/2 min + 25°C/s (LePera etch).

Fig. 45 – Optical micrographs of the microstructures of the samples after dilatometer trials. (continued).

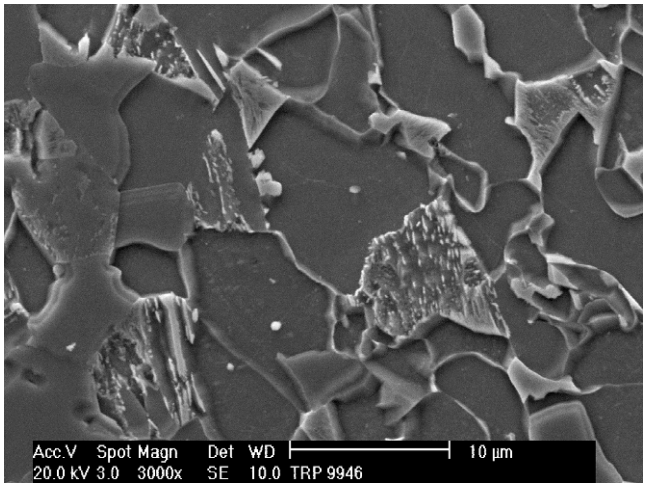

(m) DP252: 950°C/5 min + 10°C/s (Nital etch).

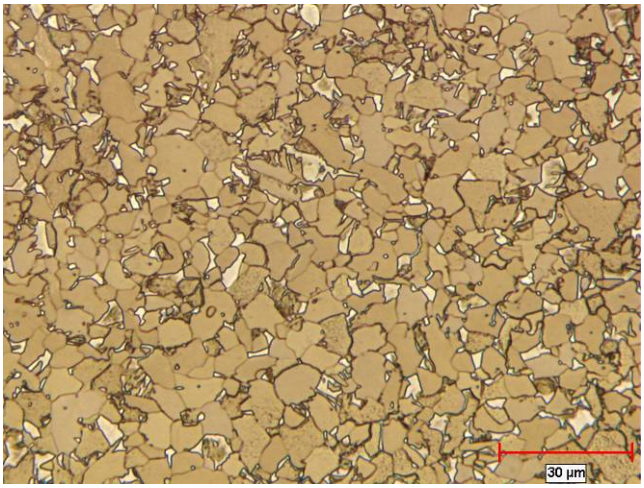

(n) DP252: 950°C/5 min + 10°C/s (LePera etch).

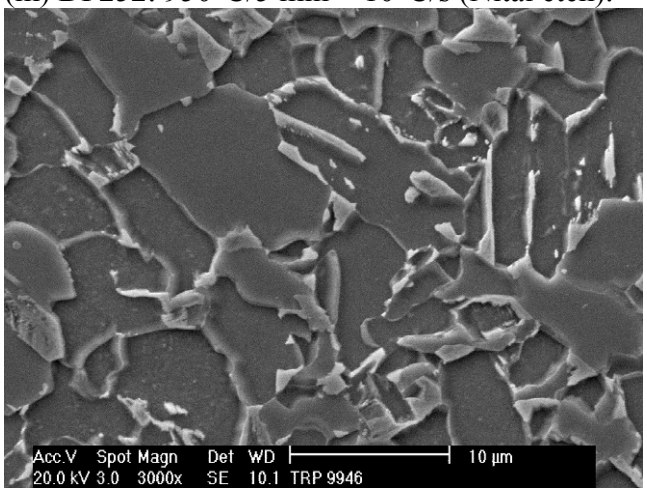

(o) DP253: 950°C/5 min + 25°C/s (Nital etch).

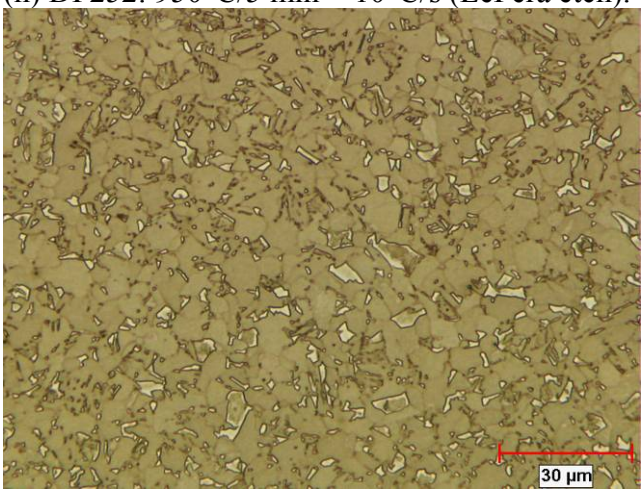

(p) DP253: 950°C/5 min + 10°C/s

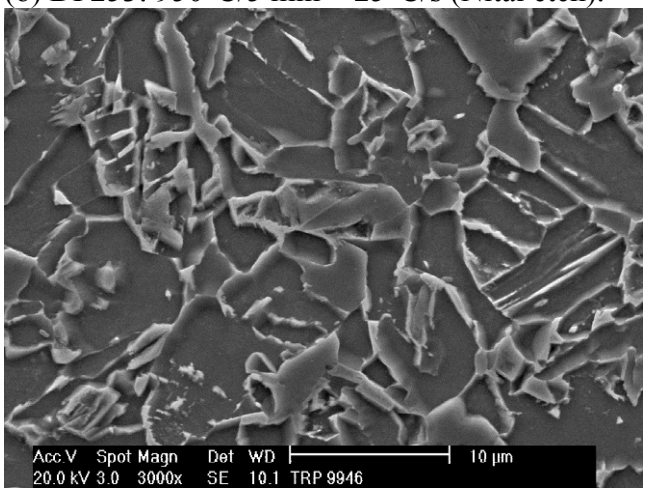

(q) DP255: 950°C/5 min + 50°C/s (Nital etch).

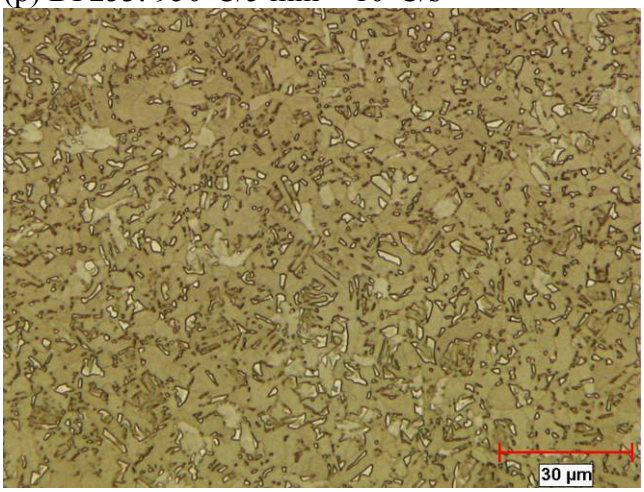

(r) DP255: 950°C/5 min + 50°C/s

Fig. 45 – Optical micrographs of the microstructures of the samples after dilatometer trials (continued)

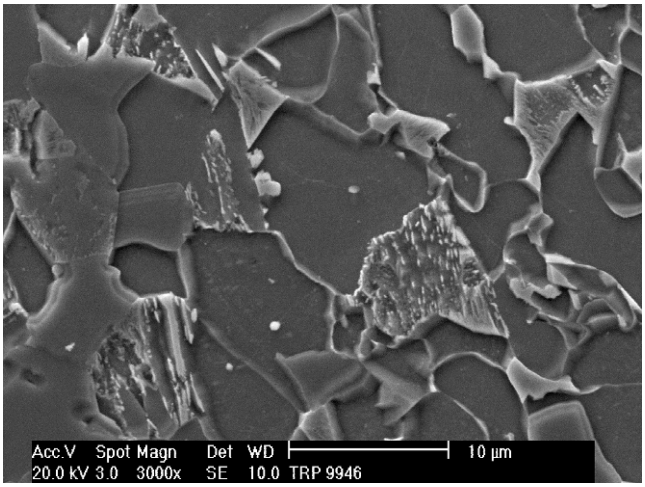

(s) DP254: DP254 820°C/2 min + 10°C/s + 460°C/1 min (Nital etch)

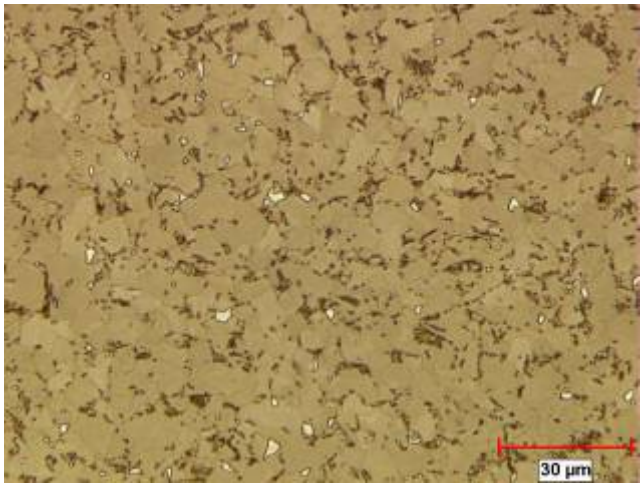

(t) DP254: DP254 820°C/2 min + 10°C/s + 460°C/1 min (LePera etch)

Fig. 45 – Optical micrographs of the microstructures of the samples after dilatometer trials (continued)

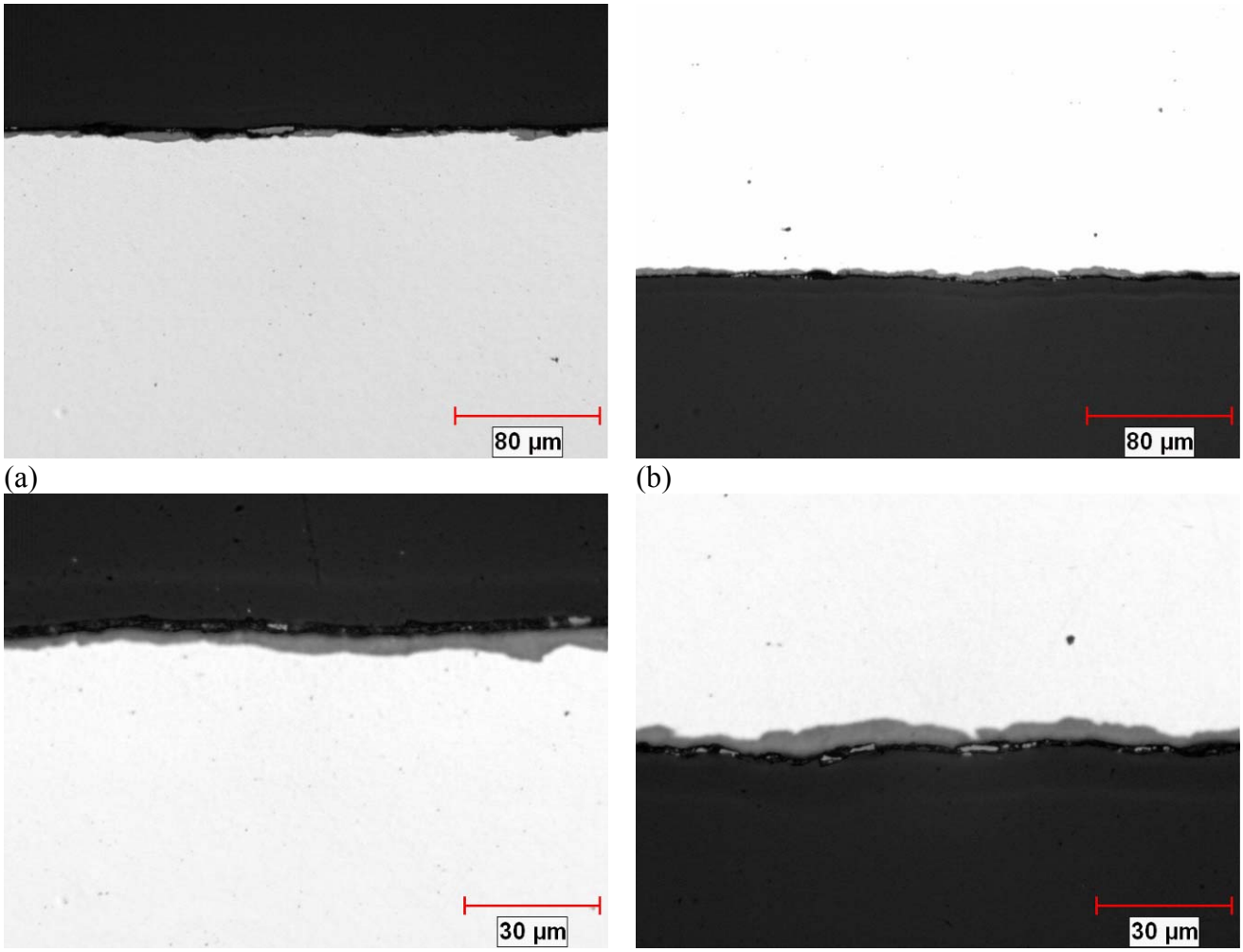

Fig. 46 – Optical micrographs of the polished longitudinal cross-section of hot-rolled TRIP steel.

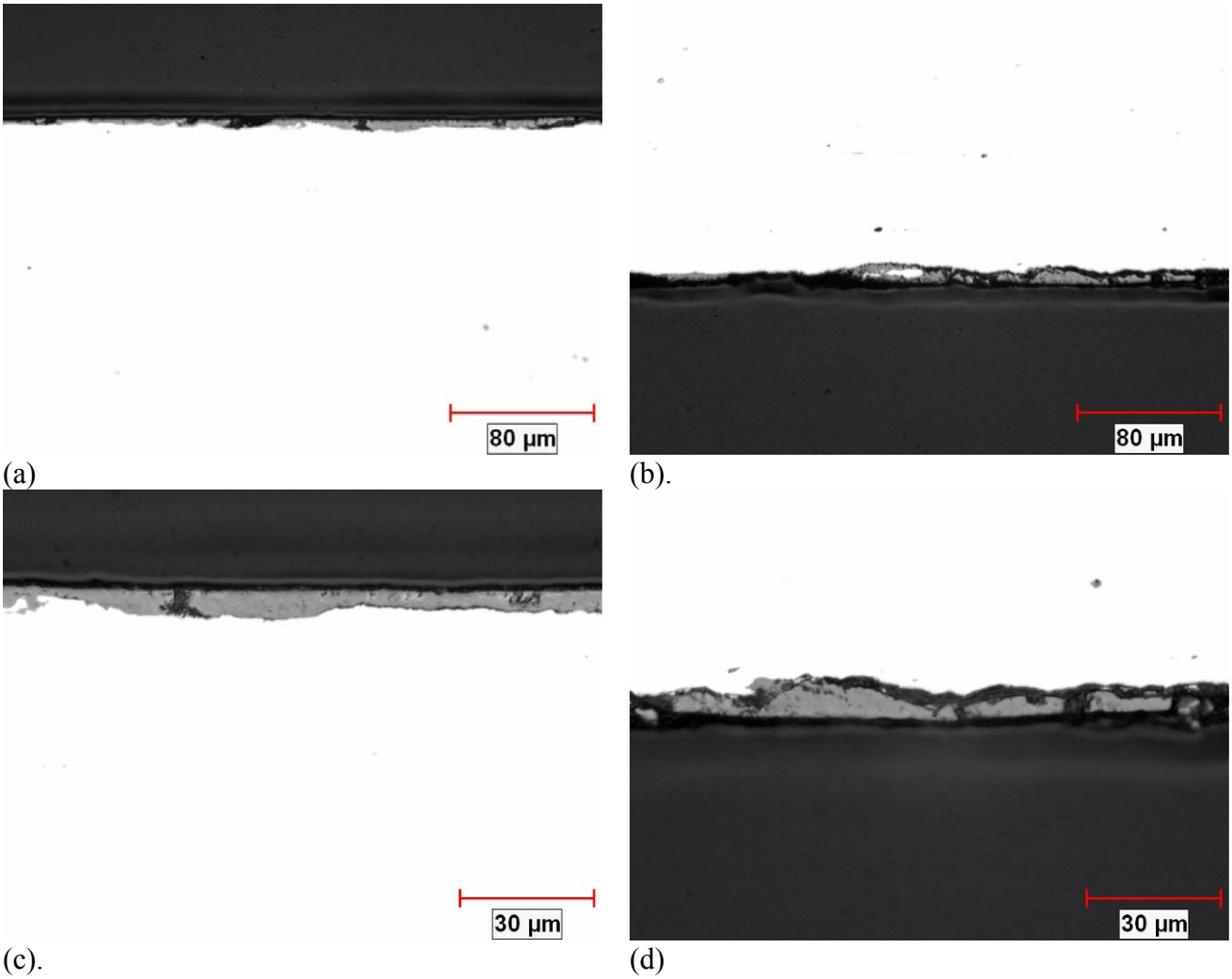

(a) (b). (c). (d)

Fig. 47 – Optical micrographs of the polished transverse cross-section of hot-rolled TRIP steel.

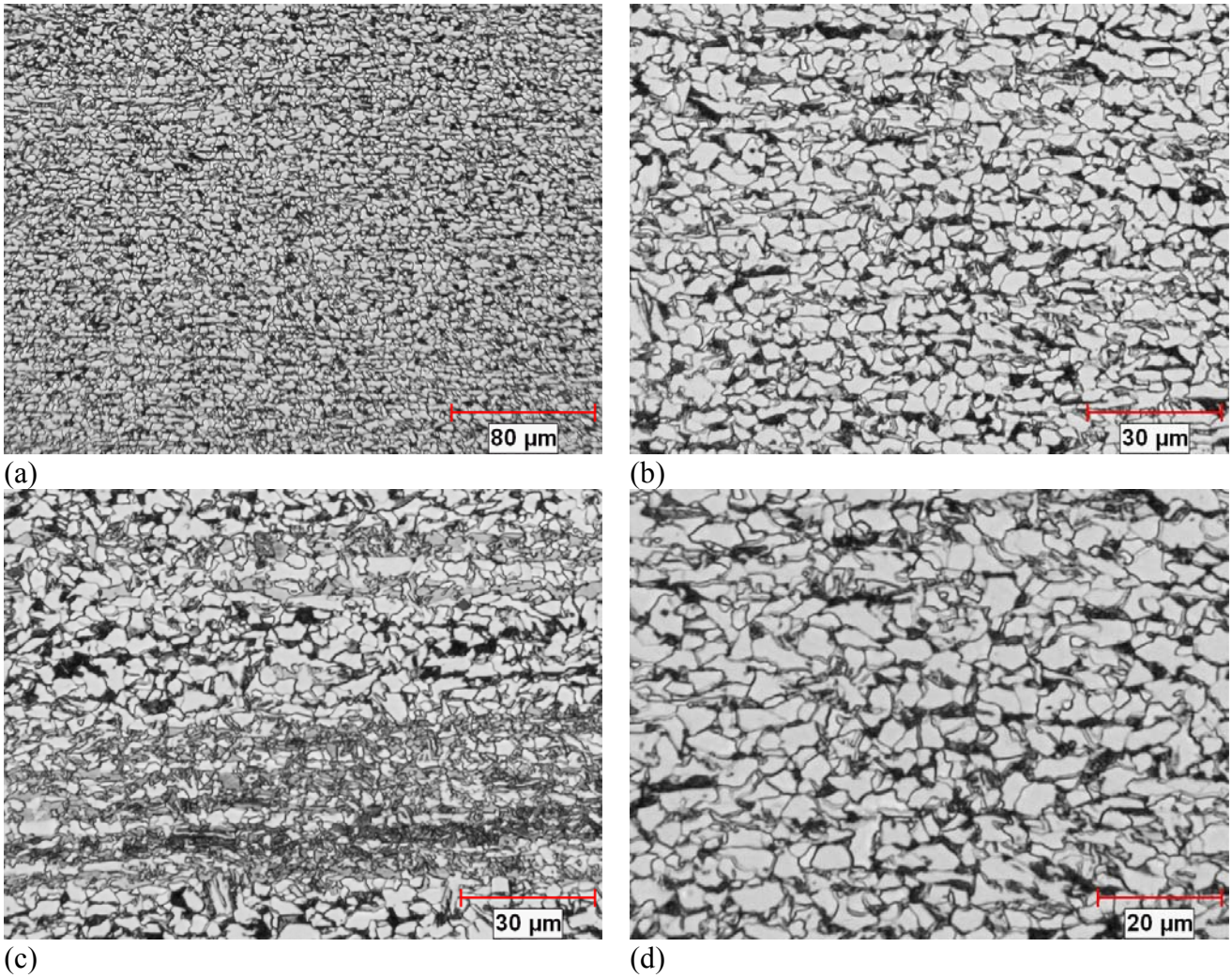

Fig. 48 – Optical micrographs of the longitudinal cross-section of hot-rolled TRIP steel etched with Nital.

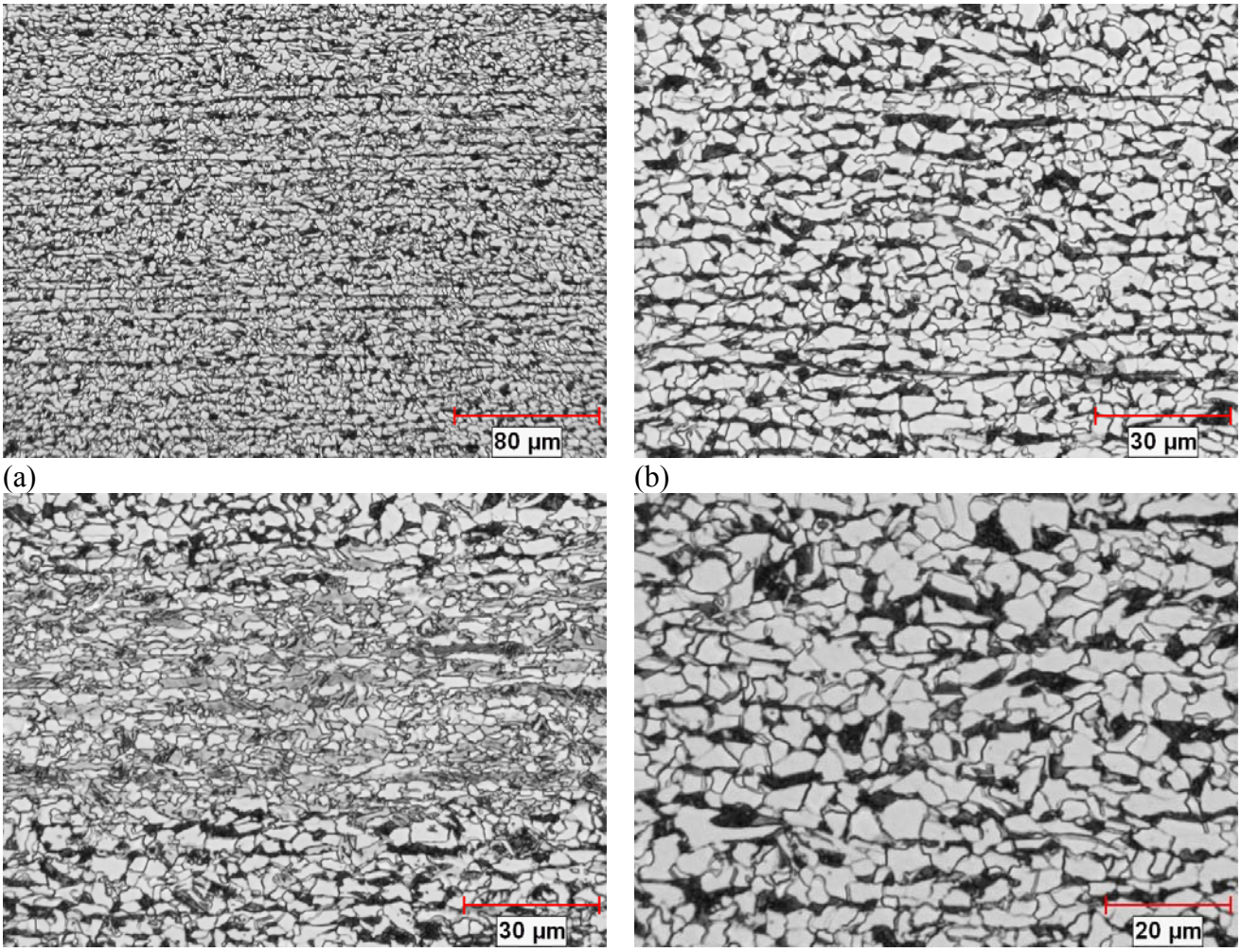

Fig. 49 – Optical micrographs of the transverse cross-section of hot-rolled TRIP steel etched with Nital.

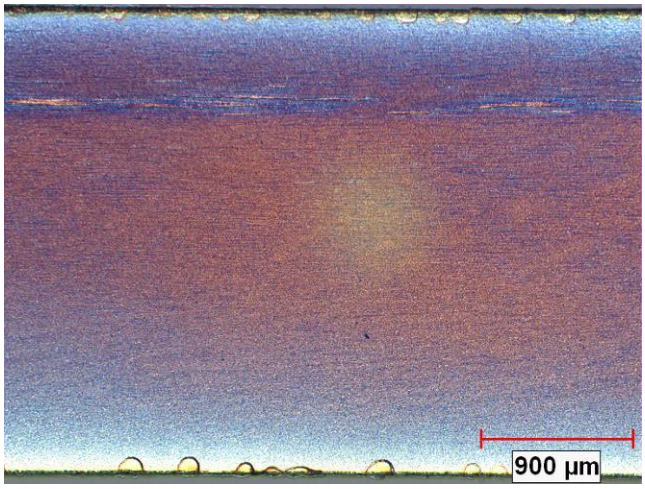

(a)

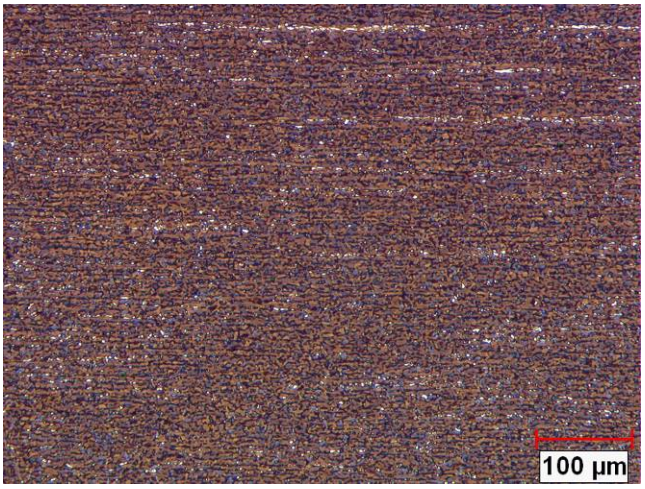

(b)

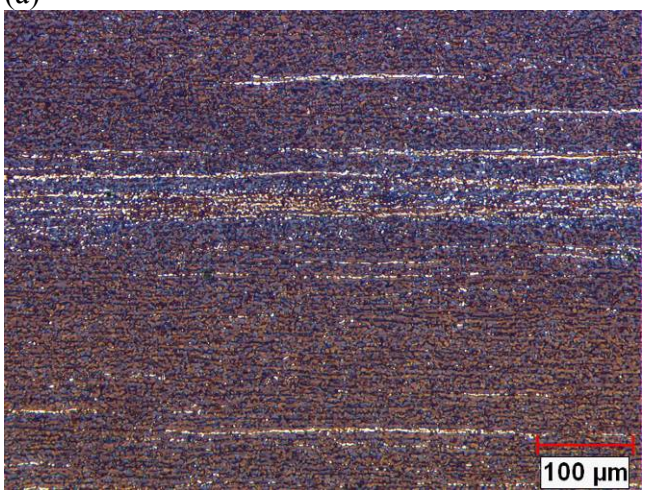

(c)

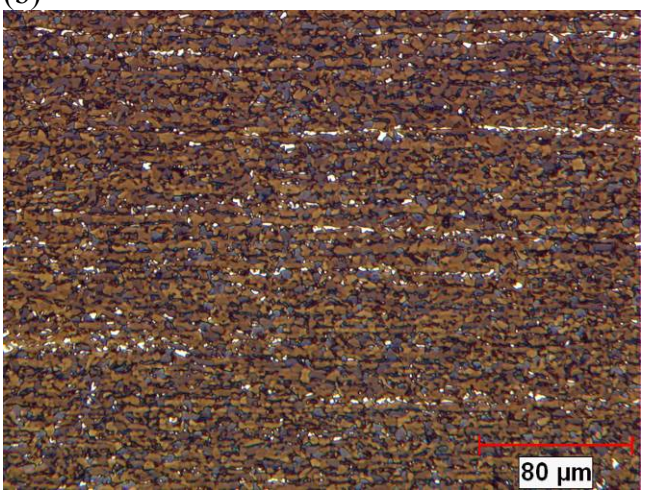

(d)

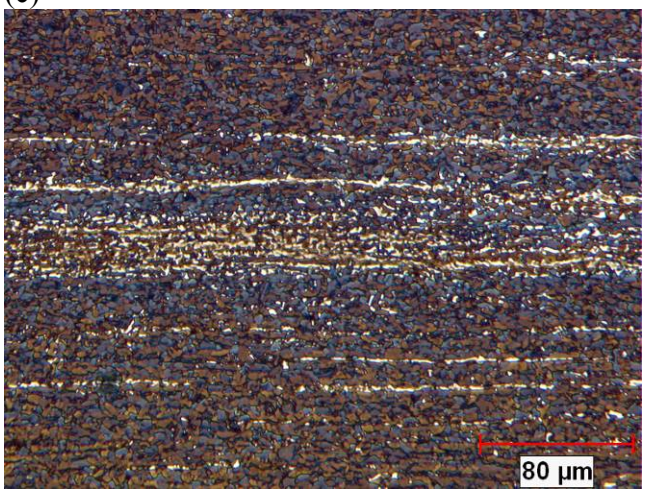

(e)

Fig. 50 – Optical micrographs of the longitudinal cross-section of hot-rolled TRIP steel etched with LePera reactive (sample near the edge of the rolling strip).

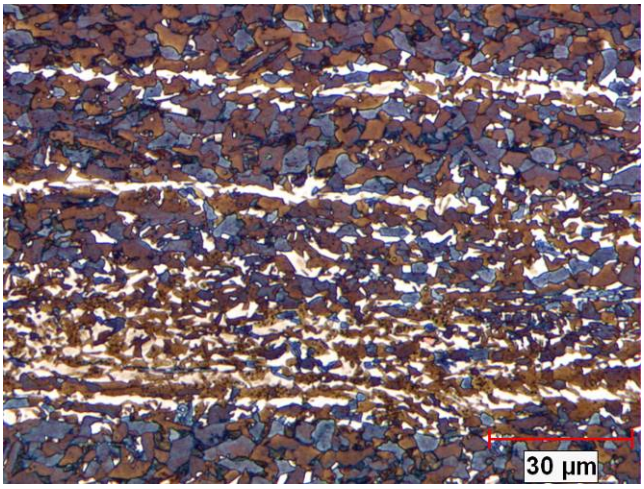

(f)

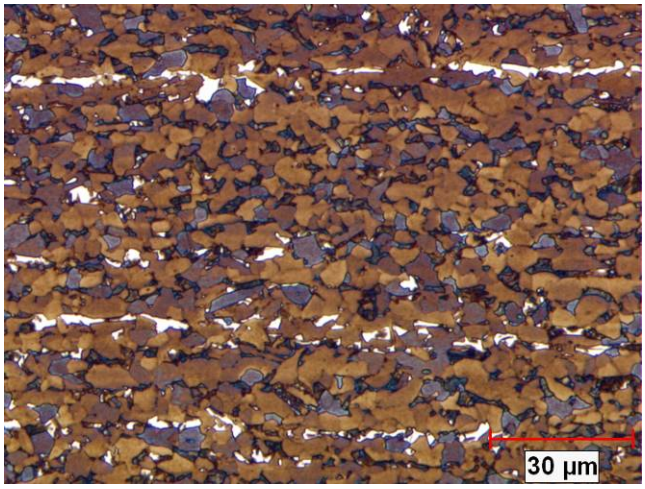

(g)

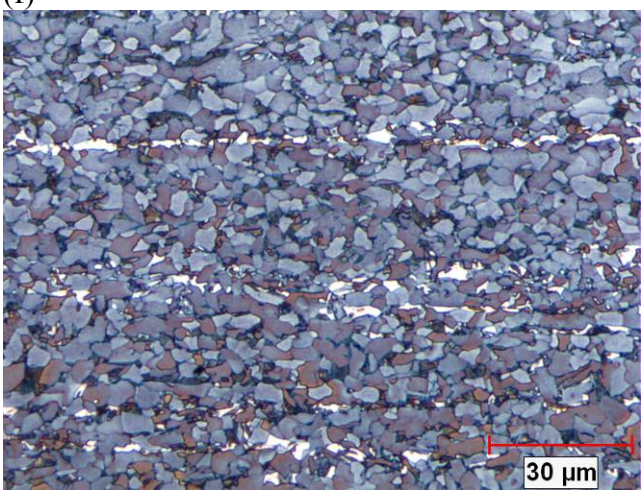

(h)

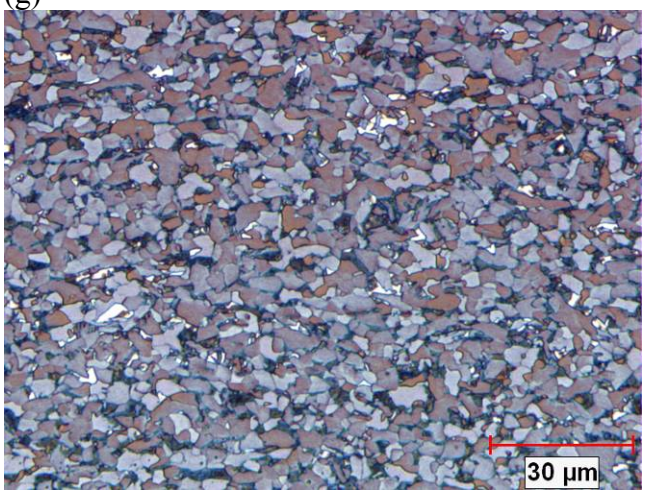

(i)

Fig. 50 – Optical micrographs of the longitudinal cross-section of hot-rolled TRIP steel etched with LePera reactive (sample near the edge of the rolling strip) (continued).

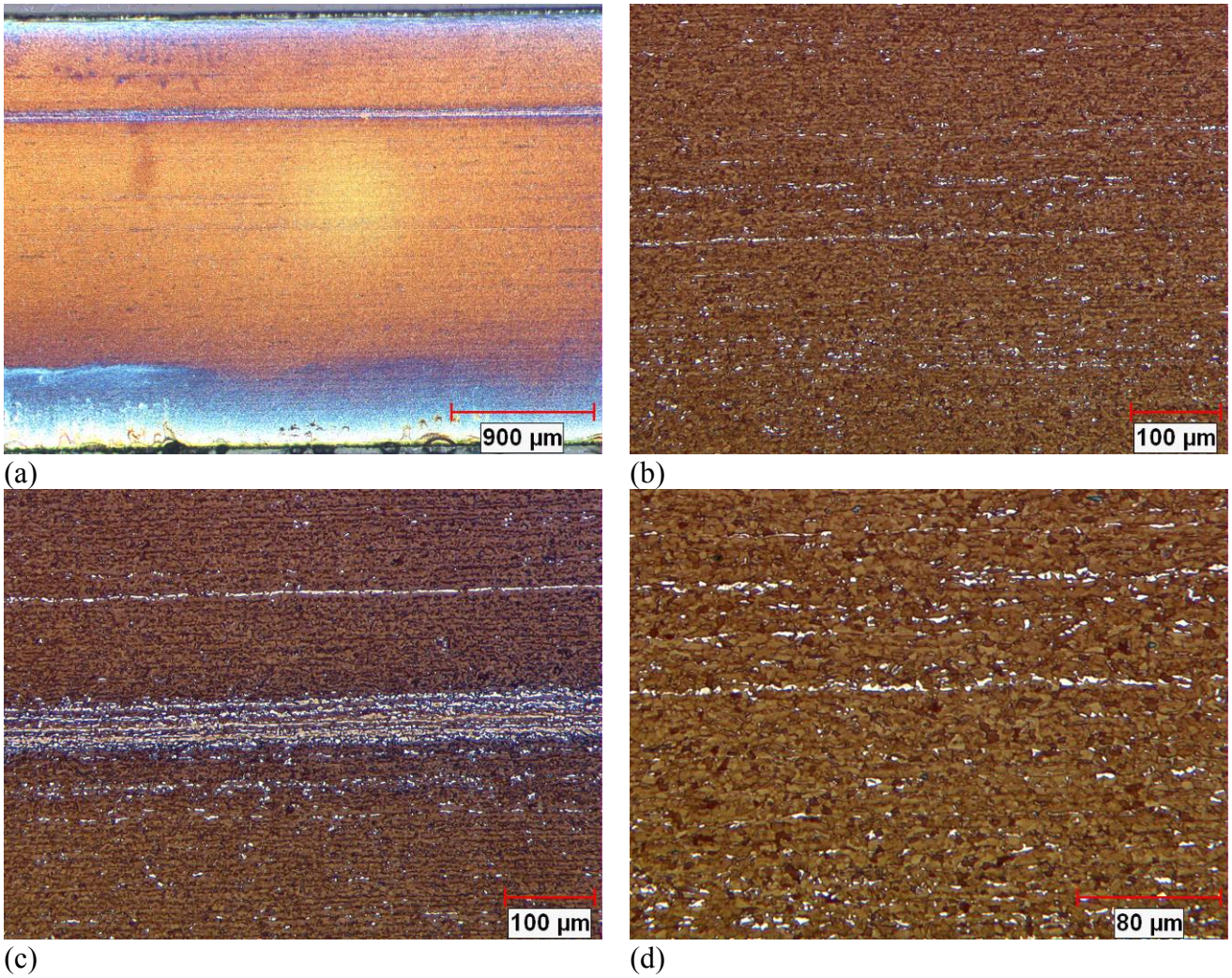

Fig. 51 – Optical micrographs of the transverse cross-section of hot-rolled TRIP steel etched with LePera reactive (sample near the edge of the rolling strip).

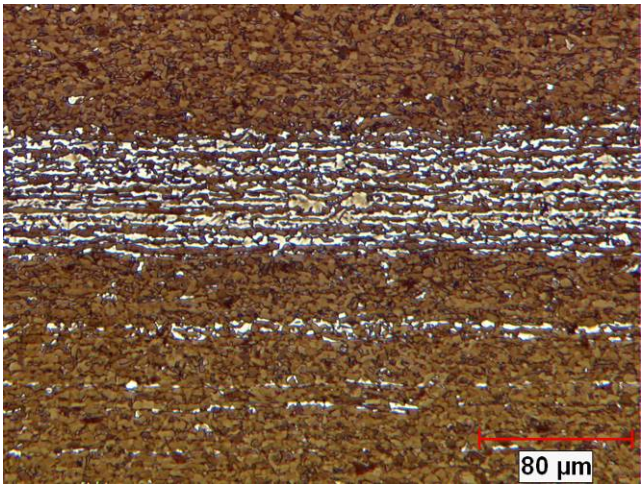

(e)

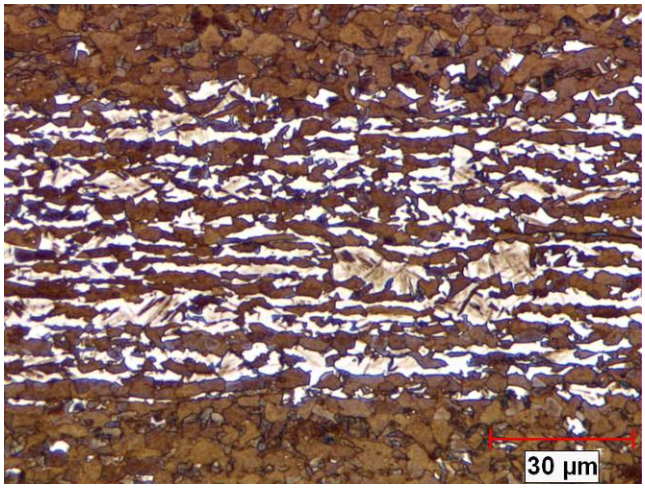

(f)

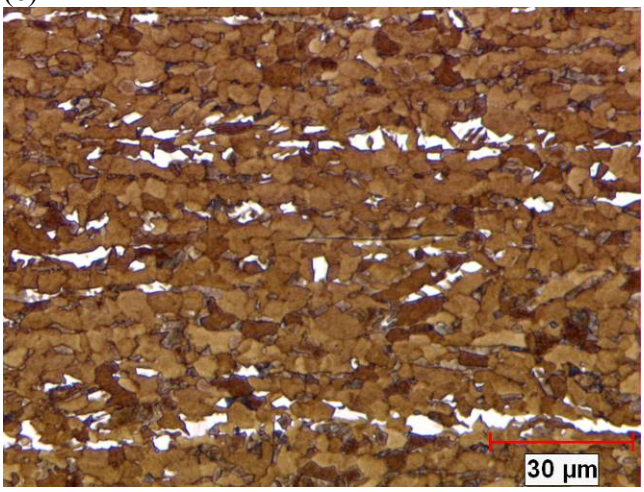

(g)

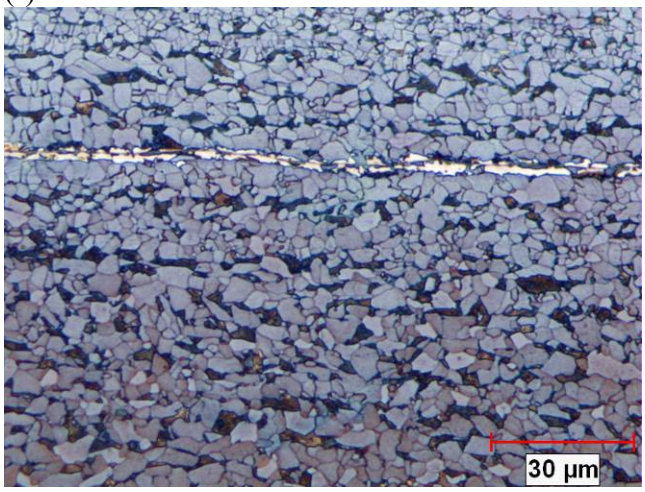

(h)

Fig. 51 – Optical micrographs of the transverse cross-section of hot-rolled TRIP steel etched with LePera reactive (sample near the edge of the rolling strip) (continued).

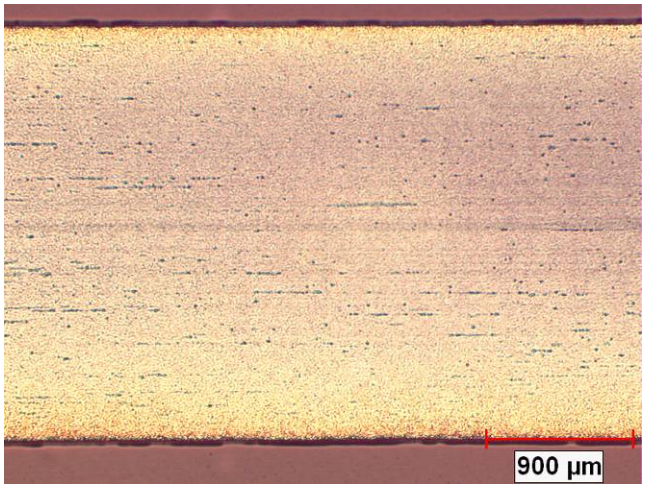

(a) longitudinal cross-section

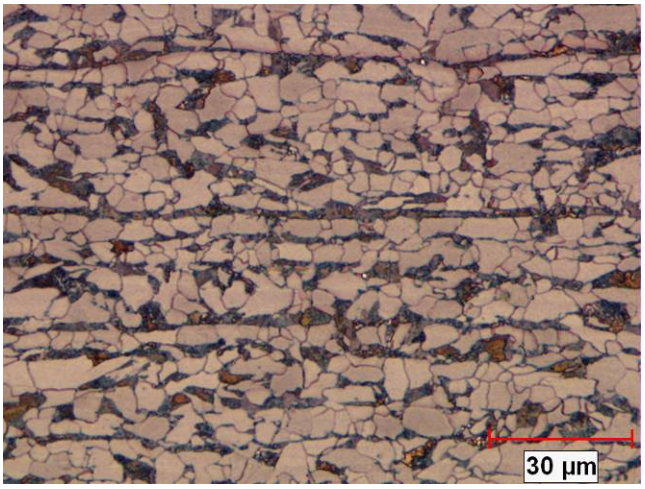

(b) longitudinal cross-section

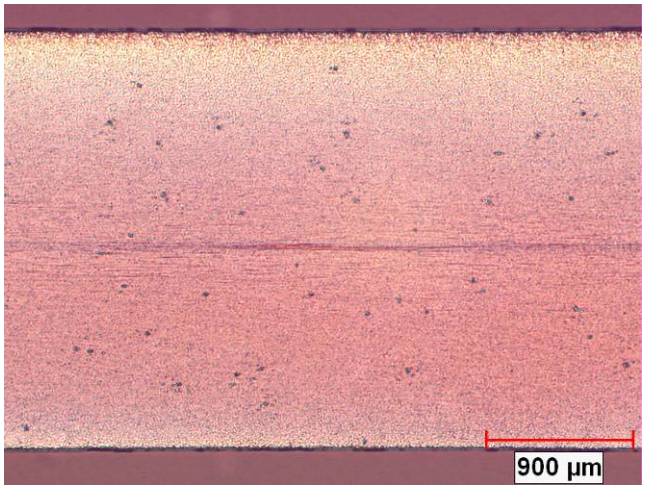

(c) transverse cross-section

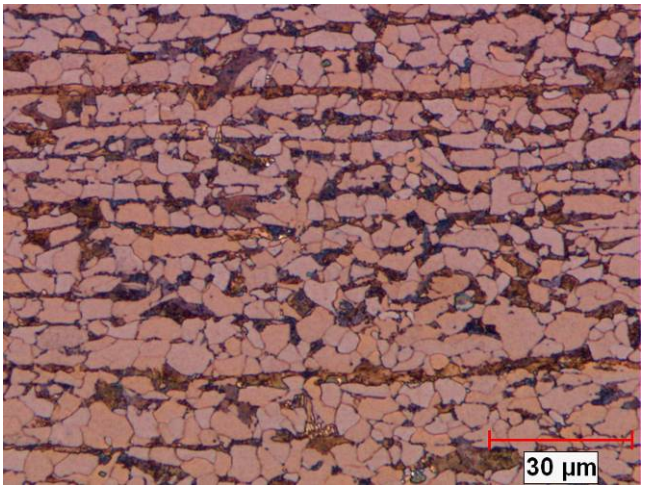

(d) transverse cross-section

Fig. 52 – Optical micrographs of hot-rolled TRIP steel etched with LePera reactive (middle of the plate).

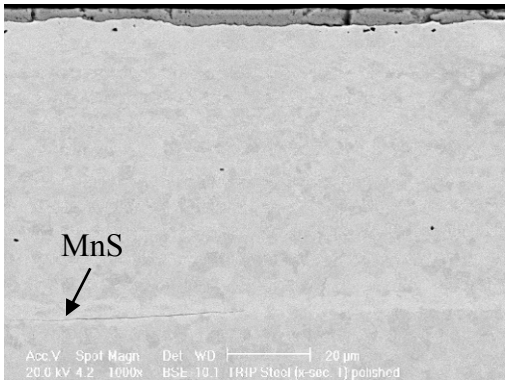

(a) BSE image of the sample near the edge

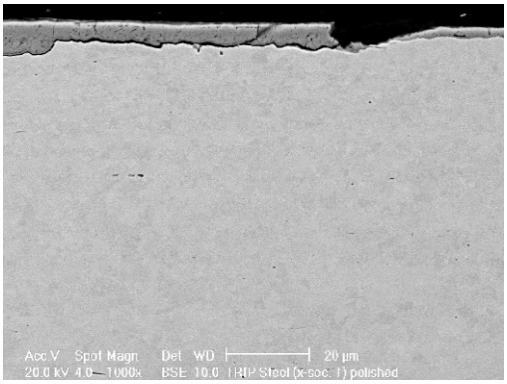

(b) BSE image of the opposite edge

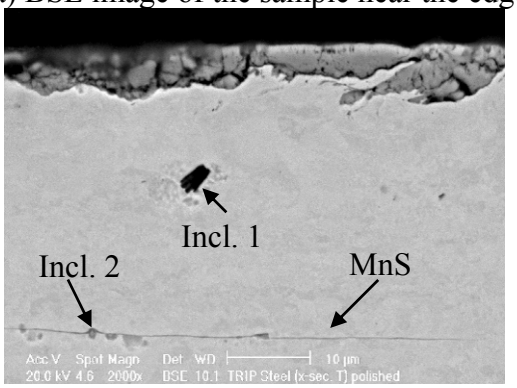

(c) BSE image of the polished sample revealing the inclusions

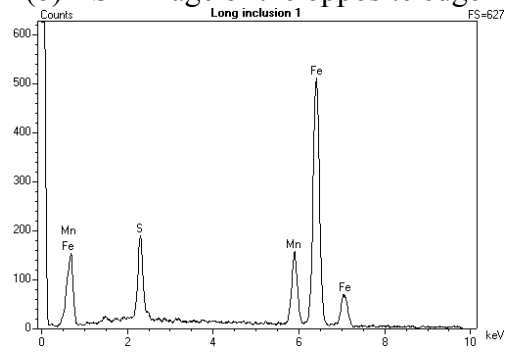

(d) EDS spectrum of the elongated MnS inclusions

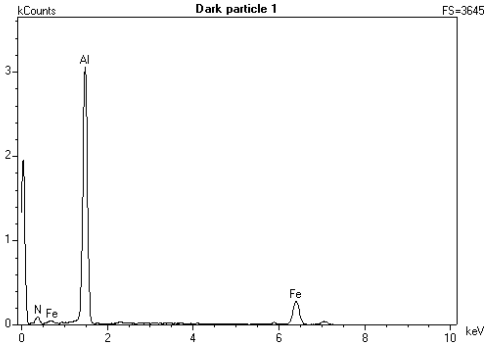

(e) EDS spectrum of inclusion 1

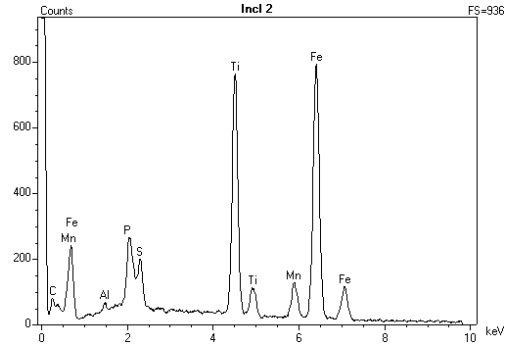

(f) EDS spectrum of inclusion 2

Fig. 53 – SEM BSE images and EDS spectra of the inclusions present in the TRIP steel sample in the hot-rolled condition (polished transverse cross-section).

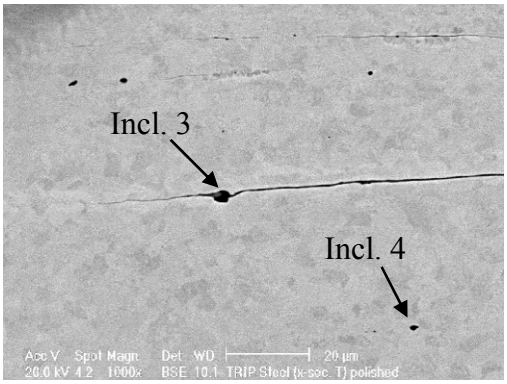

(g) BSE image of the inclusions present in the steel

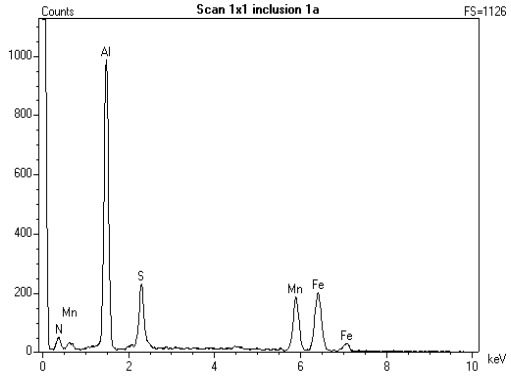

(h) EDS spectrum of the complex inclusion 3

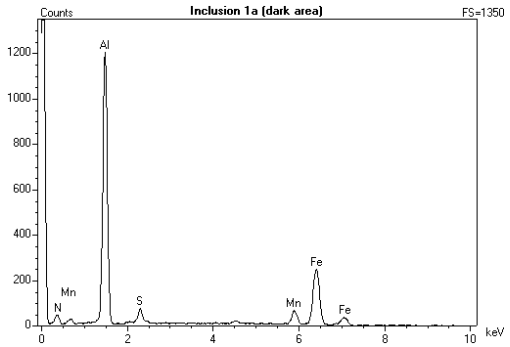

(i) EDS spectrum of dark area of inclusion 3

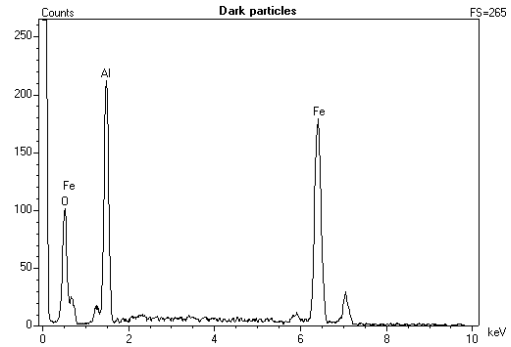

(j) EDS spectrum of inclusion 4

Fig. 54 – SEM BSE images and EDS spectra of the inclusions present in the TRIP steel sample in the hot-rolled condition (polished transverse cross-section) (continued)

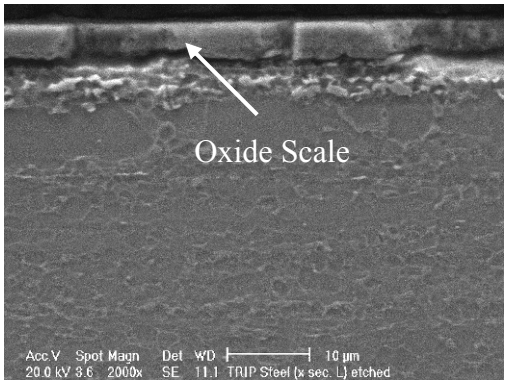

(a) SE image of the sample near the edge

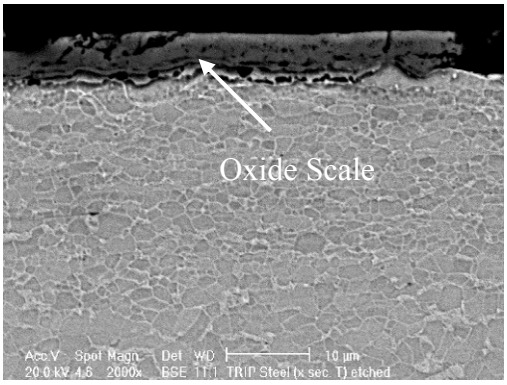

(b) BSE image of the opposite edge

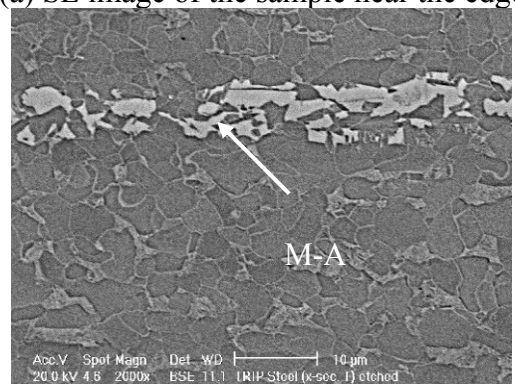

(c) BSE image shows a layer of M-A present in the matrix

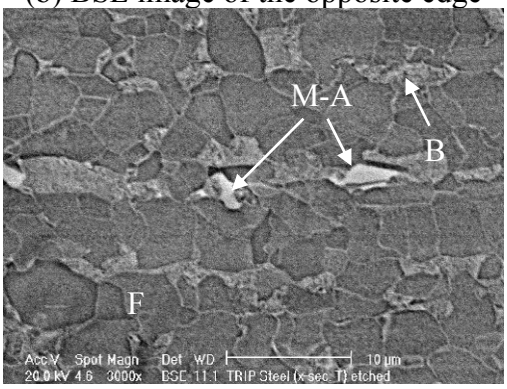

(d) Higher magnification BSE image shows three phases (Ferrite, Bainite and M-A)

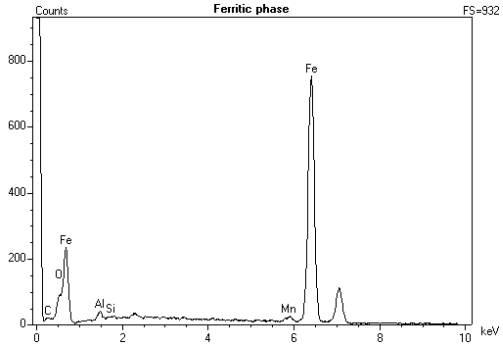

(e) EDS spectrum from ferritic phase

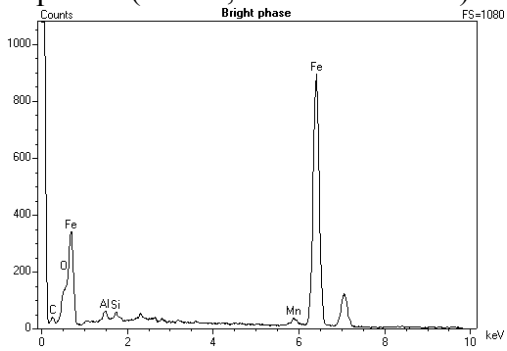

(f) EDS spectrum from M-A-phase

Fig. 55 – SEM images and EDS spectra of the etched TRIP steel sample in the hot-rolled condition (transverse cross-section, LePera etch).

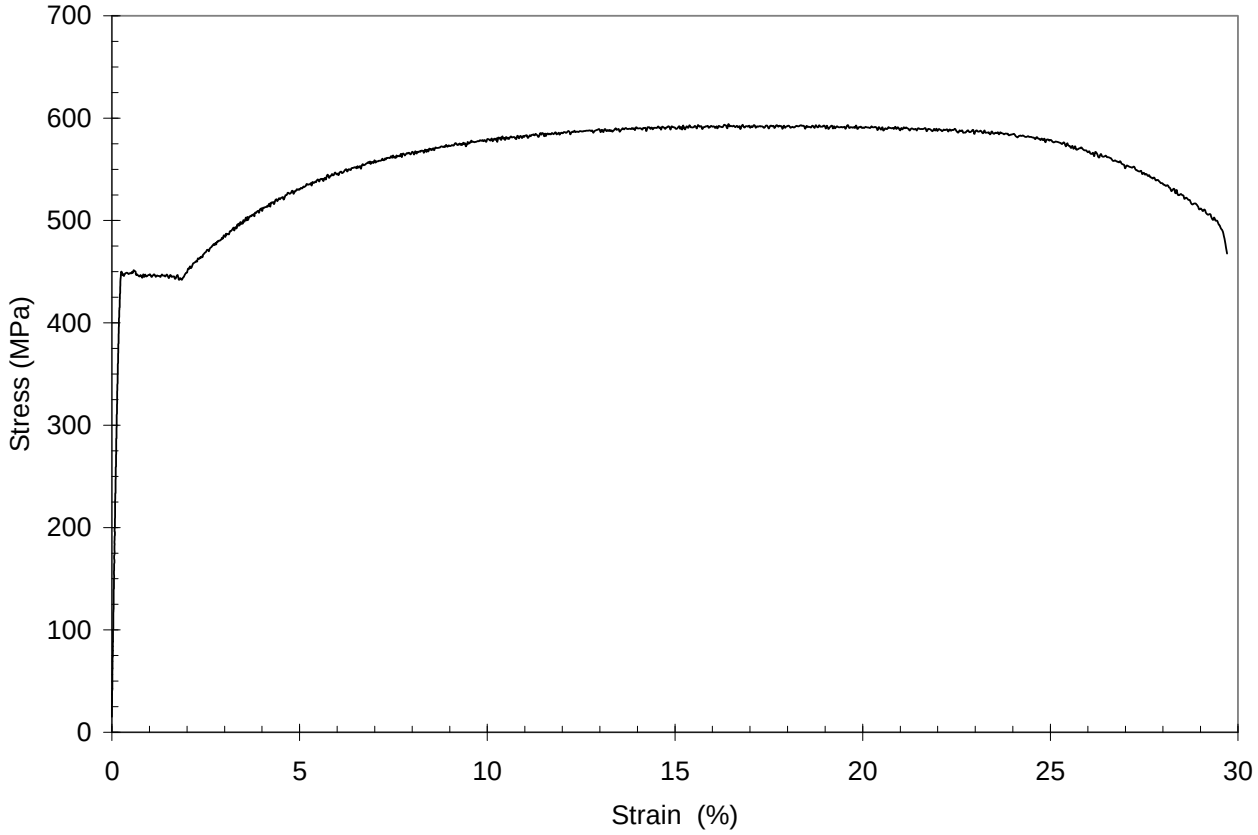

Fig. 56 – Representative engineering stress versus engineering strain plot for the as-received hot-rolled TRIP steel.

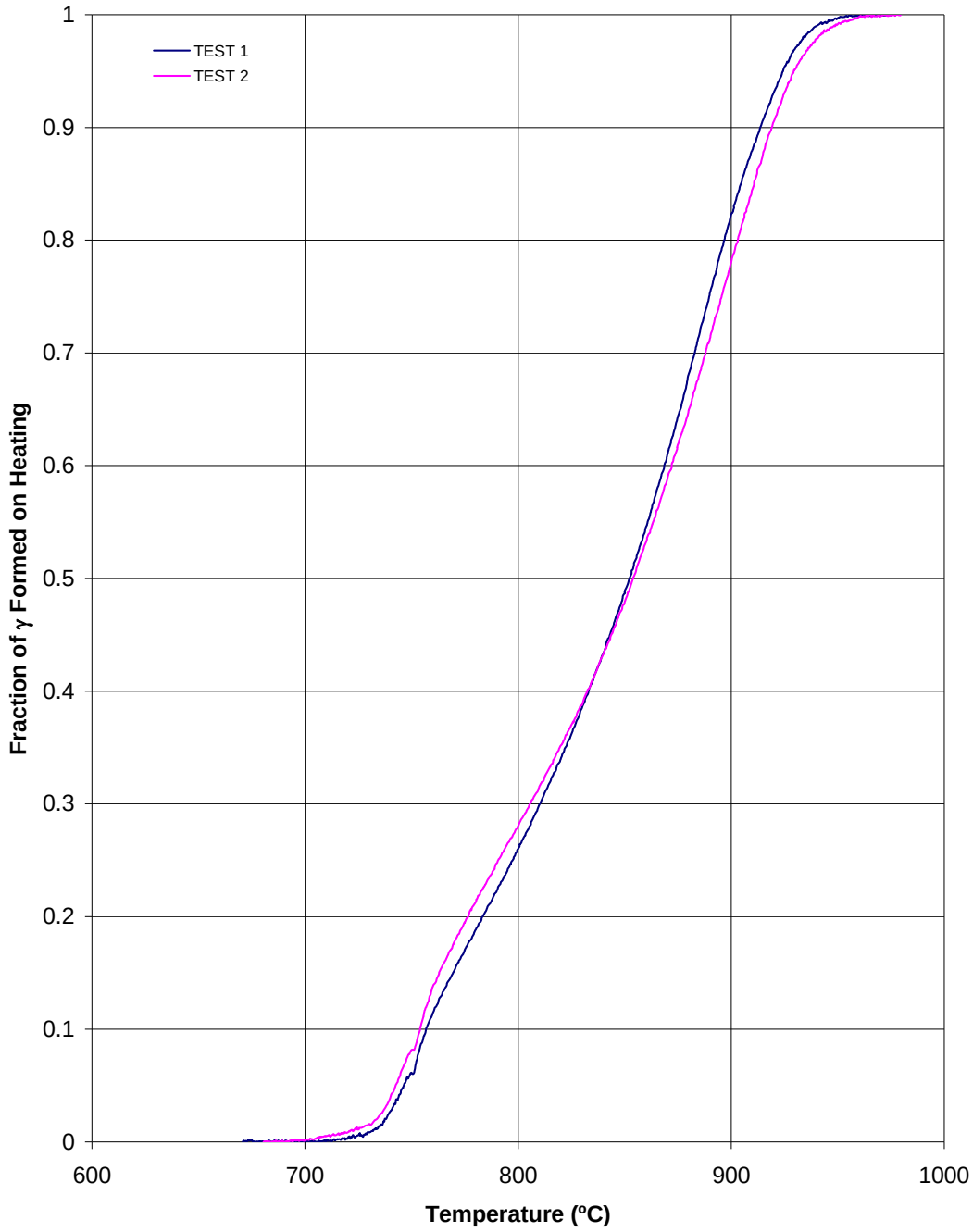

Fig. 57 – Formation of austenite on heating of TRIP steel.

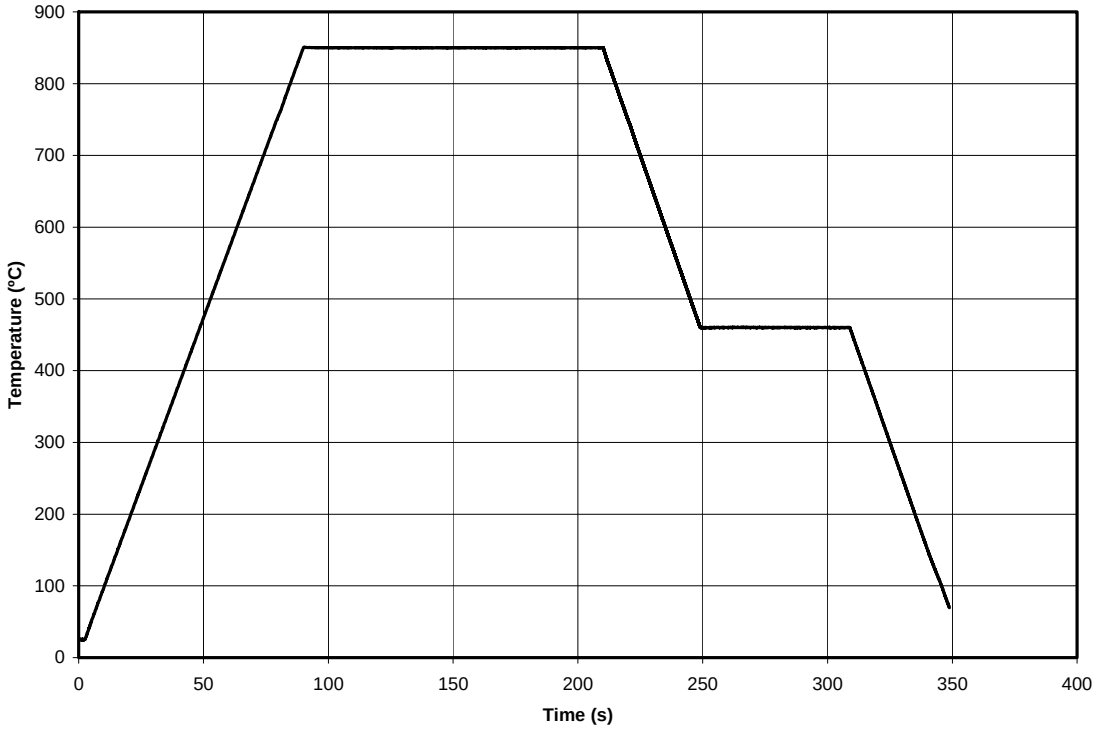

HT-1

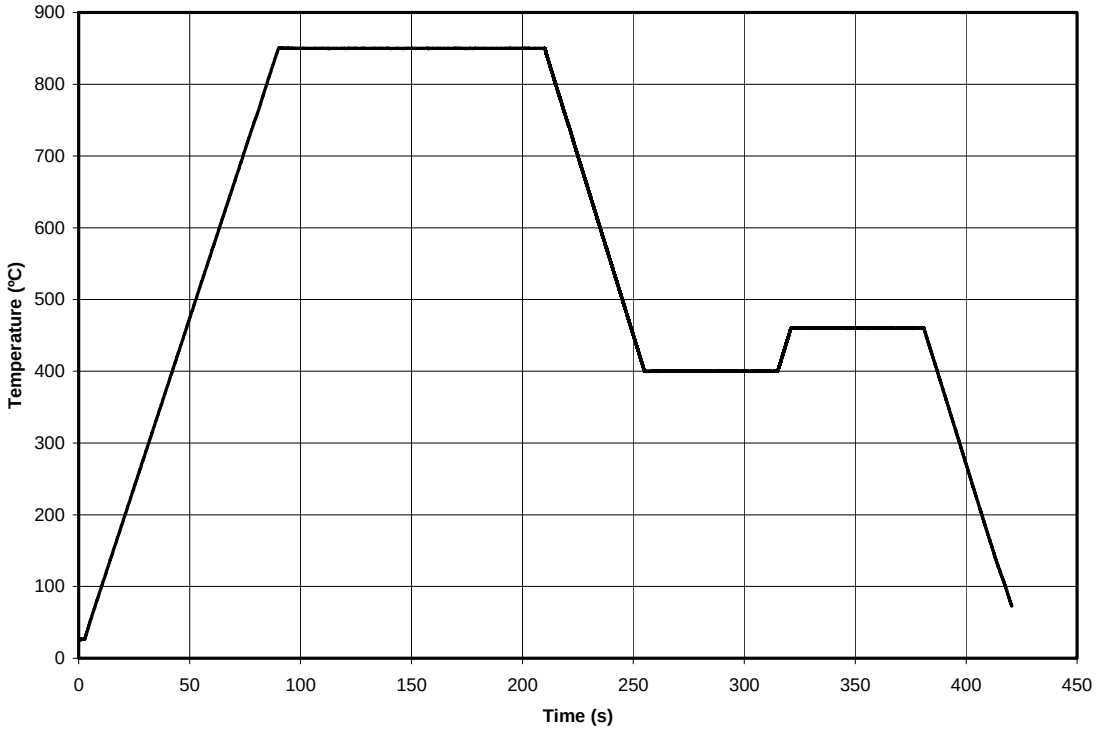

HT-3

Fig. 58 – Examples of temperature profiles during heat treatment of TRIP steel in the dilatometer.

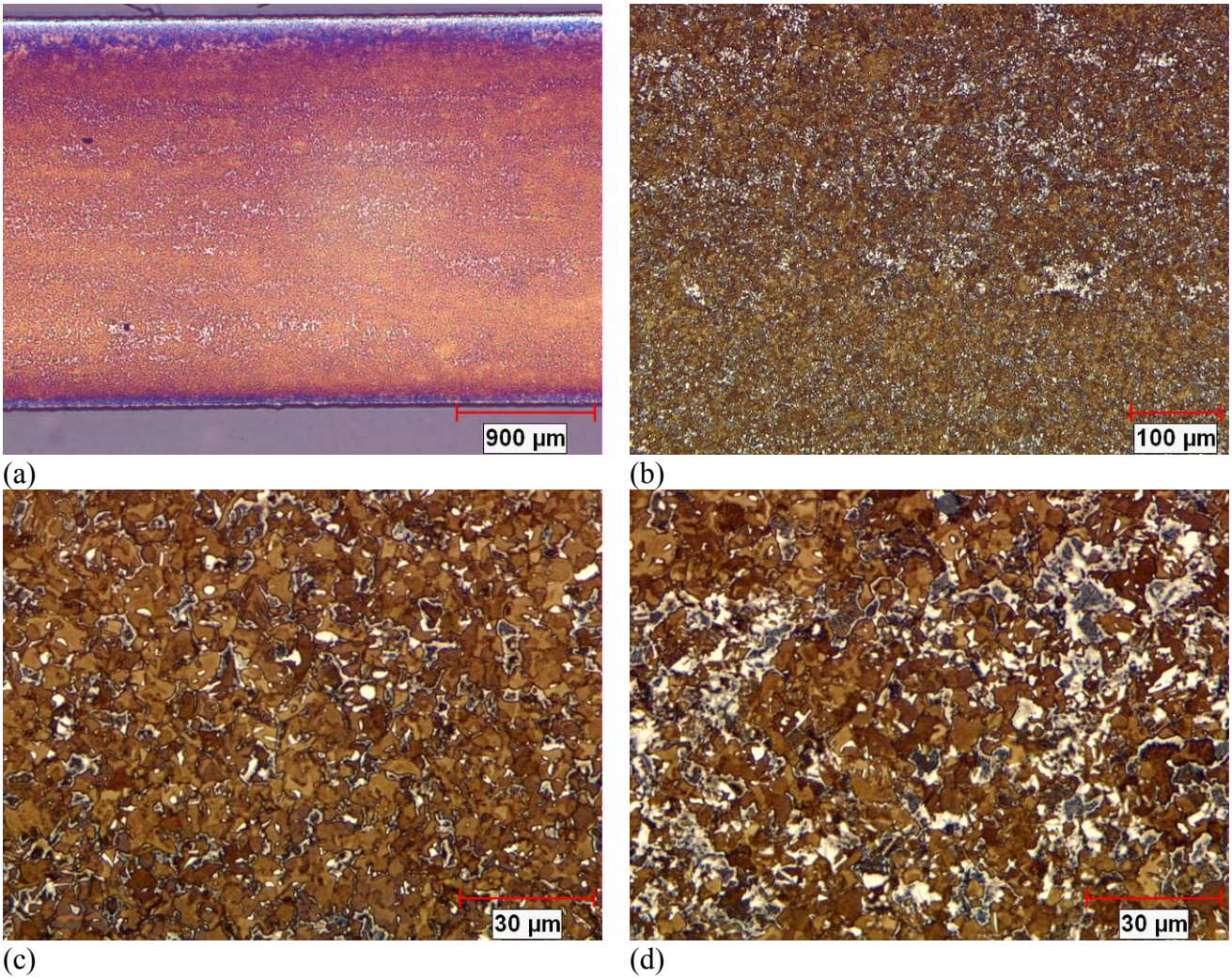

Fig. 59 – Optical micrographs of the TRIP steel sample 012 heat treated in the dilatometer according to regime HT1 (LePera etch).

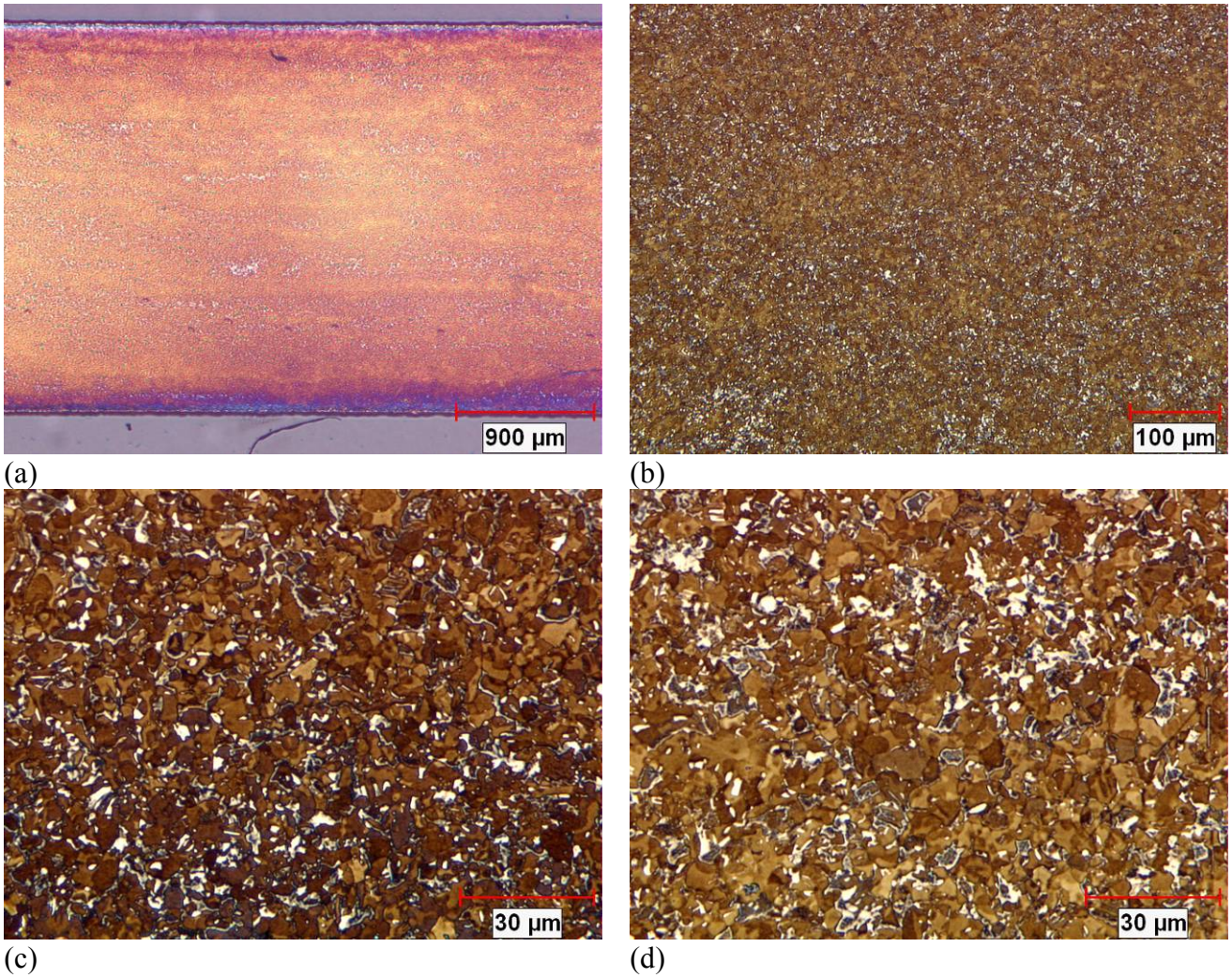

(a) (b)

(c) (d)

Fig. 60 – Optical micrographs of the TRIP steel sample 013 heat treated in the dilatometer according to regime HT1 (LePera etch).

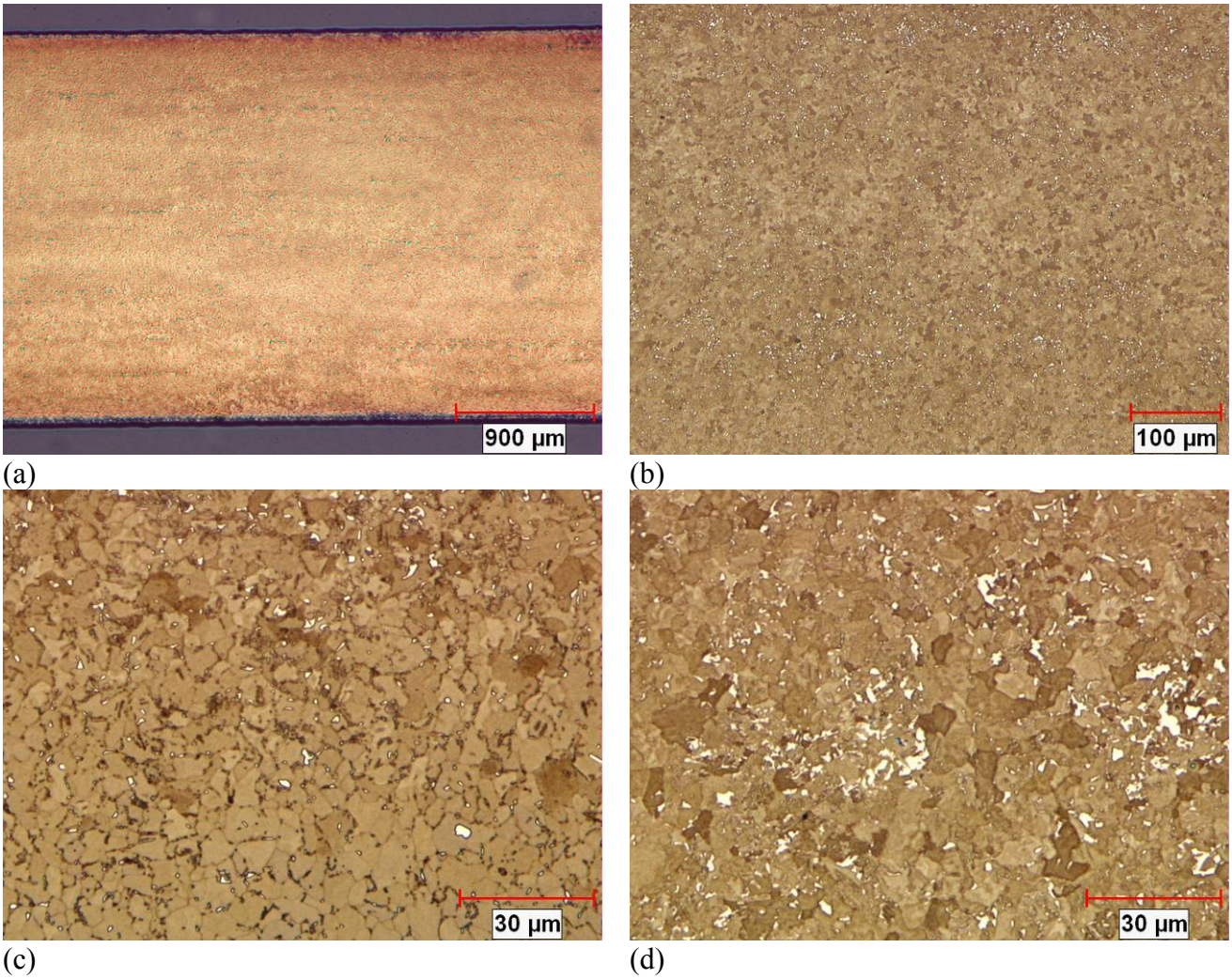

Fig. 61 – Optical micrographs of the TRIP steel sample 014 heat treated in the dilatometer according to regime HT3 (LePera etch).

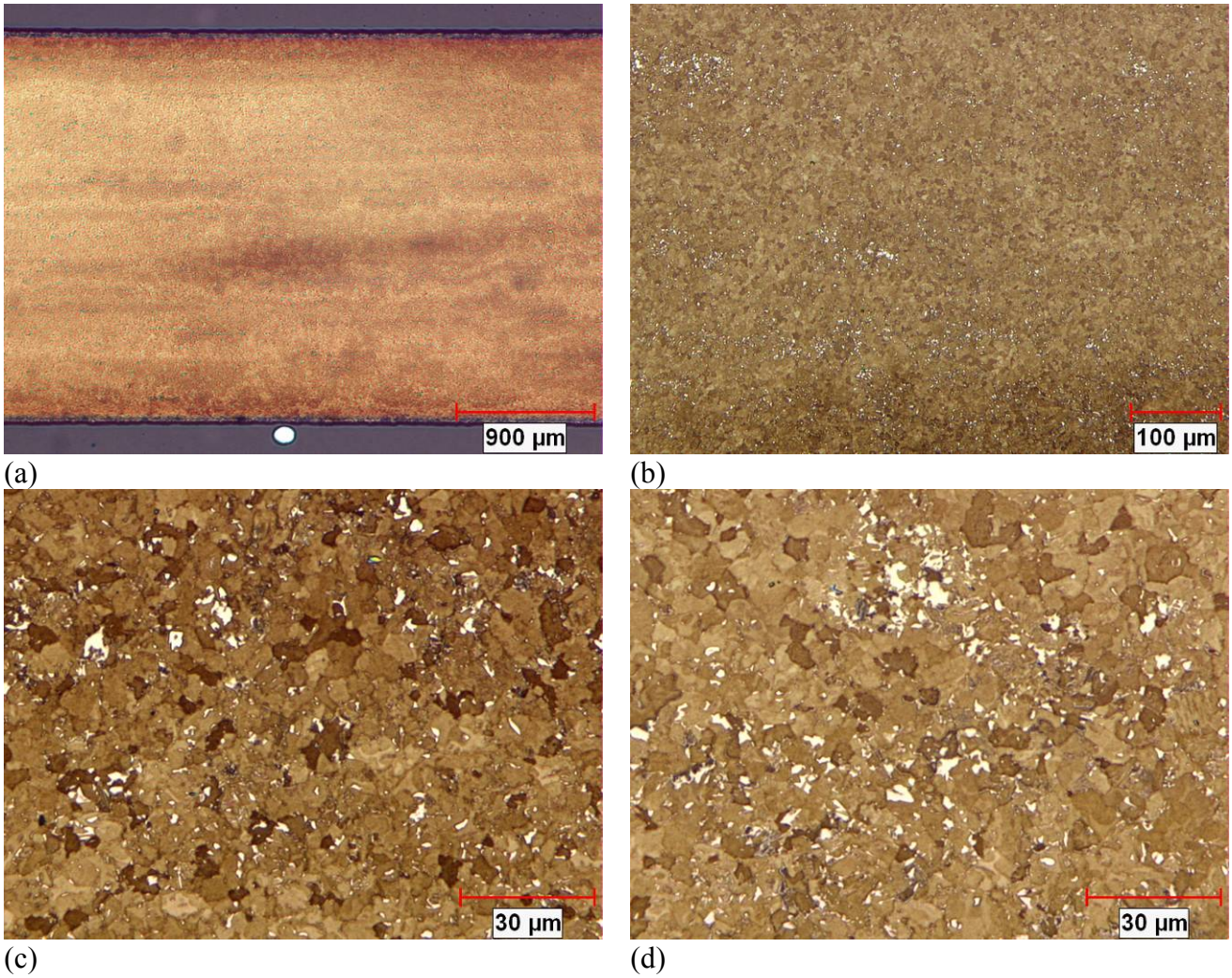

Fig. 62 – Optical micrographs of the TRIP steel sample 015 heat treated in the dilatometer according to regime HT3 (LePera etch).

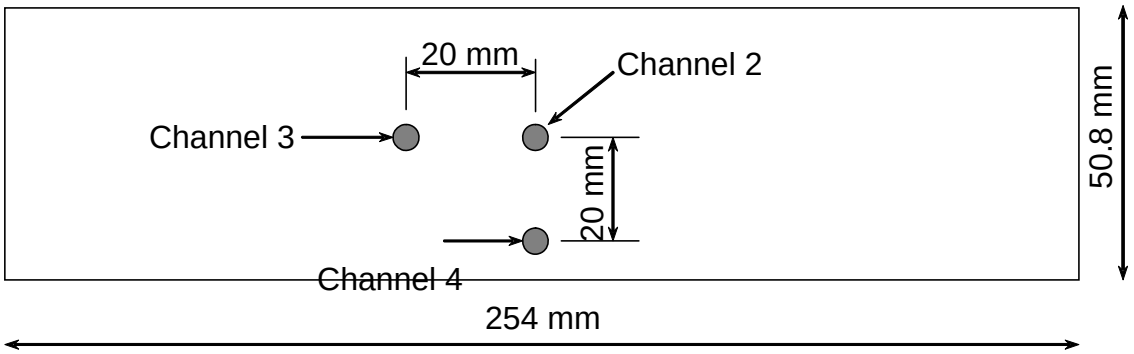

Fig. 63 – Schematics of the sample heat treated in the Gleeble simulator.

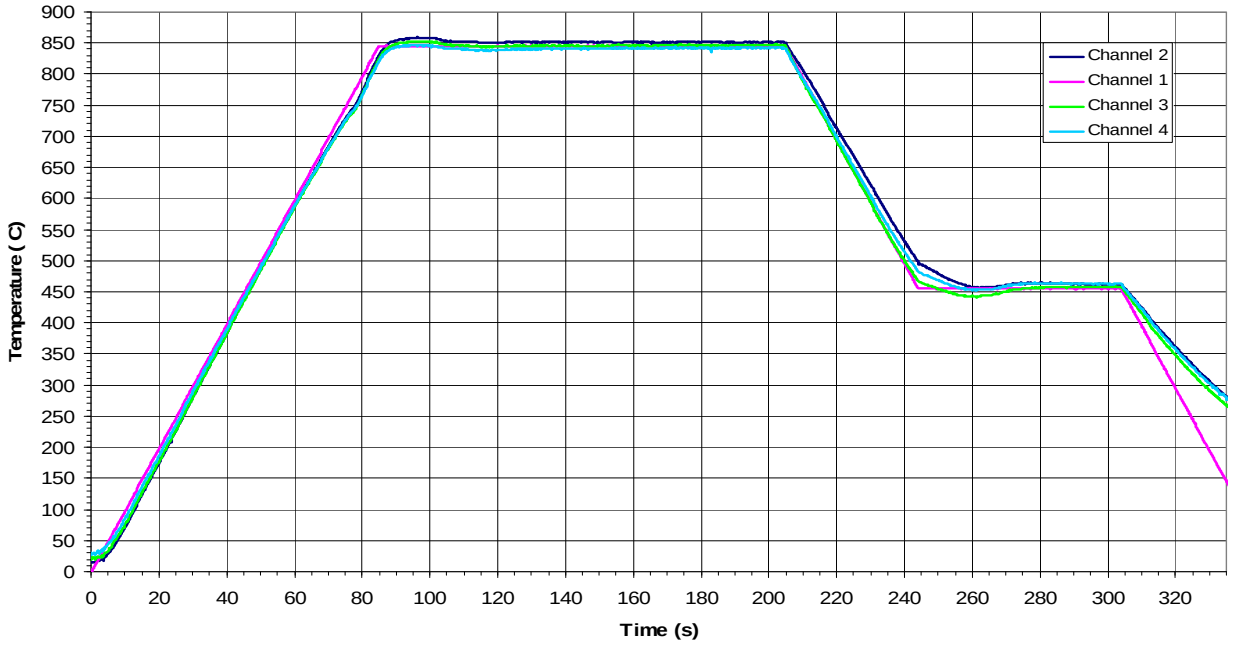

HT1

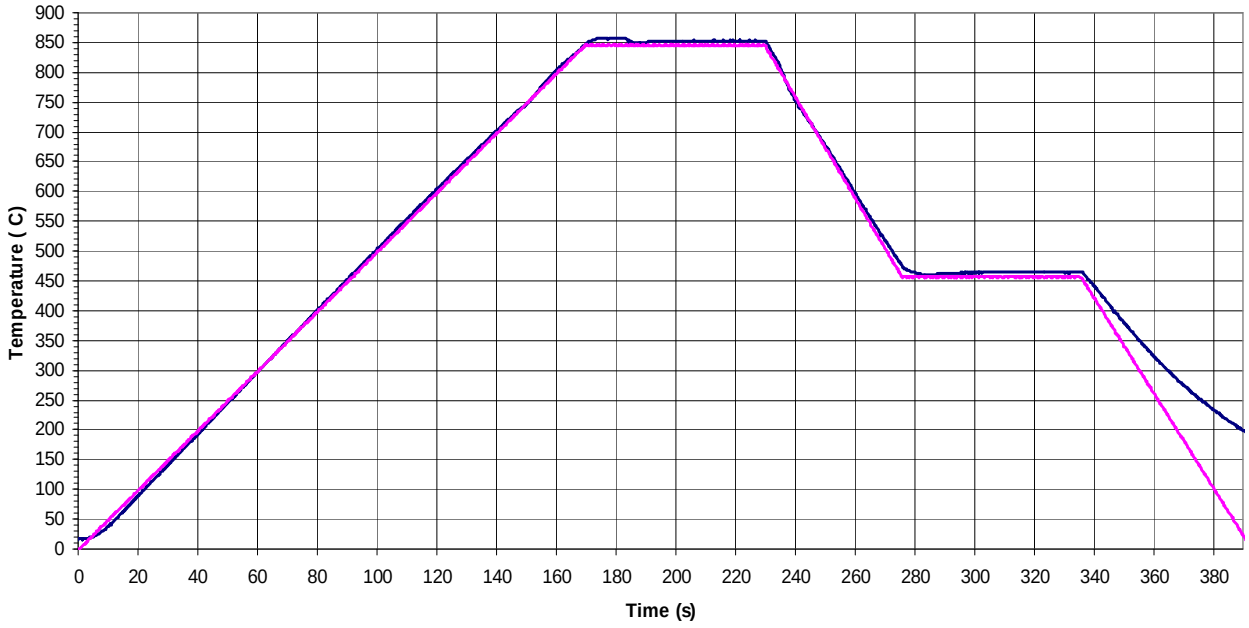

HT2

Fig. 64 – Examples of temperature profiles during Gleeble heat treatment of TRIP steel. Channel 1 – input, channels 2 to 4 – thermocouple readings.

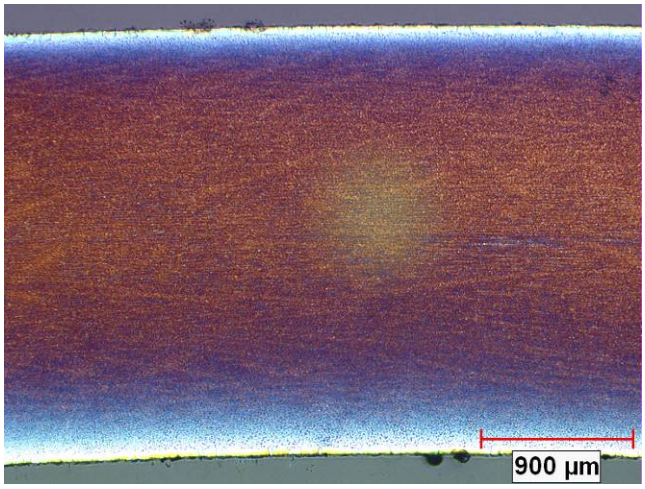

(a)

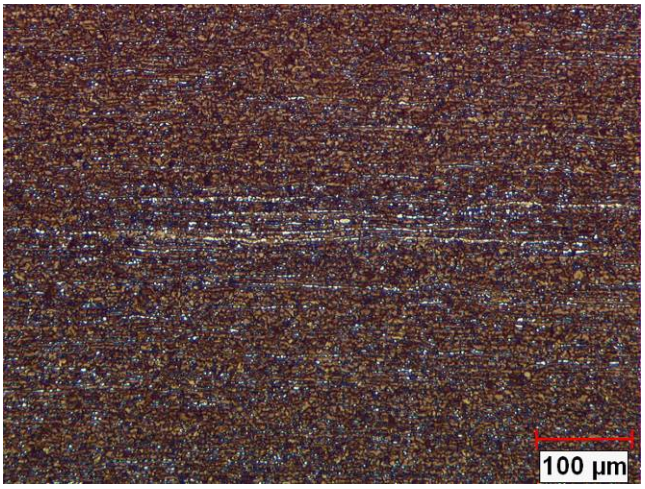

(b)

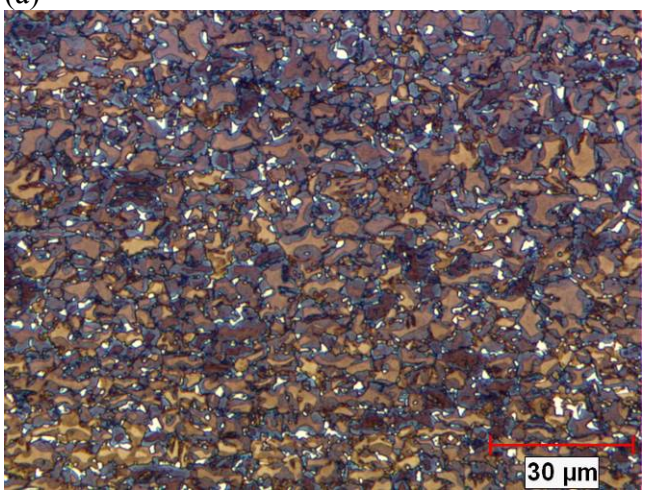

(c)

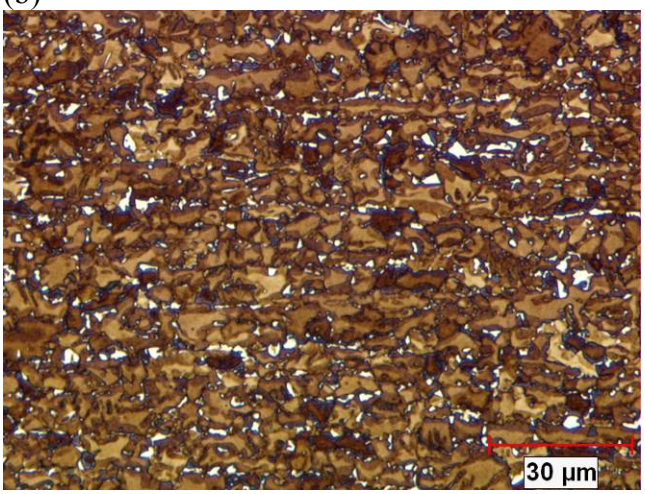

(d)

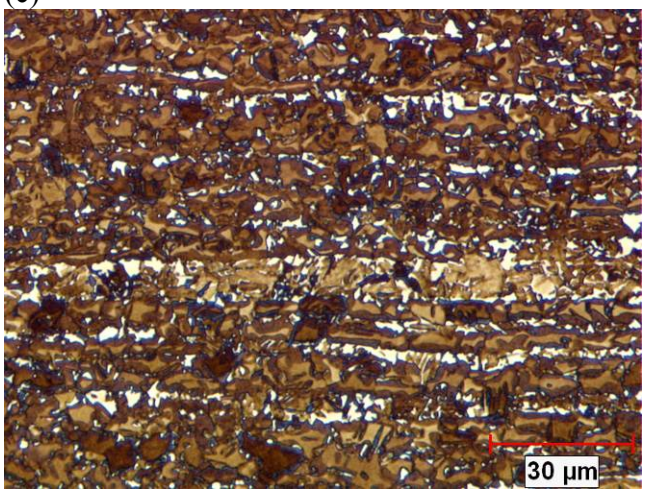

(e)

Fig. 65 – Optical micrographs (LePera etch) of Tube 1 made of TRIP heat treated according to regime HT1.

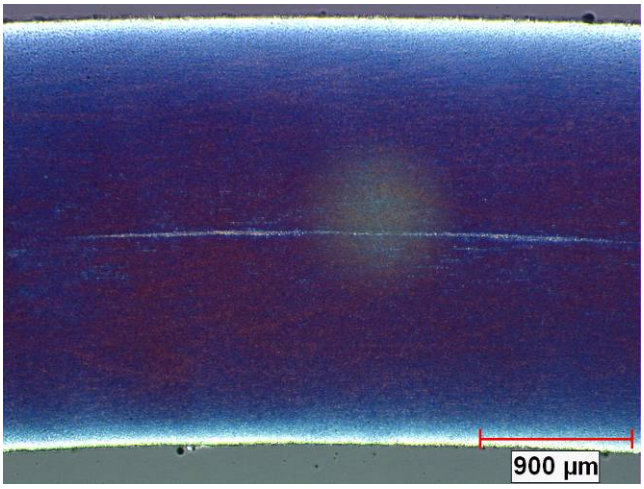

(a)

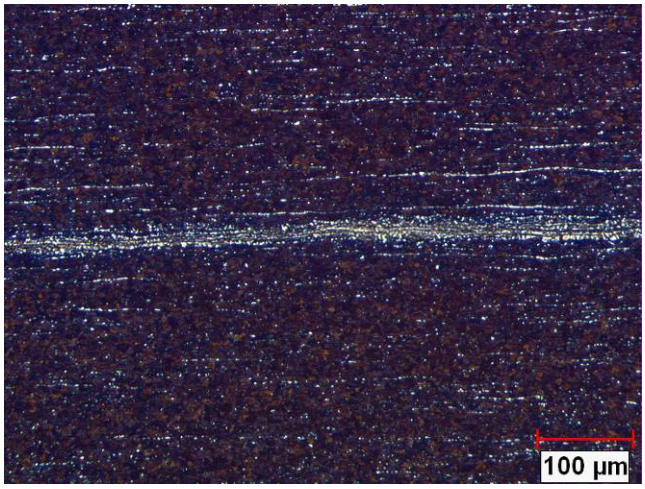

(b)

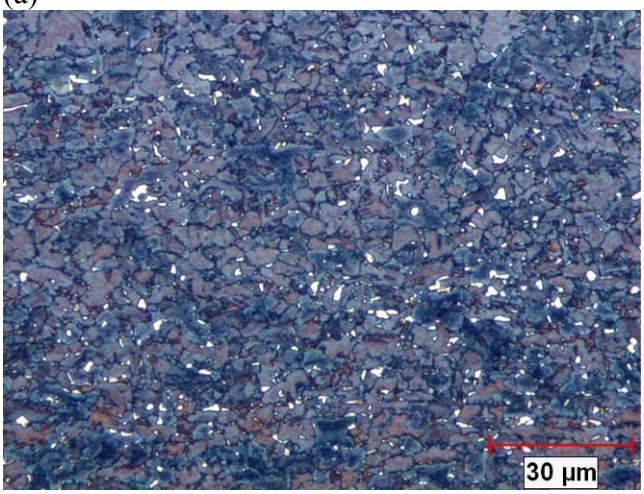

(c)

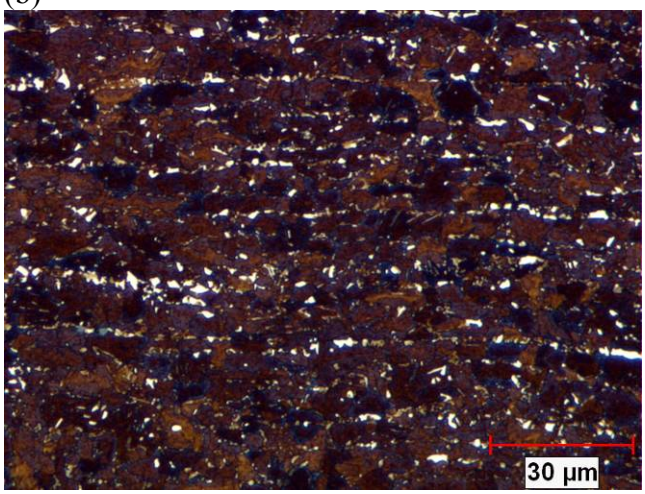

(d)

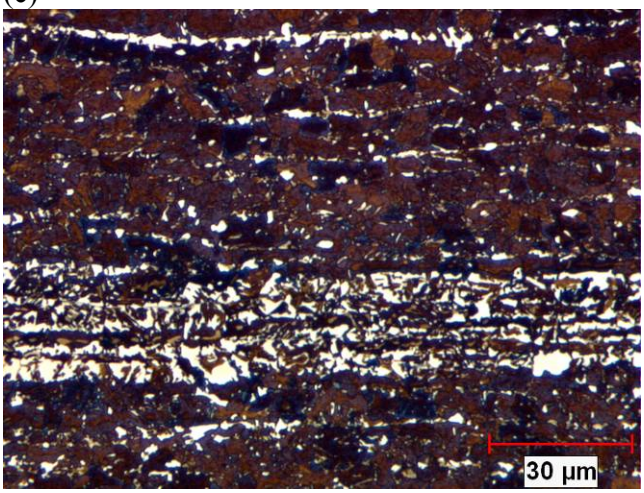

(e)

Fig. 66 – Optical micrographs (LePera etch) of Tube 2 made of TRIP heat treated according to regime HT1.

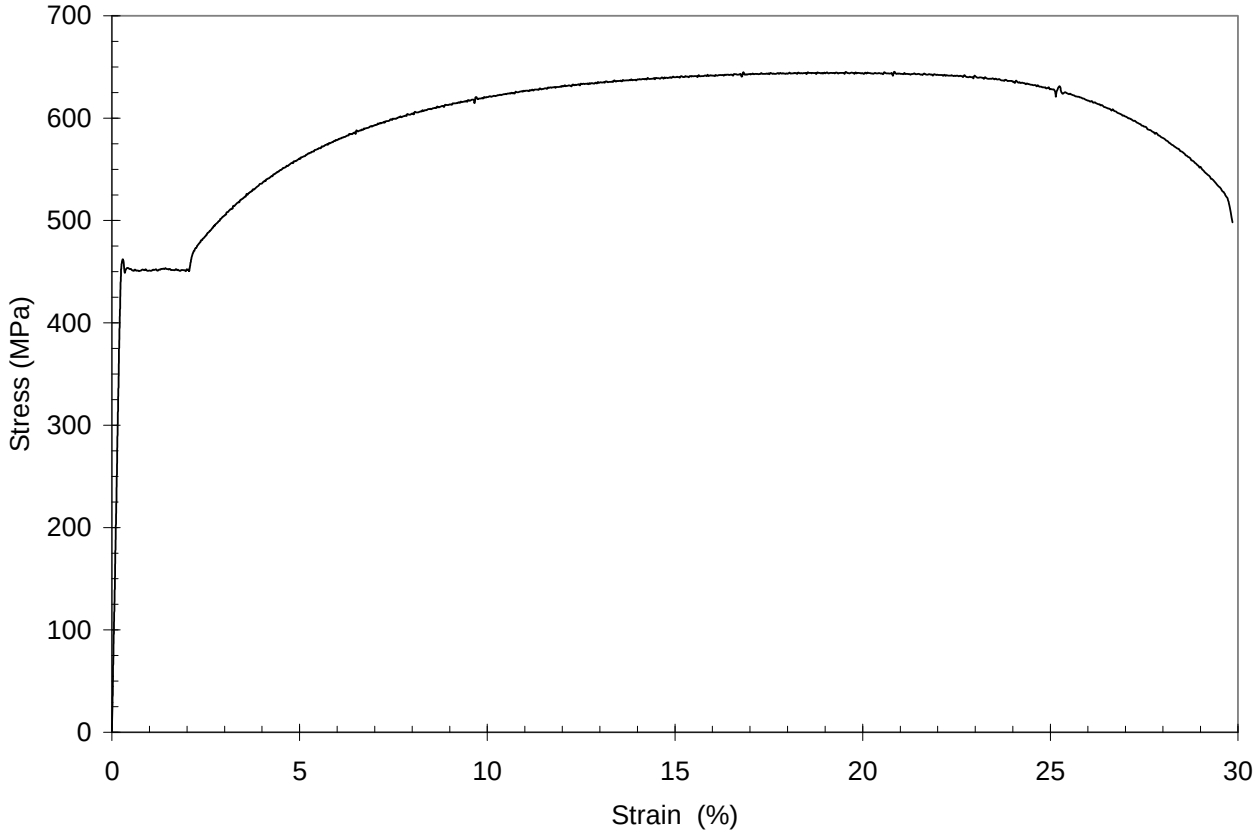

Fig. 67 – Representative engineering stress versus engineering strain plot for the heat treated TRIP steel.

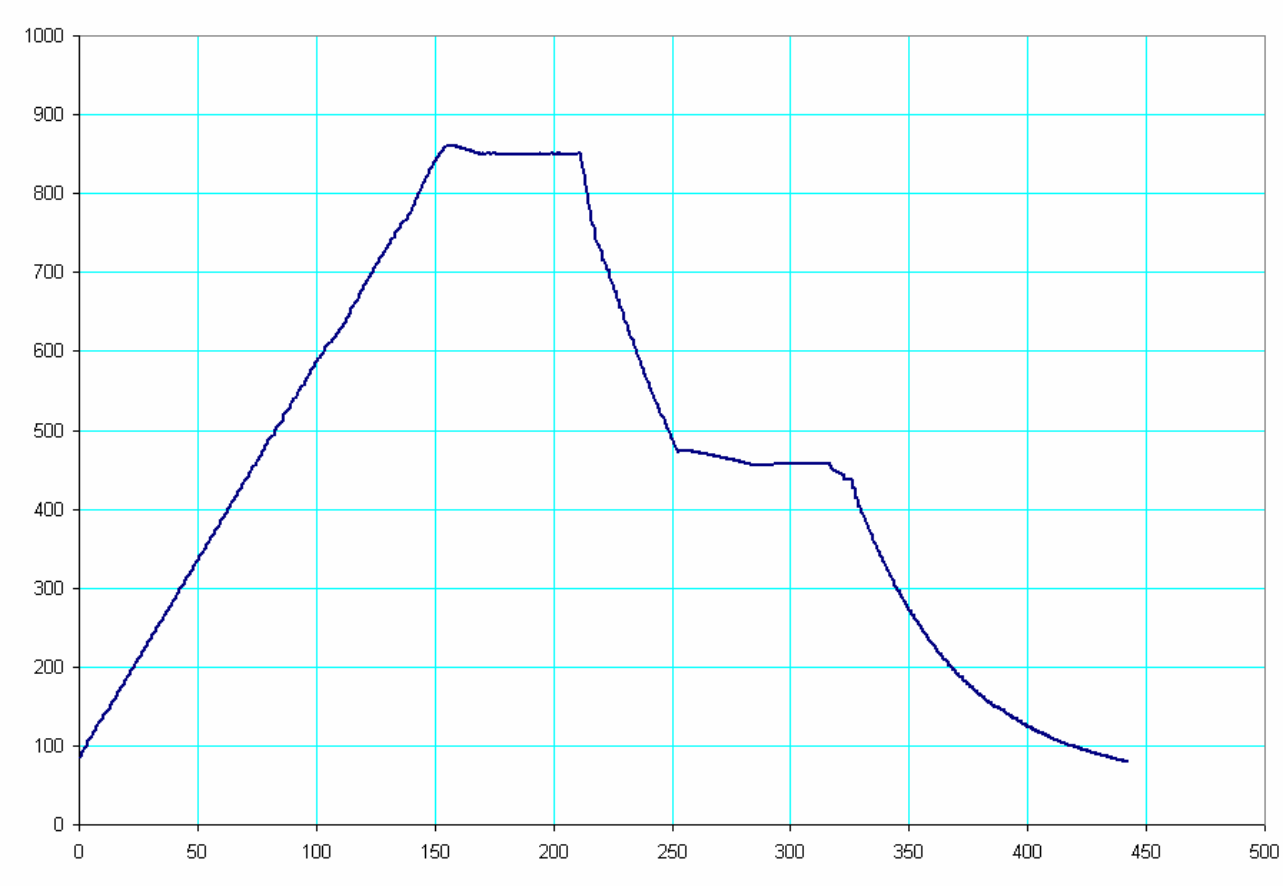

Fig. 68 – Example of temperature profile during galvanizing of TRIP steel.

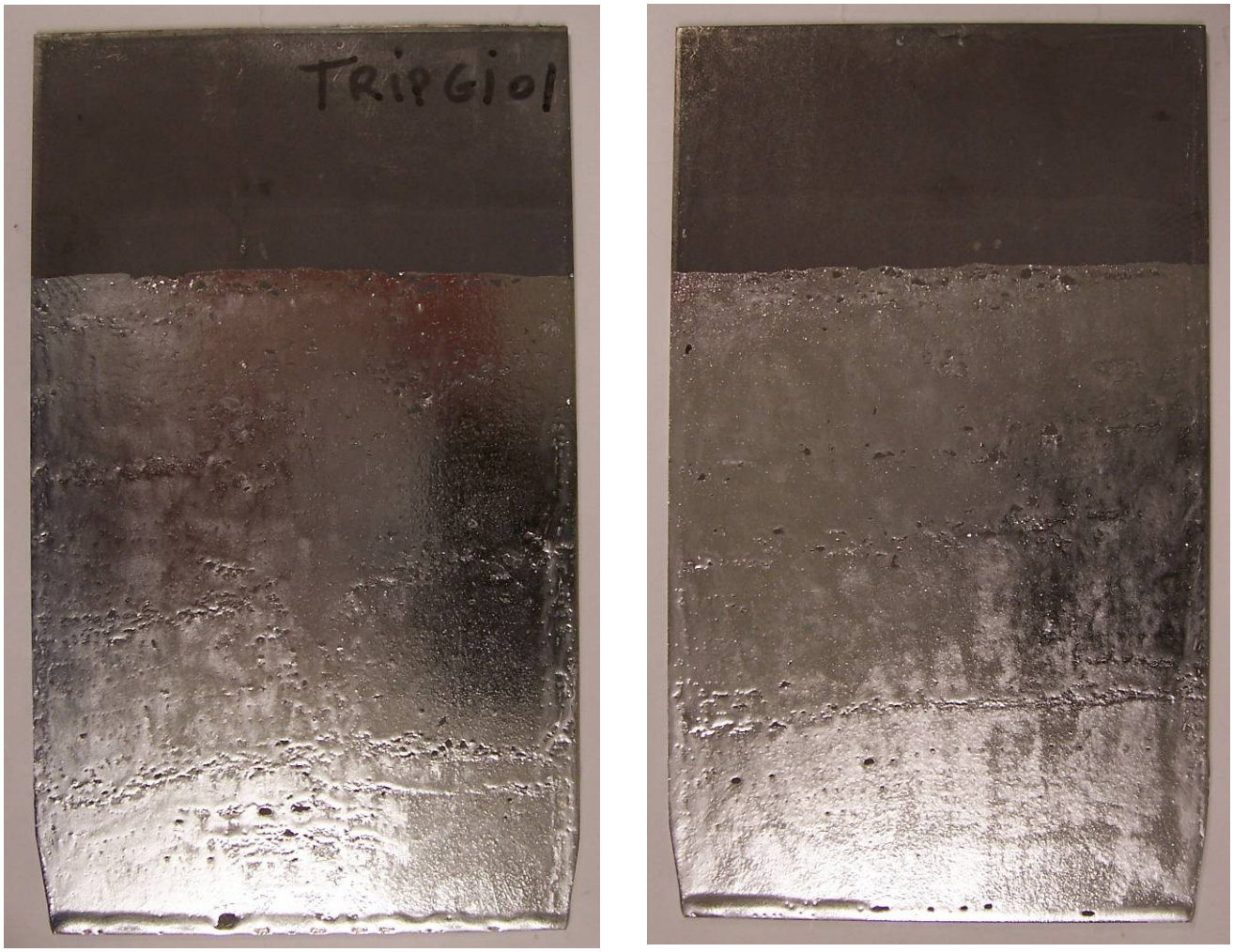

Fig. 69 – Example of a TRIP coupon galvanized according to schedule TRIP-GI01 (see Table 16).

Fig. 70 – Example of a TRIP coupon galvanized according to schedule TRIP-GI02 (see Table 16)

Fig. 71 – Example of a TRIP coupon galvanized according to schedule TRIP-GI03 (see Table 16).

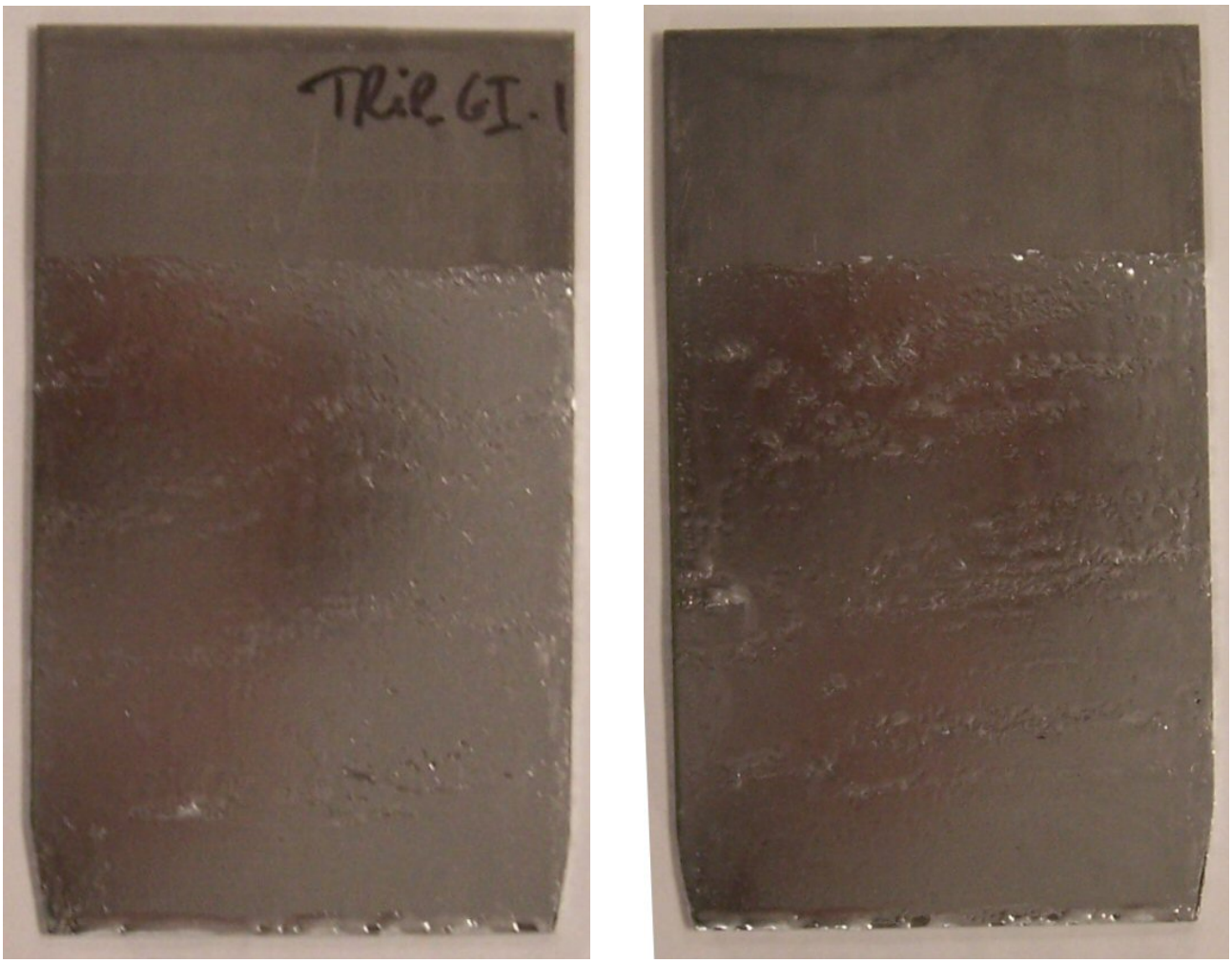

Fig. 72 – Example of a TRIP coupon galvanized according to schedule TRIP-GI03 (see Table 16).

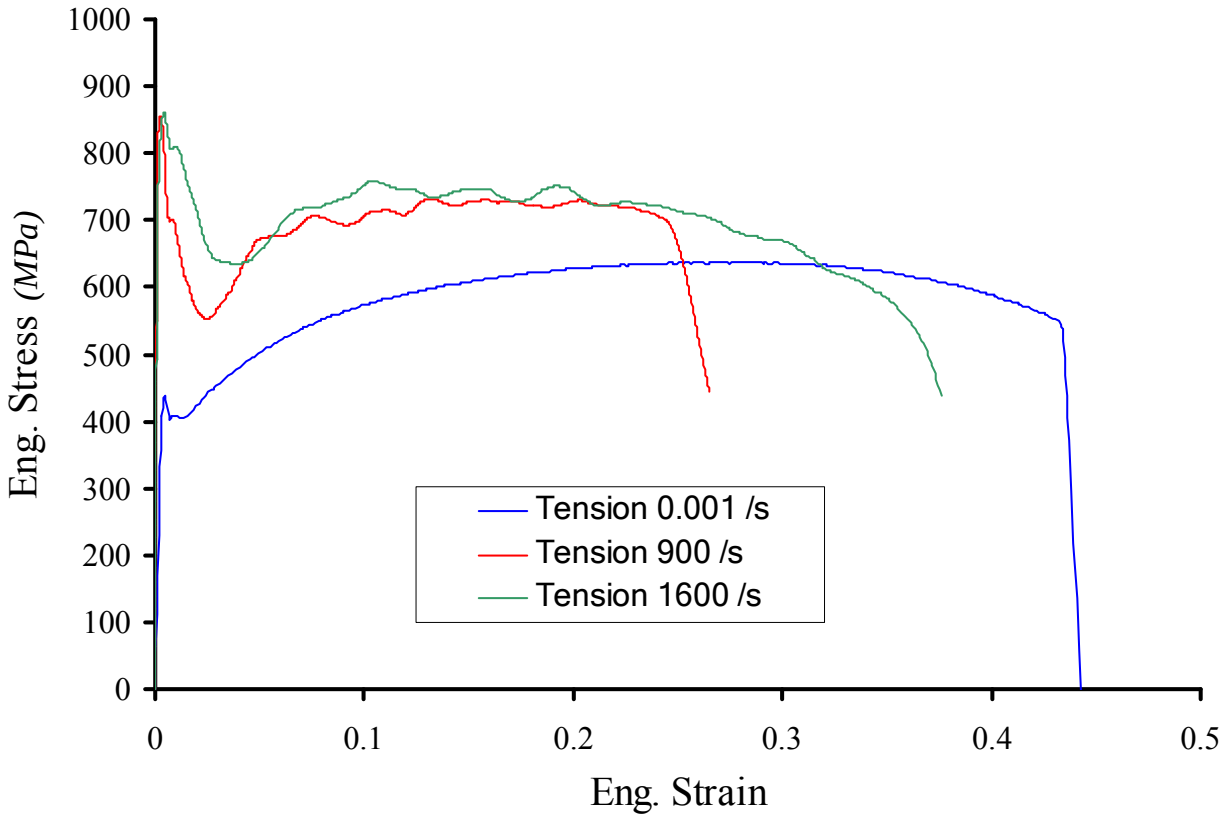

Fig. 73 – Examples of stress-strain curves (TRIP steel).

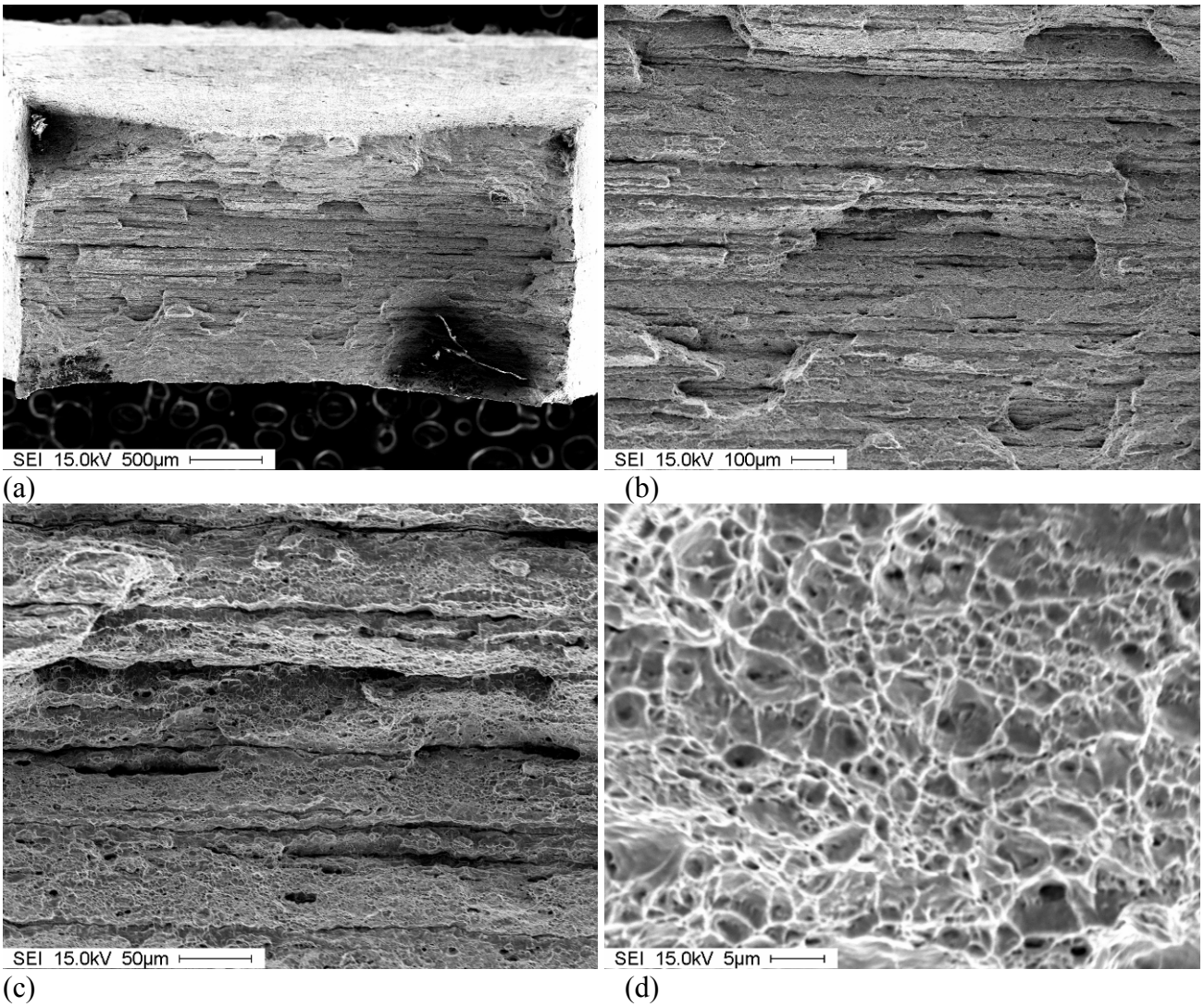

Fig. 74 – Examples of fractographic examination of the TRIP steel samples after quasi-static tensile tests.

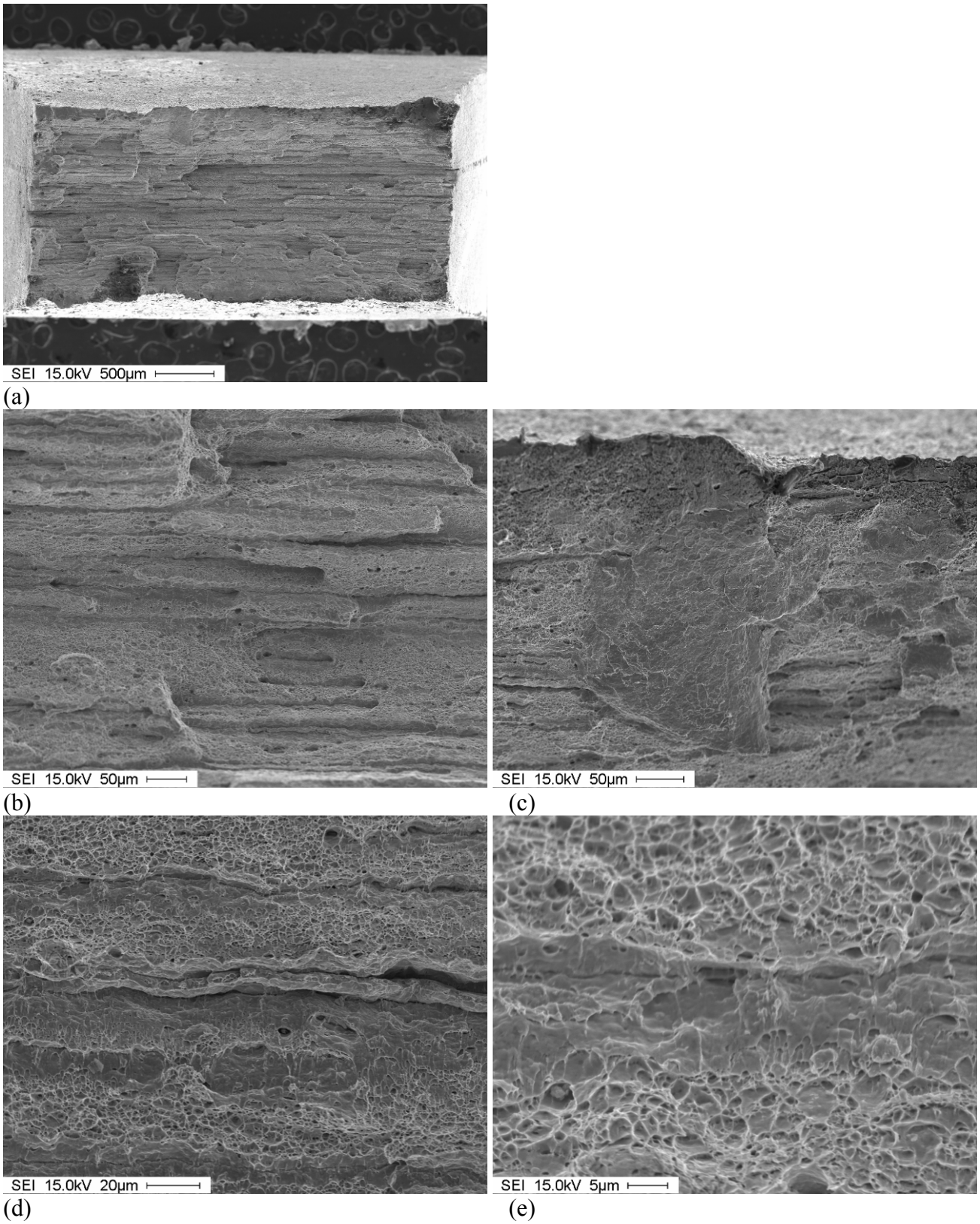

Fig. 75 – Examples of fractographic examination of the TRIP steel samples after high strain rate tensile tests.

APPENDIX 1 – MCMASTER GALVANIZING SIMULATOR

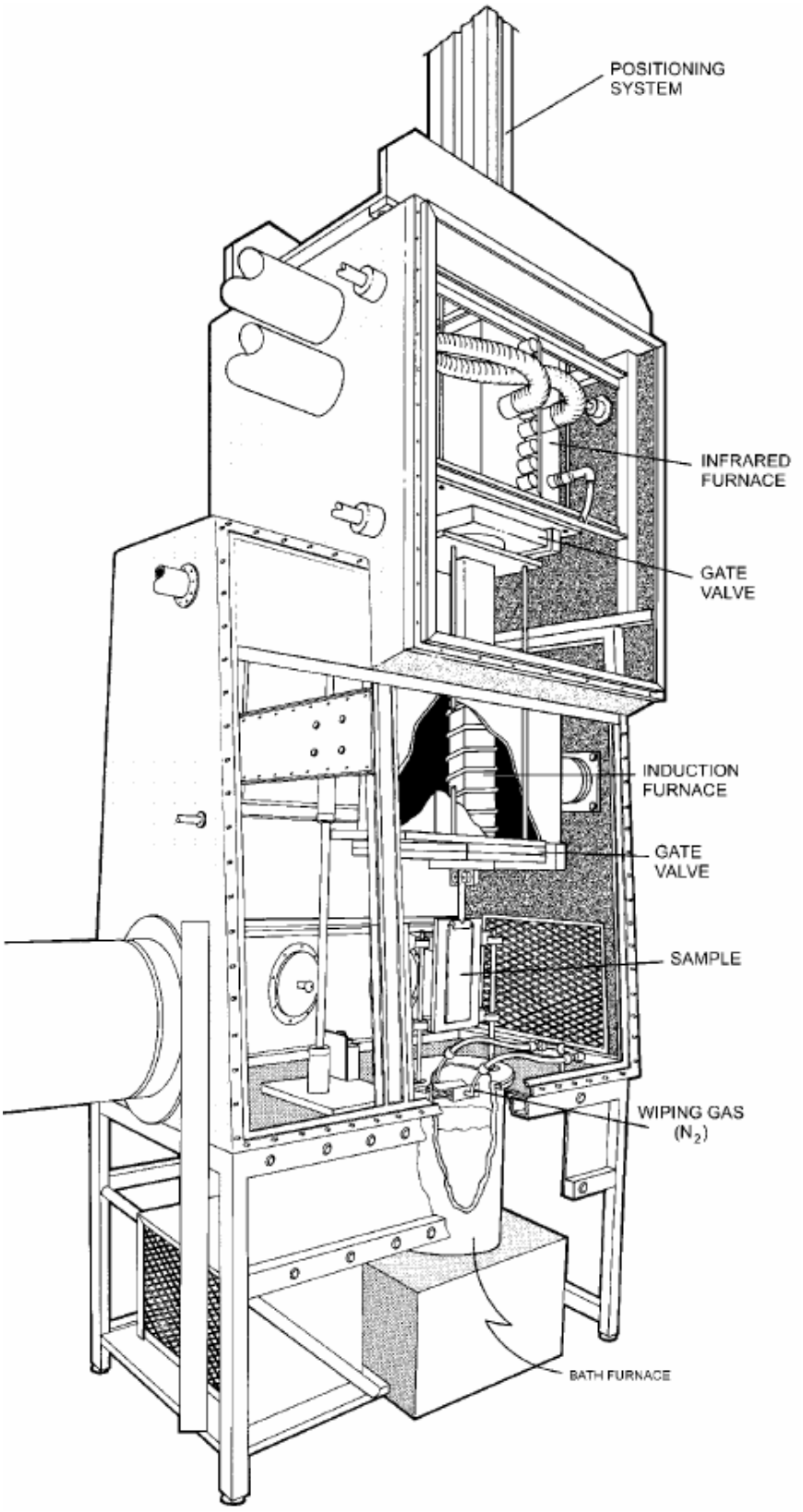

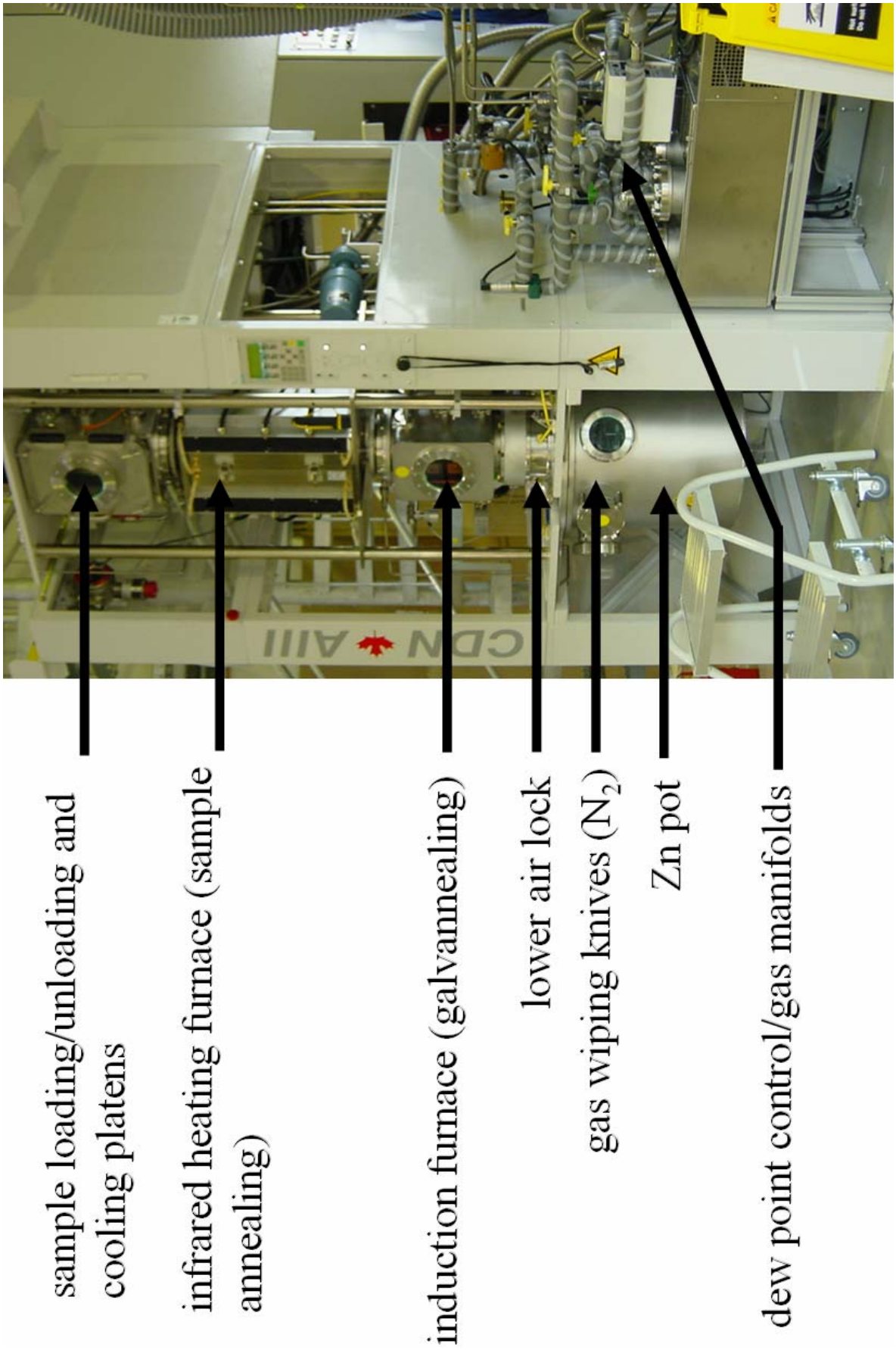
sample loading/unloading and cooling platens
infrared heating furnace (sample annealing)
induction furnace (galvannealing)
lower air lock
gas wiping knives (N_2)
Zn pot
dew point control/gas manifolds

Components	Specifications		Remarks
Glove Box	Total volume: 88 ft^3 (2.5 m^3)		- Closed environment for safety, reduced contamination, and clean operation.
	Operating Atmosphere	Mixture of 4% H_2 in N_2 O_2 < 100 ppm Dew point: -50 to 10°C	
Sample	Maximum size: 4 x 12 in. (10.16x30.48 cm)		- Suitable for several investigations: mechanical testing, coating adhesion (Double Olsen and V-bend), corrosion, welding, metallographic cross-sections.
	Usable size: 3.25 x 7 in (8.25x17.78 cm)		
	Thickness: 0.0125-0.1000 in (0.318-2.54 mm)		
Annealing Furnace	High Density Infrared Heater 60 kW		- Versatile annealing atmosphere control and ability to model oxidizing atmosphere such as the one of the pre-heater in the Sendzimir process. - High temperature annealing (up to 1740°F or 950°C) which is suitable for the new generation of high-strength steels.
	Heating rate	70°F/s (40°C/s)	
	Cooling Rate	In-situ: 15°F/s (10°C/s) Jet cooling: 50°F/s (30°C/s)	
	Processing Gas	Reducing: H_2/N_2 (0-100% H_2) <30 ppm O_2 -50 to 10°C D.P. Oxidizing: O_2/N_2 (0-4% O_2)	
Positioning system	Linear Slide with Servo Motor Belt Drive		- High performance positioning system which is able to produce immersion time as low as 0.3 second.
	Maximum speed: 600 ft/min (183 m/min)		
	Maximum acceleration: 64 ft/s^2 (19.5 m/s^2)		
	Working stroke: 8 ft (2.44 m)		
Zinc Pot	Resistance Heating Graphite crucible		- Virtually any kind of metallic alloys, which have a melting point below 1200°F (650°C), can be re-melted or produced.
	Dimension	5.25x12 in (13.3 x 30.5 cm)	
	Capacity	66 lb (30 kg) of liquid zinc	
Wiping Device	Compressed N_2 (N_2/H_2 mixture)		- Fully adjustable (wipes angle, vertical and horizontal position, gas flow and pressure.
	Coating weight: G20-G240 (60 g/m^2-760 g/m^2)		
Galvannealing Furnace	High-Frequency Induction Furnace 20 kW at 2.5-5 MHz		- Ability to closely model the industrial process by moving the sample in the induction coil and soaking in the infrared furnace.
	Heating rate	90°F/s (50°C/s)	
	Cooling Rate	In-situ: 15°F/s (10°C/s) Jet cooling: 50°F/s (30°C/s)	
	Processing Gas	Reducing: H_2/N_2 (0-100% H_2) <30 ppm O_2 -50 to 10°C D.P.	
Cooling System	Cooling media	Liquid Nitrogen Dry H_2-N_2 mixture	- High speed movements and high cooling rate allow for process interruption and freezing coating formation at any point.
	Cooling Rate	50°F/s (30°C/s)	
Process Control	Fully automated simulator operation, data acquisition from all the process parameters, on-line variance report generation and sample validation.		-High speed data storage offer the capability to reproduce exactly the same processing conditions (Thermal and motion profiles, atmosphere settings, …) in order to produce replicate samples.
	Temperature	Sample, Glove Box, Cooling line	
	Gas	H_2, H_2-N_2,O_2-N_2 Flow meters Gas humidifier O_2,H_2 and dew point meters	
	Motion	Linear Position Transducer	

APPENDIX 2 – PHOTOGRAPHS OF GALVANIZED COUPONS OF HSLA STEEL

side 1 side 2

side 1 side 2

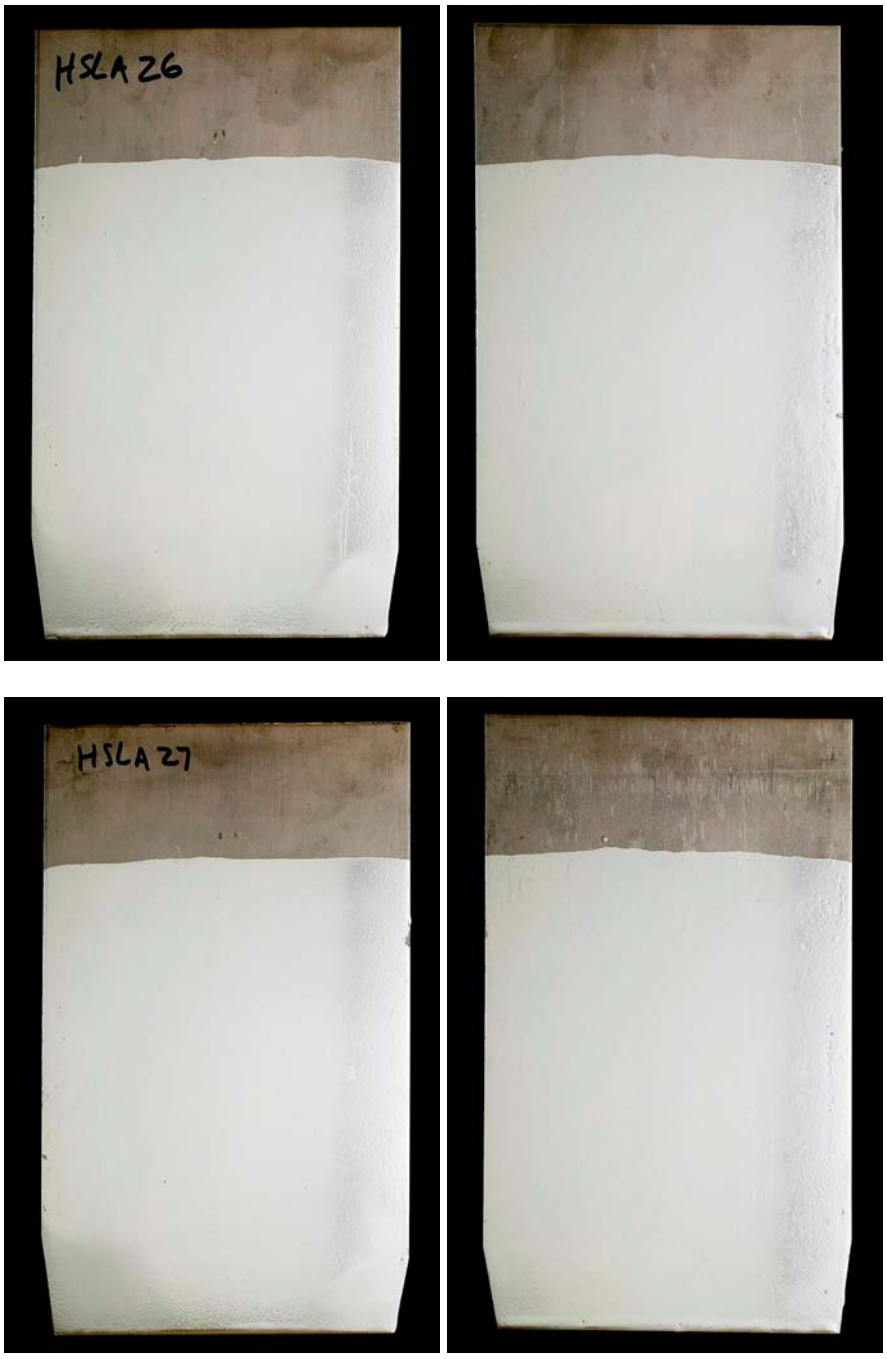

side 1 side 2

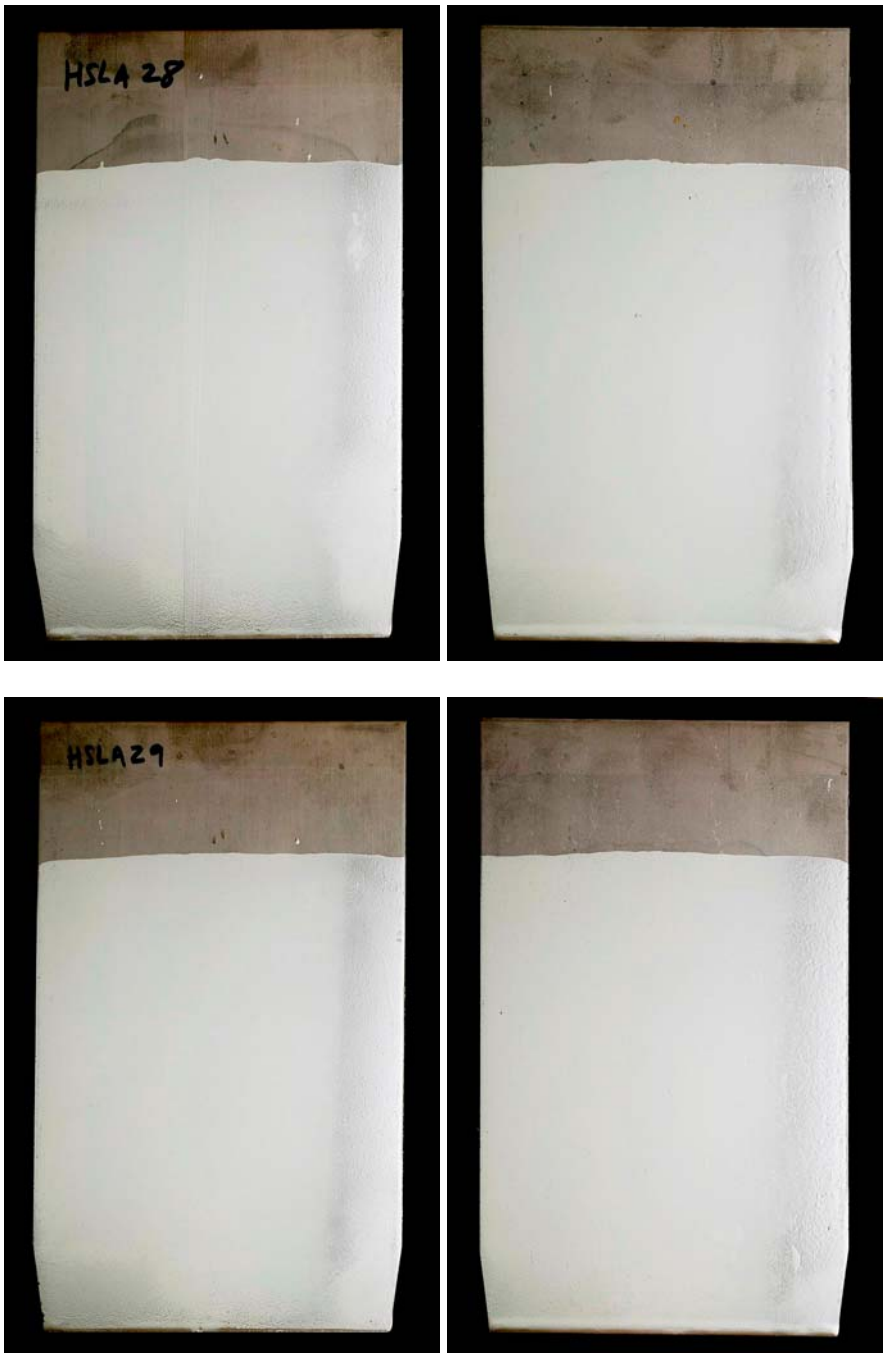

side 1 side 2

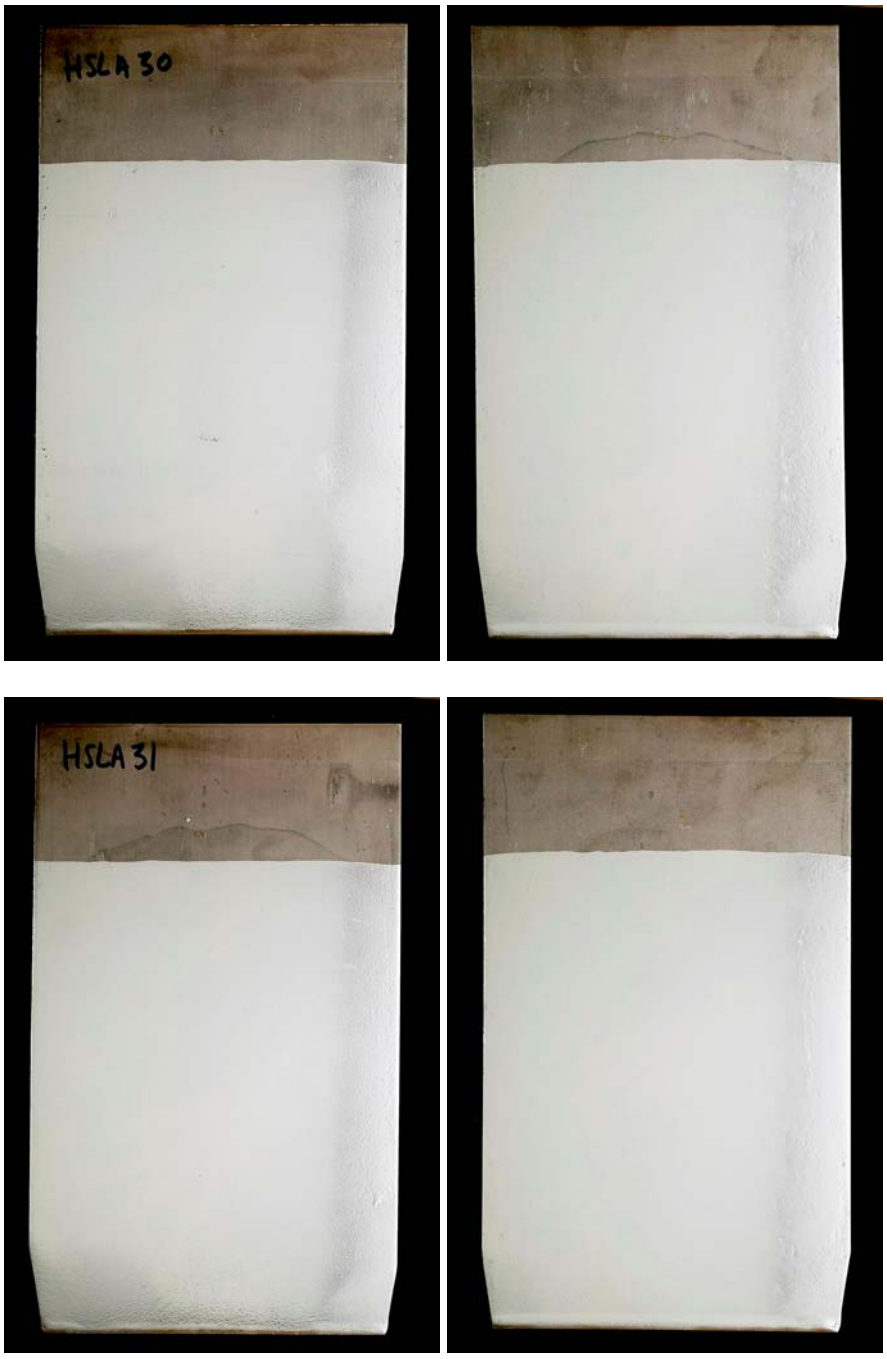

side 1 side 2

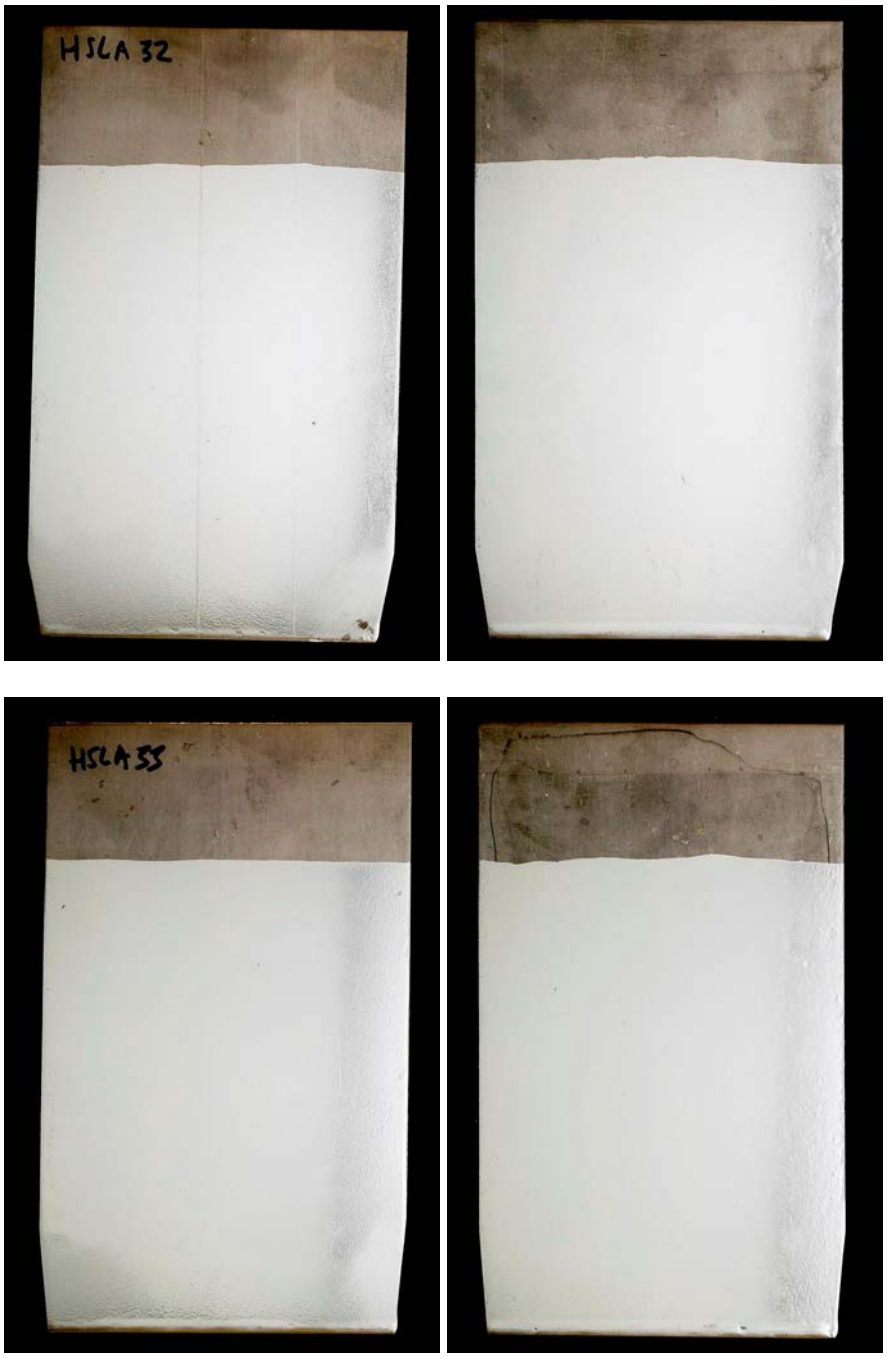

side 1 side 2

side 1 side 2

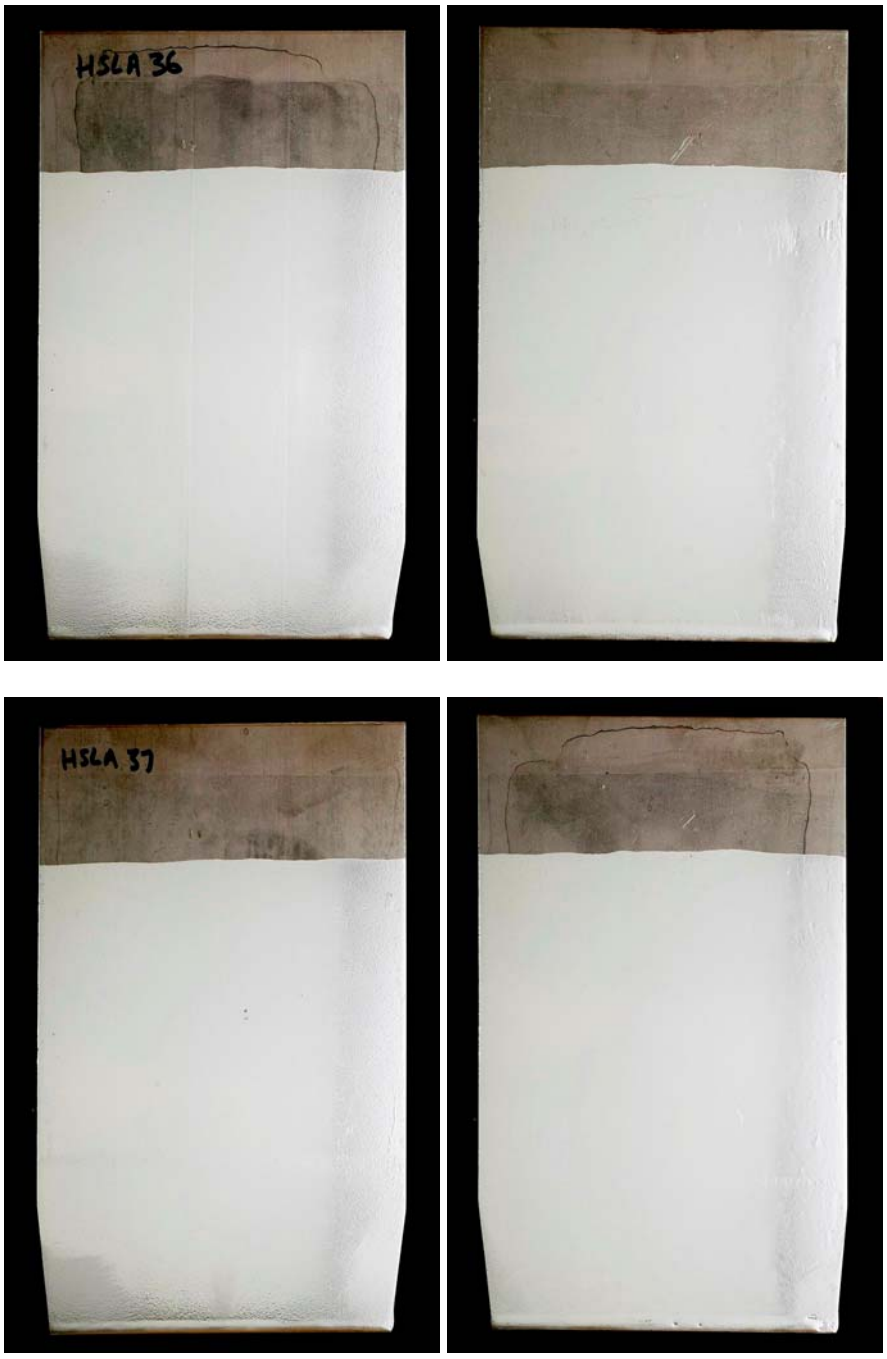

side 1 side 2

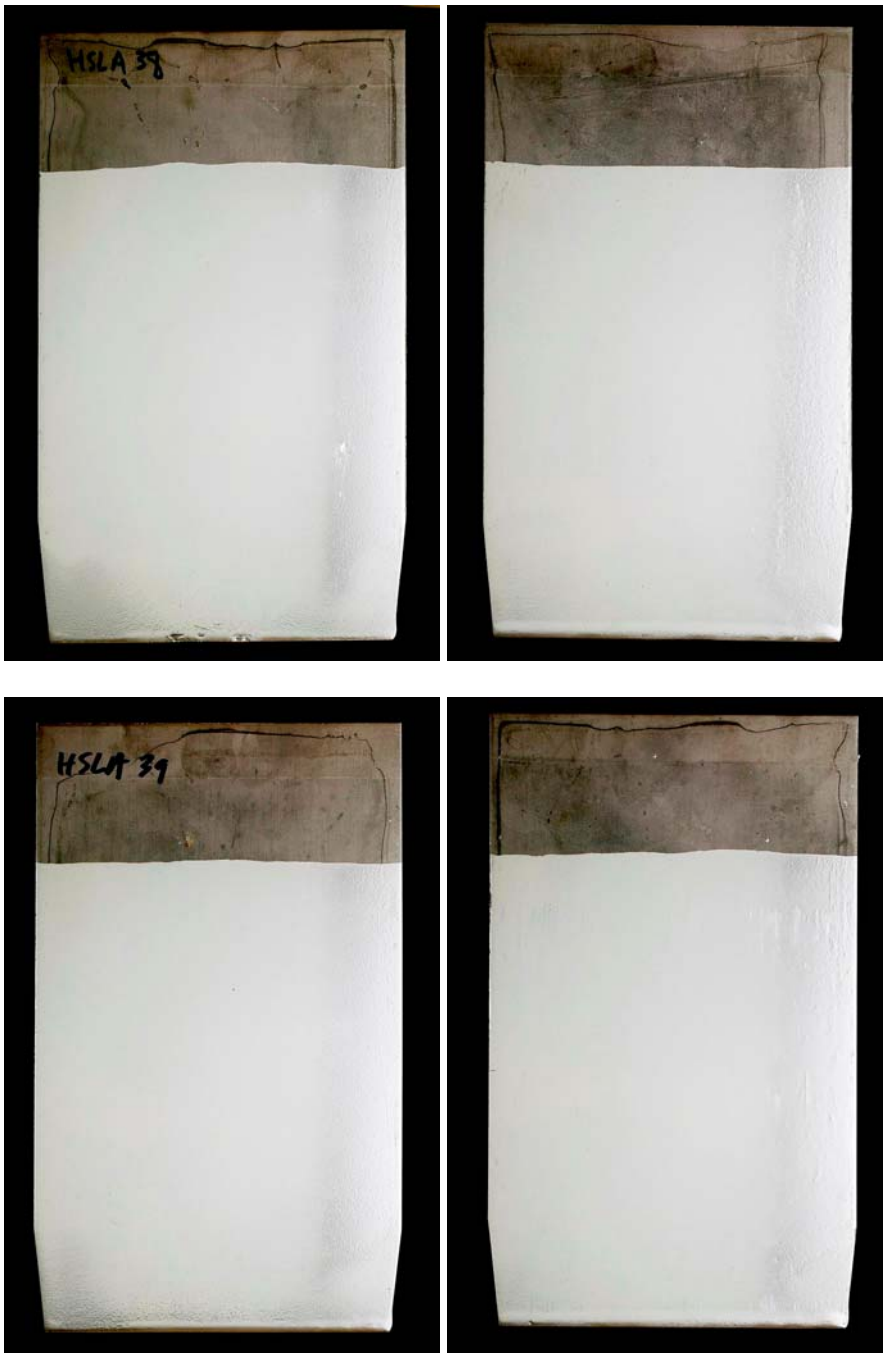

side 1 side 2

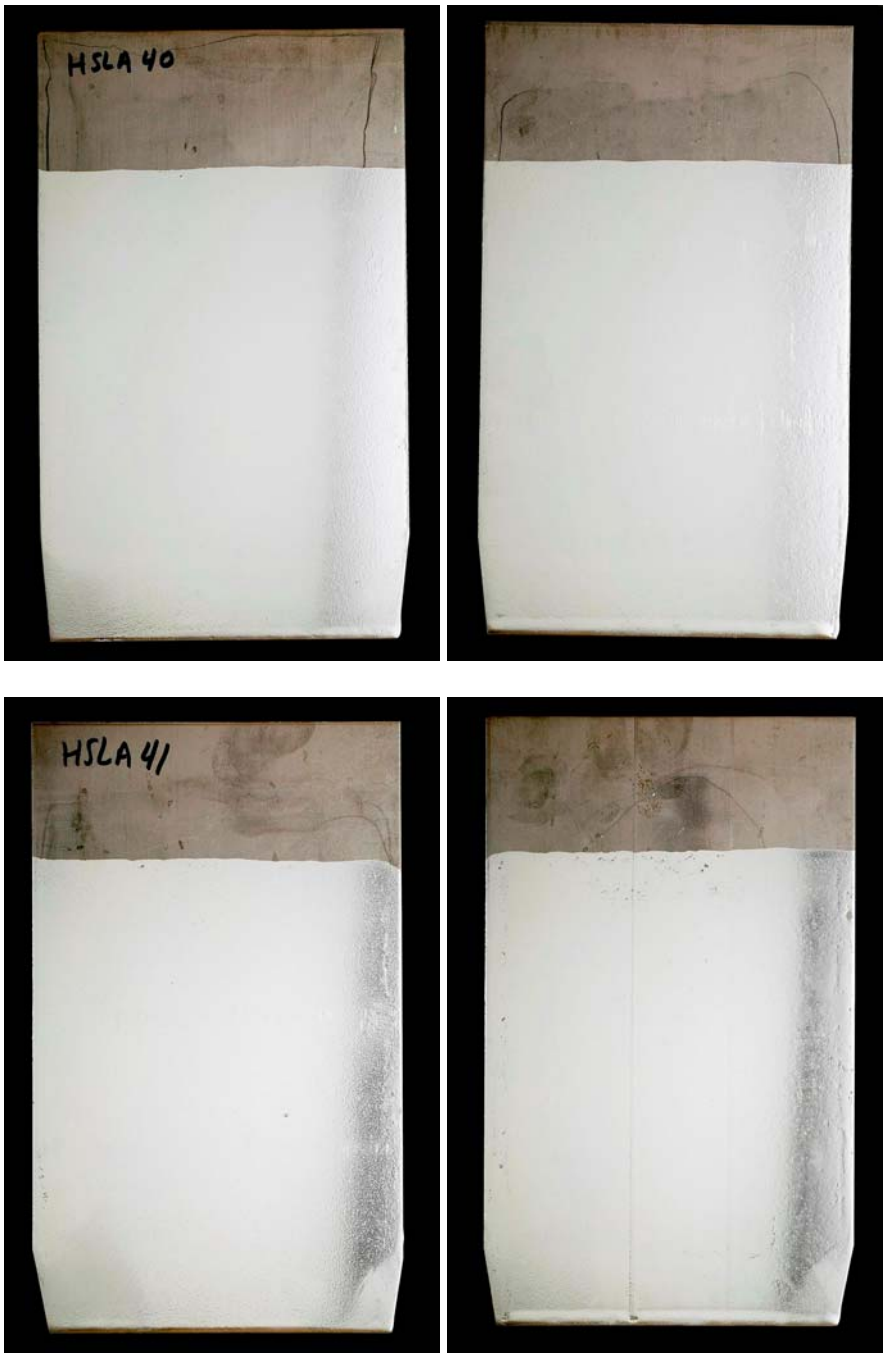

side 1 side 2

side 1 side 2

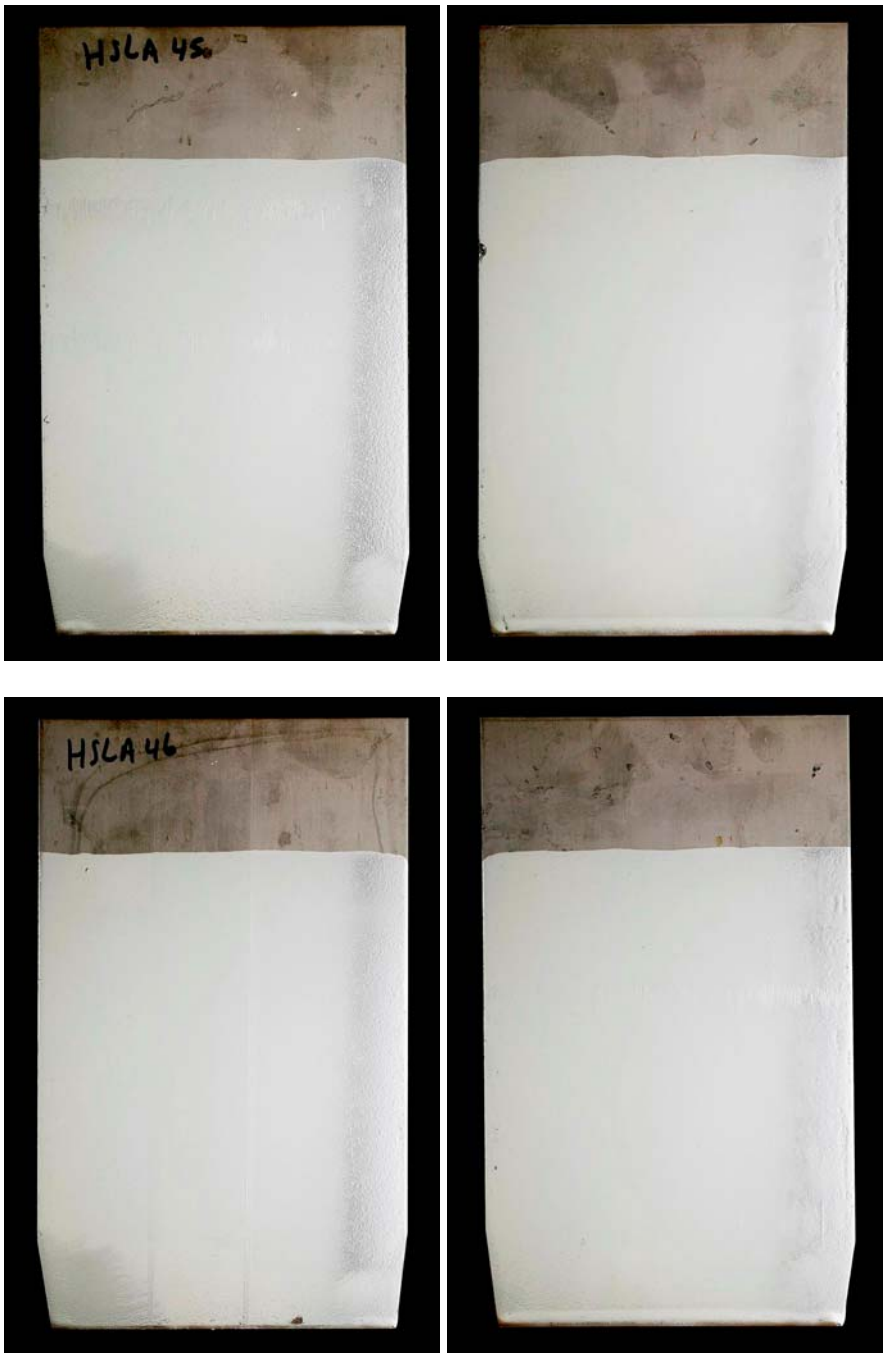

side 1 side 2

side 1 side 2

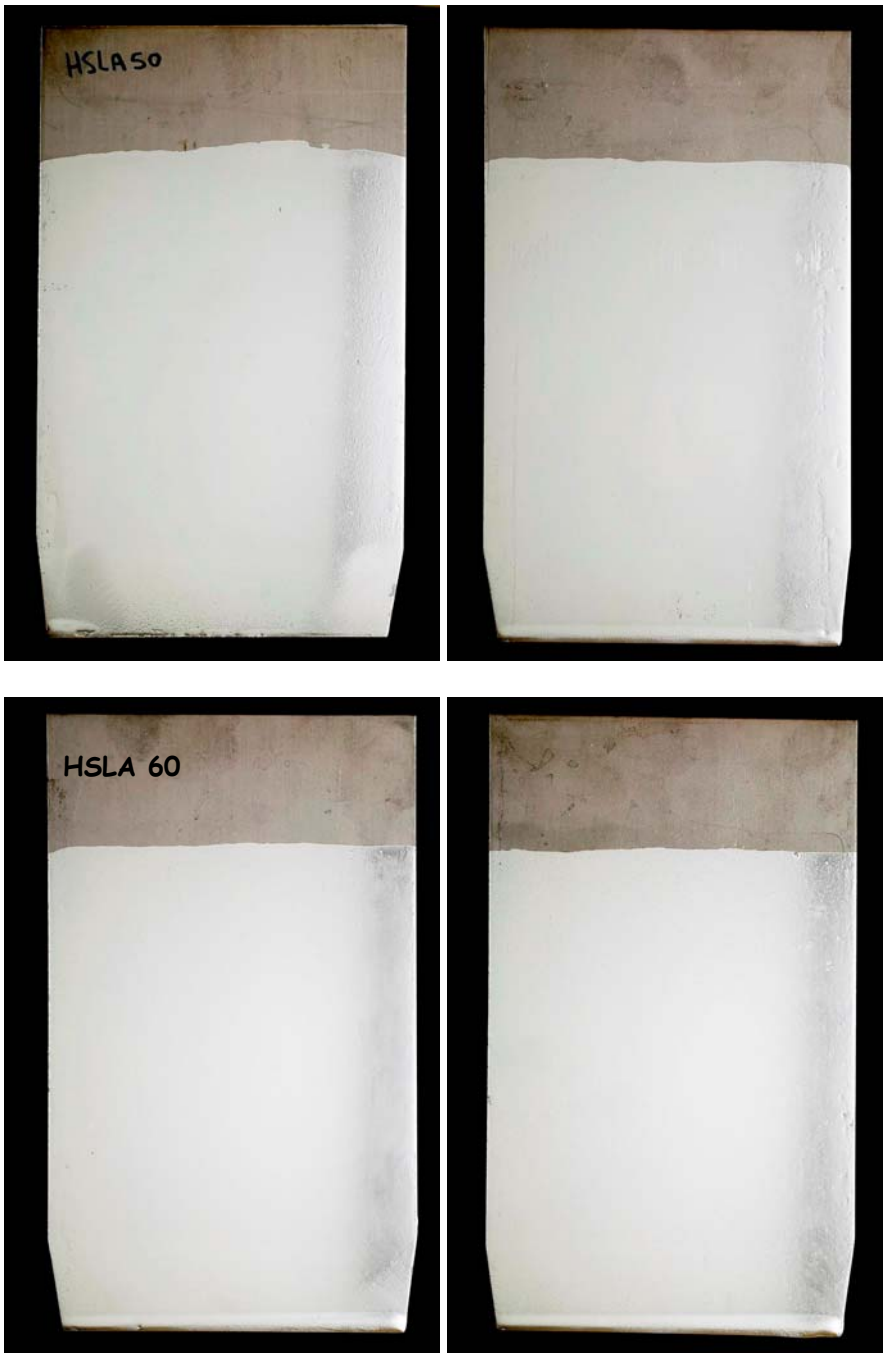

side 1 side 2

APPENDIX 3 – PHOTOGRAPHS OF GALVANNEALED COUPONS OF HSLA STEEL

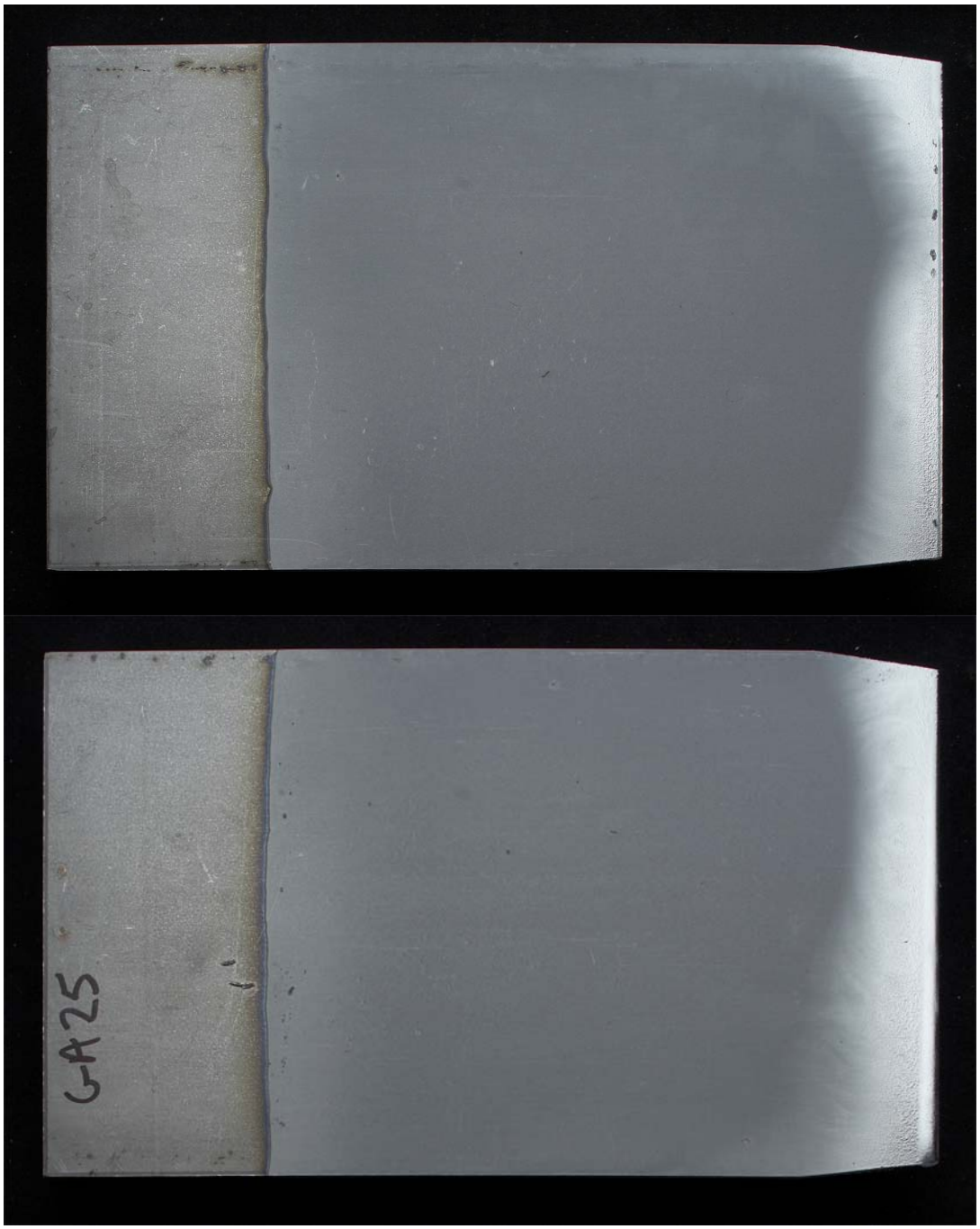

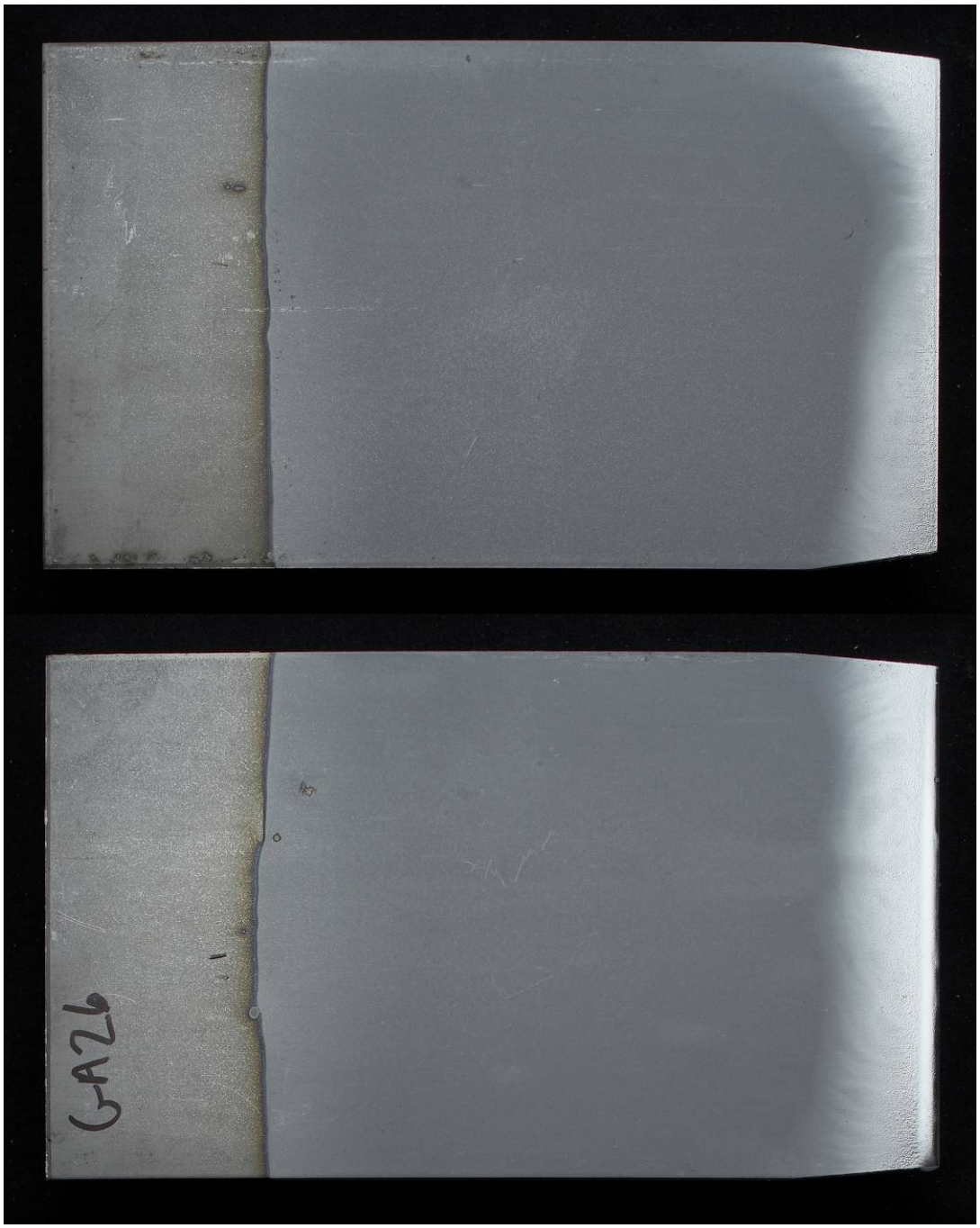
GA26

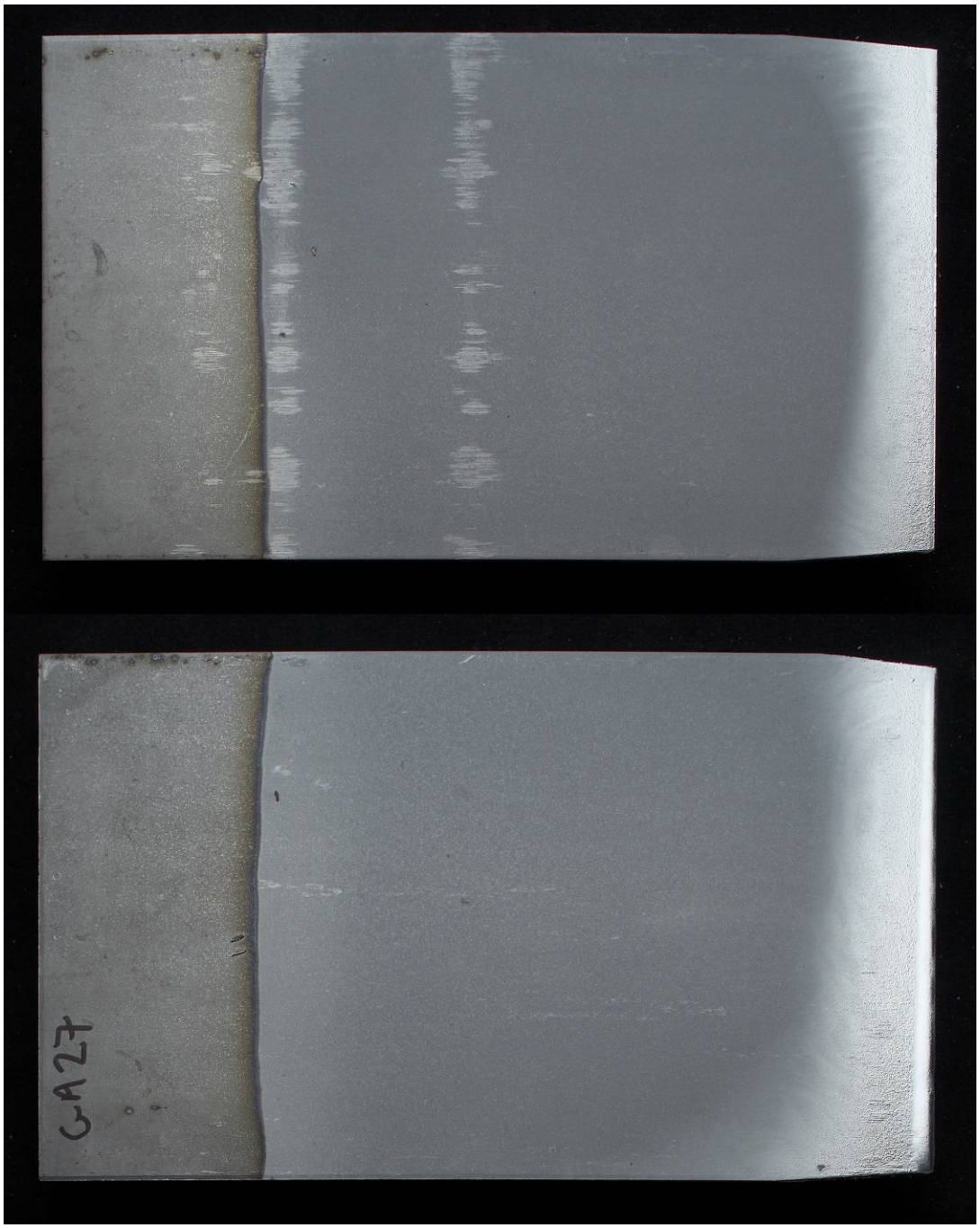
GA27

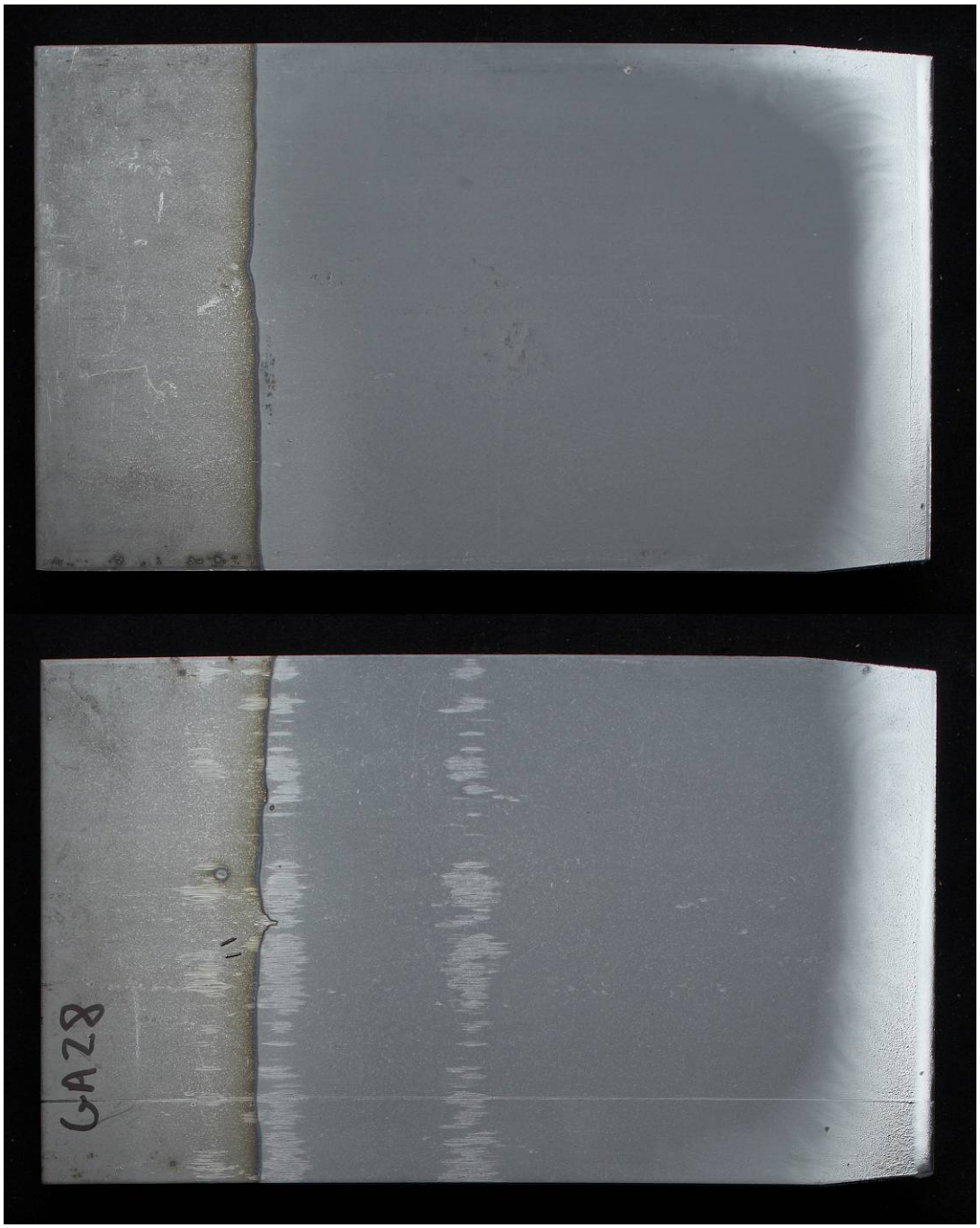
GA28

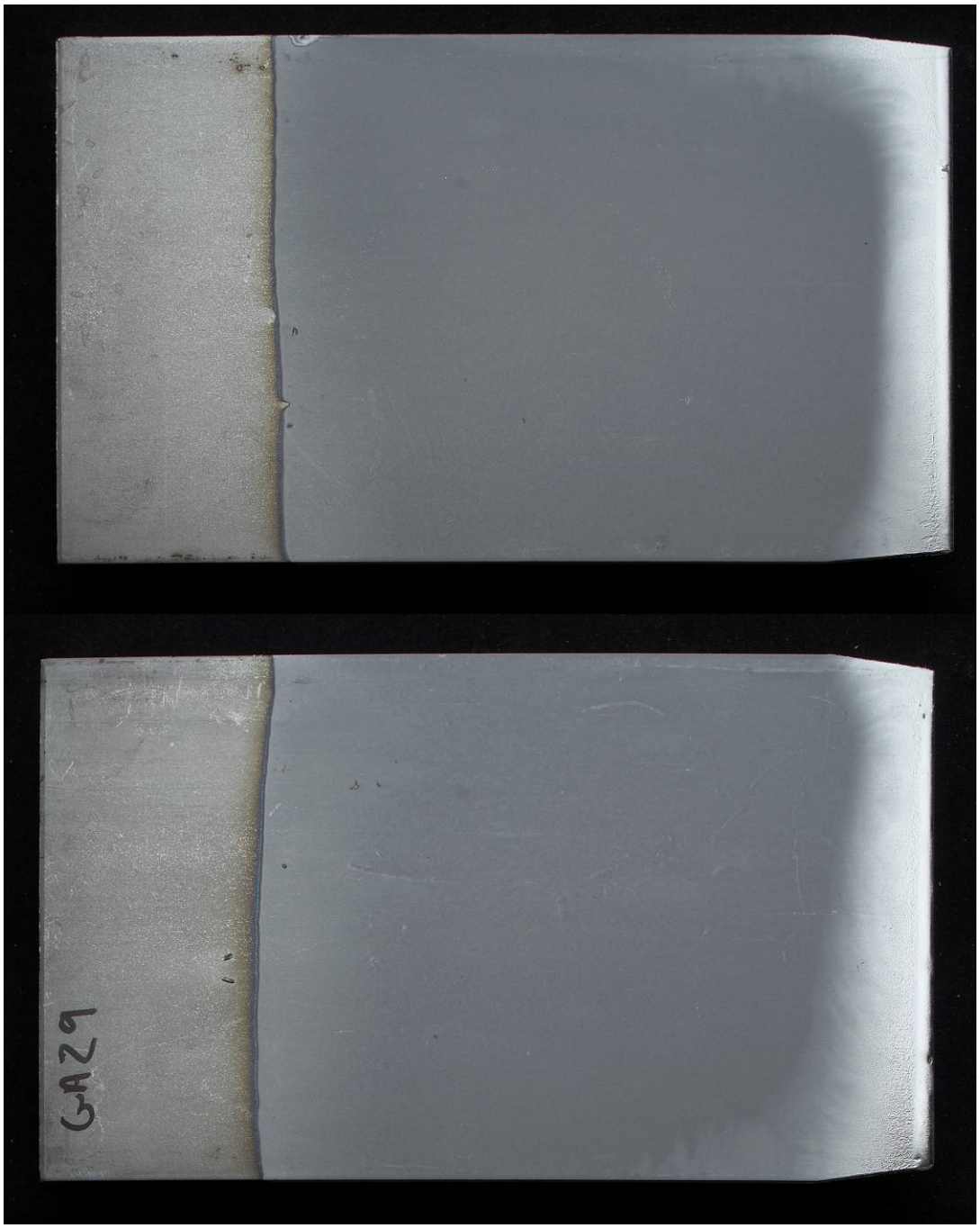
GA29

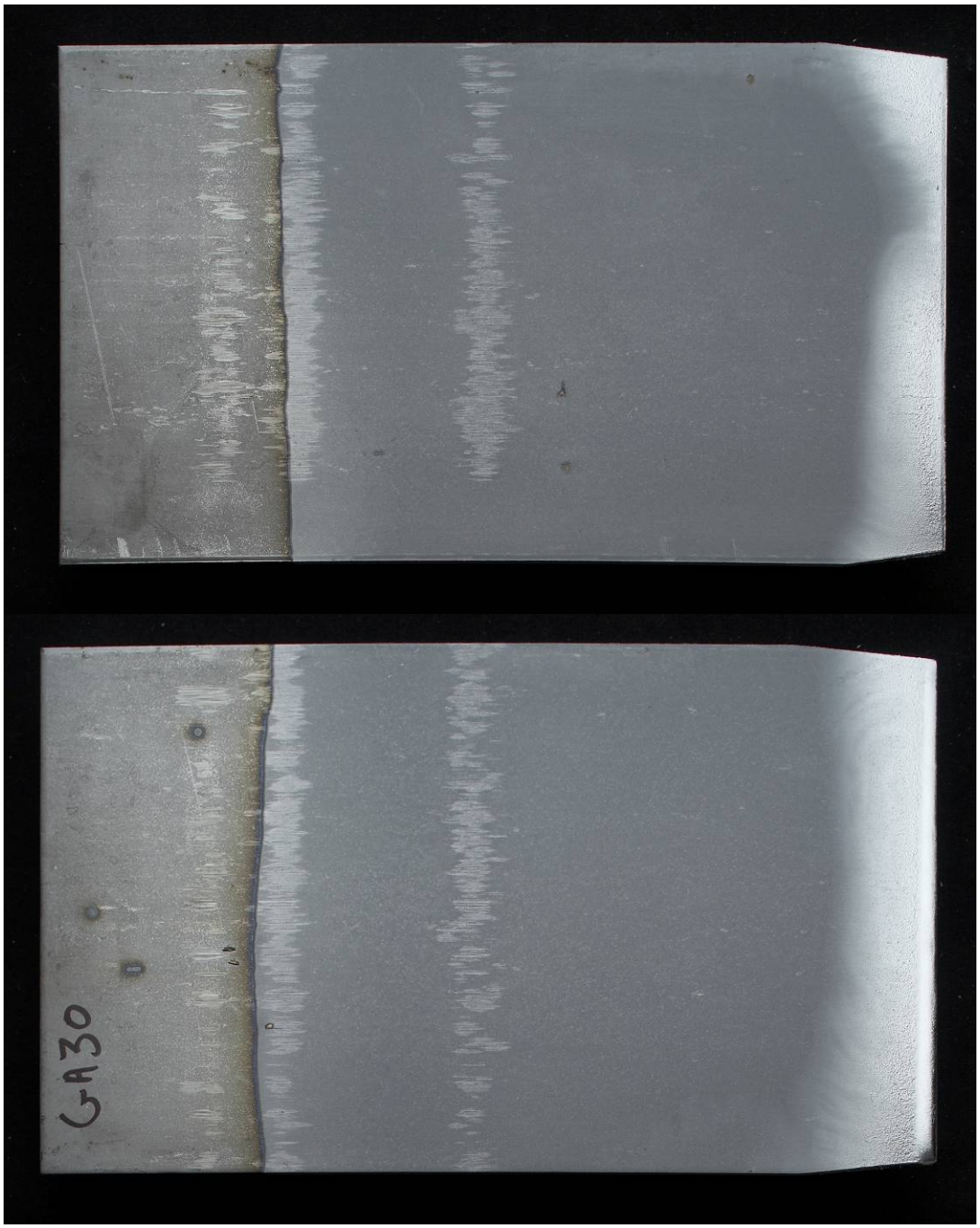
GA30

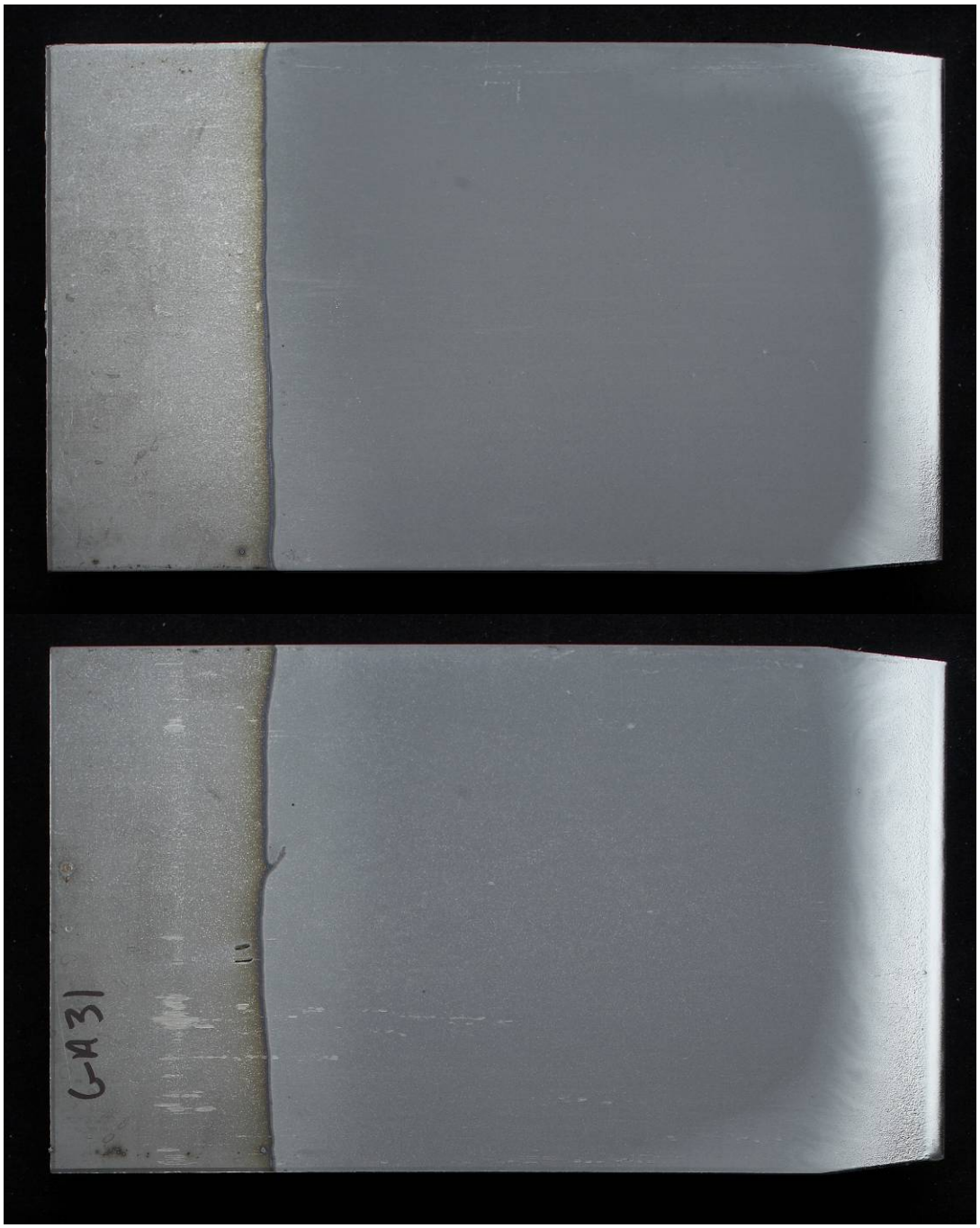
GA31

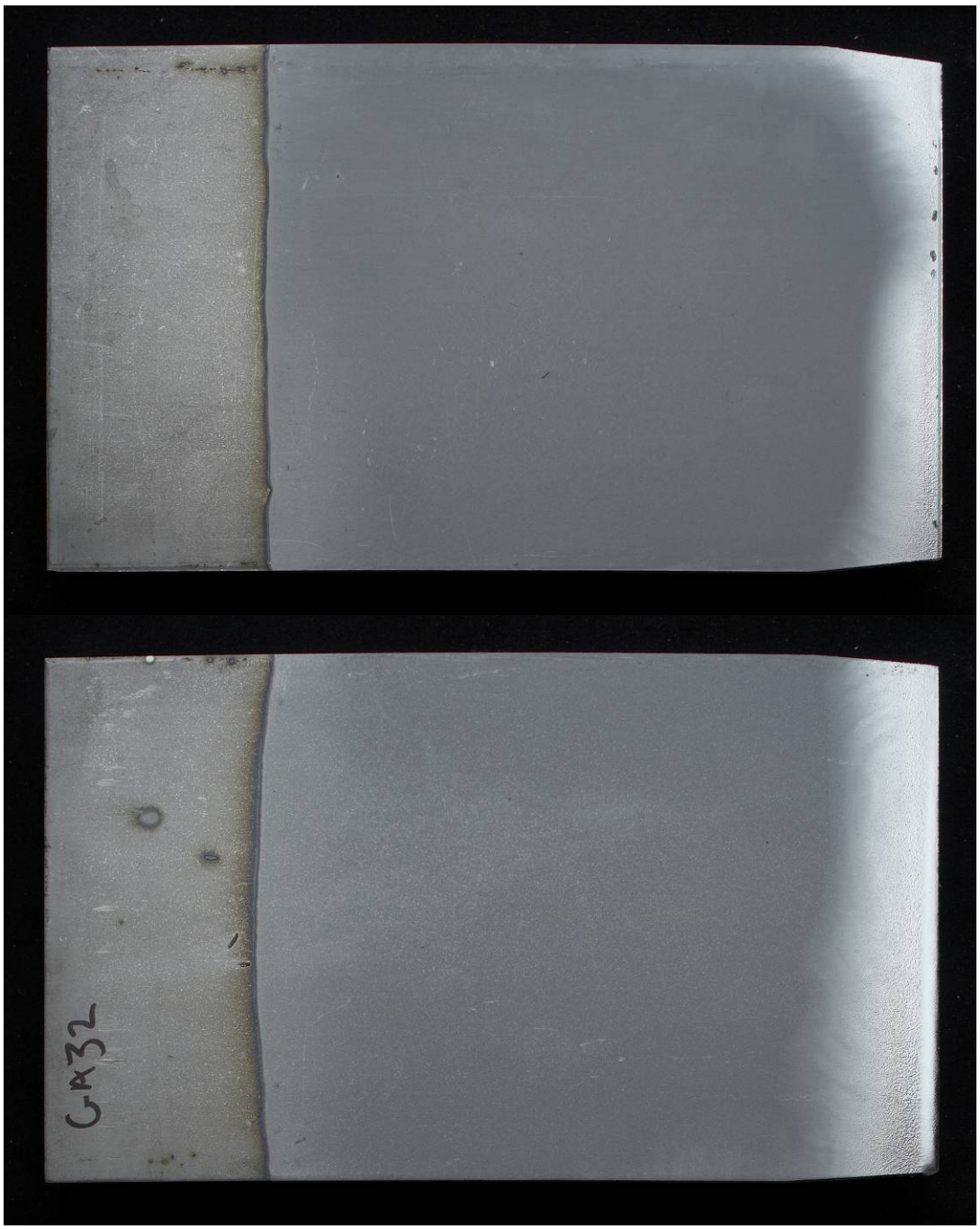
GA32

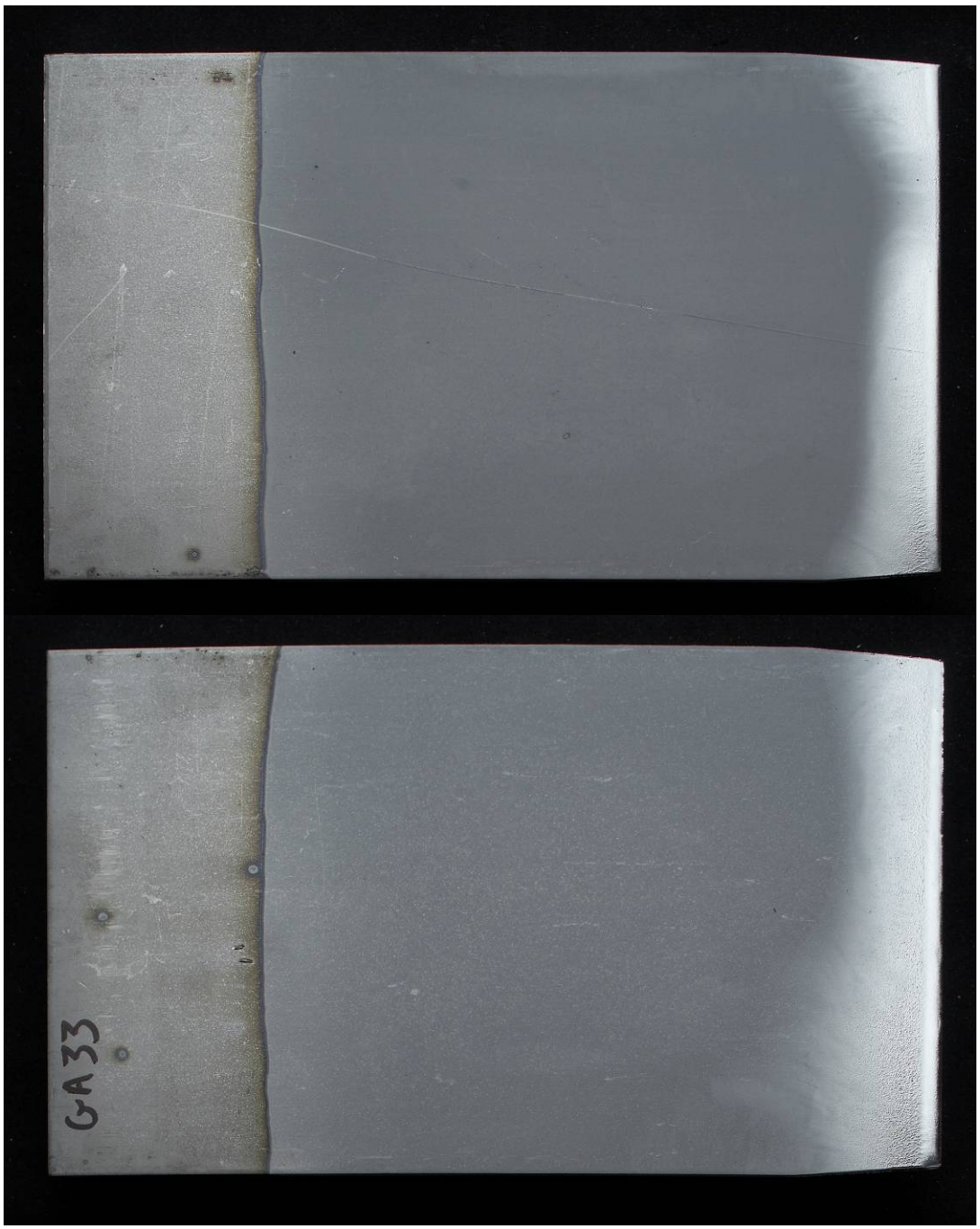
GA33

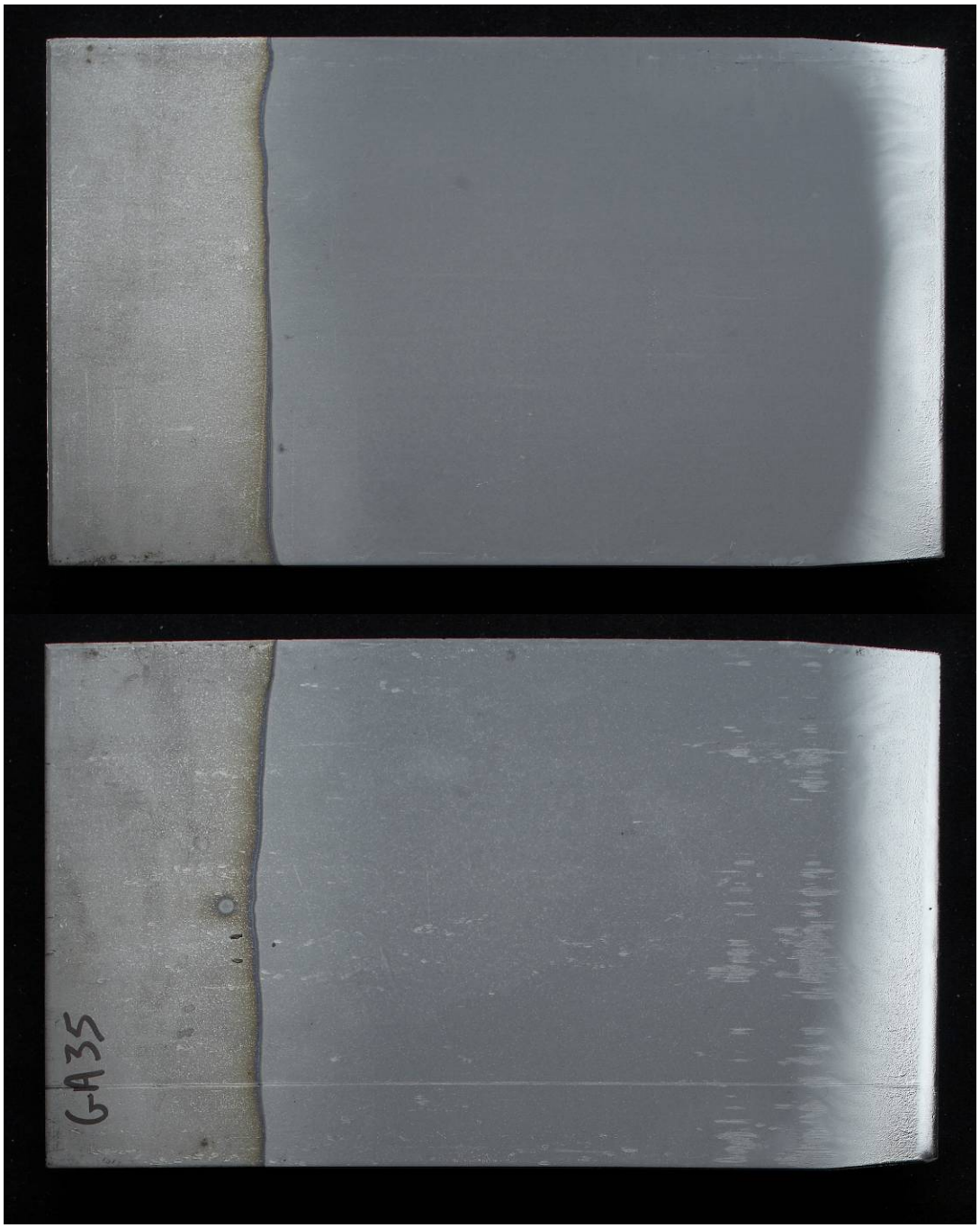
GA35

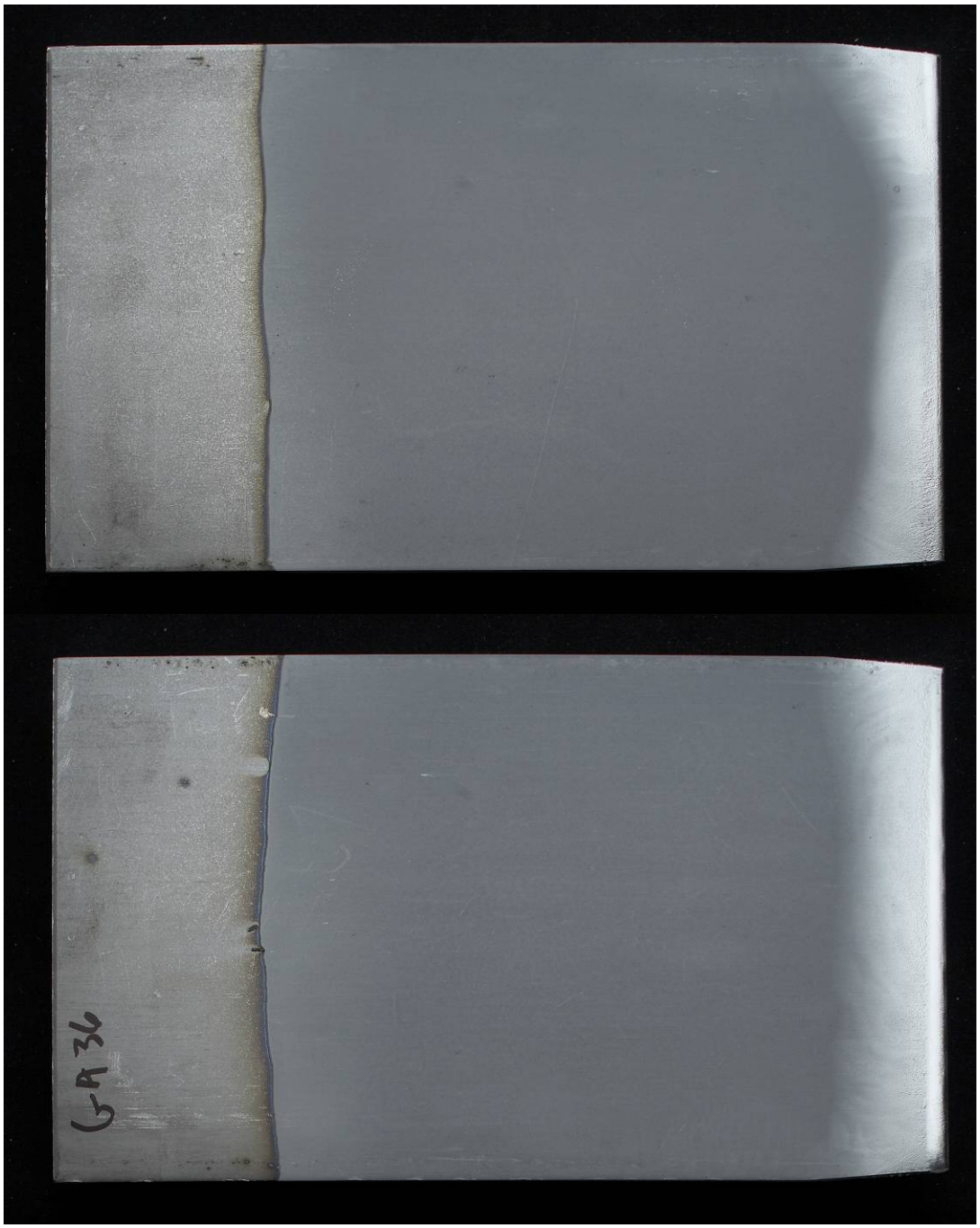
GR36

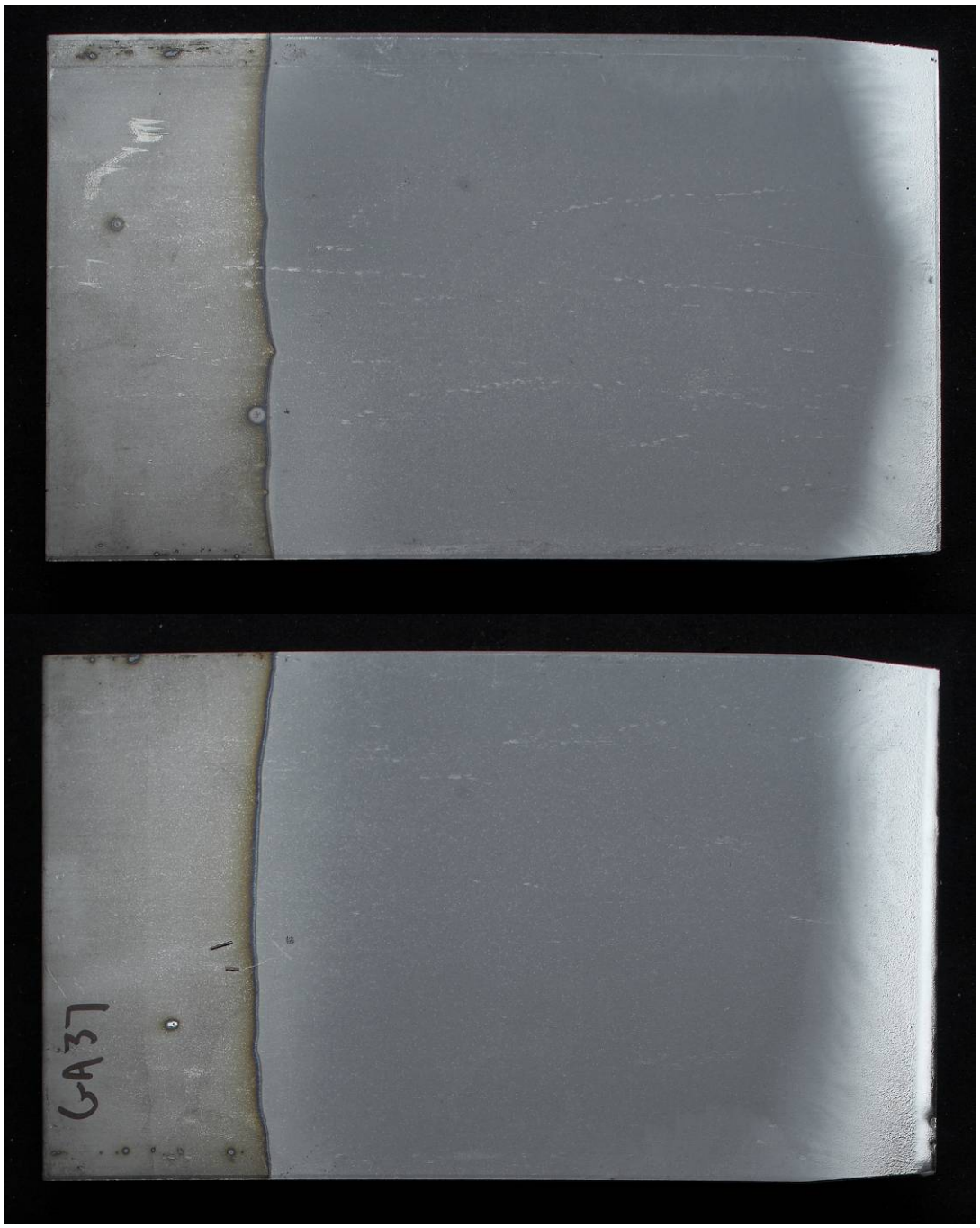
GA37


G-A38

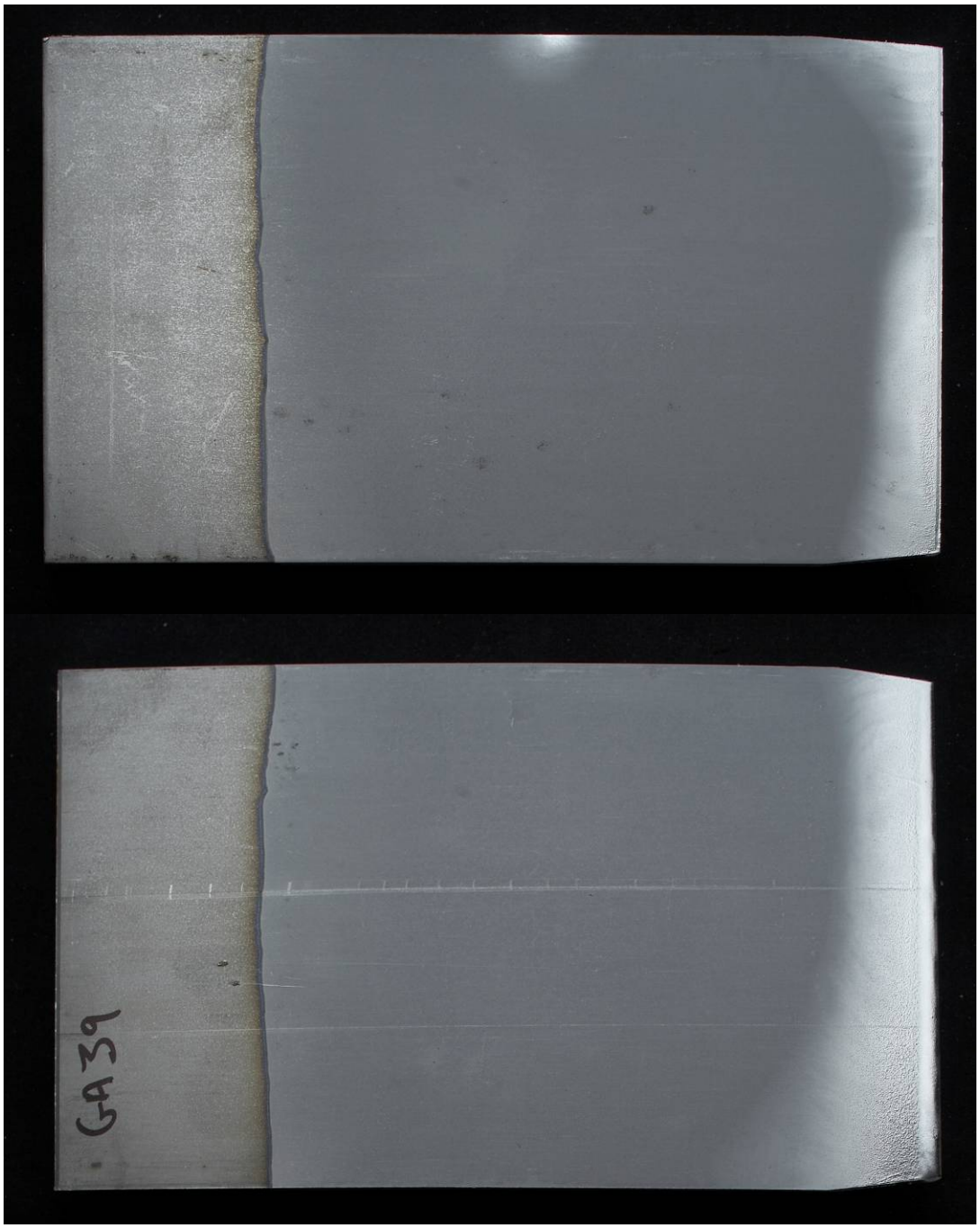
GA39

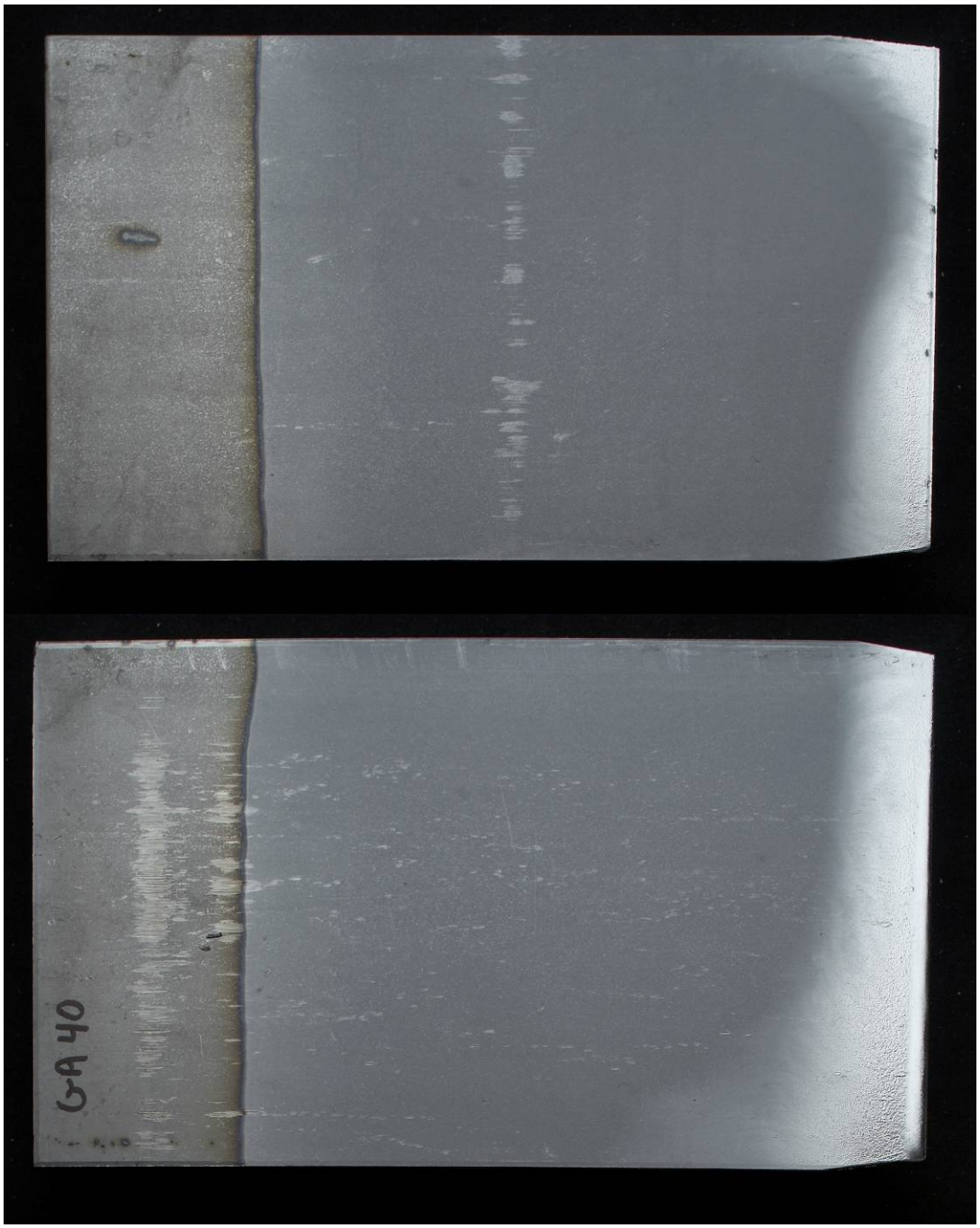
GA 40

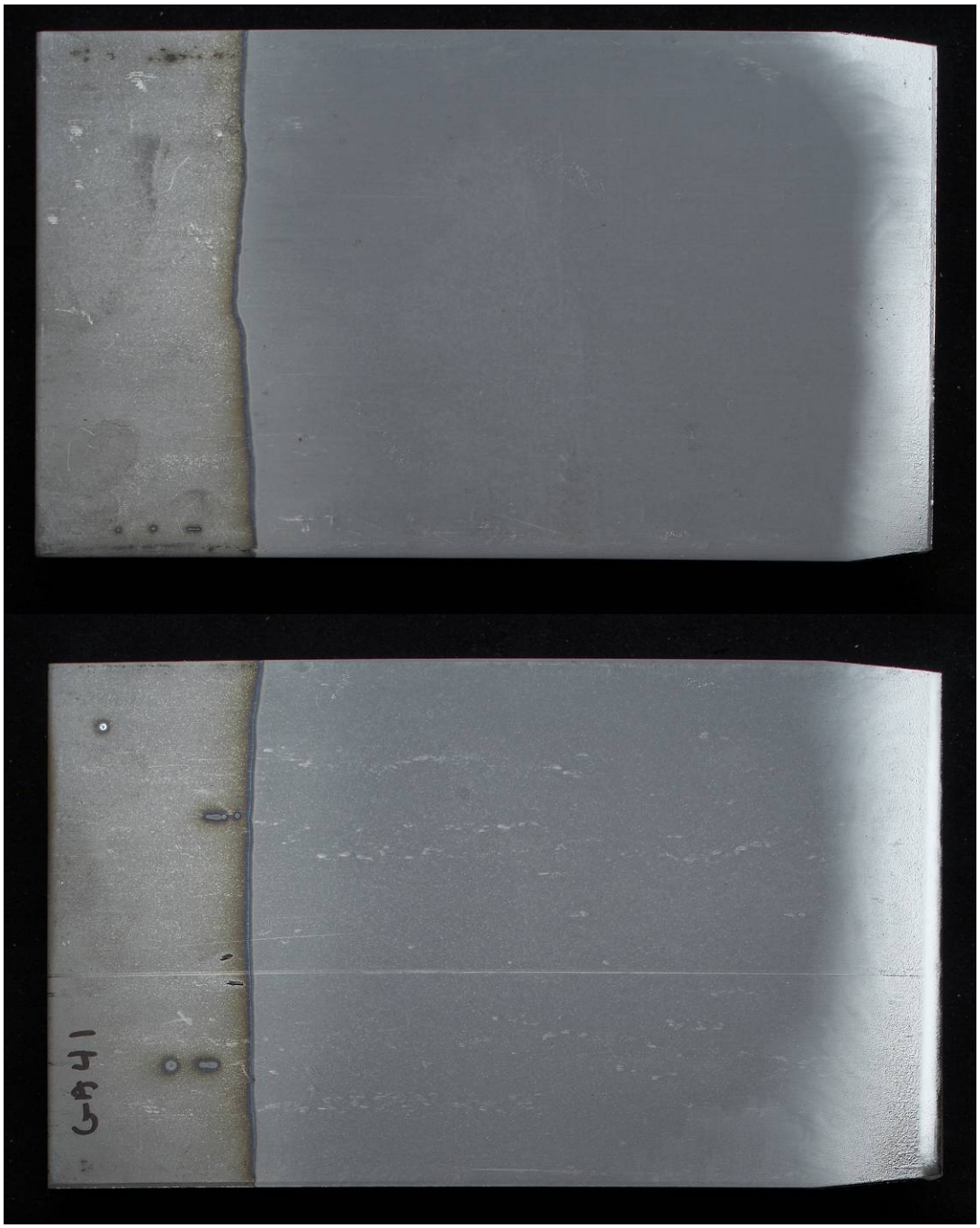


GA42

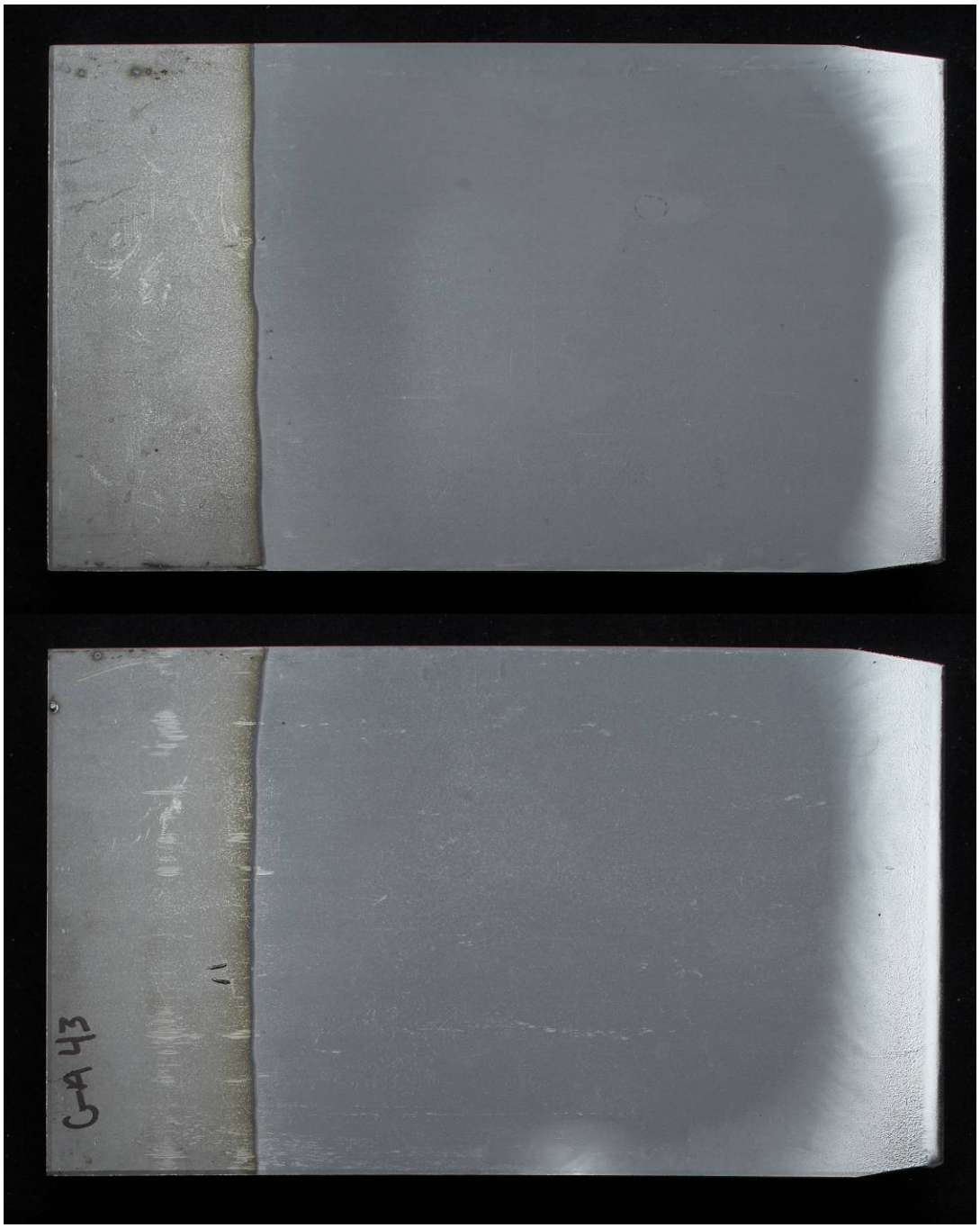
GA 43

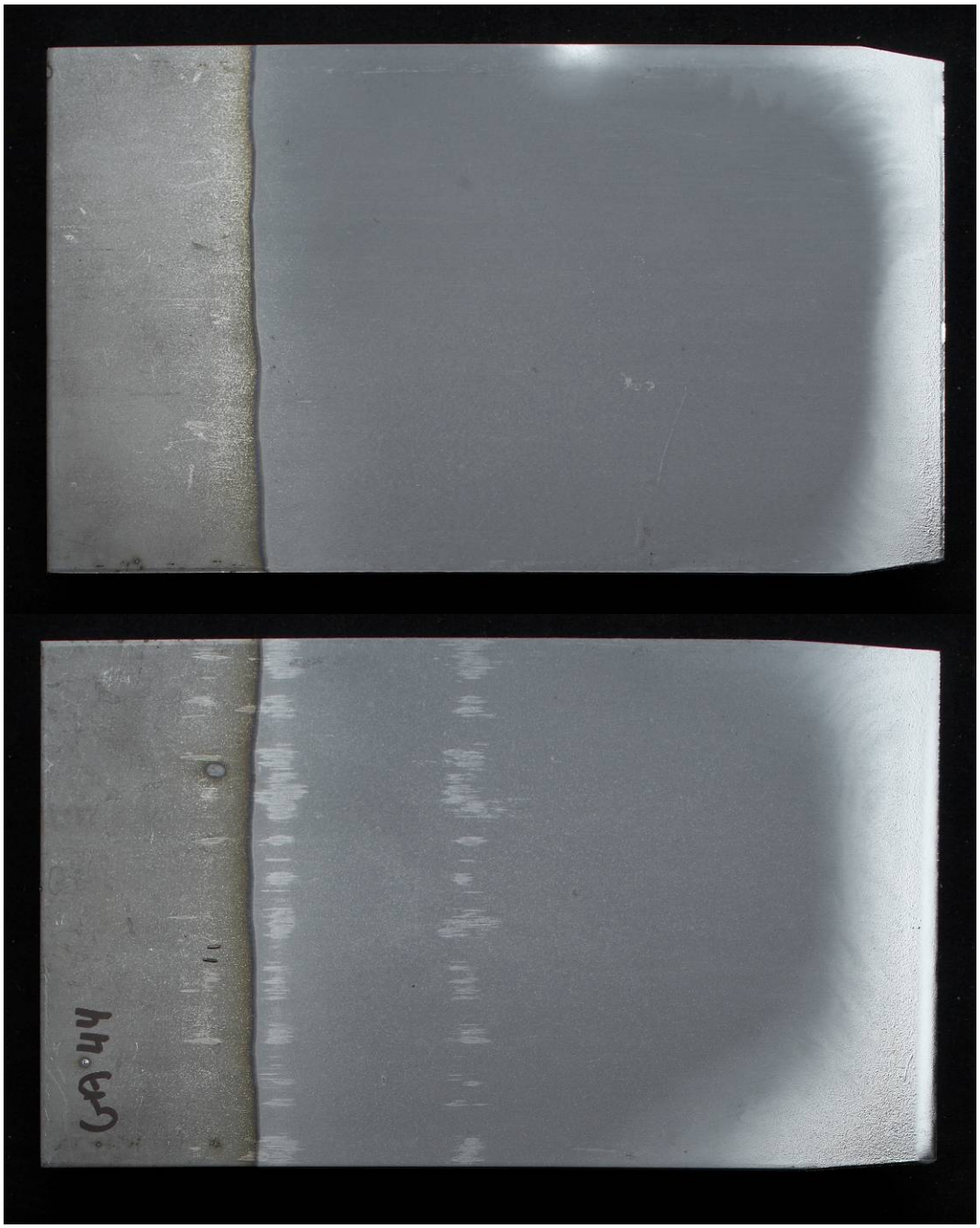

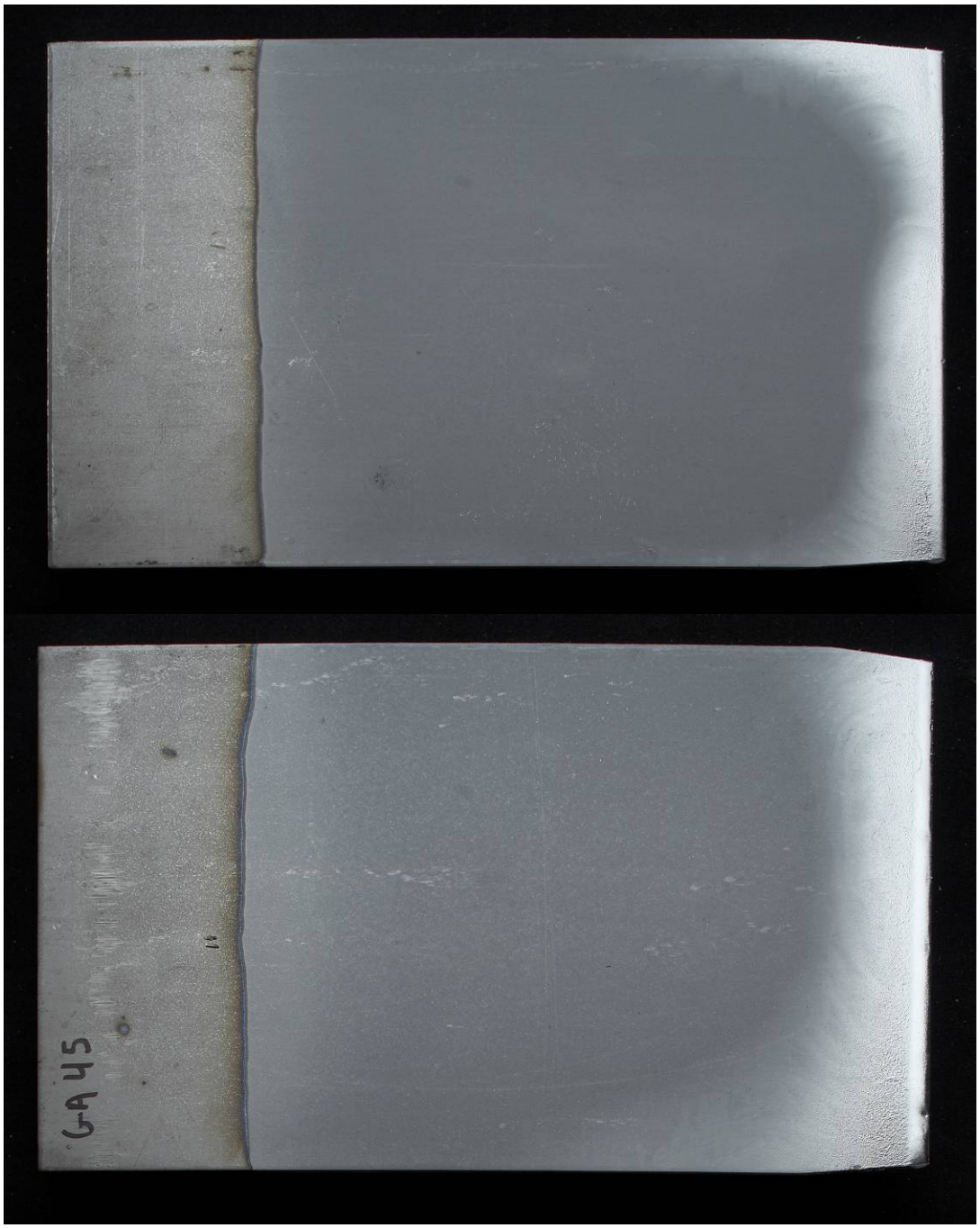
GA45

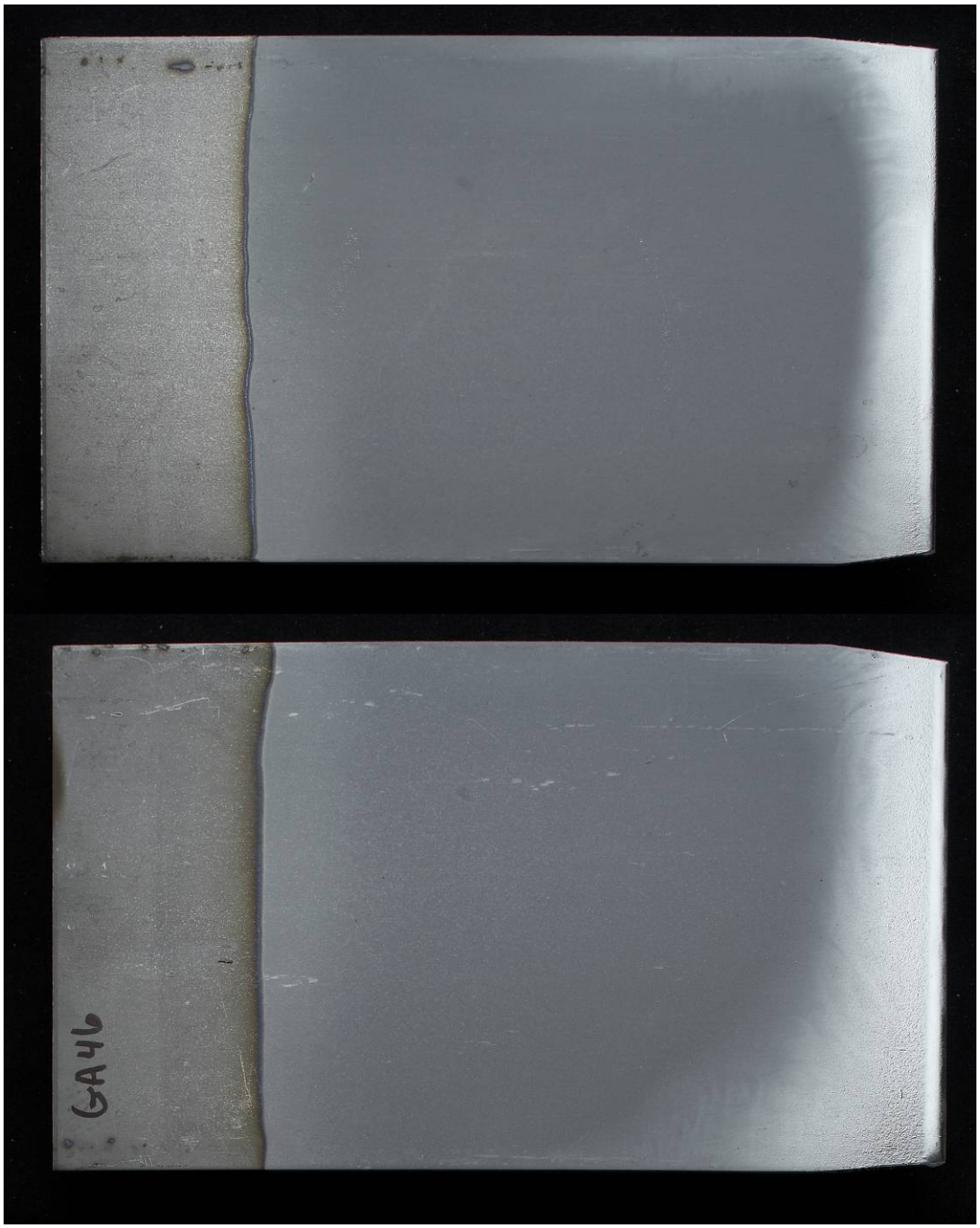
GA46

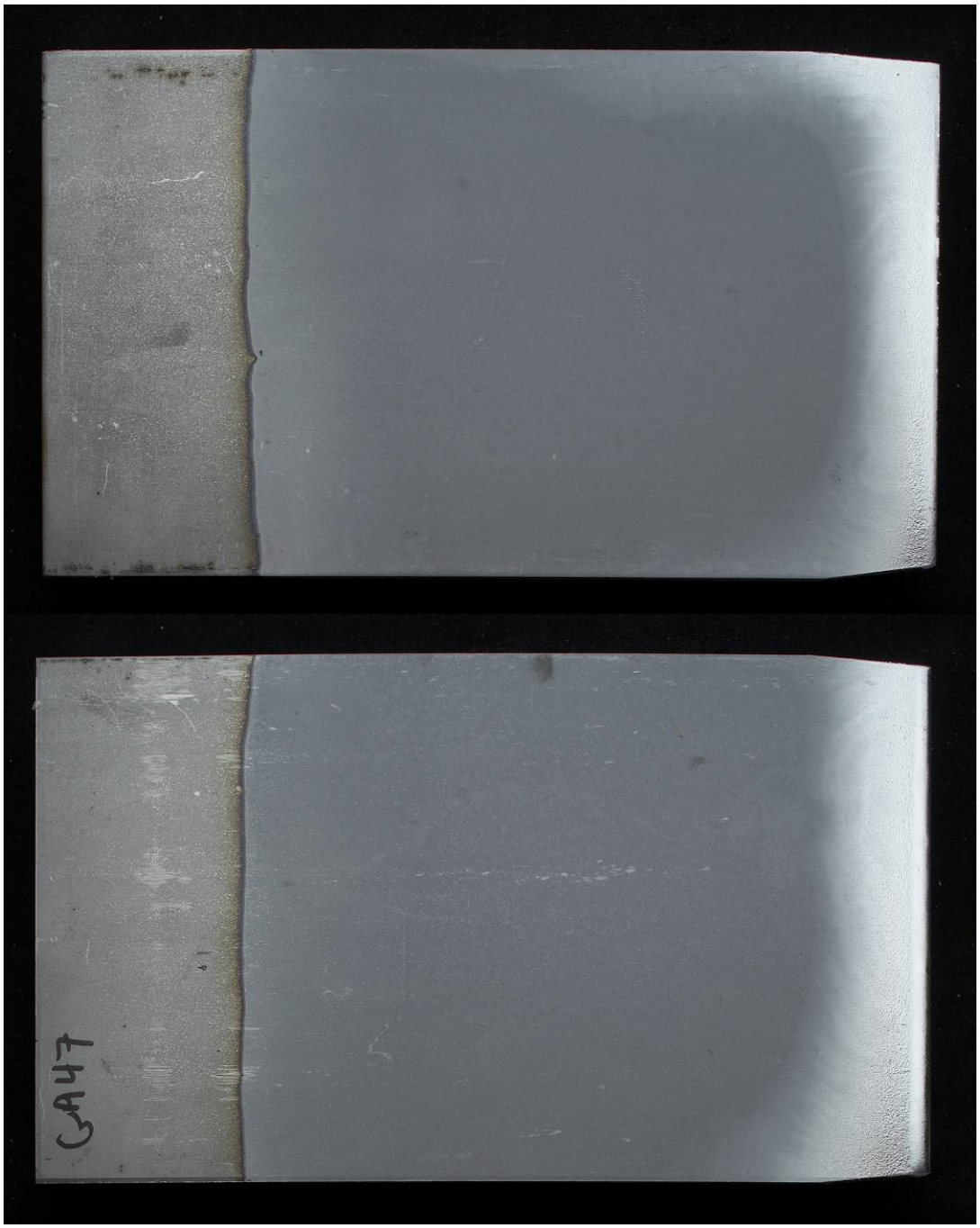
GA47

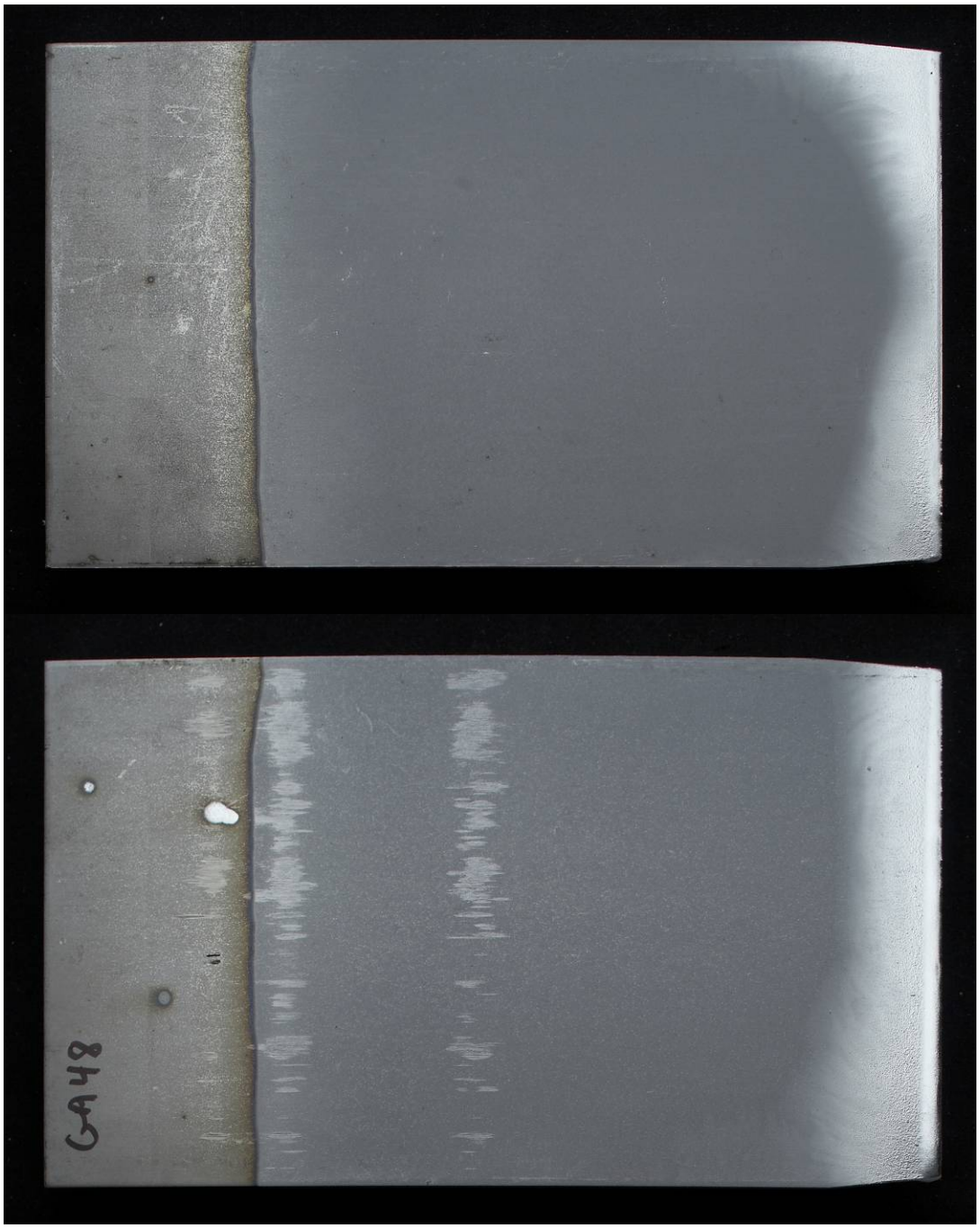
GA48


GA 49

APPENDIX 4

DYNAMIC TENSILE TESTS OF GALVANIZED HSLA STEEL

McGill University
Department of Mechanical Engineering

Quasi-static and Dynamic Tensile Strength Testing of DP, TRIP and Precipitation Hardening Steels

Semi-Annual Report, May 2007

Contract No. 23378-060599/001/SQ

Wael Dabboussi
James A. Nemes

for:

DEPARTMENT OF NATURAL RESOURCES
METALS TECHNOLOGY LAB

SCOPE

In this report the findings of laboratory experiments performed on tension coupons machined from the received HSLA galvanized plates are presented. The tension test results at quasi-static and two different high-strain rates are given in the form of stress vs. strain curves. The tested samples were subsequently examined using SEM. Images of the fractured surfaces are presented.

COUPONS

The quasi-static and high-strain rate tension tests were performed on coupons with the geometry as shown in Figure 1. The same sample geometry is used for both quasi-static and dynamic tests in order to eliminate any geometric effect on the results, hence allowing for an objective comparison and observation of the strain rate effect on the material mechanical response. The coupon geometry is dictated mainly by the nature of the high strain rate Hopkinson bar test, which requires a reduced sample length to produce the desired strain rates and in order the specimen to reach the equilibrium state faster, which leads to more reliable results. Figure 2 shows the orientation of the coupons with respect to the received plates. The shown orientation and topology is in accordance with the recommendation by MTL for minimizing any concentration of the galvanized layer and temperature gradient effect that could exist from the galvanizing process. The samples were machined using CNC.

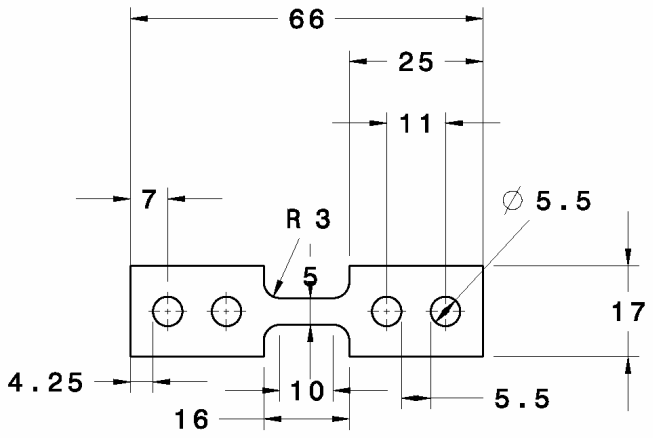

Figure 1. Coupon geometry and dimensions in mm

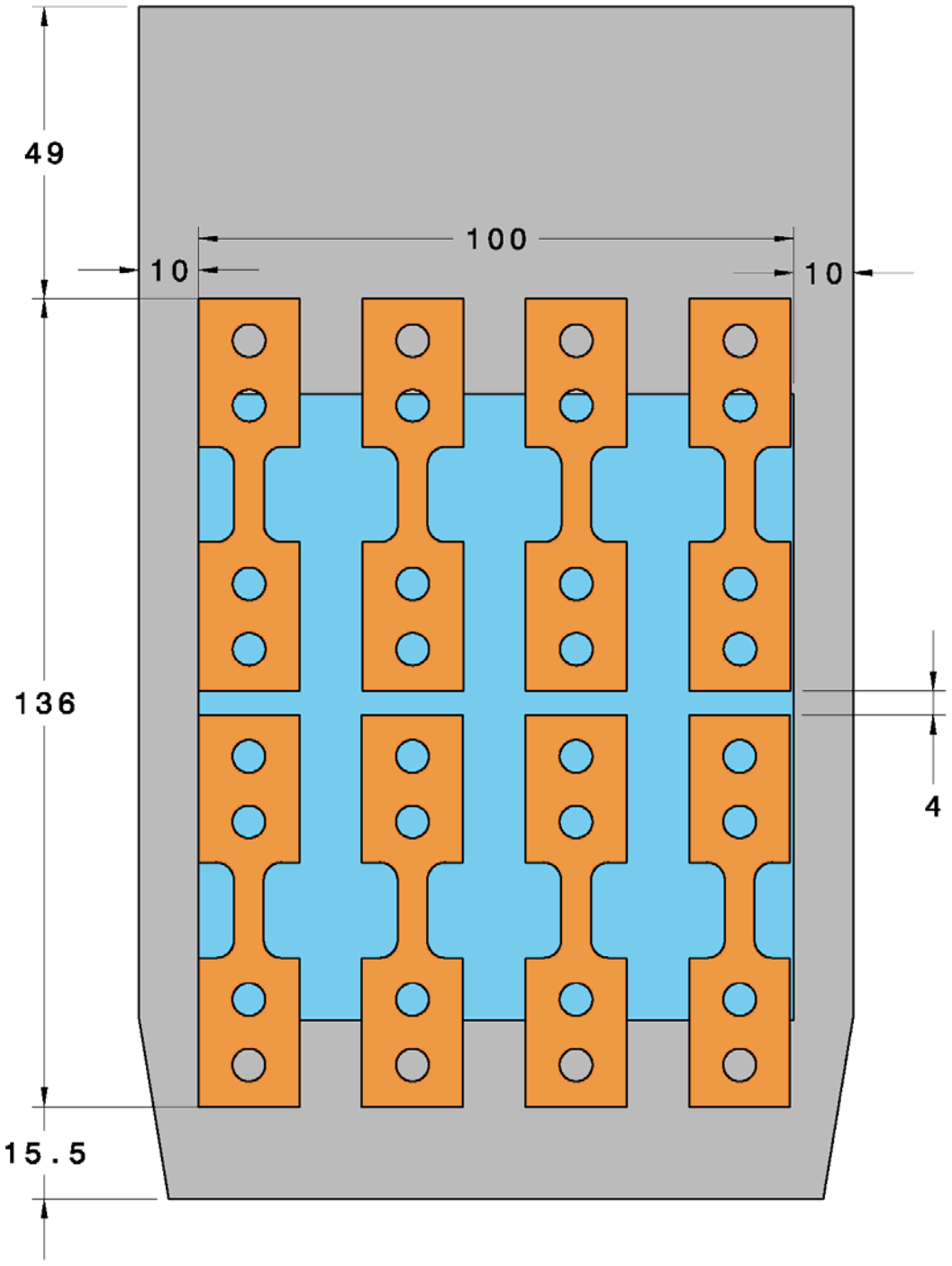

Figure 2. Dimensions of received plate (in mm) and coupon topology with respect to the plate. Blue area represents the recommended area for use.

TENSION TESTING

The tension experiments were conducted using the MTS hydraulic testing equipment for the quasi static tests whereas the direct Split Hopkinson Pressure Bars setup was used for the high strain rate tests. Three sets of data are presented in this report. The first set is of four experiments conducted at quasi-static rate, the second is of four experiments conducted at high strain rate and the third set is of experiments conducted at a different high strain rate. The dimension of the uniform gage section (10 mm) was used to determine the engineering strain for all the presented tests.

Quasi-static Tension Results

The quasi static tension test was performed on the machined coupons at room temperature and at a nominal strain rate of 10^{-3} s^{-1}. Figure 3 shows the engineering stress vs. engineering strain results, whereas Figure 4 shows the corresponding true stress vs. true strain results to the point of localization. The tests display reasonable repeatability in terms of the UTS value of 638 MPa and elongation to failure of about 36 %.

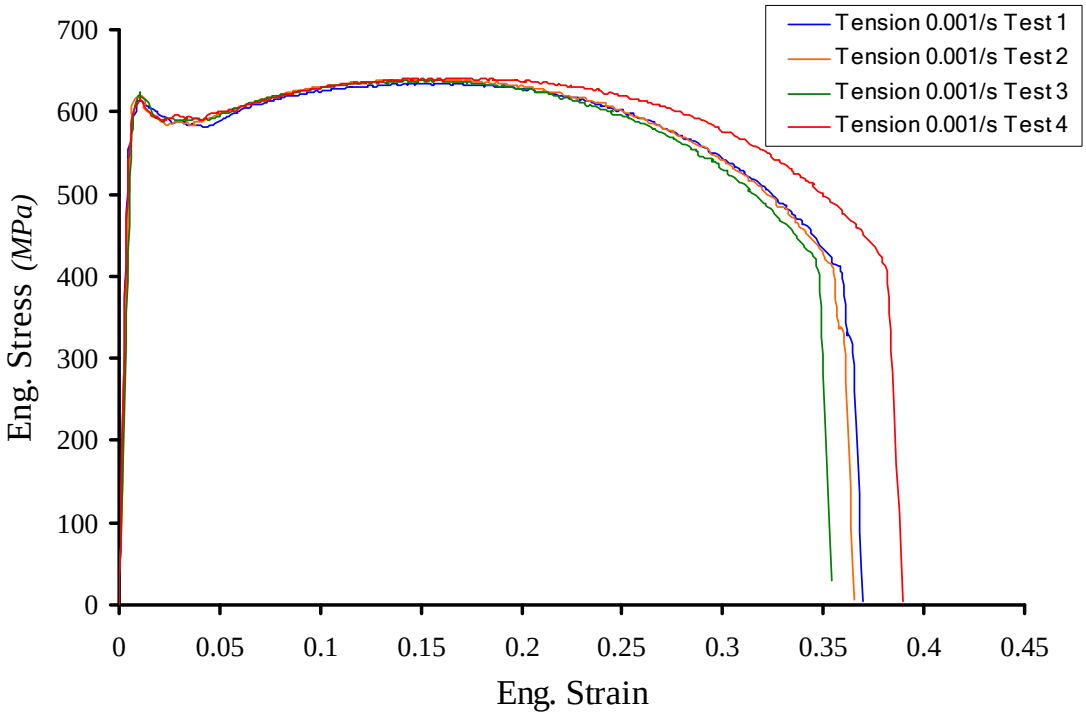

Figure 3. Quasi-static engineering stress vs. engineering strain results

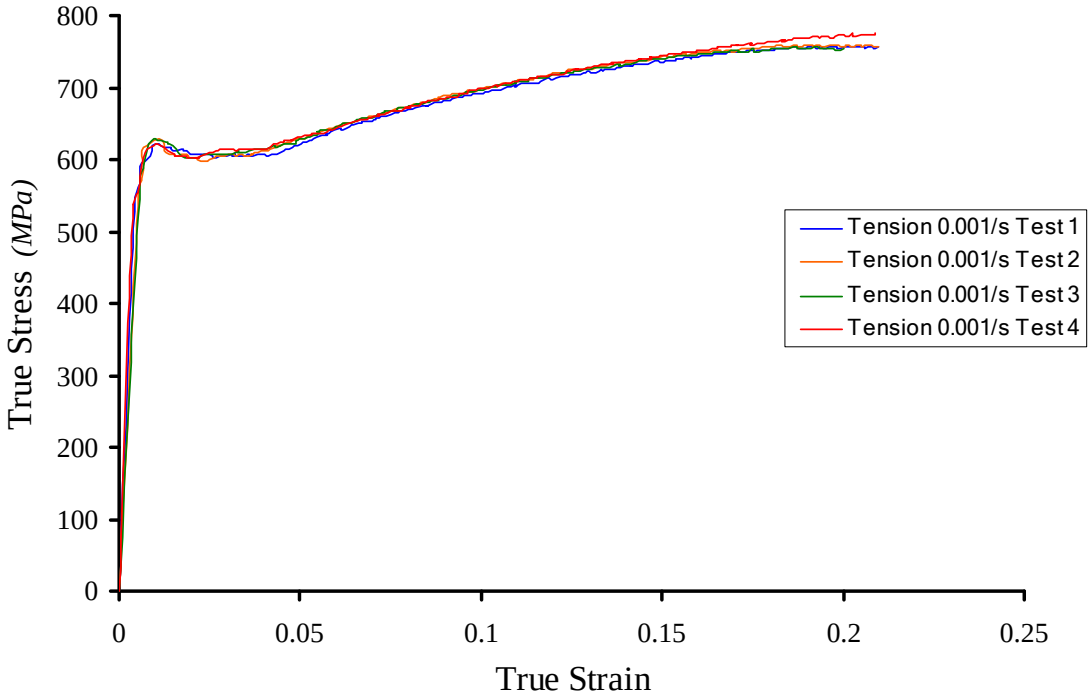

Figure 4. Quasi-static true stress vs. true strain results

High Strain Rate Tension Results

High strain rate tests were also performed on the machined coupons at 2 different rates. Figure 5 shows the engineering stress vs. engineering strain results of the tests performed at a strain rate of 900 s^{-1}. Figure 6 shows the corresponding true stress vs. true strain results. An increase in the UTS to approximately 698 MPa is observed from the plotted results, however the total elongation dropped to about 27 %.

Figure 7 shows the engineering stress vs. engineering strain of the tests performed at a strain rate of 1600 s^{-1}. Figure 8 shows the corresponding true stress vs. true strain results. An increase in the UTS to approximately 740 MPa is observed from the plotted results with the total elongation remaining comparable to that of the samples tested at 900 s^{-1}.

In order to better visualize the abovementioned effects of the variation of the strain rate on the mechanical response, one test was selected from each of the three sets and plotted together as shown in Figures 9 and 10 to show the engineering and true stress vs. strain results, respectively. The UTS and uniform elongation results for the three rates are summarized in Table 1.

Table 1. UTS and uniform elongation summary

Test	**UTS** *(MPa)*	**Uniform Elongation** *(%)*
Tension 10^{-3} s^{-1}	638 (+1/-3)	15.5 (+0.5/-0.5)
Tension 900 s^{-1}	698 (+9/-8)	10.25 (+0.75/-0.25)
Tension 1600 s^{-1}	740 (+8/-9)	9.75 (+0.25/-0.75)

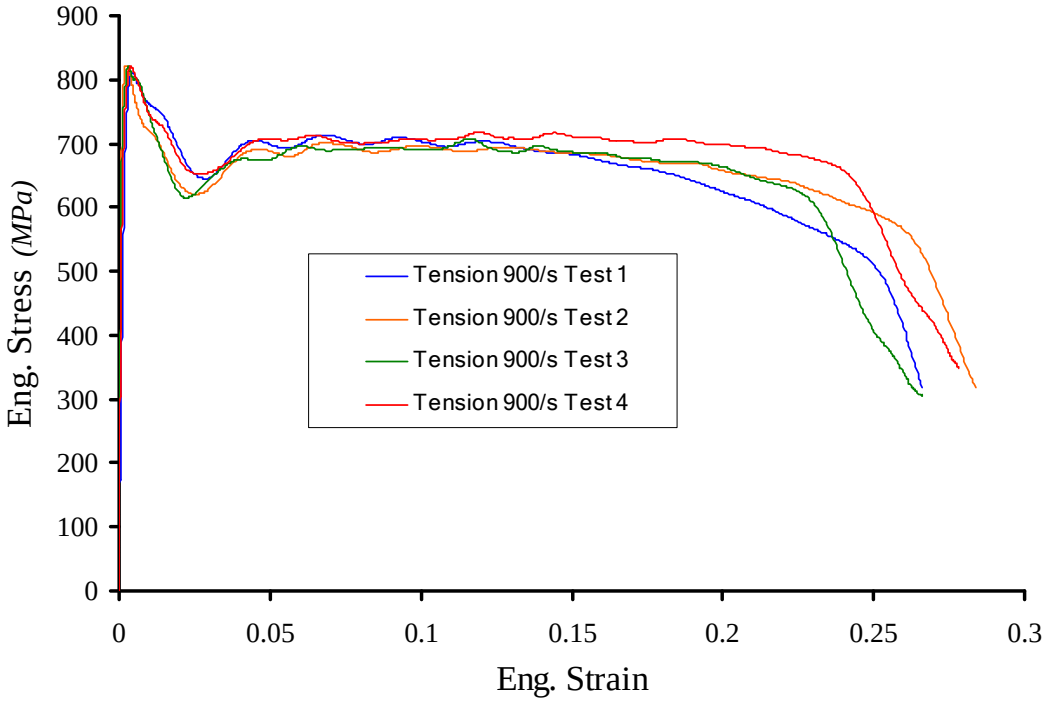

Figure 5. Dynamic engineering stress vs. engineering strain results at 900 s^{-1}

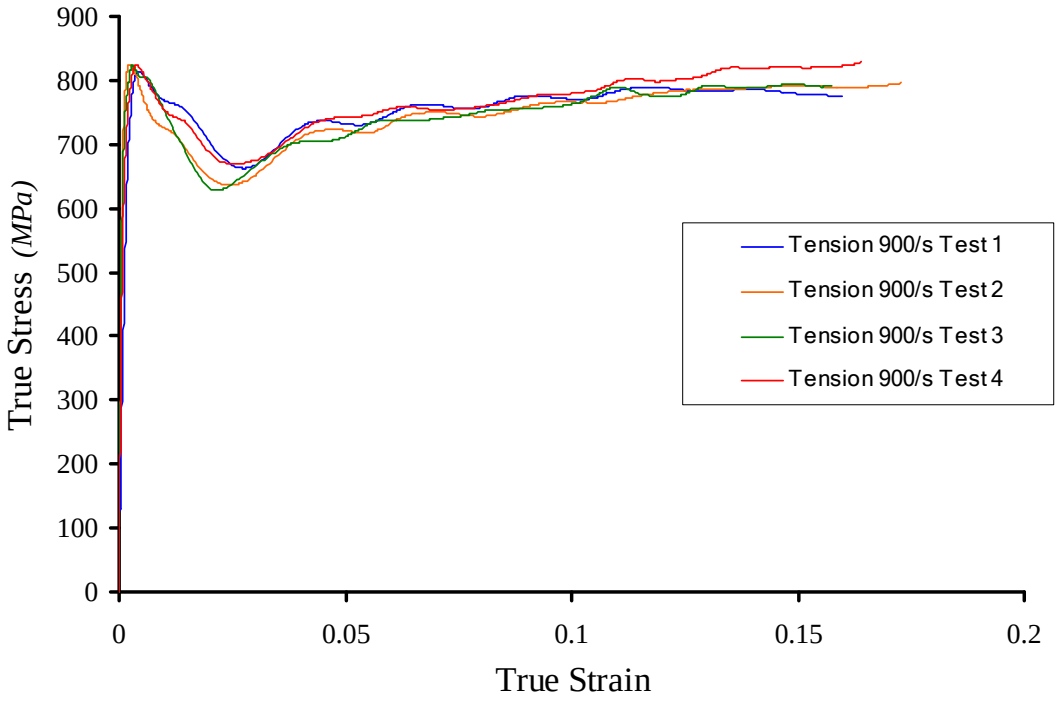

Figure 6. Dynamic true stress vs. true strain results at 900 s^{-1}

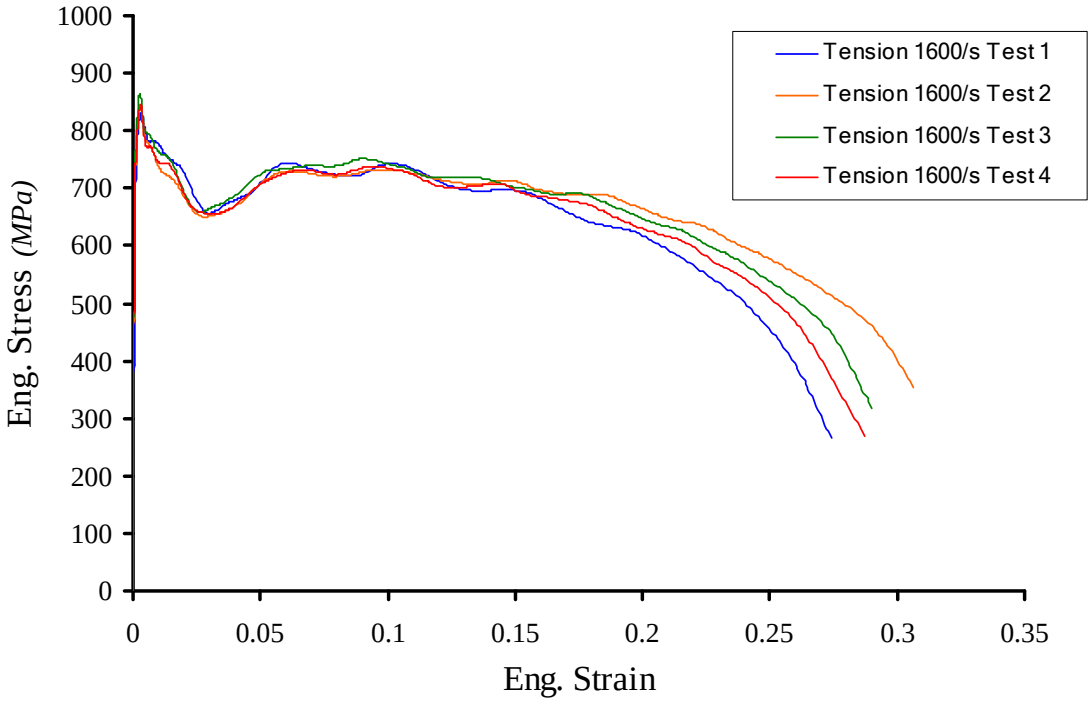

Figure 7. Dynamic engineering stress vs. engineering strain results at 1600 s^{-1}

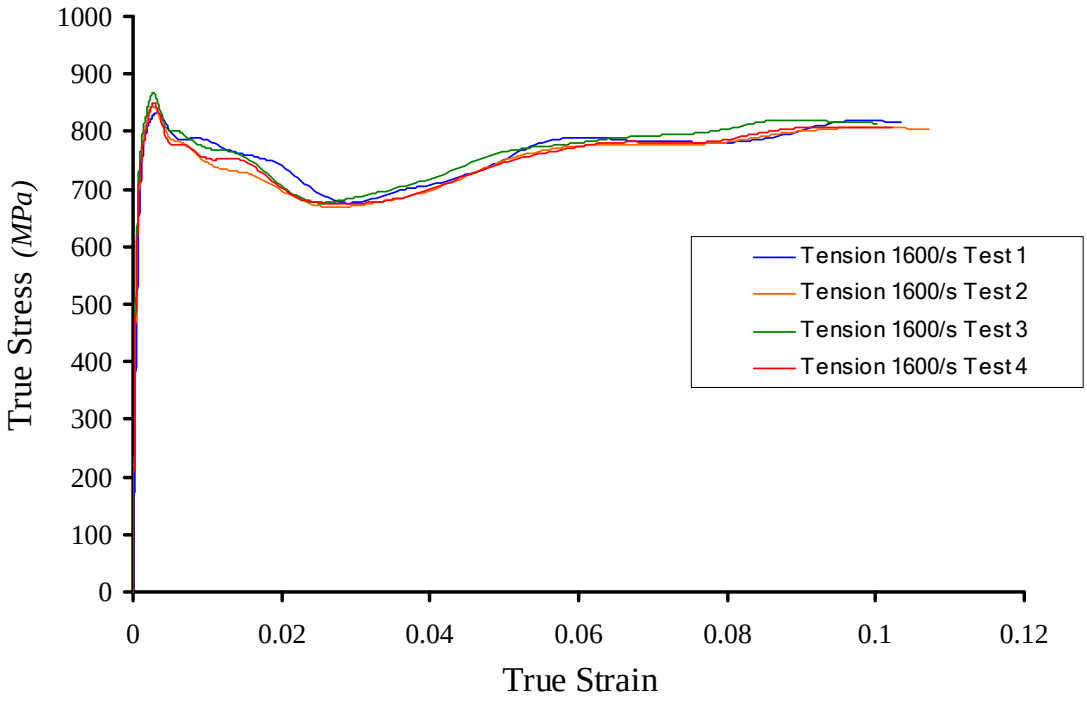

Figure 8. Dynamic true stress vs. true strain results at 1600 s^{-1}

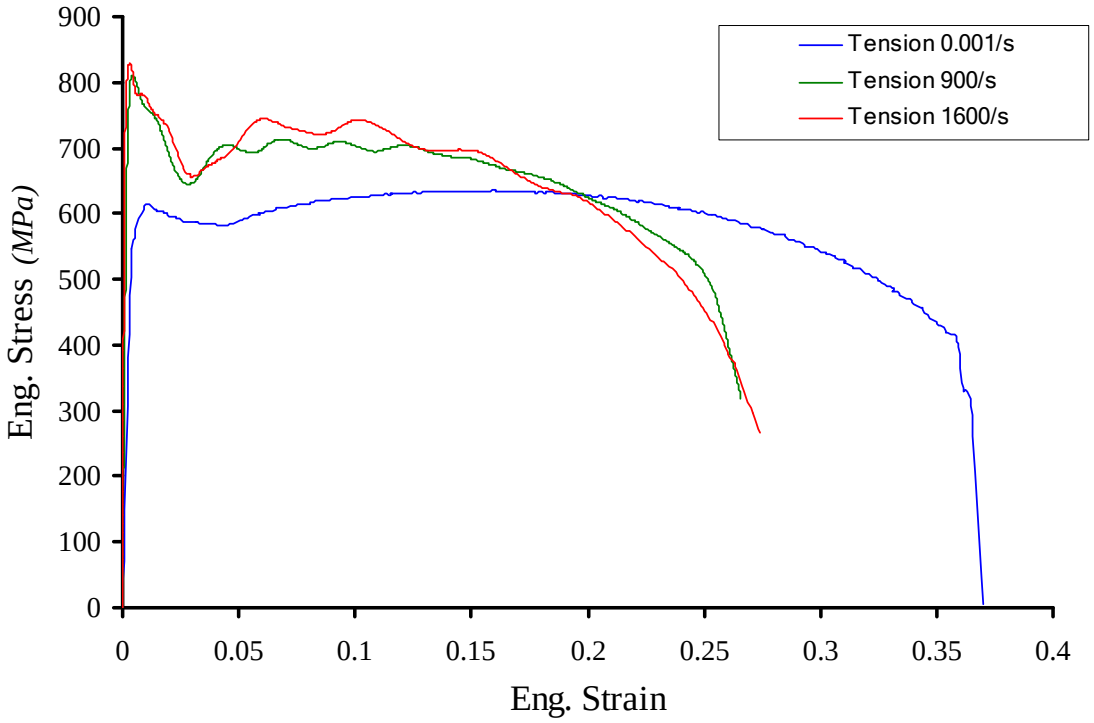

Figure 9. Engineering stress vs. engineering strain results for the three strain rates

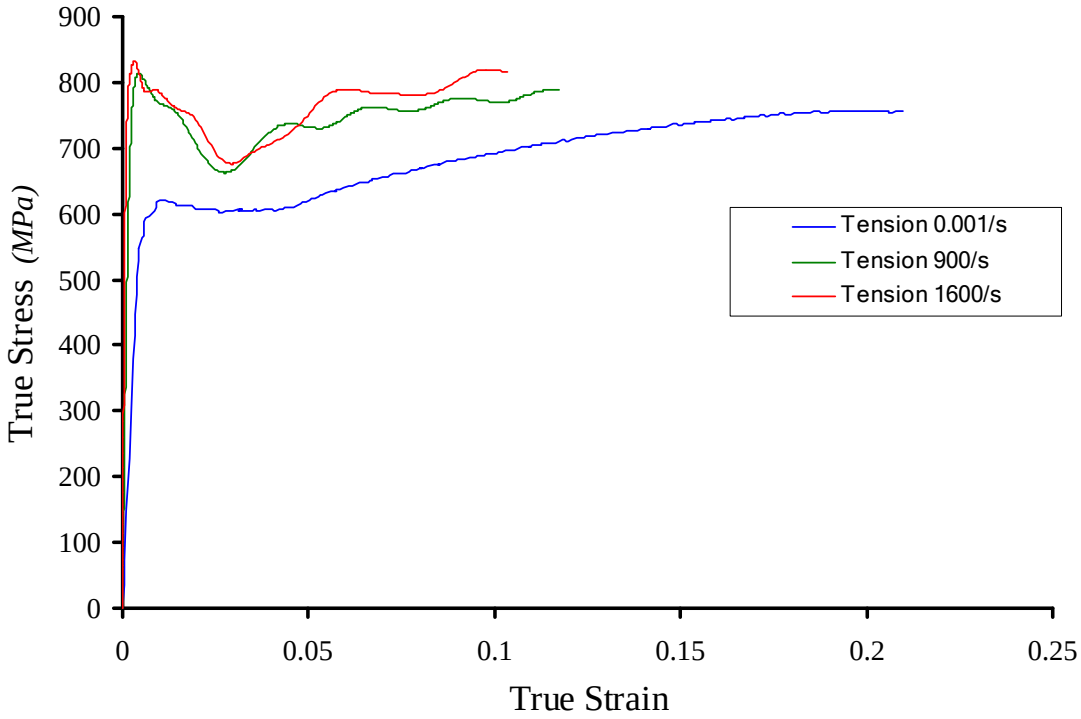

Figure 10. True stress vs. true strain results for the three strain rates

SEM FRACTOGRAPHY

Upon initial visual inspection of the tested samples it was observed that the samples tested at quasi-static strain rate had a characteristic fracture mode different from what is observed at high strain rate, with no noticeable difference of specimens tested at the two high rates.

The characteristic fracture of the quasi-static samples can be seen in Figures 11 and 12 where the central section of the sample is fractured along the medial plane (parallel to the plane containing the 5 mm width of the sample). Moreover, the resulting lips show a fracture along the 45 degrees plane as illustrated in Figure 12. Close examination of Figure 13, which is from a sample tested at the quasi-static rate, shows a dimpled texture indicating ductile fracture. The galvanized layer peeling can also be seen in Figure 14. Figures 15 and 16 of the sample tested at high strain rate indicate fracture along the 45 degrees plane; in addition a scar can be observed at the location of the fracture medial plane in the corresponding quasi-static sample. Similar to the quasi-static case, the dimpled fracture surface seen in Figures 17 and 18 is characteristic of ductile fracture.

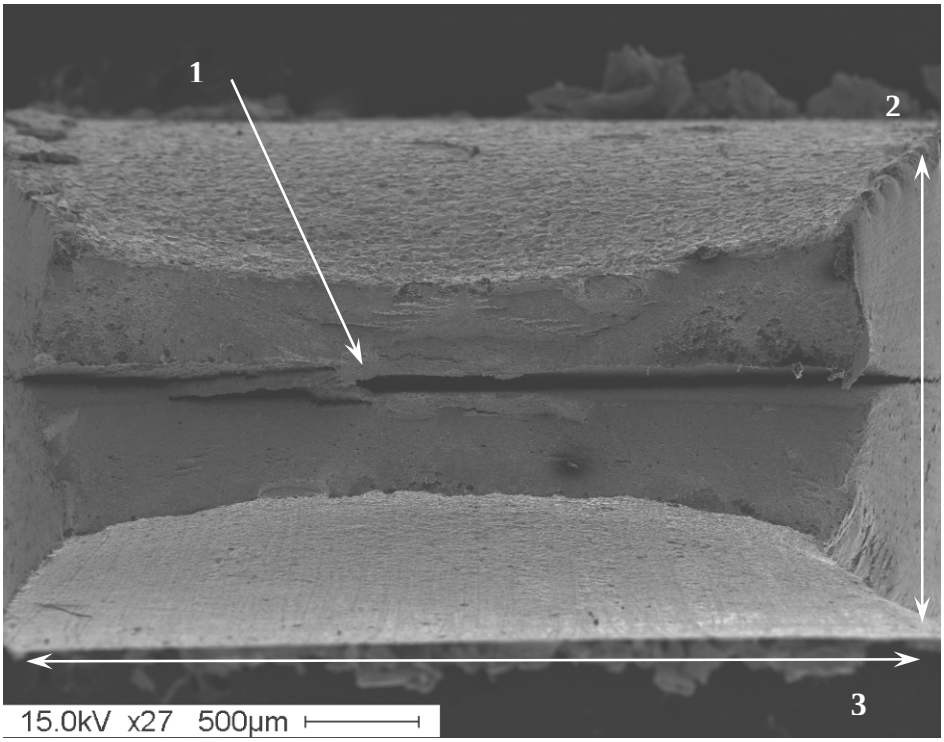

Figure 11. Quasi-static sample viewed in the direction of tension. 1) central crack, 2) thickness 2.7 mm, 3) width 5 mm.

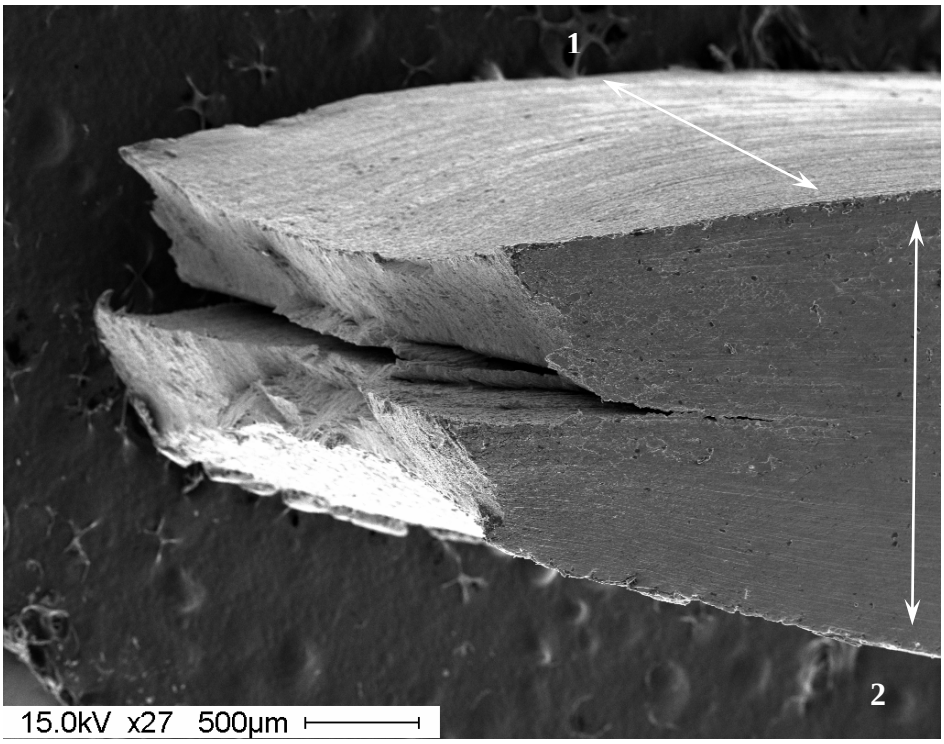

Figure 12. Quasi-static sample 1) width 5 mm, 2) thickness 2.7 mm

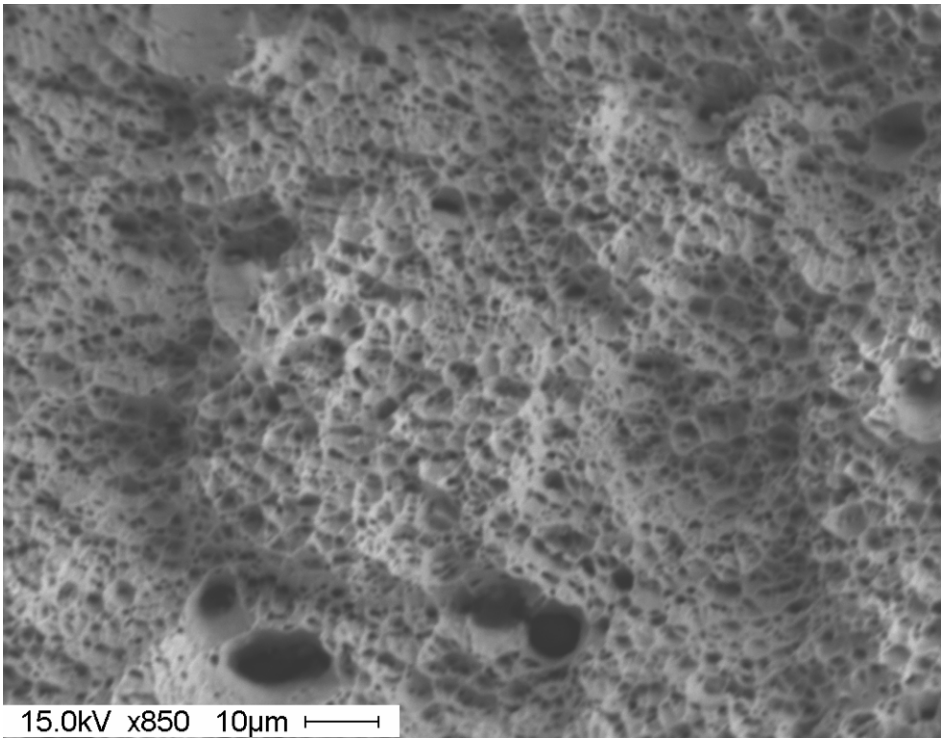

Figure 13. Quasi-static sample fracture surface closeup.

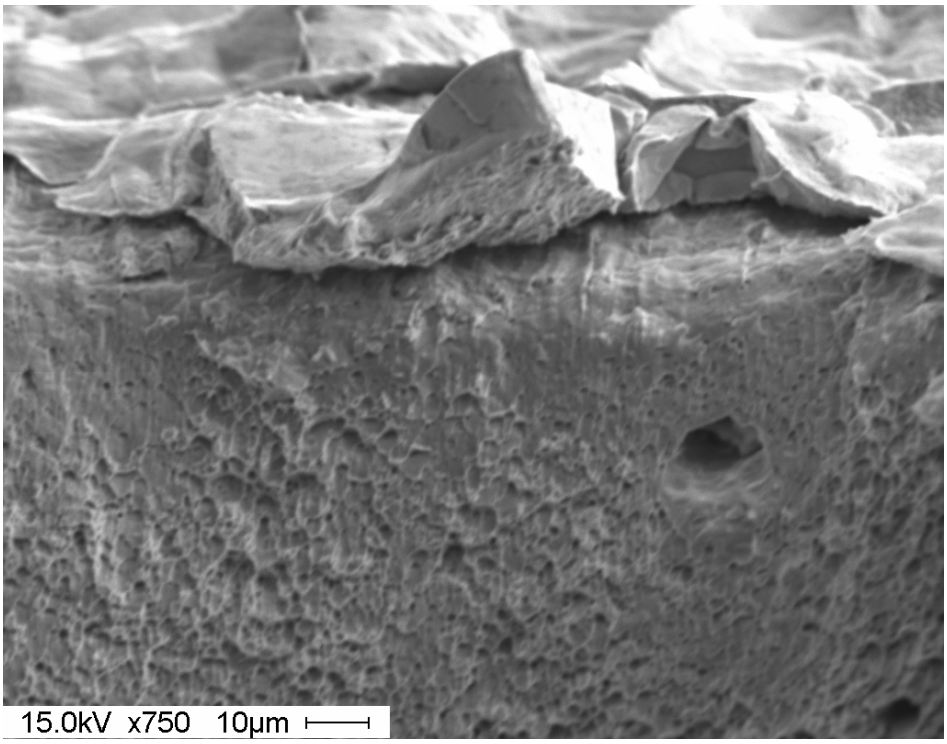

Figure 14. Quasi-static sample fracture surface closeup also showing the galvanized layer.

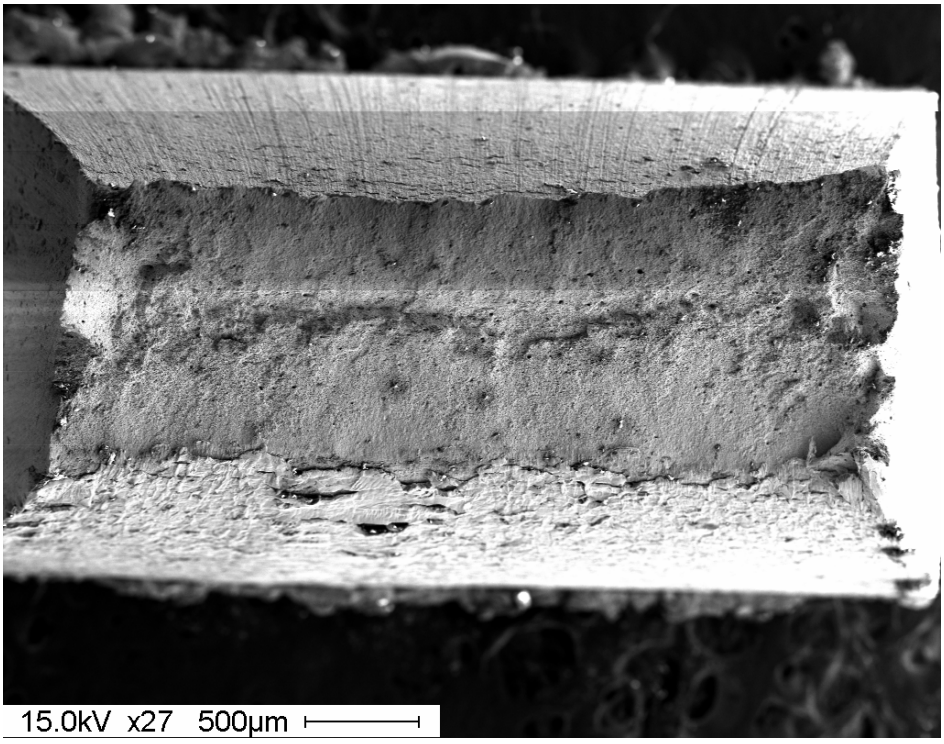

Figure 15. Dynamic sample viewed in the direction of tension.

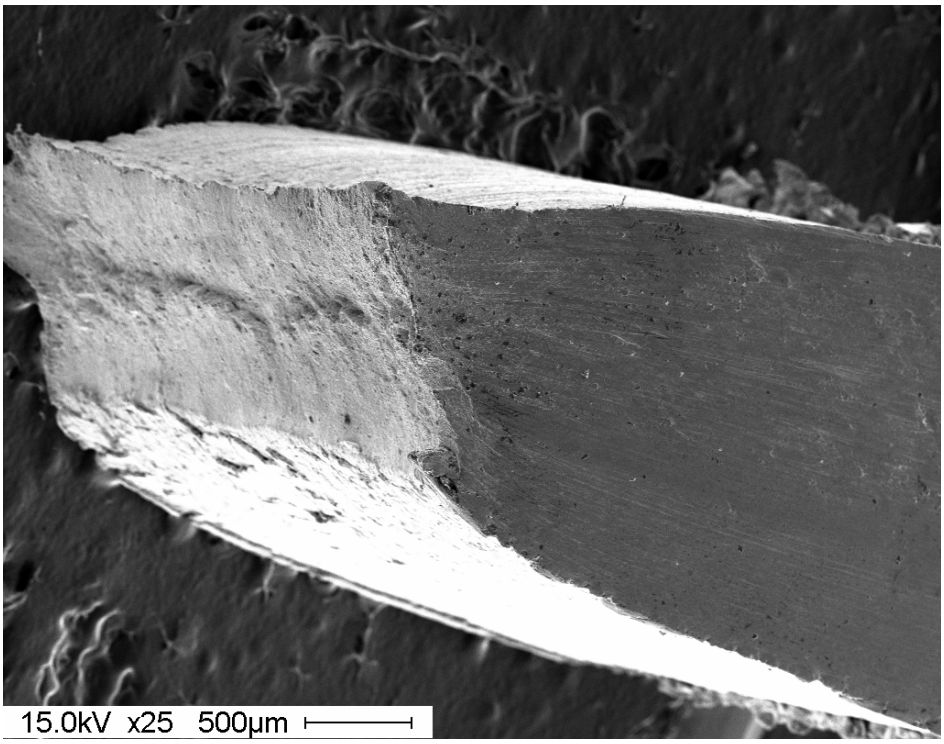

Figure 16. Dynamic sample showing the crack along the 45 degrees angle.

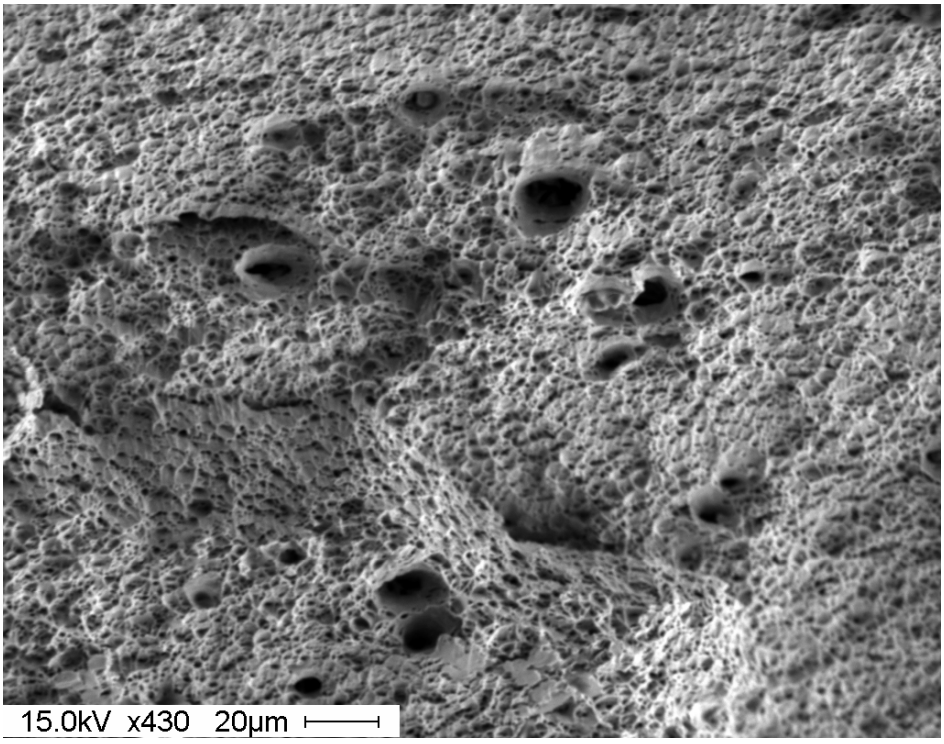

Figure 17. Dynamic sample fracture surface closeup.

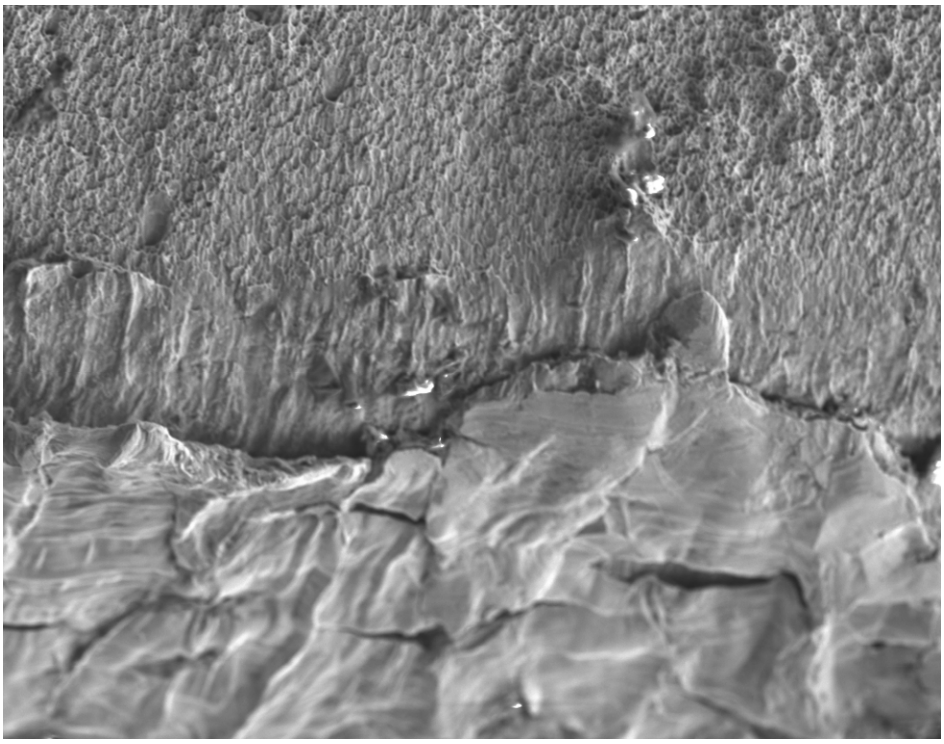

Figure 18. Dynamic sample fracture surface closeup also showing the galvanized layer.

APPENDIX 5

DYNAMIC TENSILE TESTS OF GALVANNEALED HSLA STEEL

McGill University
Department of Mechanical Engineering

Quasi-static and Dynamic Tensile Strength Testing of DP, TRIP and Precipitation Hardening Steels

Second Quarterly Report, Aug. 2007

Contract No. 23378-060599/001/SQ

Wael Dabboussi
James A. Nemes

for:

DEPARTMENT OF NATURAL RESOURCES
METALS TECHNOLOGY LAB

SCOPE

In this report the findings of laboratory experiments performed on tension coupons machined from the received HSLA galvannealed plates are presented. The tension test results at quasi-static and two different high-strain rates are given in the form of stress vs. strain curves.

COUPONS

The quasi-static and high-strain rate tension tests were performed on coupons with the geometry as shown in Figure 1. The same sample geometry is used for both quasi-static and dynamic tests in order to eliminate any geometric effect on the results, hence allowing for an objective comparison and observation of the strain rate effect on the material mechanical response. The coupon geometry is dictated mainly by the nature of the high strain rate Hopkinson bar test, which requires a reduced sample length to produce the desired strain rates and in order the specimen to reach the equilibrium state faster, which leads to more reliable results. Figure 2 shows the orientation of the coupons with respect to the received plates. The shown orientation and topology is in accordance with the recommendation by MTL for minimizing any concentration of the galvanized layer and temperature gradient effect that could exist from the galvanizing process. The samples were machined using CNC. It is to be noted that a minor discrepancy in the thickness of the received plates was observed. Plate 38 used to the 900 s^{-1} tests is 2.63 mm thick whereas plate 40 used for the 0.001 s^{-1} and the 1600 s^{-1} tests is 2.55 to 2.6 mm thick. It is unknown if such a discrepancy as any influence on the results.

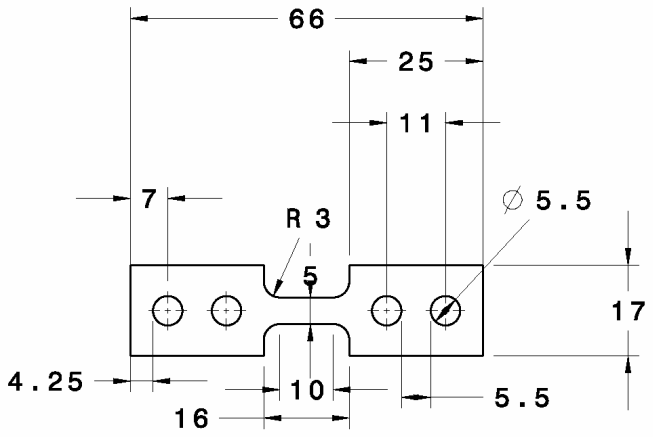

Figure 1. Coupon geometry and dimensions in mm

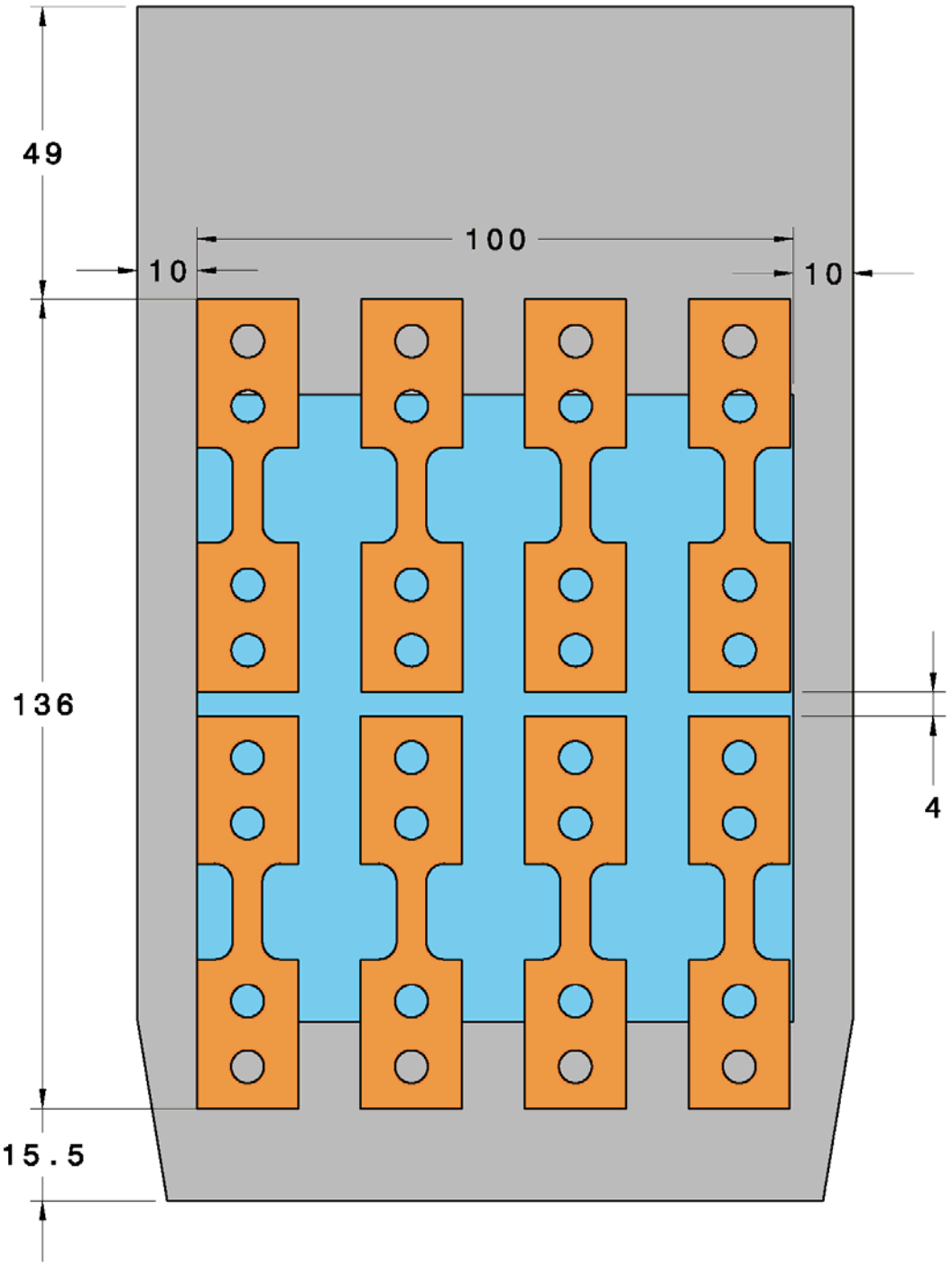

Figure 2. Dimensions of received plate (in mm) and coupon topology with respect to the plate. Blue area represents the recommended area for use.

TENSION TESTING

The tension experiments were conducted using the MTS hydraulic testing equipment for the quasi static tests whereas the direct Split Hopkinson Pressure Bars setup was used for the high strain rate tests. Three sets of data are presented in this report. The first set is of four experiments conducted at quasi-static rate, the second is of four experiments conducted at high strain rate and the third set is of experiments conducted at a different high strain rate. The dimension of the uniform gage section (10 mm) was used to determine the engineering strain for all the presented tests.

Quasi-static Tension Results

The quasi static tension test was performed on the machined coupons at room temperature and at a nominal strain rate of 10^{-3} s^{-1}. Figure 3 shows the engineering stress vs. engineering strain results, whereas Figure 4 shows the corresponding true stress vs. true strain results to the point of localization. The tests display reasonable repeatability in terms of the UTS value of 658 MPa and elongation to failure of about 38 %.

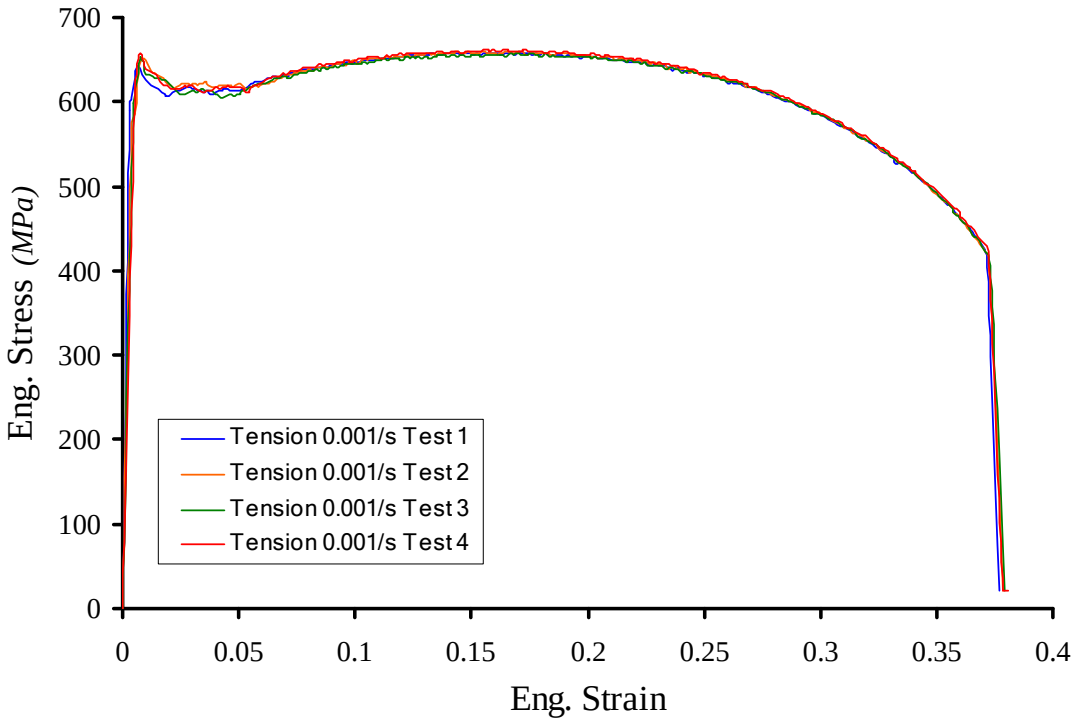

Figure 3. Quasi-static engineering stress vs. engineering strain results

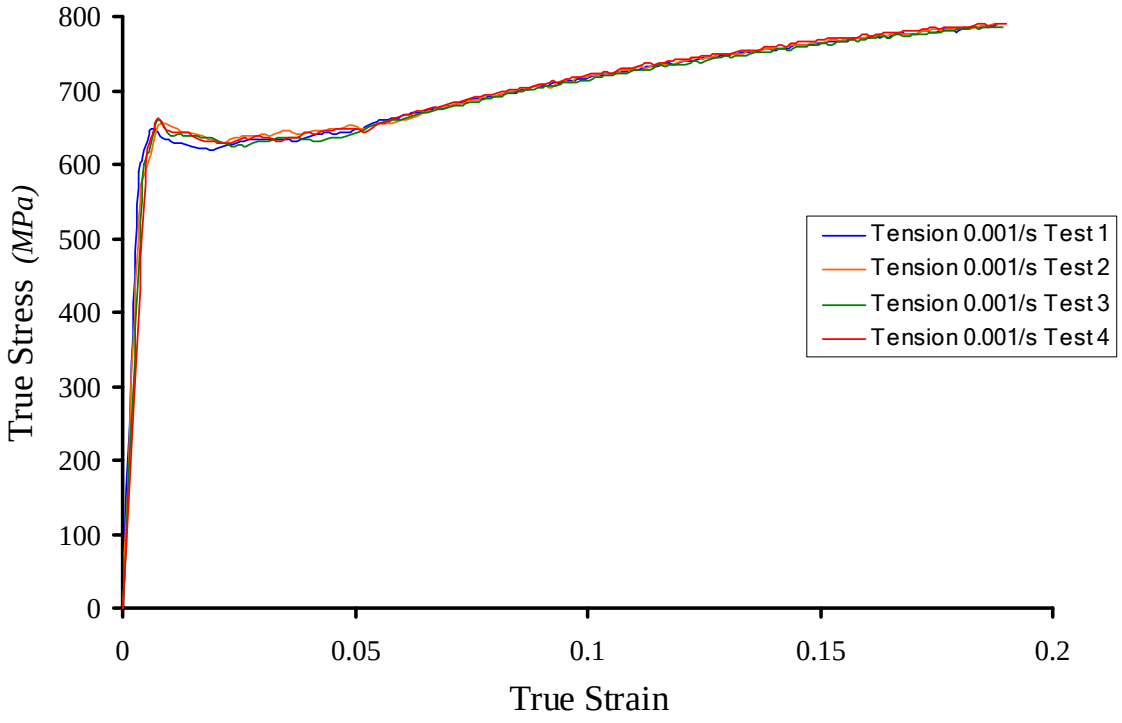

Figure 4. Quasi-static true stress vs. true strain results

High Strain Rate Tension Results

High strain rate tests were also performed on the machined coupons at 2 different rates. Figure 5 shows the engineering stress vs. engineering strain results of the tests performed at a strain rate of 900 s^{-1}. Figure 6 shows the corresponding true stress vs. true strain results. An increase in the UTS (compared to the quasi-static case) to approximately 740 MPa is observed from the plotted results; however the total elongation dropped to about 30 %. It is important to note that for this rate of testing it is not clear whether the material displays a plateau type of hardening or a well defined UTS point.

Figure 7 shows the engineering stress vs. engineering strain of the tests performed at a strain rate of 1600 s^{-1}. Figure 8 shows the corresponding true stress vs. true strain results. An increase in the UTS (compared to the quasi-static case) to approximately 736 MPa is observed from the plotted results with total elongation raging from 31 to 37 %.

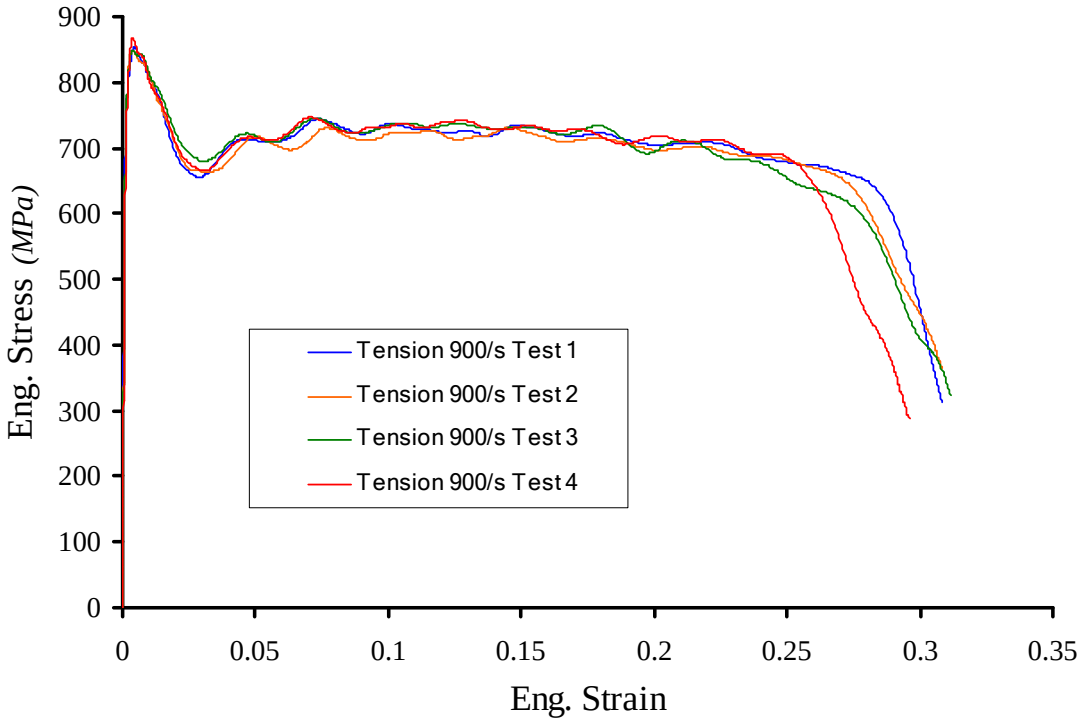

Figure 5. Dynamic engineering stress vs. engineering strain results at 900 s^{-1}

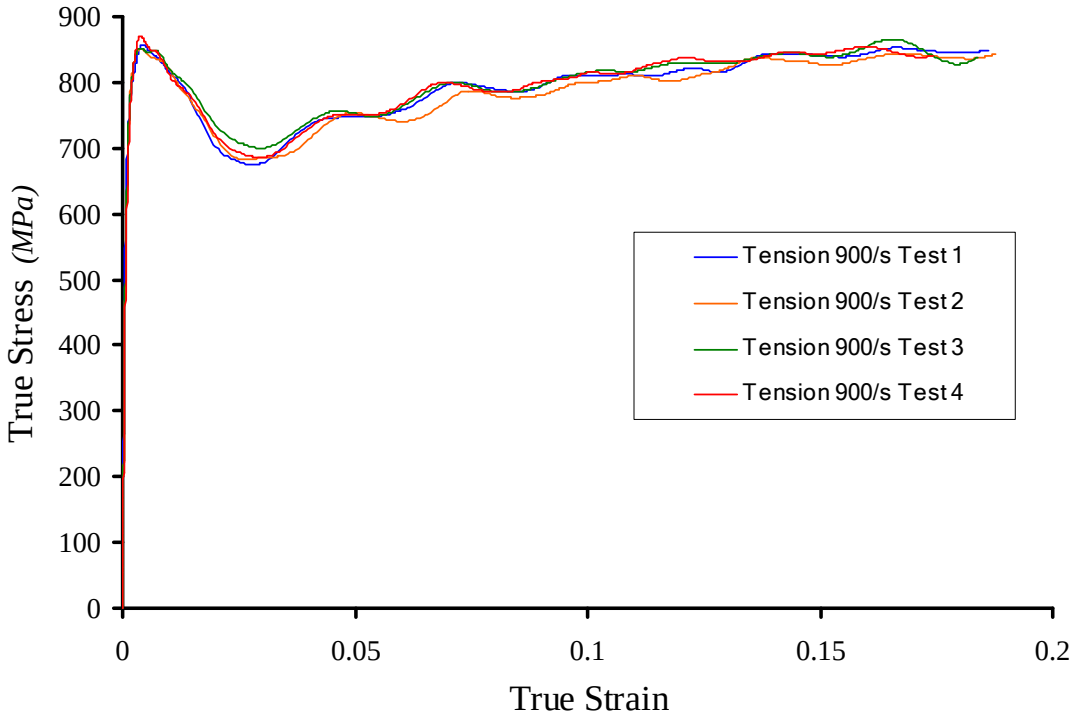

Figure 6. Dynamic true stress vs. true strain results at 900 s^{-1}

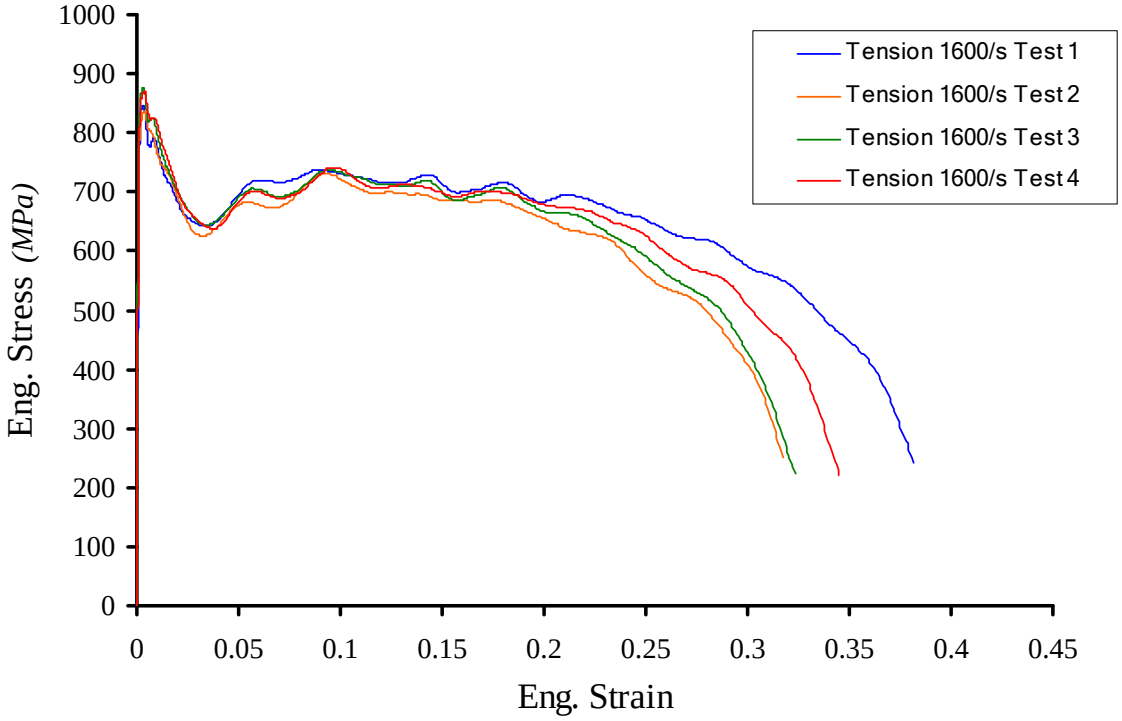

Figure 7. Dynamic engineering stress vs. engineering strain results at 1600 s^{-1}

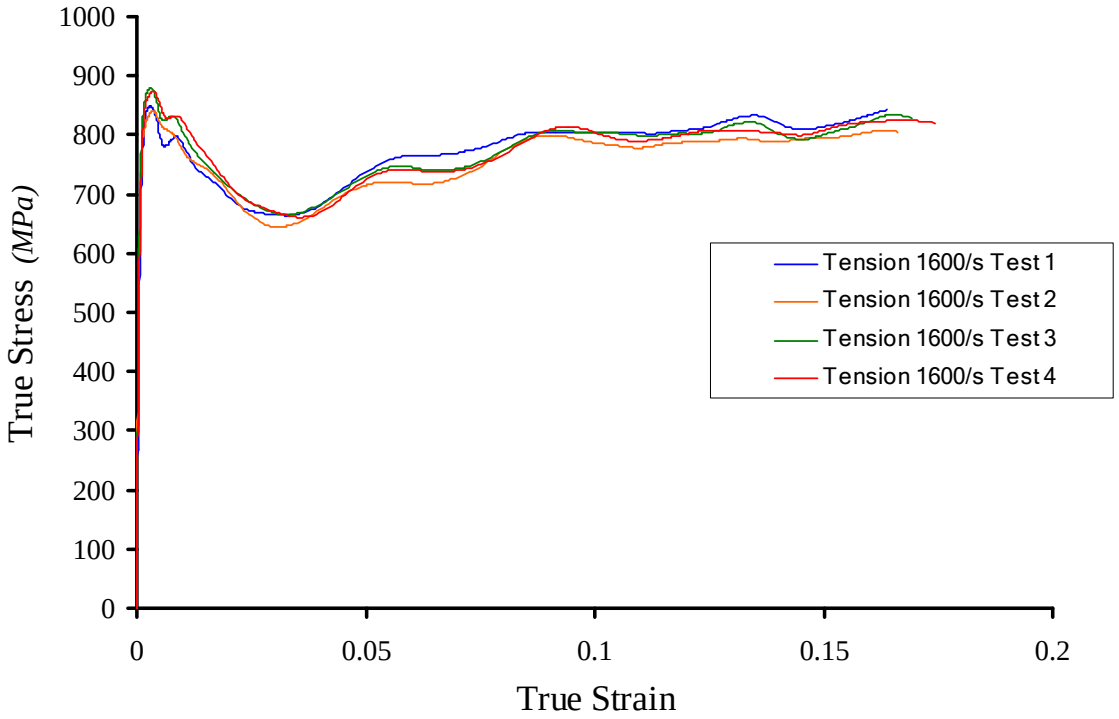

Figure 8. Dynamic true stress vs. true strain results at 1600 s^{-1}

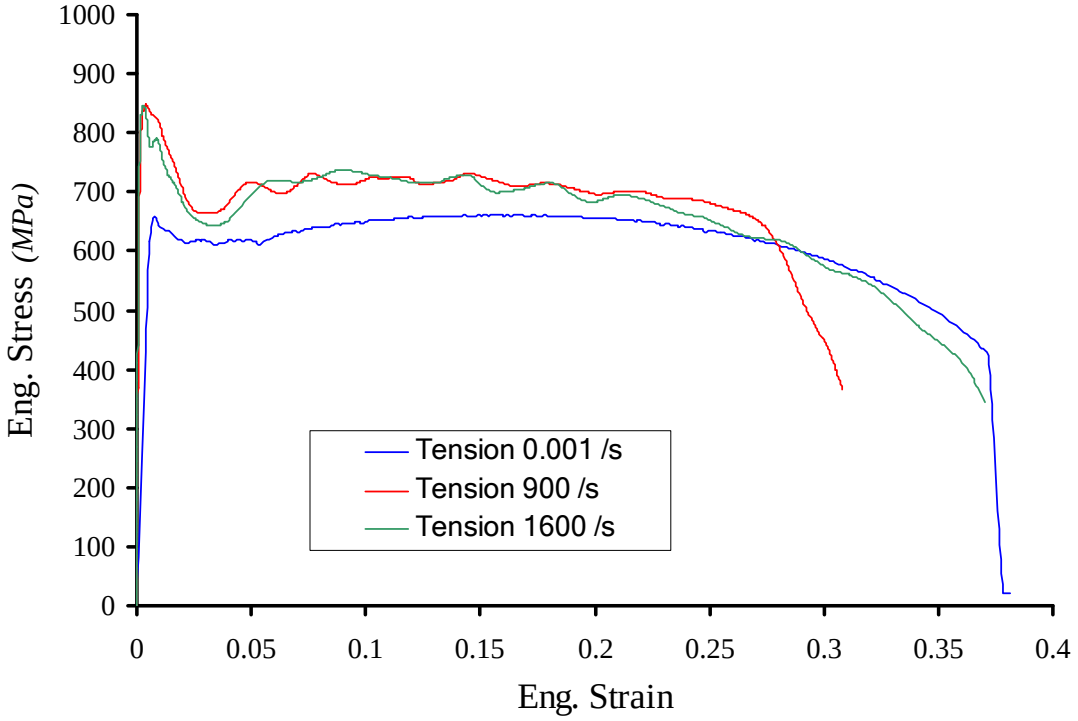

Figure 9. Engineering stress vs. engineering strain results for the three strain rates

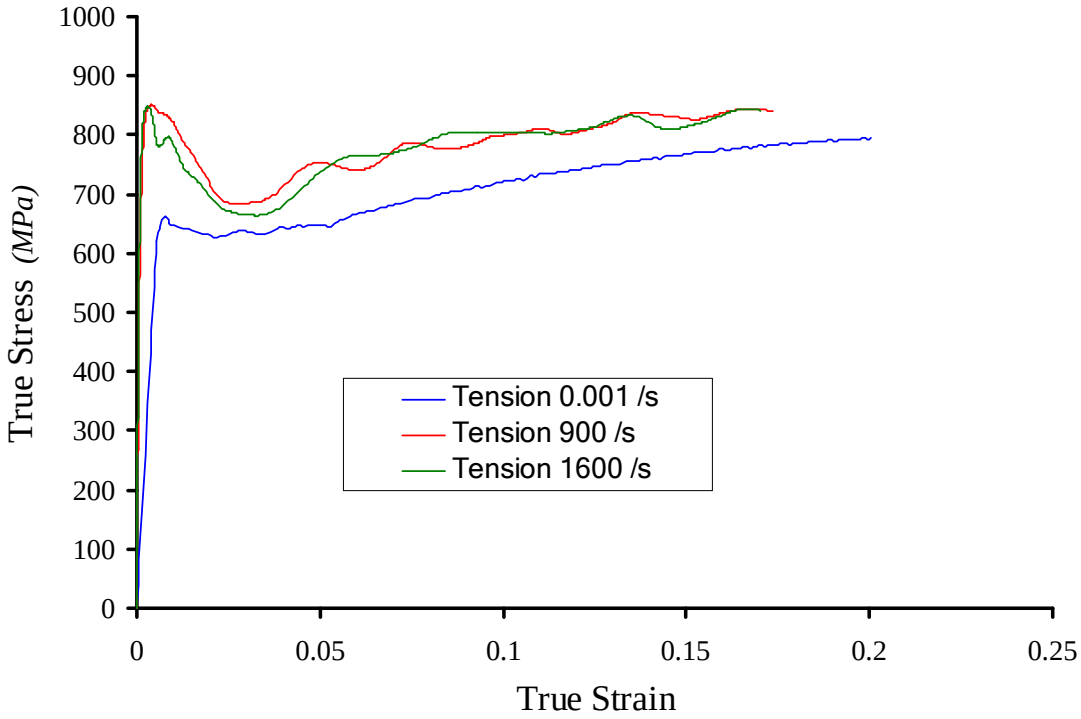

Figure 10. True stress vs. true strain results for the three strain rates

APPENDIX 6

DYNAMIC TENSILE TESTS OF TRIP STEEL

McGill University
Department of Mechanical Engineering

Quasi-static and Dynamic Tensile Strength Testing of DP, TRIP and Precipitation Hardening Steels

TRIP Steel Report, Nov. 2007

Contract No. 23378-060599/001/SQ

Wael Dabboussi
James A. Nemes

for:

DEPARTMENT OF NATURAL RESOURCES
METALS TECHNOLOGY LAB

SCOPE

In this report the findings of laboratory experiments performed on tension coupons machined from the received TRIP steel plates are presented. The tension test results at quasi-static and two different high-strain rates are given in the form of stress vs. strain curves.

COUPONS

The quasi-static and high-strain rate tension tests were performed on coupons with the geometry as shown in Figure 1. The same sample geometry is used for both quasi-static and dynamic tests in order to eliminate any geometric effect on the results, hence allowing for an objective comparison and observation of the strain rate effect on the material mechanical response. The coupon geometry is dictated mainly by the nature of the high strain rate Hopkinson bar test, which requires a reduced sample length to produce the desired strain rates and in order the specimen to reach the equilibrium state faster, which leads to more reliable results. The coupons were machined using CNC from strips of plates received from MTL and within the indicated zones.

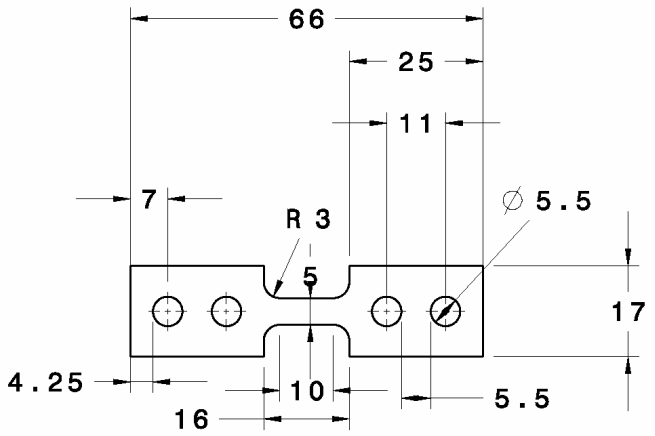

Figure 1. Coupon geometry and dimensions in mm

TENSION TESTING

The tension experiments were conducted using the MTS hydraulic testing equipment for the quasi static tests whereas the direct Split Hopkinson Pressure Bars setup was used for the high strain rate tests. Three sets of data are presented in this report. The first set is of four experiments conducted at quasi-static rate, the second is of four experiments

conducted at high strain rate and the third set is of experiments conducted at a different high strain rate. The dimension of the uniform gage section (10 mm) was used to determine the engineering strain for all the presented tests.

Quasi-static Tension Results

The quasi static tension test was performed on the machined coupons at room temperature and at a nominal strain rate of 10^{-3} s^{-1}. Figure 2 shows the engineering stress vs. engineering strain results, whereas Figure 3 shows the corresponding true stress vs. true strain results to the point of localization. The tests display reasonable repeatability in terms of the UTS value of 635 MPa with uniform elongation of about 27% and elongation to failure of about 43 %.

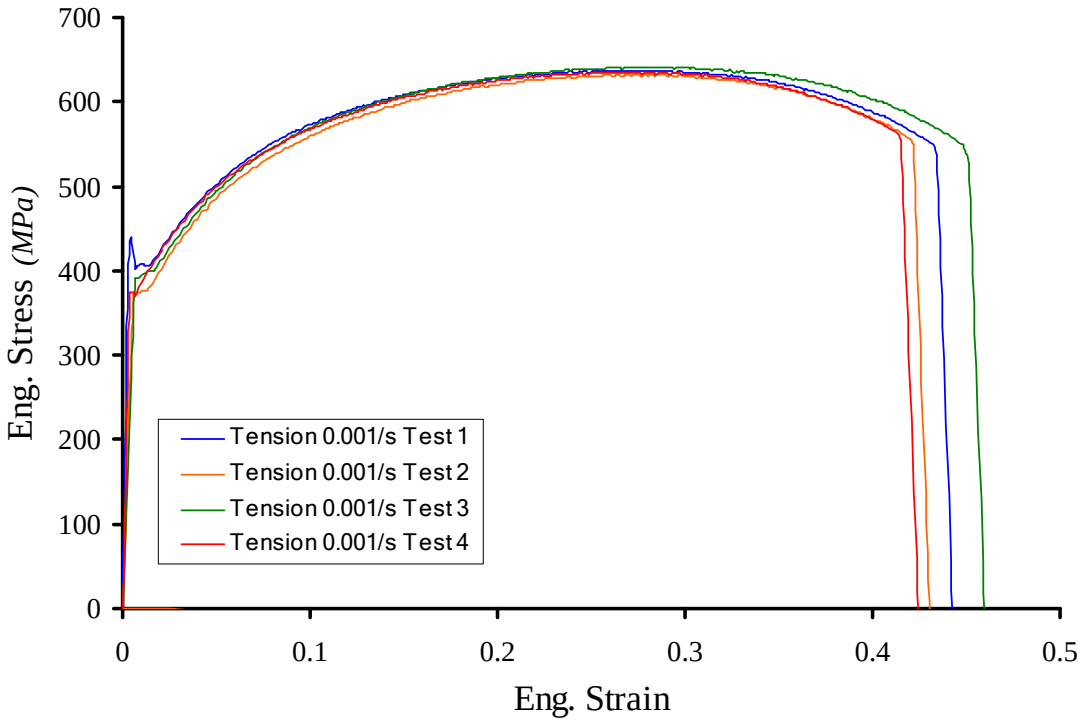

Figure 2. Quasi-static engineering stress vs. engineering strain results

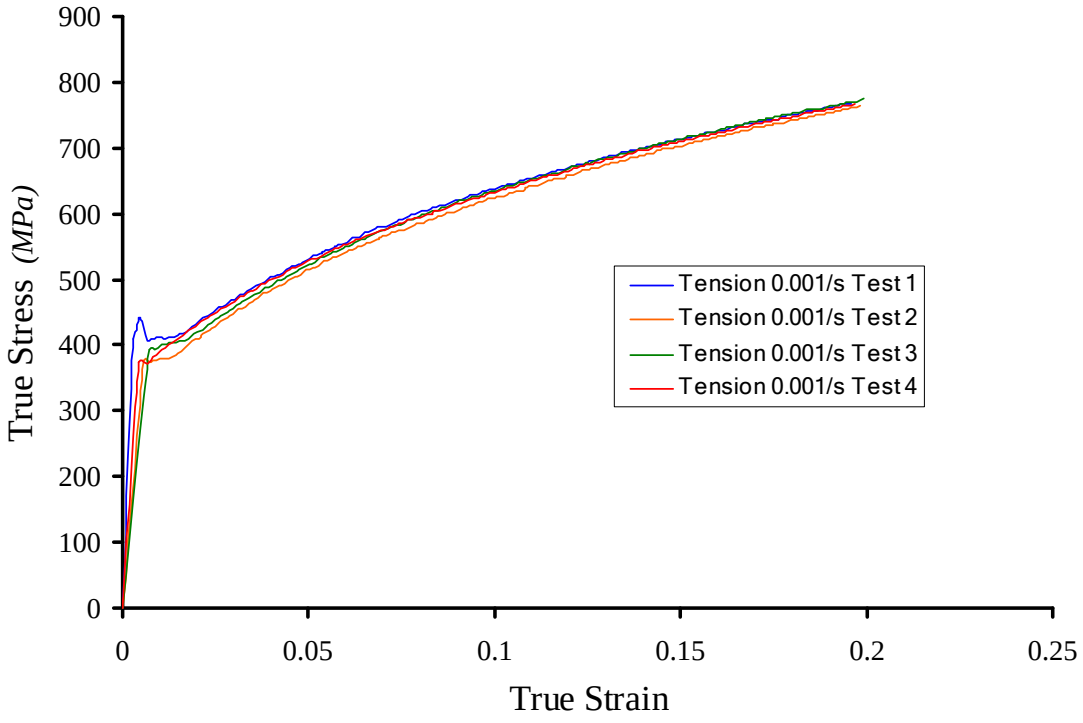

Figure 3. Quasi-static true stress vs. true strain results

High Strain Rate Tension Results

High strain rate tests were also performed on the machined coupons at 2 different rates. Figure 4 shows the engineering stress vs. engineering strain results of the tests performed at a strain rate of 900 s^{-1}. Figure 5 shows the corresponding true stress vs. true strain results. An increase in the UTS (compared to the quasi-static case) to approximately 720 MPa is observed from the plotted results; however the total elongation dropped to about 26 %. It is important to note that for this rate of testing it is not clear whether the material displays a plateau type of hardening or a well defined UTS point.

Figure 6 shows the engineering stress vs. engineering strain of the tests performed at a strain rate of 1600 s^{-1}. Figure 7 shows the corresponding true stress vs. true strain results. An increase in the UTS to approximately 750 MPa is observed together with an increase in total elongation to 36%.

Figures 8 and 9 are the stress vs. strain results for a selected sample of each strain rate.

The detailed results for UTS, uniform elongation and final elongation are shown in Table 1. The absorbed energy results for the tests shown in Figure 8 are shown in Tables 2-4 for 10, 15 and 20 % strain, respectively.

Table 1. TRIP steel

Test	**UTS** *(MPa)*	**Uniform Elongation** *(%)*	**Final Elongation** *(%)*
Tension 10^{-3} s^{-1}	635 (+2/-3)	26.75 (+0.25/-0.75)	43.25 (+1.75/-1.25)
Tension 900 s^{-1}	~ 720	*	25.75 (+1.25/-1.75)
Tension 1600 s^{-1}	~ 750	*	36 (+2/-1.5)

Table 2. Absorbed energy at 10 % strain

Test	**TRIP** *(N/m^2)*
Tension 10^{-3} s^{-1}	48.7
Tension 900 s^{-1}	66.2
Tension 1600 s^{-1}	70.7

Table 3. Absorbed energy at 15 % strain

Test	**TRIP** *(N/m^2)*
Tension 10^{-3} s^{-1}	78
Tension 900 s^{-1}	102
Tension 1600 s^{-1}	108

Table 4. Absorbed energy at 20 % strain

Test	**TRIP** *(N/m^2)*
Tension 10^{-3} s^{-1}	109
Tension 900 s^{-1}	139
Tension 1600 s^{-1}	145

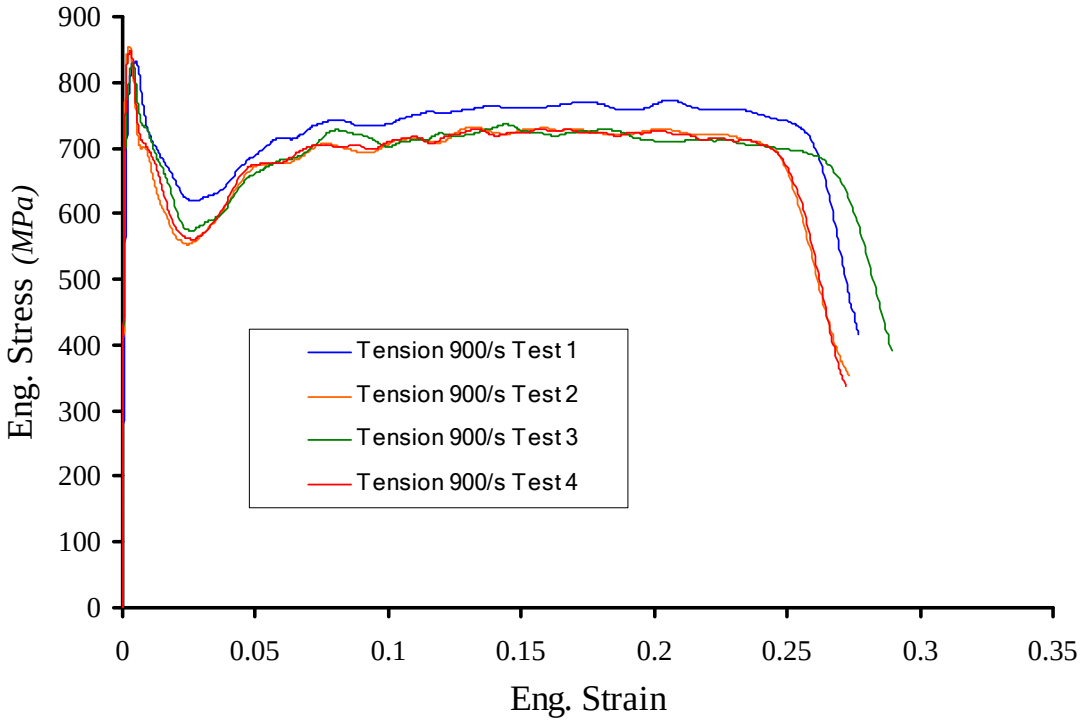

Figure 4. Dynamic engineering stress vs. engineering strain results at 900 s^{-1}

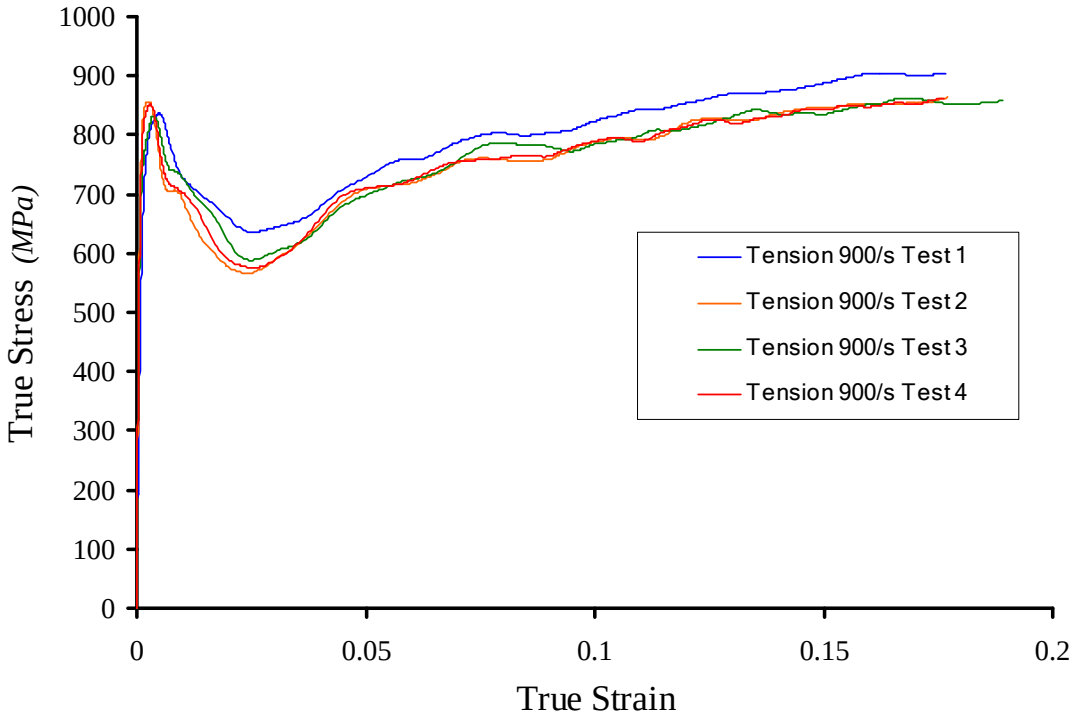

Figure 5. Dynamic true stress vs. true strain results at 900 s^{-1}

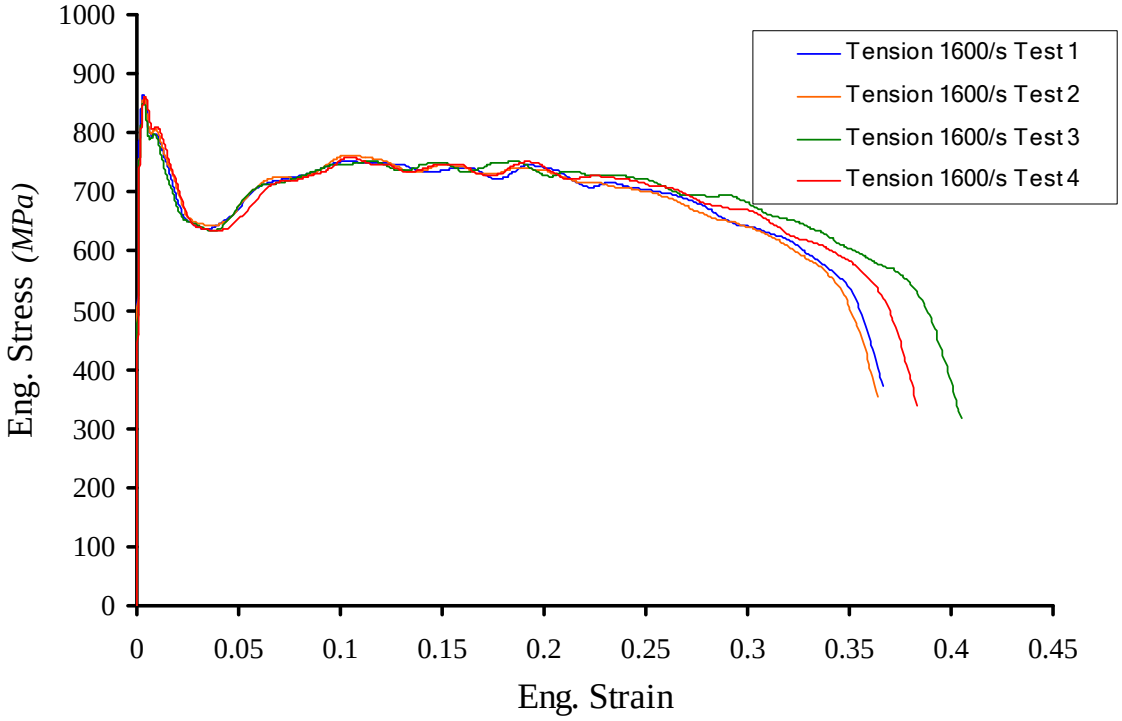

Figure 6. Dynamic engineering stress vs. engineering strain results at 1600 s^{-1}

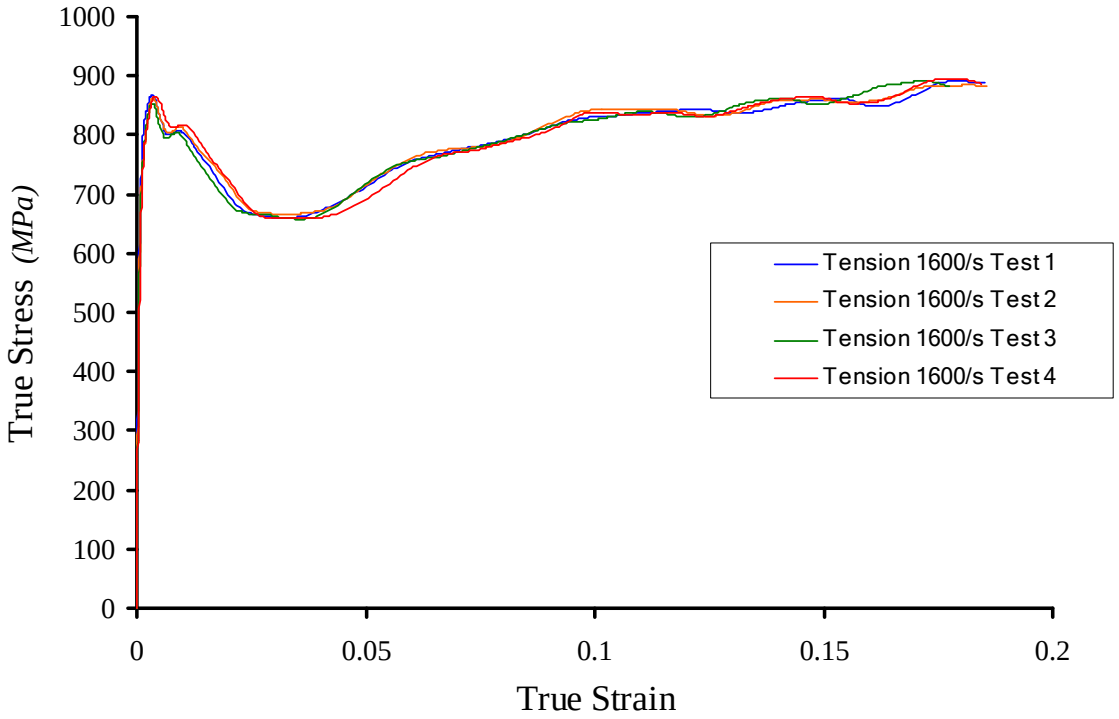

Figure 7. Dynamic true stress vs. true strain results at 1600 s^{-1}

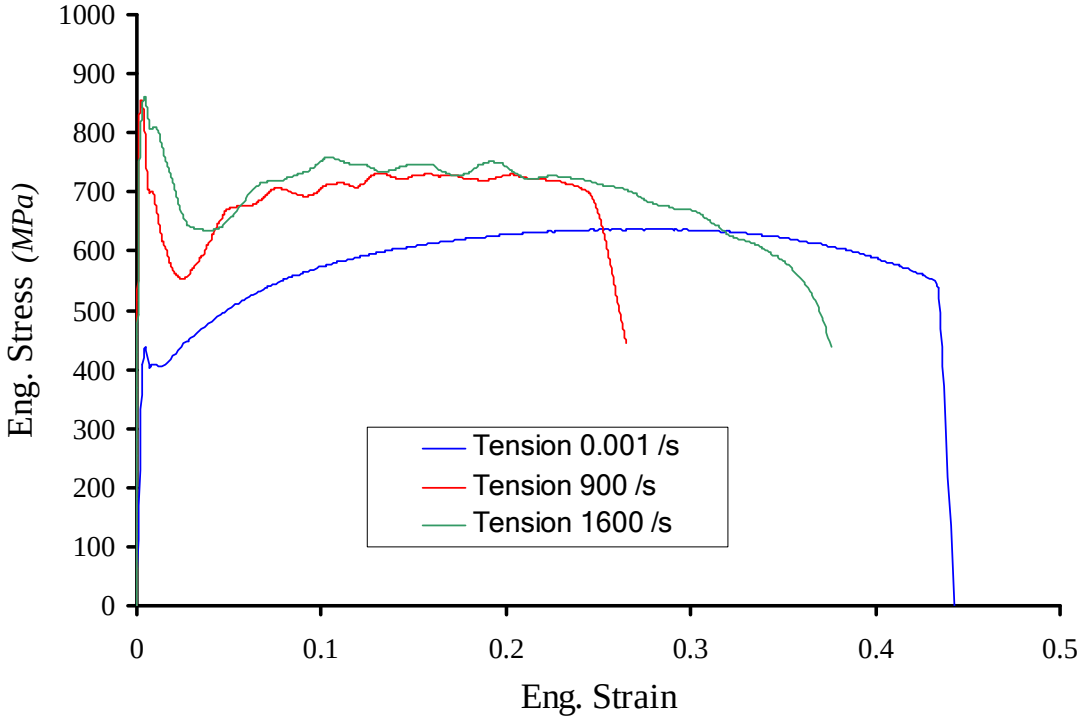

Figure 8. Engineering stress vs. engineering strain results for the three strain rates

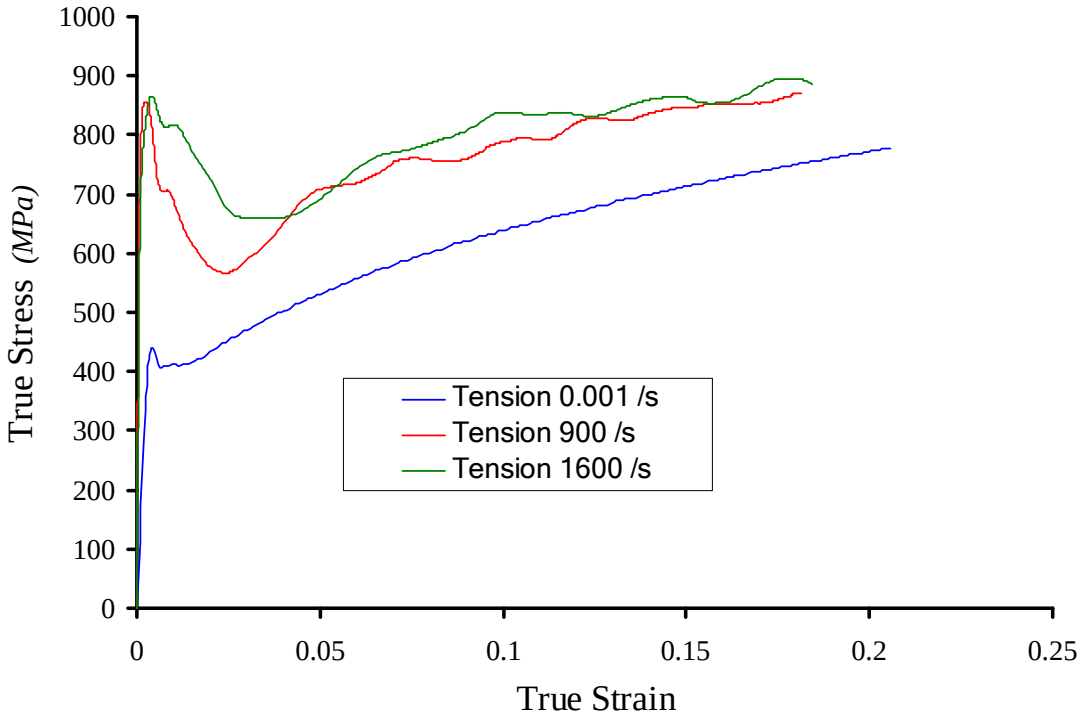

Figure 9. True stress vs. true strain results for the three strain rates

FRACTOGRAPHY

This section contains the fractographic analysis for the HSLA Galvannealed and the TRIP steel received from MTL. For each material a representative quasi-static and high-strain rate sample are examined as shown below.

The HSLA galvannealed samples showed a dimpled fracture surface both at quasi-static and high strain rate indicating a ductile fracture.

The TRIP samples displayed a striated texture on low magnification and the fracture surface shows the dimpled texture, however not exclusively.

HSLA Galvannealed

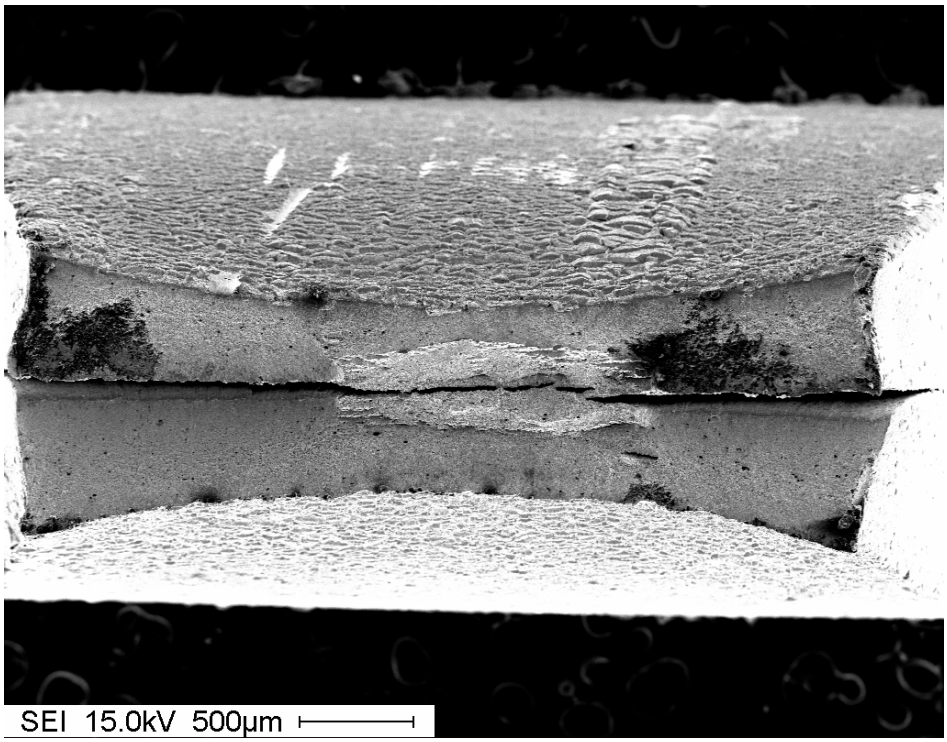

Figure 1. 27x, quasi-static sample. Top view.

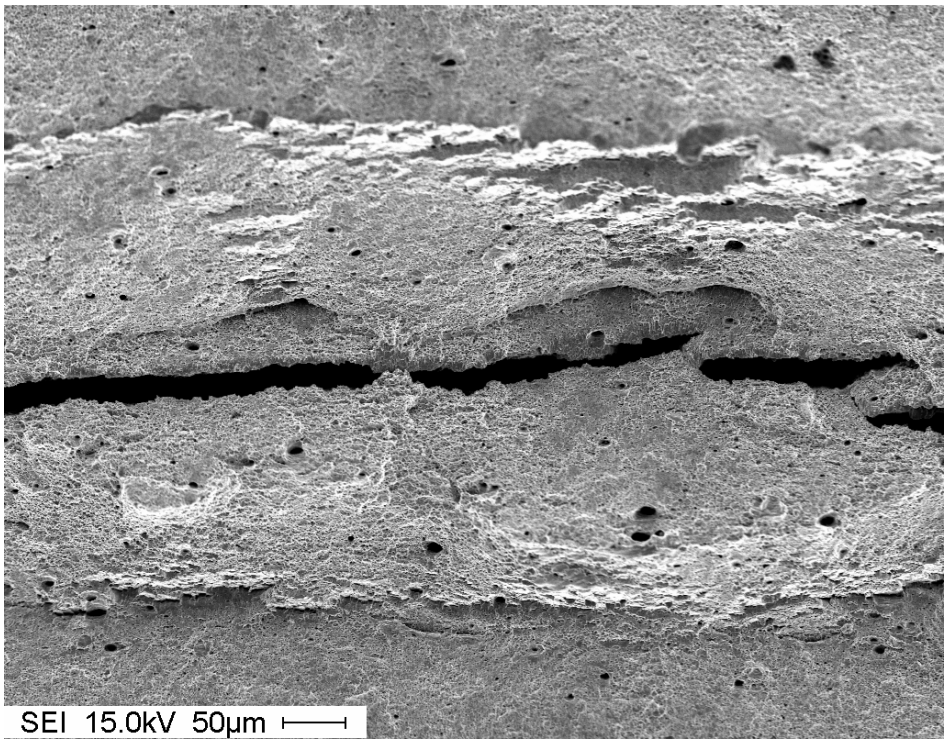

Figure 2. 150x, quasi-static sample. Middle crack.

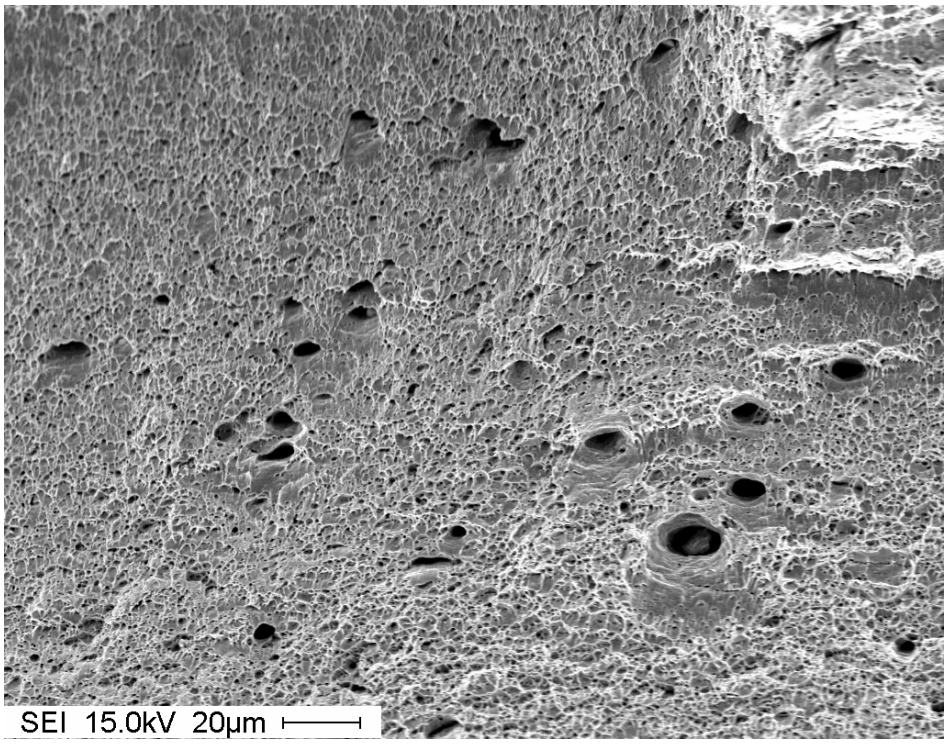

Figure 3. 450x, quasi-static sample. Dimple texture.

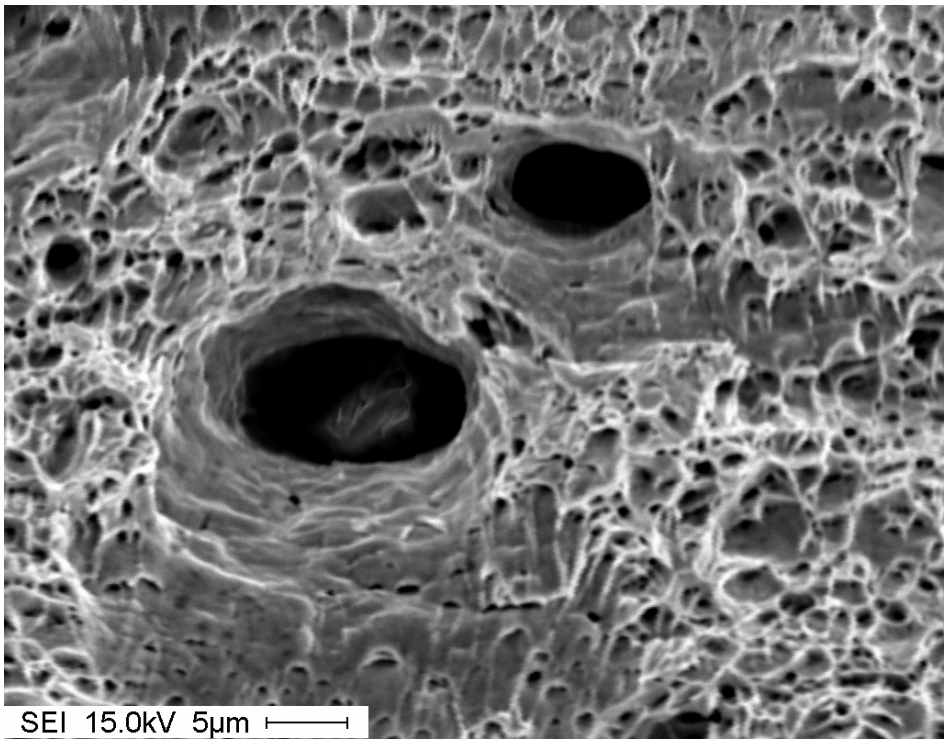

Figure 4. 1900x, quasi-static sample. Dimple texture close-up on inclusion.

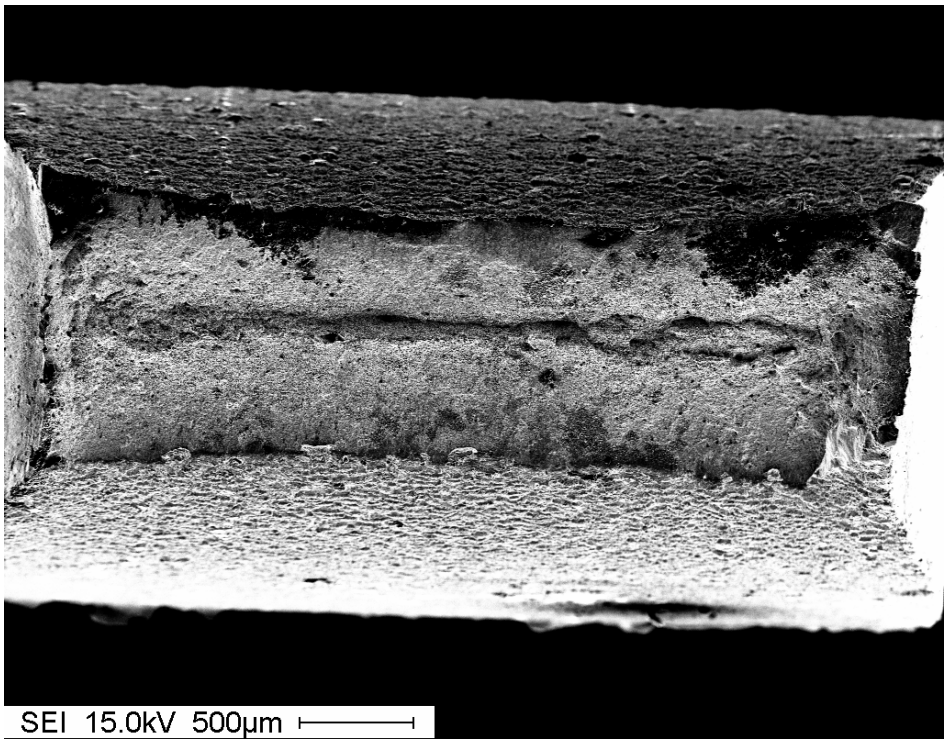

Figure 5. 27x, high strain rate sample. Top view.

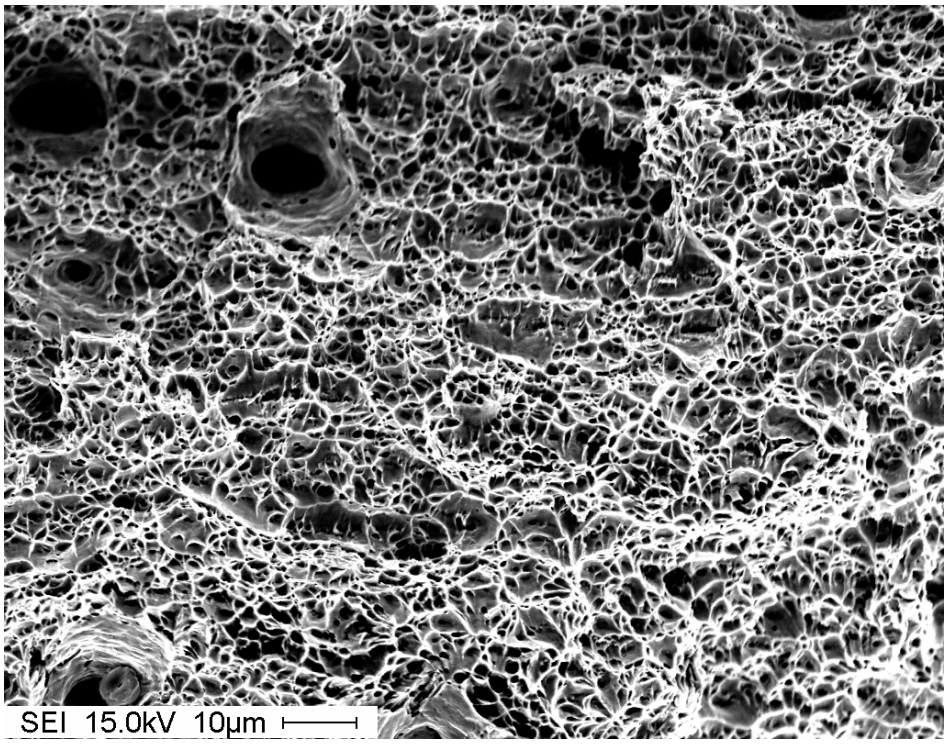

Figure 6. 850x, high strain rate sample. Dimple texture.

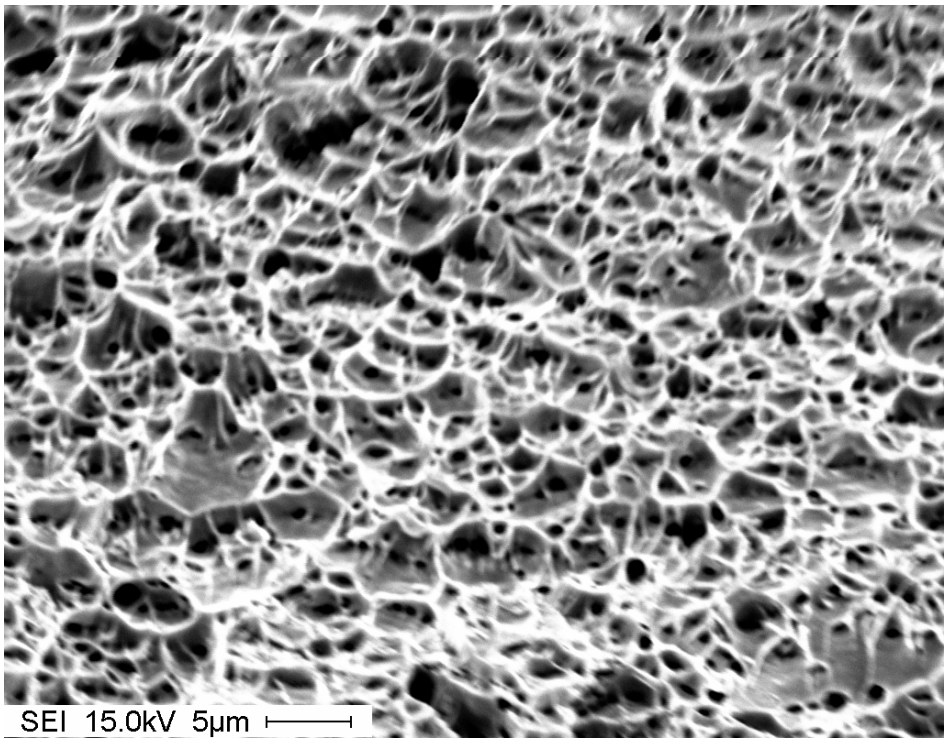

Figure 7. 2000x, high strain rate sample. Dimple texture close-up.

TRIP Steel

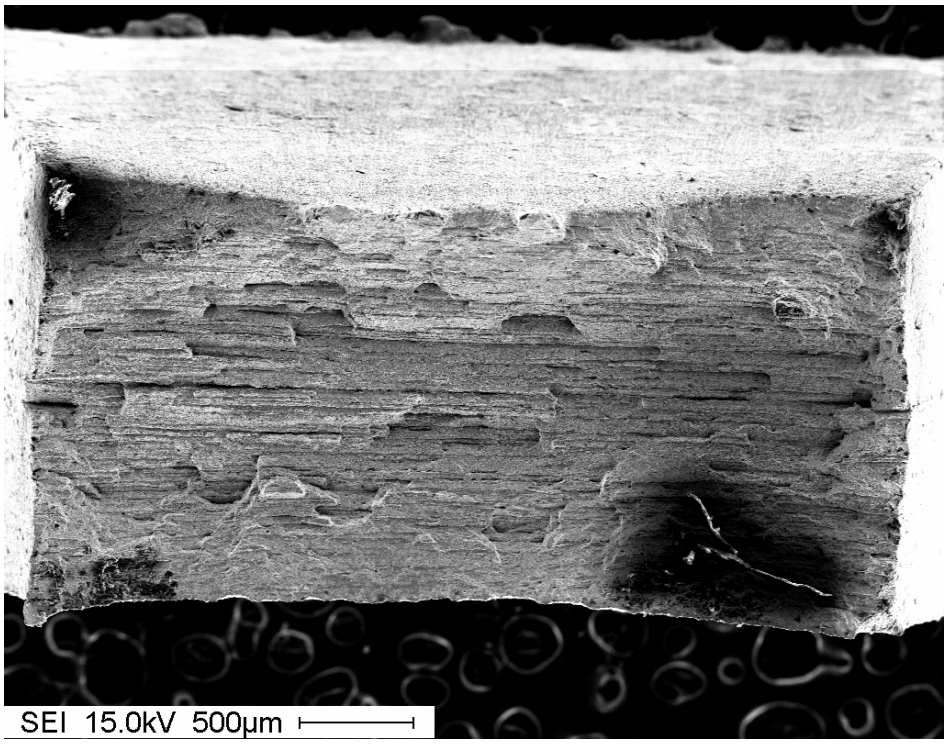

Figure 8. 27x, quasi-static sample. Top view.

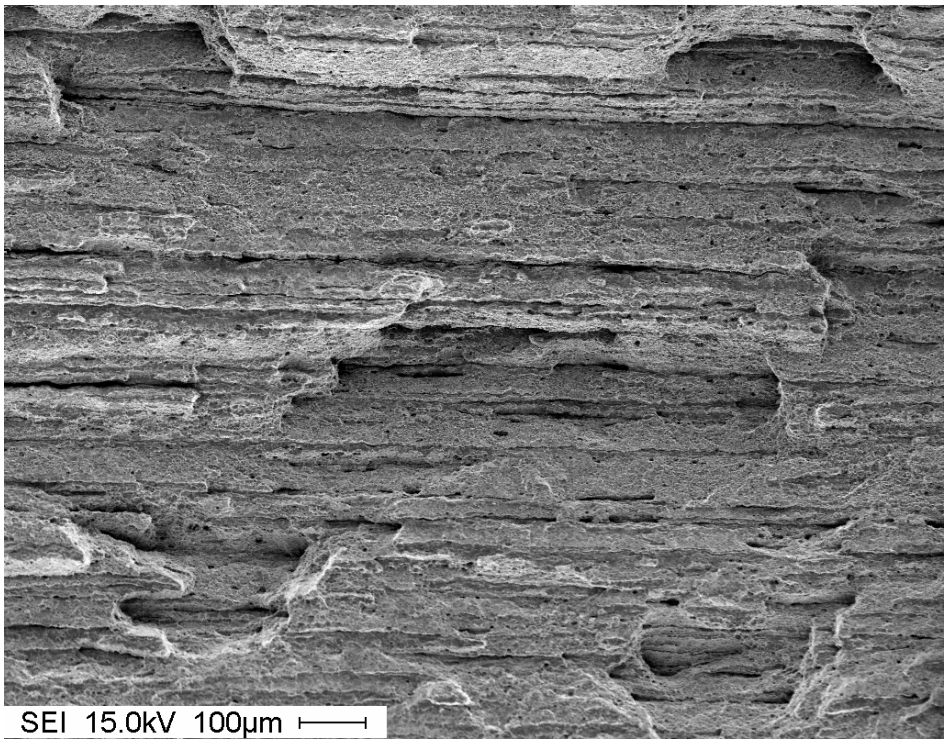

Figure 9. 80x, quasi-static sample. Top view close up.

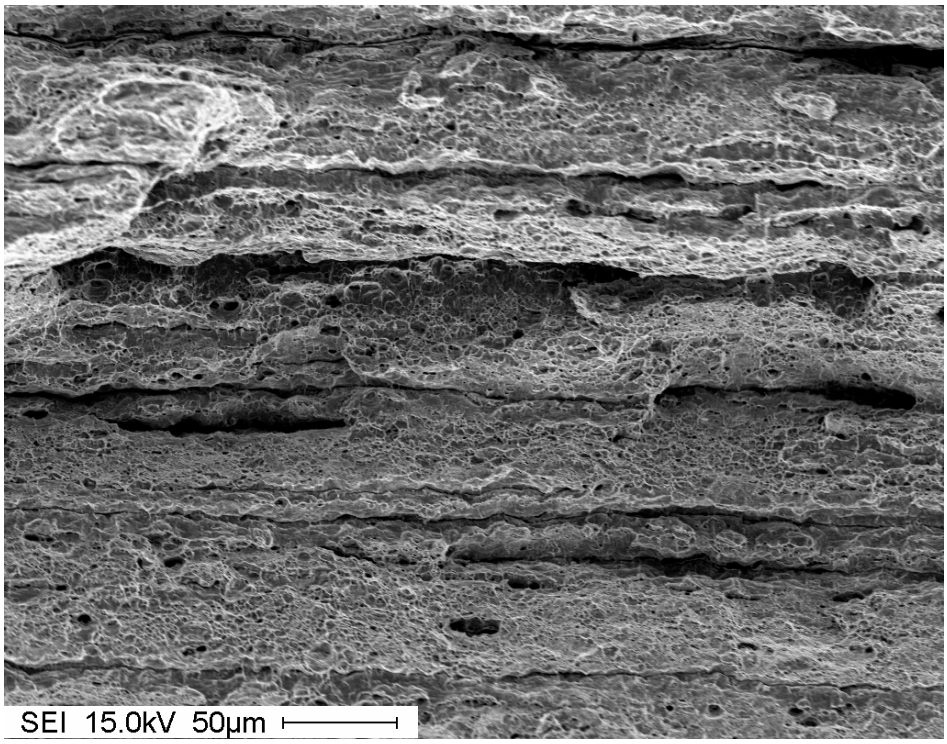

Figure 10. 270x, quasi-static sample.

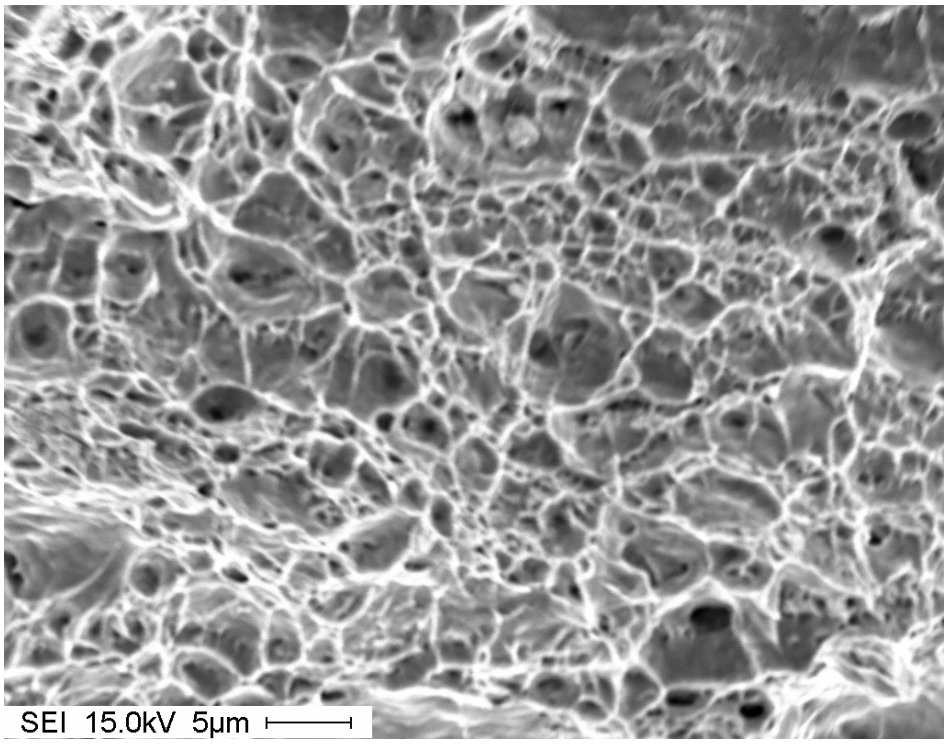

Figure 11. 2000x, quasi-static sample viewed in the direction of tension.

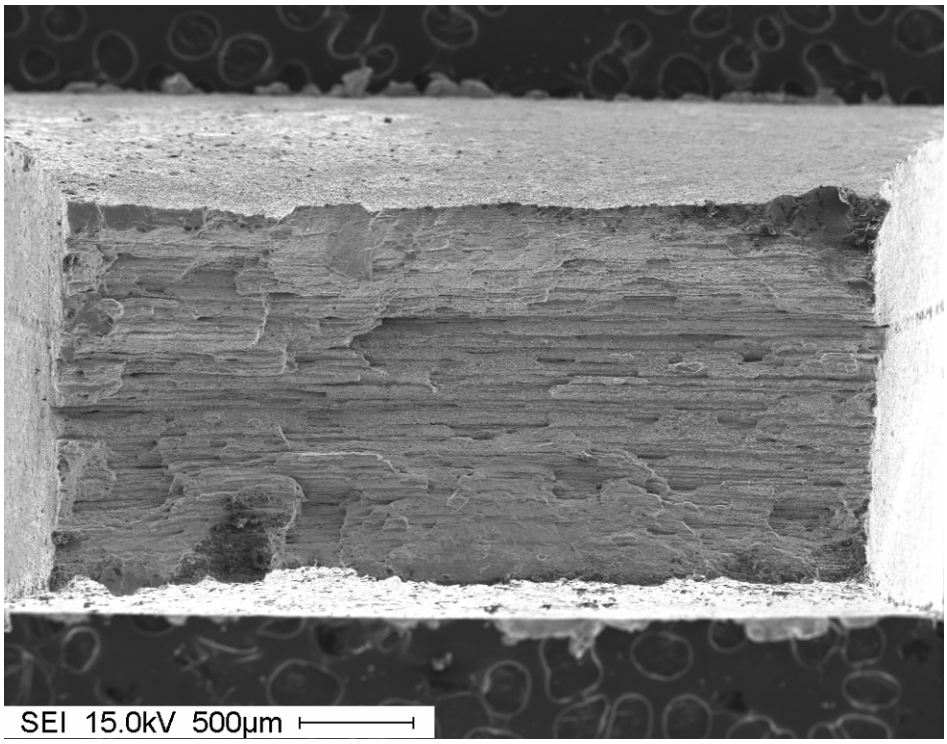

Figure 12. 27x, high strain rate sample.

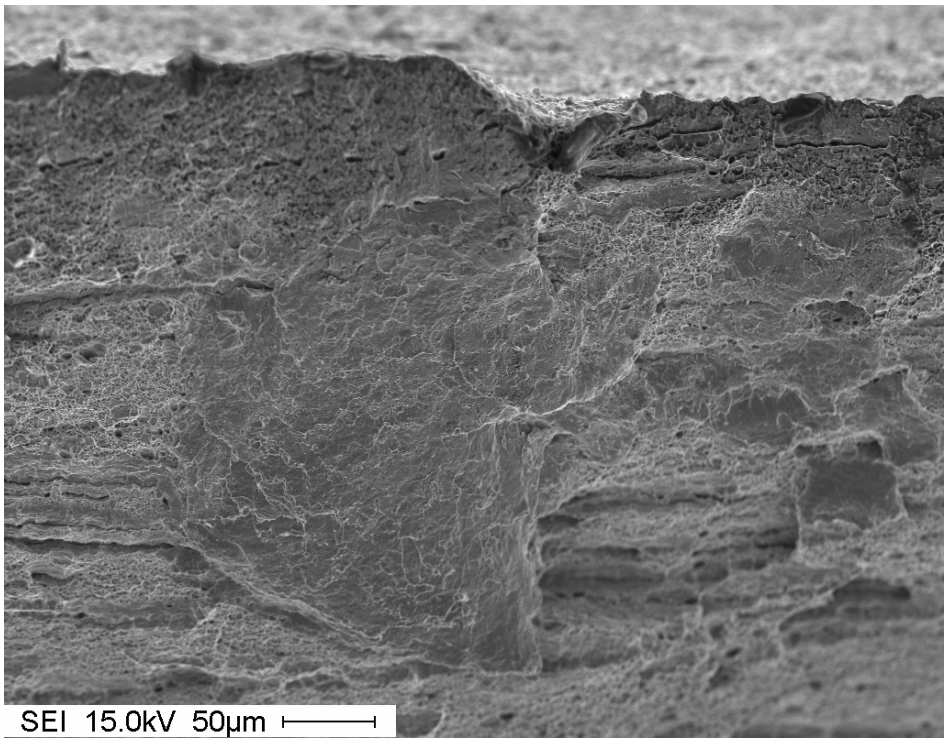

Figure 13. 220x, high strain rate sample.

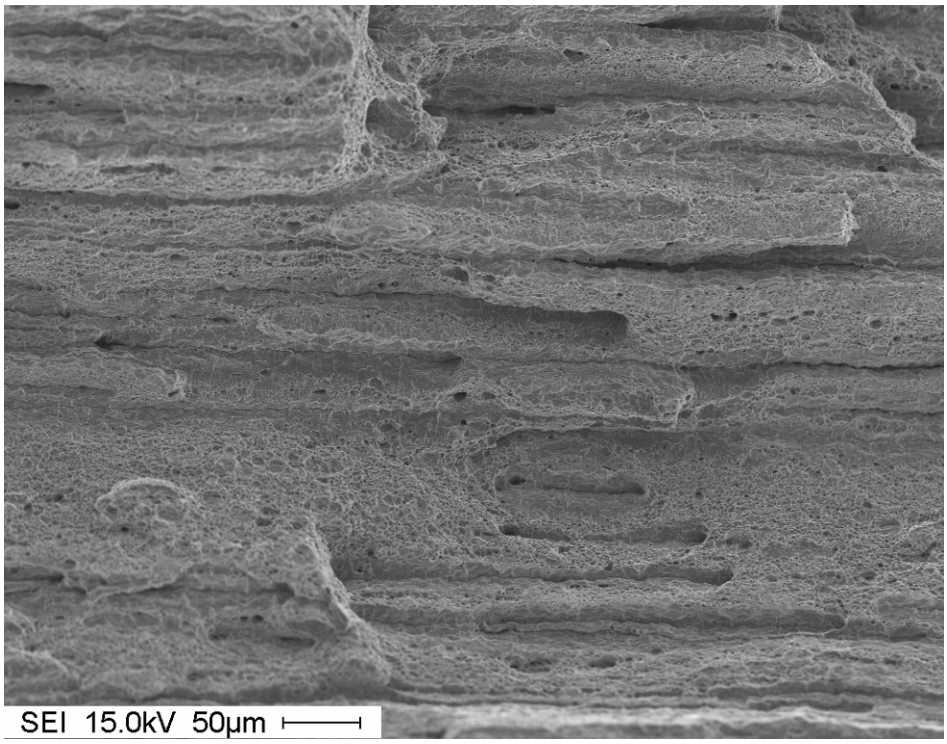

Figure 14. 180x, high strain rate sample.

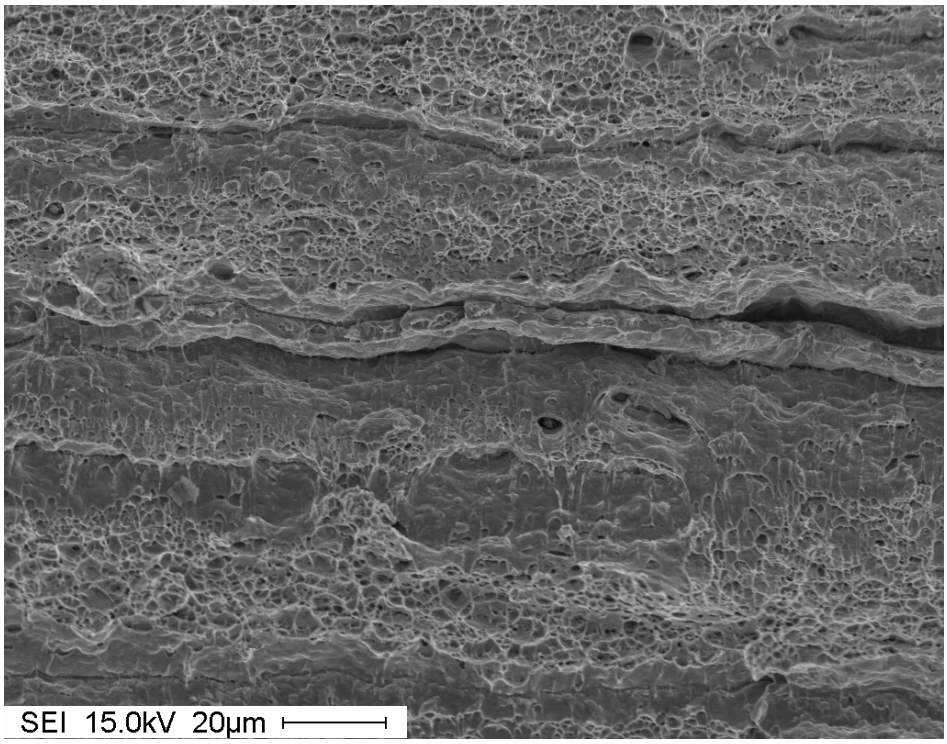

Figure 15. 600x, high strain rate sample.

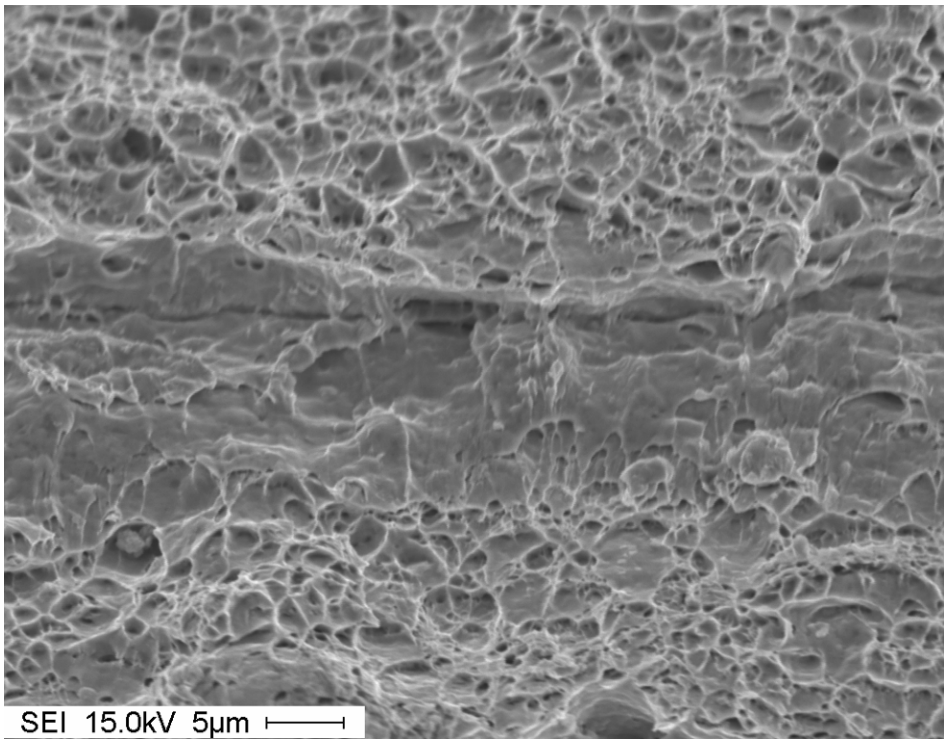

Figure 16. 1800x, high strain rate sample.

APPENDIX 7 – COUPONS AFTER HOLE EXPANSION TESTS

GALVANIZED COUPONS

HSLA-25

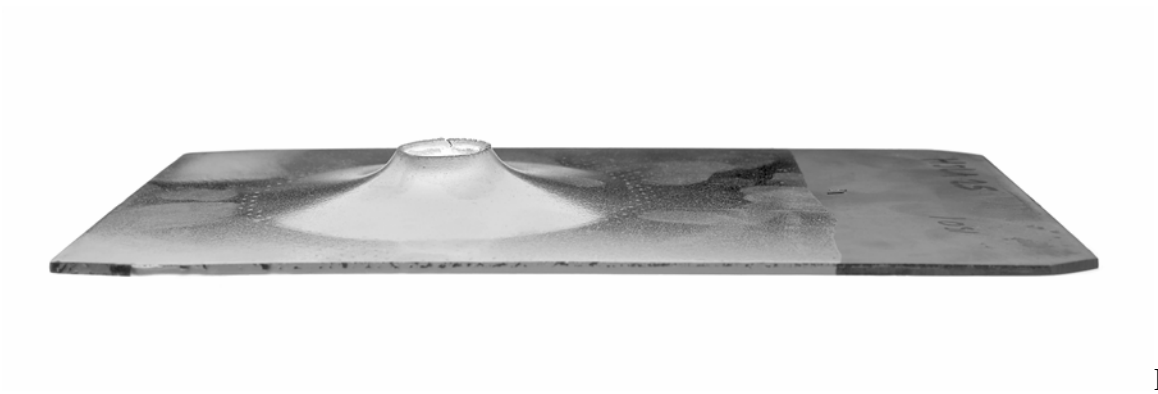

HSLA-32

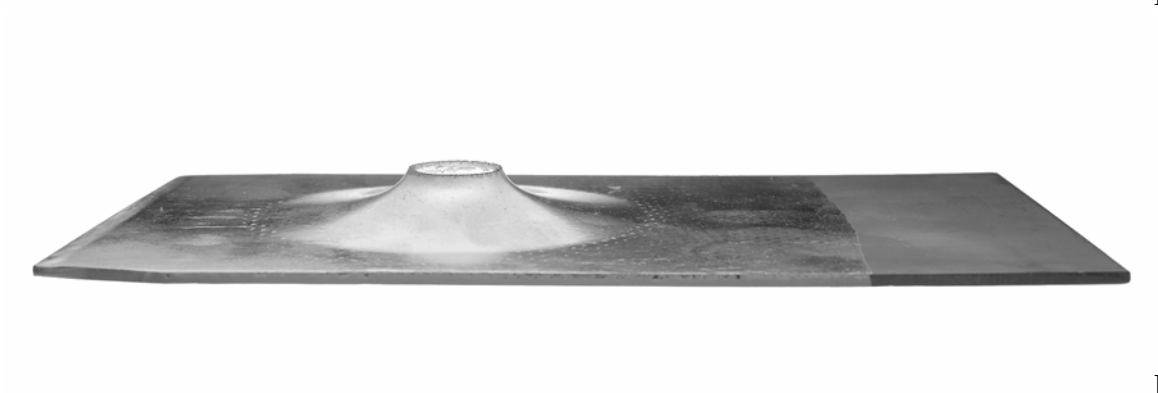

HSLA-36

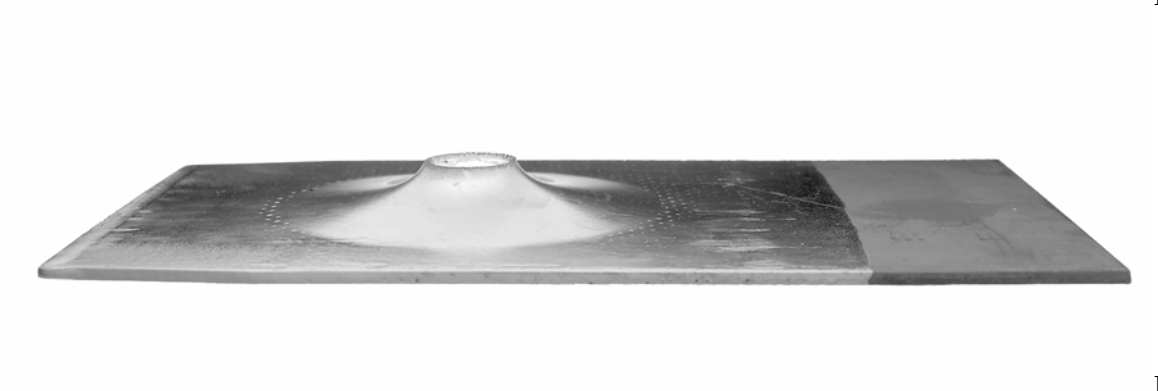

HSLA-41

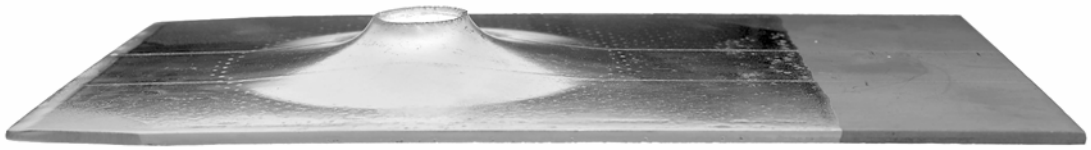

HSLA-46

HSLA-60

GALVANNEALED COUPONS

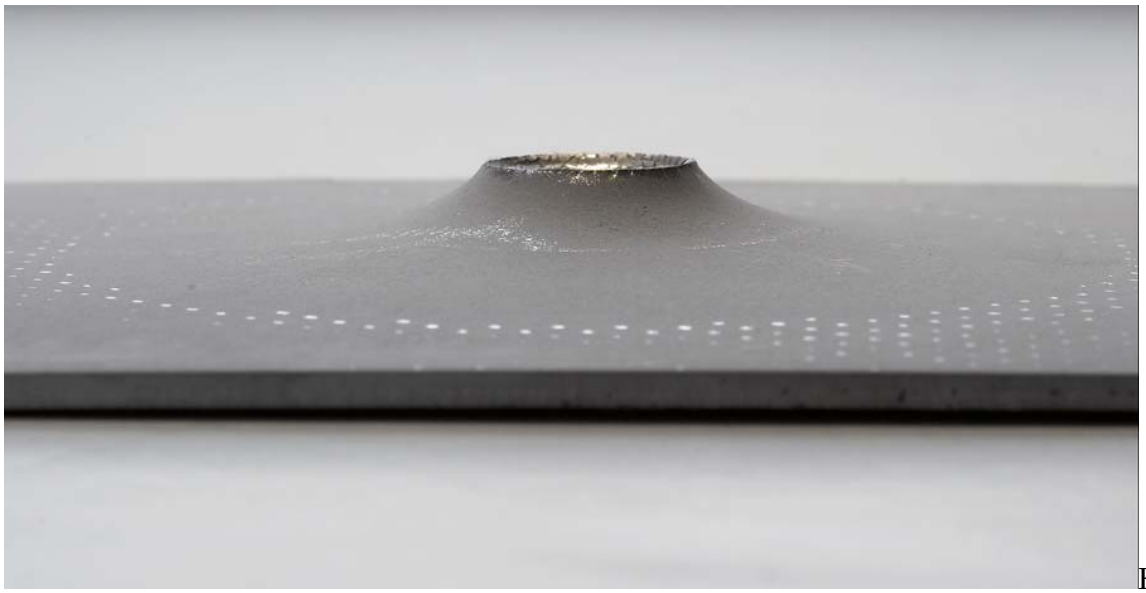

HSLA-GA30

HSLA-GA33

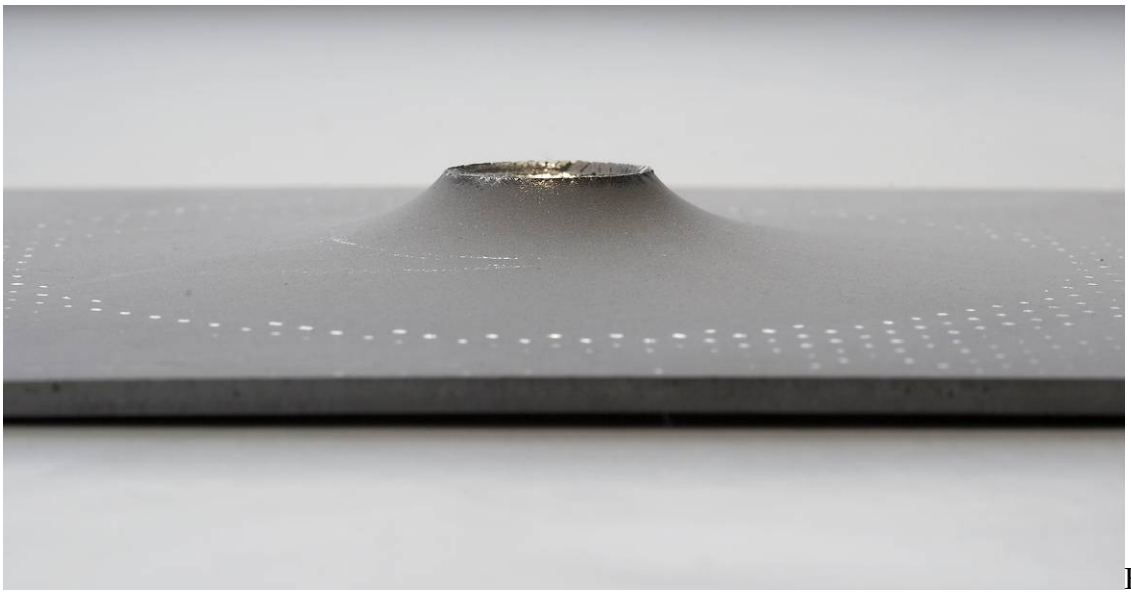

HSLA-GA35

HSLA-GA36

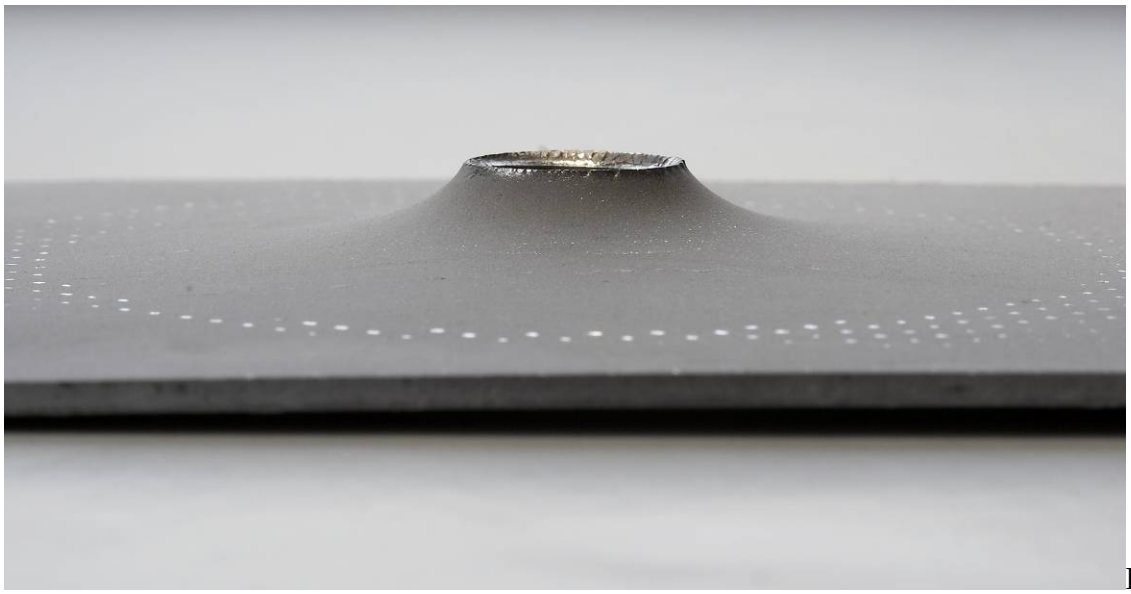

HSLA-GA37

Appendix 8 – X-RAY MEASUREMENTS OF RETAINED AUSTENITE

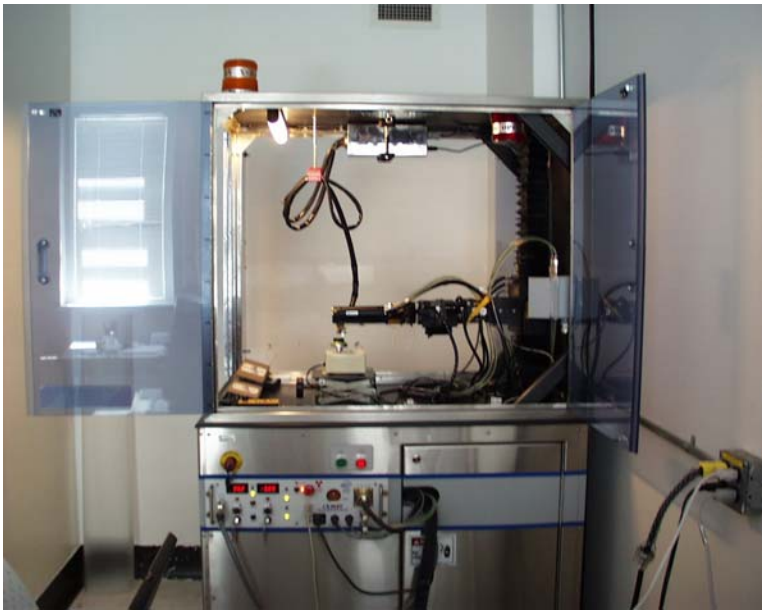

Fig. – Proto X-Ray Diffractometer (iXRD)

The industrial X-ray diffractometer built by Proto Manufacturing Ltd. (Oldcastle, Ontario, Canada) can be used to measure the stress state at the surface of ferrous and non-ferrous materials, and is also capable of measuring retained austenite in steel and ductile iron. Using X-ray diffraction offers significant benefits compared to other methods because it is a non-destructive technique. This equipment is portable which means that measurements can be made in an industrial environment as well as in a laboratory.

Transverse cross-section samples of TRIP steels were used for the measurements of the volume fraction of retained austenite. This samples were prepared by mechanical polishing and cleaning with ethanol. Care was taken to avoid significant damage of the surface layer during preparation, since retained austenite might transform to martensite due to deformation. This sample was attached to a rotating goniometer, which provided more accurate measurements for all grain orientations.

The volume fraction of retained austenite was determined using X-ray diffractomentry in which the Average Peak method was applied in the analysis of results. The Proto X-ray diffractometer is equipped with a Cr-Kα_1 tube which produces X-rays with the wavelength of λ=2.29Å. The X-rays are generated by the interaction of electrons with the Cr-target using an accelerating voltage of 20 kV applied to a tungsten filament. A V-filter was attached to the detector to eliminate Kβ irradiation. In the Average Peak method only one detector and only one peak are used at a time. The detector was moved manually to four peak positions. The following four peaks were used:

1. Ferrite (211), Bragg angle 2θ=156.3°
2. Ferrite (200), Bragg angle 2θ=106.3°
3. Austenite (220), Bragg angle 2θ=128°
4. Austenite (200), Bragg angle 2θ=79°